UNIVERSITY OF BELGRADE
FACULTY OF MECHANICAL ENGINEERING

Stefan S. Rudaković

A NOVEL APPROACH TO STABILITY ASSESSMENT OF RIVER-SEA SHIPS

Ph.D. thesis

Belgrade, 2020

УНИВЕРЗИТЕТ У БЕОГРАДУ
МАШИНСКИ ФАКУЛТЕТ

Стефан С. Рудаковић

ИНОВАТИВНИ ПРИСТУП ПРОЦЕНИ СТАБИЛИТЕТА РЕЧНО-МОРСКИХ БРОДОВА

докторска дисертација

Београд, 2020.

Supervisor and the Committee

Supervisor: Associate professor Dr. Igor Bačkalov
University of Belgrade, Faculty of Mechanical Engineering

Committee members: Associate professor Dr. Igor Bačkalov
University of Belgrade, Faculty of Mechanical Engineering

Full professor Dr. Milorad Motok
University of Belgrade, Faculty of Mechanical Engineering

Associate professor Dr. Marcos Míguez González
Escola Politecnica Superior, Universidade da Coruña

Thesis defence date: _____

Acknowledgements

First of all, I would like to express my sincere gratitude to my supervisor Prof. Igor Bačkalov for his permanent guidance and support, from the very beginning of my Ph.D. studies. He created many opportunities for my scientific advancement, that I tried to seize as much as I was able to. Hopefully, this is reflected through the thesis.

An important part of the research for the thesis was carried out during the four-month stay at the University of Trieste in 2018, under the supervision of Prof. Gabriele Bulian. I cannot thank him enough for his time and the knowledge he transferred to me, and for our discussions that clarified plenty of my doubts. I would also like to thank him for the cross-checks of codes, providing me with the confidence I much needed.

I am grateful to Mr. Jean-Michel Chatelier and Mr. Nzengu Wa Nzengu for the possibility to undertake an internship at Bureau Veritas DNI Rules Development & Training department in Antwerp. It proved to be an important step at an early stage of my studies.

I would like to thank Gennaro Rossano from the University of Naples Federico II for the cross-check of the Excessive Acceleration criterion code. It gave me a better insight and different view of the matter.

Finally, I would like to thank my colleagues, friends and family for the encouragement and support.

Abstract

A novel approach to stability assessment of river-sea ships

The goal of the thesis is to conceive a novel procedure for intact stability assessment of river-sea ships taking into account realistic environmental conditions and advanced hydrodynamics. River-sea ships are primarily inland navigation vessels that are allowed to operate in coastal areas, if technical requirements are met and environmental conditions are favourable. Although they take part in coastal operations, in general, they are not designed in compliance with international maritime regulations intended for sea-going ships. Instead, individual national regulatory bodies conceived their own sets of regulations. However, these regulations employ deterministic semi-empirical procedures based on design practice and particular operational experience in the designated area, and as such, are inevitably location-specific. Therefore, the possibility to apply the Second Generation Intact Stability Criteria (SGISC), particularly the Vulnerability Level 2 of the SGISC, to river-sea ships is analysed in the thesis. The SGISC is the state-of-the-art set of intact stability criteria for sea-going ships, laid down by International Maritime Organization. However, several methods and procedures within the SGISC need to be altered in order to successfully implement the framework on river-sea ships. Therefore, the thesis investigates the effects on stability assessment of: the modification of environmental conditions, the adjustment of roll damping estimation method, and the use of advanced methods for effective wave slope coefficient and natural roll period calculations. Furthermore, the thesis makes use of the concept of operational limitations of river-sea ships with respect to the maximum significant wave height, and proposes a set of indices for evaluation of operability of vessels from the point of view of stability in seaway. Finally, the thesis proposes a simple stability assessment procedure suitable for use at the Vulnerability Level 1 of the Dead Ship Condition, based on regression analysis.

Сажетак

Иновативни приступ процени стабилитета речно-морских бродова

Циљ тезе је осмислити нови поступак за процену стабилитета речно-морских бродова у неоштећеном стању, узимајући у обзир реалне временске услове и напредну хидродинамику. Речно-морски бродови су пре свега речни бродови који могу да плове у обалним подручјима, под условом да су испуњени одређени технички и временски услови. Иако плове у приобалним подручјима, у суштини нису пројектовани у складу са међународним прописима предвиђеним за морске бродове. Стога су различита национална регулаторна тела осмислила скуп прописа којим регулишу овај тип пловидбе. Међутим, ови прописи се базирају на детерминистичким полу-емпиријским методама прилагођеним орђеним бродовима и областима пловидбе. У дисертацији је због тога анализирана могућност примене Друге генерације критеријума стабилитета брода у неоштећеном стању, пре свега другог нивоа овог критеријума. То је најсавременији скуп критеријума за морске бродове који је предложила Међународна поморска организација (International Maritime Organisation). Међутим, потребно је изменити одређене методе и поступке садржане у критеријумима, како би се успешно применили на речно-морске бродове. Због тога се следеће теме испитују у дисертацији, како би се установио њихов утицај на стабилитет брода: прилагођавање временских услова, модификација методе за процену пригушења услед ваљања и примена напредне методе за процену ефективног нагиба таласа и сопствене фреквенције ваљања брода. Такође, у тези се користи коцепт операционих ограничења речно-морских бродова у погледу максималне значајне висине таласа, а уводи се и појам индекса операционих ограничења. За крај, предложен је једноставан поступак процене стабилитета који одговара првом нивоу критеријума, а базиран је на регресионој анализи.

Кључне речи:	брод, речно-морски брод, ваљање брода, стабилитет брода, бродска хидродинамика, бродоградња, Друга генерација критеријума стабилитета брода у неоштећеном стању, превртање брода, попречна убрзања
Научна област:	машинско инжењерство
Ужа научна област:	бродоградња
УДК:	629.55.051.1(043.3)

Contents

List of symbols and abbreviations

List of symbols

a	real part of the complex excitation roll moment	C_{VP}	vertical prismatic coefficient
a_{cal}	induced acceleration due to roll	C_{whm}	wind heeling moment coefficient
$\mathbf{A}$	added mass matrix	C_{WL}	waterplane area coefficient
A_{eq}	cross-section area of the "equivalent vessel"	C_{44}	restoring force coefficient
		D	depth of the ship
		$\hat{\mathbf{F}}$	vector of complex forces
A_K	total area of bilge keels	F_n	Froude number
A_L	lateral windage area	g	gravitational acceleration
a_y^*	transfer function of lateral acceleration	$\overline{GM}$	metacentric height
		$\overline{GM}_{res}$	residual metacentric height
A_{44}	roll added mass moment of inertia	$\overline{GZ}$	righting lever curve
B	breadth of the ship	$\overline{GZ}_{res}$	residual curve of statical stability
$\mathbf{B}$	damping matrix	H	absolute roll transfer function
b	imaginary part of the complex excitation roll moment	h	vertical distance from the assumed roll axis
b_{BK}	bilge keels width	h_K	distance from the keel
B_{BK}	bilge keels damping component	H_{rel}	relative roll transfer function
B_E	eddy damping component	H_S	significant wave height
$\hat{B}_E$	non-dimensional eddy damping component	$H_{S,max}$	maximum significant wave height
		K	surface drag coefficient
B_{eq}	breadth of the "equivalent vessel"	$\hat{k}$	non-dimensional wave number
B_F	friction damping component	$\overline{KB}_{eq}$	vertical position of centre of buoyancy of the "equivalent vessel"
B_L	lift damping component		
$\overline{BM}_{eq}$	transversal metacentric radius of the "equivalent vessel"		
		$\overline{KG}$	vertical centre of gravity
B_W	wave damping component	$\overline{KG}_{eq}$	vertical centre of gravity of the "equivalent vessel"
B_{44}	total roll damping		
$\hat{B}_{44}$	non-dimensional total roll damping	K_L	factor which takes into account vertical accelerations and yaw
C	roll radius of inertia coefficient	$\overline{KM}$	vertical position of metacentre
$\mathbf{C}$	restoring matrix	k_w	wave number
C_B	block coefficient	k_{xx}	roll radius of inertia
C_{BK}	bilge keels coefficient	k'_{xx}	total ("wet") roll radius of inertia
C_{DSC}	long-term DSC failure index	k_{zz}	yaw radius of inertia
$C_{DSC,s}$	short-term DSC failure index	L	length of the ships
C_{EA}	long-term EA failure index	l_{BK}	length of the bilge keels
$C_{EA,s}$	short-term EA failure index	$l_{wind,tot}$	wind heeling lever
C_M	midship section coefficient	$\mathbf{M}$	mass matrix
C_P	prismatic coefficient	M_{damp}	roll damping moment

M_{FK}	Froude-Krylov moment	V	displaced volume
M_{rest}	restoring moment	v	speed of the ship
M_{wave}	wave induced moment	V_{eq}	displaced volume of the "equivalent vessel"
M_{wind}	wind induced moment		
m_0	zeroth spectral moment	v_{max}	maximum speed of the ship
m_2	second spectral moment	W_i	weighting factor
M_{44}	roll mass moment of inertia	x	longitudinal position
$\overline{OG}$	vertical distance between water line and centre of gravity	$\mathbf{x}$	complex state vector
		Z	vertical distance from the centre of windage area to the centre of the underwater lateral area
$\overline{OG}_{eq}$	vertical distance between water line and centre of gravity of the "equivalent vessel"		
		z_T	vertical distance from the centre of lateral windage area to the waterline
OLI_1	areal operational limitation index		
OLI_2	centroidal operational limitation index	β	quadratic damping coefficient
		γ	peakedness factor
P	pressure	Δ	displacement force
Q_{ij}	mass plus added mass of motion $i,j = 2,4,6$	δ	cubic damping coefficient
		δk_{xx}	additional roll radius of inertia
r	effective wave slope coefficient	$\Delta\varphi_{res,EA+}$	residual range of stability to leeward side
r_φ	effective wave slope coefficient at natural roll frequency		
		$\Delta\varphi_{res,EA-}$	residual range of stability to windward side
RI_{EA+}	risk indices to leeward side		
RI_{EA-}	risk indices to windward side	Θ_m	roll amplitude
R_{DS0}	DSC L2 long-term standard	μ	linear damping coefficient
R_{EA2}	EA L2 long-term standard	μ_e	equivalent linear damping coefficient
R_{PLA}	PLoS L1 threshold		
R_{PR}	PR L1 threshold	ρ	density of water
R_2	EA L2 threshold	ρ_{air}	density of air
S	relative roll angle spectrum	σ_{ay}	standard deviation of the lateral acceleration
s	wave steepness factor		
S_M	roll moment spectrum	σ_φ	standard deviation of roll
S_m	non-dimensional roll moment spectrum	$\sigma_{\dot{x}}$	standard deviation of roll angular velocity
$S_{M,wave}$	roll moment spectrum due to waves		
		φ	roll angle
S_v	spectrum of the wind gust	$\dot{\varphi}$	roll angular velocity
S_x	absolute roll angle spectrum	$\ddot{\varphi}$	roll angular acceleration
S_{ZZ}	sea elevation spectrum	φ_a	roll amplitude
$S_{\alpha\alpha}$	wave slope spectrum	$\varphi_{cap,EA+}$	virtual capsize angles to leeward side
$S_{\alpha\alpha,c}$	effective wave slope spectrum		
$S_{\delta M_{wind,tot}}$	spectrum of the wind gust moment	$\varphi_{cap,EA-}$	virtual capsize angles to windward side
T	draught of the ship	$\varphi_{fail,+}$	failure angle to leeward side
t	time	$\varphi_{fail,-}$	failure angle to windward side
T_Z	zero-crossing wave period	φ_{flood}	angle of down-flooding
T_m	modal wave period	φ_i	imaginary part of the complex excitation roll moment
T_{eq}	draught of the "equivalent vessel"		
T_{exp}	exposure time	φ_r	real part of the complex excitation roll moment
$T_{Z,\varphi}$	zero-crossing roll period		
T_φ	natural roll period	φ_s	static heel angle
U_w	mean wind speed		

$\varphi_{VW,+}$	angle of vanishing stability to leeward side	ω_e	encounter wave frequency
$\varphi_{VW,-}$	angle of vanishing stability to windward side	ω_m	modal wave frequency
φ_1	angle of roll	$\omega_{Z,\varphi}$	zero-crossing roll frequency
χ	aerodynamic admittance function	ω_φ	natural roll frequency
ω	circular frequency	$\omega_{\varphi,e}$	modified natural roll frequency close to the heel angle
$\hat{\omega}$	non-dimensional circular frequency		

List of abbreviations

BV	Bureau Veritas
CEMT	Conférence Européenne des Ministres des Transports
CESNI	Comité Européen pour l'Élaboration de Standards dans le Domaine de Navigation Intérieure
DSA	direct stability assessment
EA	Excessive Acceleration
ES-TRIN	European Standard laying down Technical Requirements for Inland Navigation vessels
G	centre of gravity
IMO	International Maritime Organisation
IS	Intact Stability
LPG	liquefied petroleum gas
L1	Level 1
L2	Level 2
MAD	median absolute deviation
PLoS	Pure Loss of Stability
PR	Parametric Roll
RAO	response amplitude operator
OG	operational guidance
OL	operational limitation
RF	regression formula
SGISC	Second Generation Intact Stability Criteria
SLF	Stability and Load Lines and on Fishing Vessels' Safety
TEU	twenty-foot equivalent unit
UNECE	United Nations Economic Commission for Europe
1DOF	one-degree-of-freedom
2D	two-dimensional
2DOF	two-degree-of-freedom
3D	three-dimensional
3DOF	three-degree-of-freedom

Chapter 1

Introduction

1.1 Scope of research and objectives of the thesis

A common approach to safety issues of river-sea vessels (akin to international regulatory framework instituted by IMO conventions) does not exist. In practice, the safety assessment is largely based on diverse (semi-)empirical, approximate and simplified or incomplete methods, which in some cases may unnecessarily limit the operation of the vessels. It is believed that a proper stability assessment procedure would not only contribute to the safety of river-sea ships but that it may even be beneficial for their efficiency; if a more accurate mathematical model of stability-related physical phenomena is employed, its application could result in a less conservative stability assessment and, hence, in expansion of safe navigation conditions. Therefore, the goal of the research is to conceive a procedure for intact stability assessment of river-sea ships when sailing in maritime environment, accounting for realistic environmental conditions and advanced hydrodynamics. The possibility to derive a procedure based on the Second Generation Intact Stability Criteria framework should be examined, while each component should be tested for applicability to river-sea ships, and modified or reconsidered accordingly.

The definition of "river-sea ship" is sometimes used to describe very dissimilar ship types, or even used interchangeably. However, in this thesis the term "river-sea ship" follows Bačkalov (2019), where river-sea ships are defined as primarily inland navigation vessels which are supposed to make short sea trips in coastal zones on a regular basis, provided that certain technical and environmental conditions are met. Although the stability of inland navigation vessels is well-established in national and classification society rules and to some extend harmonised (see UNECE, 2019; CESNI, 2019), the focus of the thesis is on the intact stability of river-sea ships in maritime environment. Furthermore, only self-propelled cargo vessels are considered, disregarding pushed convoys and coupled formations. River-sea ships are in operation in coastal areas of France, Belgium, Russia, India, China, etc. However, the common international regulatory framework for river-sea ships does not exist, not even on the European level. Instead, national regulations and classification rules employing very dissimilar approaches are being used throughout the world, see Bačkalov (2012, 2019) and Chatelier et al. (2017). Such regulations, being location-specific, are inevitably semi-empirical and tailored so as to take into account the design features of typical ships used in the designated navigation area, as well as the particular operational experience with such ships. In other words, the regulations successfully applied in one coastal zone may not be appropriate for different ships sailing in another area.

It is, therefore, necessary to conduct a proper assessment of stability of river-sea ships in appropriate environmental conditions. On the other hand, because of their unconventional design (in comparison to standard sea-going ships), the suitability of the present mandatory ship stability regulations laid out in IMO 2008 IS Code (see IMO, 2008a), involving semi-empirical and simplified analytical methods, may not be appropriate. A rational solution could

be possibly found in the application of the methods under development in the framework of Second Generation Intact Stability Criteria (SGISC) to river-sea ships, with some modifications reflecting the specific design and operational features of this type of vessels.

The Second Generation Intact Stability Criteria represents the state-of-the-art procedure in ship stability assessment, developed by IMO. It is conceived as applicable to sea-going ships, which can have diverse hull forms and ship particulars, taking advantage of advanced hydrodynamic models. IMO has recognized five stability failure modes to which sea-going ships could be vulnerable: Dead Ship Condition, Excessive Acceleration, Parametric Roll, Pure Loss of Stability and Surf-riding/Broaching. Nevertheless, these advanced hydrodynamical models can be extremely complex and impractical for everyday use. Therefore, the SGISC is organized in multiple tiers, each being less complex and more conservative than the previous one: Direct Stability Assessment (DSA), Vulnerability Level 2 (L2), Vulnerability Level 1 (L1), plus an extra level – Operational Guidance/Operational Limitations (OG/OL).

After a preliminary analysis was conducted, it was concluded that, out of five stability failure modes, river-sea ships are vulnerable to the following two: Dead Ship Condition (DSC) and Excessive Acceleration (EA). River-sea ships are considered not to be vulnerable to other three modes either due to hull shape or due to low forward speed. Therefore, the governing equation for the two dangerous modes is the non-linear differential equation of ship roll where, in general, excitation moments are beam wind and waves.

The novel approach to stability assessment of river-sea ships, proposed in this thesis, is based on the calculation of operational limitations in the designated navigation area, making use of the L2 procedures for DSC and EA. At this moment (2020), the IMO procedures for L1 and L2 failure modes are finalized, and the draft guidelines for DSA are prepared. The latest complete procedures for DSC and EA are given in IMO (2019a). However, within L1 and L2 procedures, several semi-empirical methods are foreseen to be used. These methods are used to estimate the natural roll frequency, the roll damping coefficients, and the effective wave slope coefficient. They were, however, developed primarily for hull forms of conventional sea-going ships. Therefore, the applicability of these methods to river-sea ships is doubtful and requires a reconsideration. For the purpose of the research, computer codes were developed for the Vulnerability Level 2 calculations. The codes were validated based on the available test cases provided in IMO documents (IMO, 2013, 2016e). Furthermore, the codes were cross-checked in cooperation with other researchers.

The overall goal of the thesis is to provide a novel procedure for intact stability assessment of river-sea ships. Therefore, first, an overview of presently available stability regulations for river-sea ships is given in Chapter 2, followed by the review of the Second Generation Intact Stability Criteria in Chapter 3, where a possibility of implementation of the SGISC to river-sea ships is discussed. Accordingly, applicability of the Dead Ship Condition and Excessive Acceleration criteria to river-sea ships is tested in Chapter 4. In Chapter 5, environmental conditions that determine excitation moments due to wind and wave are reconsidered, resulting in adoption of a new wind and wave climate formulation. Because of unfavourable conclusions suggesting an issue with the damping estimation, Chapter 6 is dedicated to an analysis of the Simplified Ikeda's method (see Kawahara et al., 2009) application to river-sea ships, resulting in a modification of eddy damping component. Then, an important parameter in proper estimation of wave excitation, the effective wave slope coefficient, is thoroughly analysed in Chapter 7, with an advanced hydrodynamic estimation method proposed. The same method was proposed for natural roll frequency estimation within Chapter 8. However, the method is somewhat cumbersome for use, therefore, in Chapter 9 simple regression formulae for the effective wave slope coefficient and natural roll frequency estimation are derived. In order to provide river-sea ships with possibility to extend the acceptable range of loading condition and minimising the suspension of navigation, Chapter 10 is focused on operational limitations with

respect to maximum significant wave height. In Chapter 11, unified procedures for stability assessments of river-sea ships based on the SGISC Vulnerability Level 2, developed in the thesis, are presented. Moreover, a derivation procedure of simple and conservative Vulnerability Level 1 criteria is given. Furthermore, after each modification of the original SGISC procedure, stability of three test vessels is assessed and presented, pointing out the significance of the modification.

1.2 Vessels database

For the purpose of the research presented in the thesis, a database of typical inland vessels and river-sea ships was gathered from different sources. For most of the vessels, available information comprised tables of offsets, as well as general arrangements, and only occasionally actual loading conditions. Based on this data, the hull geometry of the vessels was reconstructed as well as other design data required for stability assessment.

In total, 33 existing self-propelled vessels were gathered, comprising 24 tankers, 4 general cargo vessels, 4 container vessels and 1 LPG tanker. It should be noted, however, that the hull shape and the dimensions of European inland vessels are not significantly influenced by the vessel type, and that the underwater hull part share similarities between them. The typical propulsion arrangement consists of two propellers in stern tunnels, although some vessels in the database have a single screw. These vessels, in general, have low forward speeds, usually in range $8 \, \mathrm{kn} \div 12 \, \mathrm{kn}$. Presently (2020), most of the vessels were approximately from 8 to 15 years in service.

In Table 1.1, the main particulars of the vessels from the database are given. Additionally, the main characteristics of the vessels in the database are given in Appendix A in form of histograms. The dimensions of inland navigation vessels are, to a large extent, determined by the waterway in which they are designed to sail. In this database, the length of vessels ranges from 66 m (for small inland navigation vessels) up to 135 m (corresponding to the largest contemporary inland self-propelled vessels in Western Europe). According to the Classification of European Inland Waterways (CEMT, 1992) created by the European Conference of Ministers of Transport (known as CEMT - Conférence Européenne des Ministres des Transports), these vessels are in range from CEMT III class up to CEMT VIb class. The inland vessels have full hull forms, with block coefficients up to $C_B \approx 0.92$, due to long parallel middle bodies in combination with full midship coefficients (C_M typically exceeding 0.99). Due to restrictions in waterway dimensions, inland vessels have relatively small draught, which is compensated with greater beam, resulting in somewhat high B/T ratios, in the range of $2.5 \div 4.5$ for the scantling draught, and much higher ratios for lower draughts. They often make use of maximum practical length for a certain waterway, resulting in wide range of L/B ratios, in range of $5.5 \div 12$, for scantling draught. On the other hand, the beam of inland navigation vessels are restricted by the width of locks, resulting in repetitive beam dimensions among them. For instance, from the presented database, 19 vessels in total have the beam close to $11.4 \, \mathrm{m}$ (see Figure A.1), which corresponds to the maximum vessel beam, which can fit into lock chambers of $12 \, \mathrm{m}$ width. Furthermore, the air draught of inland vessels is restricted by bridge height, restricting the maximal number of container tiers to, as usual for Western Europe, three or four. Consequently, inland vessels typically have retractable, hydraulically-driven wheelhouses, enabling them to pass under low bridges (when the wheelhouse is lowered), and to attain sufficient visibility from the bridge (when the wheelhouse is elevated).

Additionally, body plans of several vessels will be presented in this Chapter. In all cases, the cross-sections are equally spaced at $500 \, \mathrm{mm}$ distance whereby "0" represents the aftmost section. All body plans of inland vessels given are in the same drawing scale.

Table 1.1: Vessel database

vessel	vessel type	L_{WL} [m]	B [m]	T [m]	D [m]	C_B [-]	C_P [-]	C_M [-]	B/T [-]
T1	tanker	66.83	10.50	3.45	4.00	0.8099	0.8132	0.9959	3.04
T2	tanker	84.30	9.56	3.10	3.50	0.9129	0.9141	0.9987	3.08
T3	tanker	85.07	10.50	3.60	3.85	0.8766	0.8766	0.9969	2.92
T4	tanker	85.20	11.40	4.30	5.00	0.8514	0.8540	0.9969	2.65
T5	tanker	85.77	10.95	2.80	2.95	0.8535	0.8551	0.9982	3.91
T6	tanker	85.79	14.15	3.00	5.00	0.9164	0.9220	0.9940	4.72
T7	tanker	85.83	9.45	2.50	3.60	0.9111	0.9119	0.9991	3.78
T8	tanker	85.98	9.60	3.35	3.65	0.8762	0.8795	0.9962	2.87
T9	tanker	86.23	9.51	3.25	3.50	0.8873	0.8914	0.9953	2.92
T10	tanker	86.23	9.40	3.07	3.62	0.8703	0.8710	0.9992	3.06
T11	LPG tanker	94.76	11.40	3.50	4.10	0.8933	0.8952	0.9980	3.26
T12	tanker	100.60	11.40	3.20	3.60	0.8656	0.8667	0.9987	3.56
T13	tanker	108.10	11.35	2.50	4.00	0.8745	0.8751	0.9993	4.54
C14	container v.	108.40	11.40	2.46	3.70	0.8683	0.8714	0.9964	4.63
T15	tanker	109.59	11.40	4.30	4.65	0.8967	0.8983	0.9982	2.65
T16	tanker	109.62	11.35	3.00	3.75	0.8810	0.8822	0.9986	3.78
T17	tanker	109.69	11.41	3.75	3.90	0.8860	0.8873	0.9985	3.04
T18	tanker	109.75	11.47	3.50	3.80	0.8885	0.8906	0.9977	3.28
T19	tanker	109.76	13.59	3.50	4.40	0.8607	0.8663	0.9935	3.88
T20	tanker	109.78	13.50	3.50	4.40	0.8643	0.8663	0.9977	3.86
C21	container v.	109.81	11.45	2.60	3.65	0.8738	0.8751	0.9986	4.38
T22	tanker	109.92	11.41	3.60	4.00	0.8808	0.8822	0.9985	3.17
T23	tanker	110.13	11.35	3.55	4.00	0.8900	0.9242	0.9982	3.20
T24	tanker	110.80	11.40	3.30	3.60	0.9005	0.9019	0.9985	3.45
T25	tanker	124.33	11.40	4.30	6.00	0.8967	0.8970	0.9996	2.65
C26	container v.	133.75	14.50	3.80	4.20	0.9313	0.9353	0.9957	3.82
C27	container v.	134.27	11.41	3.50	4.15	0.9198	0.9221	0.9974	3.26
C28	container v.	134.30	14.50	4.50	5.70	0.9145	0.9166	0.9978	3.22
C29	container v.	134.78	11.45	3.21	3.90	0.8998	0.9017	0.9979	3.57
C30	container v.	134.79	11.41	3.75	4.50	0.9240	0.9524	0.9974	3.04
T31	tanker	135.02	16.80	4.55	5.00	0.8832	0.8847	0.9984	3.69
C32	container v.	135.20	11.40	3.50	3.65	0.9156	0.9173	0.9981	3.26
T33	tanker	135.22	11.40	3.20	3.90	0.9124	0.9145	0.9978	3.56

Inland vessels have different design characteristics than standard sea-going ships. Inland navigation vessels have, in general, fuller hull forms than sea-going ships. For instance, sea-going bulk carriers, ships considered to have typically high block coefficient, may have $C_B = 0.8 \div 0.85$ (Watson, 1998; Lamb, 2004), while inland vessels often have $C_B > 0.9$. Furthermore, sea-going ships have smaller B/T ratios, which are in range $B/T = 2.2 \div 2.9$ (Watson, 1998), while restrictions in inland waterways depth has resulted in increased inland vessels beam, thus higher B/T ratios. However, if L/B ratio of inland vessels are compared to the same ratio for sea-going ship, which is in range of approximately $L/B = 5.0 \div 7.5$ and sometimes up to $L/B = 9$ for sea-going container ships (Watson, 1998; Lamb, 2004), it can be seen that also length of inland vessels is increased in order to compensate for the lower draught. Furthermore, inland vessels usually do not have bulbous bow, however they have stern aprons, which form tunnels for the propellers. All of these make inland vessels a unique ship types, unconventional in terms of design.

1.2.1 Test vessels

Three test vessels were chosen from the database of river-sea ships, in order to demonstrate the effects of modifications of the methods used in the SGISC - vessels T4, C14 and C32. For the sake of simplicity, hereinafter, they will be referred to as vessel A, vessel B and vessel C, respectively. It is considered that they are credible representatives of this ship type. The test vessels particulars for the scantling draught are shown in Table 1.2. Inland navigation vessels are often built without bilge keels, which is reflected in the same table. The actual vertical centre of gravity is not known, thus only position of metacentre $\overline{KM}$ is reported, obtained by the hydrostatic calculations based on input hull forms. However, the expected ranges of metacentric heights will be estimated for each test vessel. In order to achieve that, information on the lightship mass for the exact or similar vessels are used, together with information on the cargo hold dimensions. Although the vertical centre of gravity of the lightship is unknown, it is assumed to be around the half of the vessel height. Following the assumption of lightship mass and position of centre of gravity and cargo distribution within the cargo hold, and using the obtained position of metacentre, ranges of metacentric heights were possible to estimate.

Table 1.2: The particulars of the test vessels.

	Vessel A Tanker	Vessel B Container vessel	Vessel C Container vessel
L_{WL} [m]	85.2	108.4	135.2
B [m]	11.4	11.4	11.4
T [m]	4.3	2.46	3.5
C_B [-]	0.8514	0.8683	0.9156
C_P [-]	0.8540	0.8714	0.9173
$\overline{KM}$ [m]	4.871	5.76	4.636
A_L [m^2]	175.3	647.2	718.4
Z [m]	3.254	4.558	5.486
l_{BK} [m]	0	0	0
b_{BK} [m]	0	0	0
φ_{flood} [°]	28.0	21.3	13.1
h_K [m]	9.5	12.6	13.8
x [m]	10.4	15.7	16.3
v_{max} [kn]	13.3	9.1	9.8

Although the obtained values are approximate, they will be used for analyses in the thesis. Furthermore, the maximum position where crew can be expected (typically at the wheelhouse at its highest position) measured from the keel h_K is reported in the Table as well. Although the vessel design speed is not known, an information regarding the maximum recorded speed could have been gathered from a ship tracking intelligence website. Therefore, a row in Table 1.2 also reports the maximum speed recorded v_{max}.

Test vessel A is a tanker, designed as a river-sea ship. According to the CEMT classification of inland vessels given by CEMT (1992), it can be classed as a CEMT Va vessel due to its beam, but it has a length corresponding to CEMT IV class. It is the smallest vessel in the test group, with the small windage area and the low wheelhouse position. Moreover, angle of flooding φ_{flood} is the largest between the three. The metacentric height is estimated to be in the range of $\overline{GM} = 1\,\mathrm{m} \div 2\,\mathrm{m}$, at the design draught. The body plan of the test vessel A is presented in Figure 1.1.
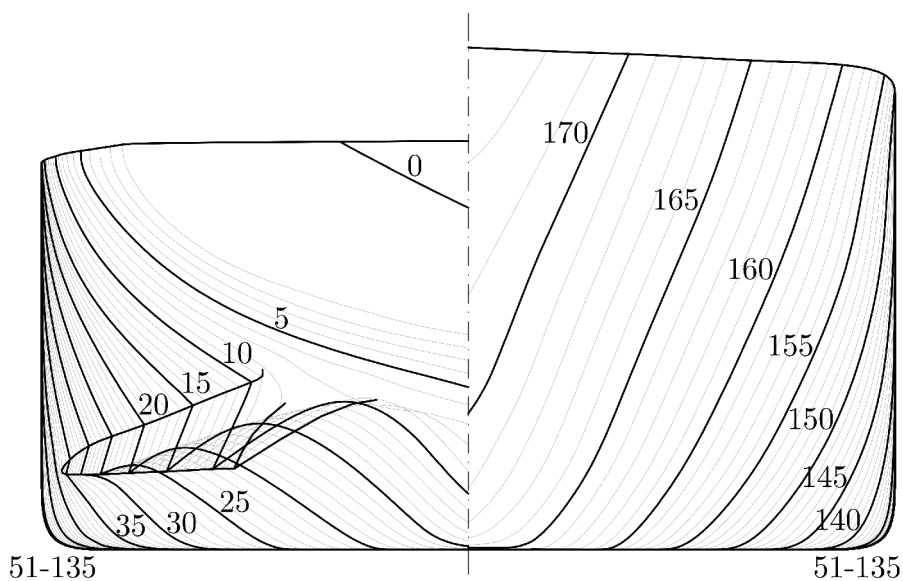
Figure 1.1: The body plan of the test vessel A.

Test vessel B is a container vessel, also designed as a river-sea ship. It is a true representative of CEMT Va class. The ship has a single, box-shaped cargo hold, without hatch covers. When fully loaded, the ship carries 192 TEUs in four tiers, four rows and 12 bays, resulting in typically large windage area. The body plan of the test vessel B is presented in Figure 1.2. The range of attainable metacentric heights is wide due to different container arrangements, while
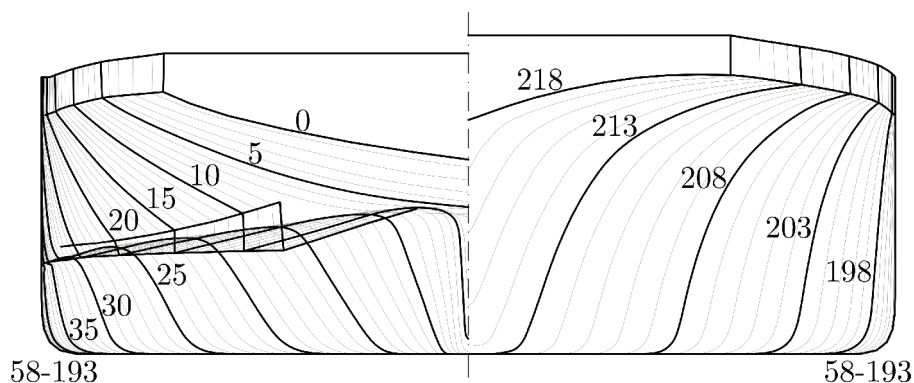
Figure 1.2: The body plan of the test vessel B.

$\overline{GM} = 1.7\,\text{m}$ corresponds to a uniform vertical distribution of cargo weight (i.e. the case in which loaded containers have equal mass). Therefore, $\overline{GM} = 1.7\,\text{m}$ could be regarded as the minimal metacentric height from the point of view of the conventional loading practice. It is considered that theoretical limits of attainable metacentric heights for the scantling draught is in the range $\overline{GM} = 0.6\,\text{m} \div 3.0\,\text{m}$, if extreme container arrangements (although not common in practice) are considered as well.

Test vessel C is an inland container vessel. It can be classed as CEMT VIb class, meaning that it is in a group of the largest inland vessels in Europe. Just like the vessel B, the vessel C has open-top, single cargo hold and retractable wheelhouse. When fully loaded, the ship carries 272 TEUs in four tiers, four rows and 17 bays, resulting in one of the largest windage areas that can be expected with this ship type. The body plan of the test vessel C is presented in Figure 1.3. The realistic range of metacentric heights goes from $\overline{GM} \approx 0.15\,\text{m}$ which approximately corresponds to the loading of containers of equal mass, and up to $\overline{GM} \approx 2.7\,\text{m}$ corresponding to the loading of heavier containers in the bottom and lighter (empty) container on top.
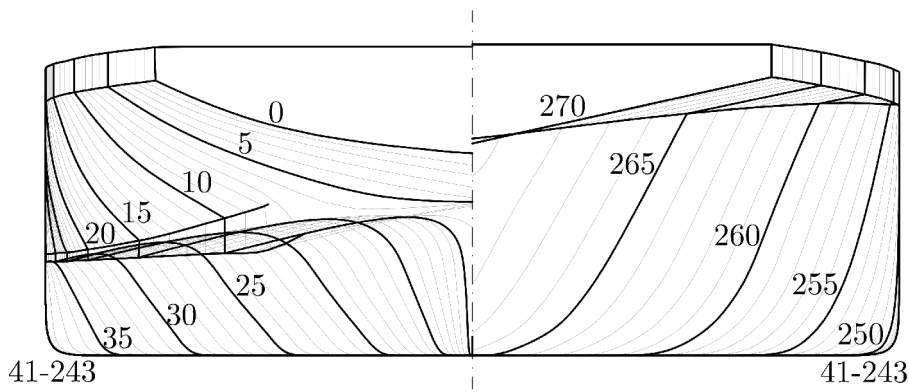

Figure 1.3: The body plan of the test vessel C.

Additionally, $\overline{GZ}$ curves of the test vessels are given in Figure 1.4. The metacentric heights used are the average values of expected $\overline{GM}$ indicated in this Section.
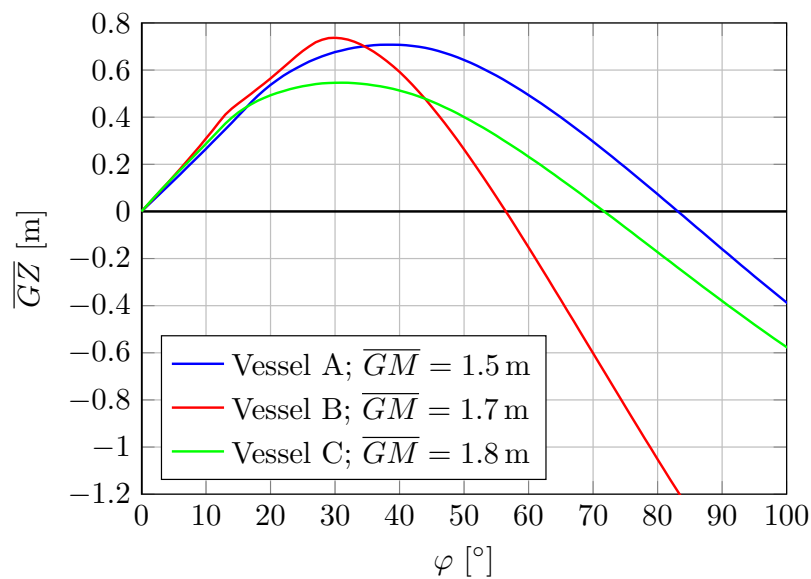
Figure 1.4: Example of $\overline{GZ}$ curve of the test vessels. Average values of the expected metacentric heights are used.

1.2.2 Validation vessels

For the purpose of validation of regression analysis, carried out in course of the thesis, two additional vessels were used - T8 and C29. For the sake of simplicity, hereinafter, they will be referred to as vessel V1 and vessel V2, respectively. They represent typical inland navigation vessels.

Although there are only two validation vessels, they are considered to be in all respects different. The vessel V1 is a small inland tanker of CEMT IV class, while the vessel V2 is a large container vessel of a CEMT VIb class. The corresponding body plans of vessel V1 and vessel V2 are given in Figure 1.5 and Figure 1.6, respectively.
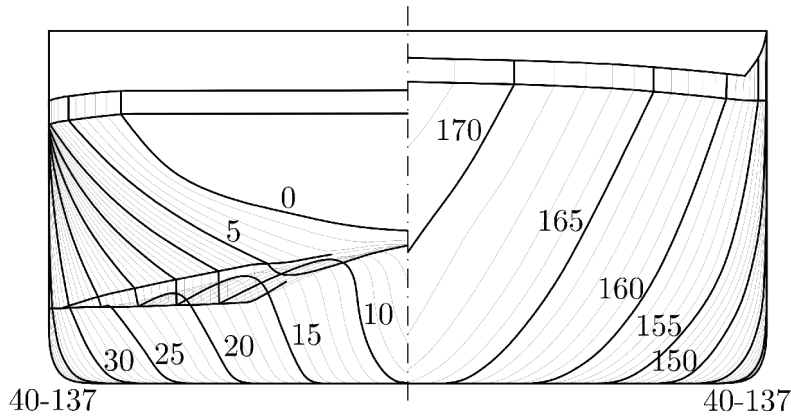
Figure 1.5: The body plan of the test vessel V1.
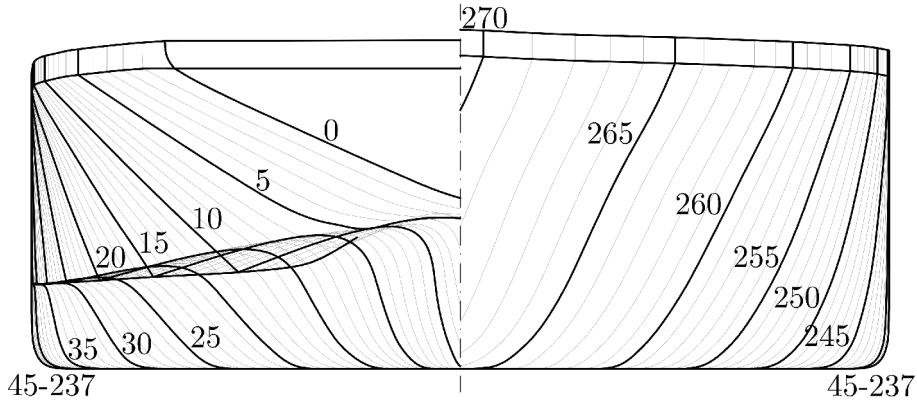
Figure 1.6: The body plan of the test vessel V2.

Chapter 2

Review of the present stability regulations for river-sea ships

2.1 Introduction

Inland vessels are not designed in compliance with IMO rules for sea-going ships. However, regulations intended for inland navigation vessels cannot guarantee required level of safety, if a vessel sails out of a river into coastal waters. Therefore, there is a need for a particular regulatory framework in order to safely and efficiently operate at sea this vessel type, which is unconventional both in terms of design and operation. Unfortunately, as it was said earlier, a common international regulatory framework for river-sea ships does not exist, not even at European level. Instead, individual national regulatory bodies and classification societies devised very dissimilar approaches throughout the world (see Bačkalov, 2012; Chatelier et al., 2017). Therefore, regulations cannot be used interchangeably between countries, as they are generally semi-empirical and developed as location-specific requirements.

In this Chapter, a brief overview of several local regulations for river-sea navigation will be presented, with a focus on intact stability requirements. Chapter is conceived as an extension of overview of river-sea ships stability regulations given by Bačkalov (2019). It is worth noticing, that most of the regulations mentioned are nationally oriented - Belgian, French, Russian and Indian national regulations, forbidding the international voyages. An exception is the regulations of the United Nations Economic Commission for Europe (UNECE), which is by its nature international.

2.2 Belgium

Belgium has a long tradition of river-sea navigation. A local term for river-sea ship is estuary vessel, as the Scheldt river creates wide river mouth toward the North Sea at which these vessels operate. According to Truijens et al. (2006), the Belgian Shipping Inspectorate has regulated estuary vessel transport since 1962 (see BSI, 1962). Based on the rules for river-sea ships, mostly tankers were operated, and their operations were practically limited to Beaufort 5 or significant wave height up to $H_S = 1.2\,\mathrm{m}$, approximately. Although deterministic by its nature and fairly limiting, the regulations from 1962 provided inland vessels with a possibility to operate in maritime environment. Nevertheless, these operational limitations were considered as too strict for contemporary river-sea transport, and ship owners have requested the extension of operational limitations to be examined (indeed, there were no reported accident corresponding to river-sea transport in Belgian waters, according to Truijens et al. (2006)). This led to the development of a new regulatory framework.

The new regulations were adopted in 2007, under the Belgian Royal Decree (see BS, 2007). They are commended as the first risk based stability regulations in the world by Vantorre et al. (2012) and Bačkalov (2012). The requirements check is based on linear seakeeping calculations, taking into account directional sea states obtained by one year successive observation of an appropriate sea. However, the wind effects are neglected in the calculations, which is the main shortcoming of the current regulation, affecting accuracy of stability assessment. Perhaps to cope with this, it is foreseen that river-sea ships should comply with 2008 IS Code (IMO, 2008a), which, in terms of stability requirements, means Criteria regarding righting lever curve properties as well as Severe wind and rolling criterion (Weather Criterion). Furthermore, detailed instructions for all procedures are not given, leaving a user with a freedom and responsibility to select, for example, the best method for damping estimation, or the most adequate sea spectrum.

The Belgian Royal Decree is conceived so as to give maximum allowable significant wave height at which a vessel can sail out to an open sea, if short-term weather forecast is favourable. The limiting significant wave height is obtained based on probability estimations that certain critical events will occur once in a lifetime or once in a year (depending on the event considered). For this purpose, it is assumed that the vessel would perform 300 round trips a year. Therefore, maximum allowable significant wave height is estimated for the following criteria:

- Emergence of keel at the bow, with a return period of once a year;

- Shipping of green water at the bow, with a return period of once in a lifetime;

- Immersion of a specified critical point at the side, with return period of once in a lifetime;

- Shipping of green water at the stern, with return period of once in a lifetime;

- Roll angle corresponding to two-thirds of an angle at which unprotected openings are immersed, or two-thirds of an angle of maximum of $\overline{GZ}$ curve, or 15 degrees, with return period of once in a lifetime;

- Critical value of lateral accelerations of the telescopic wheelhouse in its highest position, with return period of once in a lifetime;

- Critical value of lateral accelerations of cargo on deck, with return period of once in a lifetime;

- Critical value of vertical bending moment, with return period of once in a lifetime;

- Critical value of torsional moment, with return period of once in a lifetime.

2.3   France

In December 2014, a decree was issued in France (see Journal officiel de la République Française, 2014), with a purpose of regulating the access to La Havre port, and the newly built terminal Port 2000, by inland (mainly container) vessels. By the content, it is akin to Belgium Royal Decree, with which it shares the same requirements mentioned in the previous subsection. Therefore, only the significant differences will be mentioned here.

Differences can be found in an assumption that vessels are making minimum 100 round trip a year, and if a vessel is to make more than 100 round trips a year, the actual value should be used in the calculations. Another stability related difference is that requirements regarding the Weather Criterion are modified, such that wind pressure is reduced to $P = 300\,\mathrm{Pa}$, and roll angle due to wind action is calculated by means of seakeeping calculation, as the maximum roll angle with a return period of once in a lifetime.

2.4   Russian Federation

In Russian Federation, river-sea navigation (as defined in Chapter 1) is regulated by the Russian River Register (2015). Four different classes of inland navigation vessels are defined: "Л", "Р", "О" and "М", and three classes of inland vessels that are allowed to operate at sea: "О-ПР", "М-ПР" and "М-СП", each with precisely defined permissible areas, seasons of navigation and maximum significant wave heights. Each successive vessel class is allowed to sail in more severe weather conditions, and has stricter requirements. Here, only stability requirements for the latter three will be discussed, as they correspond to river-sea navigation.

According to the rules, a vessel is considered to be safe from the stability point of view, if it complies with the following criteria:

- Main stability criterion

- Additional stability requirements, depending on a vessel type

- Requirements to static stability curve parameters

- Requirements to initial stability

Main stability criterion employs the Weather Criterion scenario. There are, however, noticeable differences and an increased complexity. As the criterion is designed for local areas of navigation only, the dynamic wind pressure is limited to 304 Pa for "О-ПР", and 324 Pa for "М-СП" and "М-ПР" classes, for the case when centre of lateral windage area (measured from the waterline) is $z_T \geq 6.0$ m. The assumed dynamic wind pressure gradually reduces as the centre of lateral windage area is lower, according to a formula. Interestingly, and unlike the Weather Criterion, wind heeling arm composing wind heeling moment is corrected considering the influence of water resistance to lateral drift and inertia forces, thus, semi-empirically, taking into account coupling with other motions. Estimation of the angle of roll due to wave action is calculated in an elaborated way, and also separate procedures for "М-ПР" and "О-ПР" classes and for "М-СП" class are provided.

Additional stability requirements amend criteria that different vessel types have to comply with. For example, "М-СП" container vessels should be tested for excessive heel angle due to steady turning, furthermore additional requirements for vessels carrying cargo in bulk, tugs, fishing vessels, etc., are provided. Moreover, "М-СП" class bulk carriers should comply with an acceleration criterion, i.e. the induced acceleration due to roll a_{cal} should be smaller than $0.3g$, where g is the gravitational acceleration. The estimated acceleration is in correlation with the main stability criterion, as it is obtained using some of the same parameters: roll amplitude Θ_m, ship breadth B and coefficient m_1 which describes the natural roll frequency.

Requirements to static stability curve parameters are mainly defined for "М-СП" class. Only one requirement is defined for other classes, for "М" and "М-ПР" - the maximum value of righting arm as a function of a vessel length. For "М-СП" class, the following requirements are defined: the maximum value of righting arm as a function of vessel length; the angle of vanishing stability or downflooding angle; and the area under the $\overline{GZ}$ curve as defined in 2008 IS Code.

The last criteria mentioned is the requirement to initial stability. It is simply defined as $\overline{GM}_{min} = 0.2$ m, corrected for free surface effect for all vessels, and taking into account corrections due to icing for "М-СП" class.

2.5   Europe (UNECE)

The harmonisation of inland navigation in Europe began in 1975 with adoption of recommendations of Technical Requirements for Inland Navigation Vessels, given in Resolution No.17,

by the United Nations Economic Commission for Europe (UNECE). It has been revised ever since, and a significant change was made in 2006, when the Resolution No.61 was adopted (see UNECE, 2016). Nevertheless, requirements regarding river-sea navigation haven't been addressed until the Chapter 20B: Special provisions applicable to river-sea navigation vessels, was annexed. Currently, the latest adopted document, which includes the Chapter 20B, is published by UNECE (2019). It should be noted that, considering all regulations mentioned in this Chapter, only the Resolution No. 61 has foreseen the possibility of an international voyage, which is the actual spirit of the regulation.

Stability recommendations in the Resolution No. 61 are influenced by Russian River Register (as mentioned by Bačkalov, 2019), most noticeable in the modified Weather Criterion, laid out by UNECE. Nevertheless, this criterion is designed for inland navigation vessels, while the stability of a river-sea ship is regarded as sufficient if it satisfies the requirements of the 2008 IS Code. There are also additional stability requirements for specific vessel types, which define additional loading conditions to be checked by the Weather Criterion, together with specific operational requirements for some vessel types, for example $\overline{GM}$ for vessels carrying cargo in bulk or on deck shall be $\overline{GM}_{min} \geq 0.2\,\mathrm{m}$, tugs shall be checked for stability under the dynamic effect of a towline jerk, etc.

2.6   Europe (ES-TRIN)

CESNI (Comité Européen pour l'Élaboration de Standards dans le Domaine de Navigation Intérieure – European Committee for drawing up Standards in the field of Inland Navigation) released ES-TRIN (European Standard laying down Technical Requirements for Inland Navigation vessels), as a uniform set of technical requirements concerning inland navigation vessels. Chapter 25 of the document (CESNI, 2019), is referring to the safety of river-sea ships (in the regulation, noted as sea-going vessels).

Stability of river-sea ships is just briefly mentioned, in the Chapter 25 of the regulation, as an additional requirement corresponding to the river-sea ships navigating on the Rhine river. It is required that a river-sea ship should comply with relevant national and international provisions regarding the matter. However, additional requirements are given in Chapter 25 of the CESNI (2019) amending the Chapter 27 dealing with vessels carrying containers, where it is stated:

> Chapter 27 shall be deemed to have been complied with when stability complies with current IMO Resolutions, the corresponding stability-related documents have been endorsed by the competent authority and the containers are secured in the customary maritime navigation manner. (p. 179)

Therefore, if a new set of international regulations is adopted, river-sea ships, at least according to ES-TRIN, would have to comply with them. This means that the regulation could be too strict for river-sea ships in the future, resulting in an excessive restriction of navigation.

2.7   India

The latest document that regulates the river-sea transport in India is given by Directorate General of Shipping (2013). It defines additional requirements in terms of structural integrity, fire safety, prevention of pollution, etc., and also stability requirements, that inland navigation vessels have to comply with in order to sail in maritime conditions. The rules are organised according to division of river-sea ships in 4 types:

- Type 1 – Ship-to-Shore Service: Vessels engaged in ship-to-shore operations;

- Type 2 – Nearby Ports Service: Vessels engaged in operations between Indian ports, operating the maximum distance that can be covered during the daylight hours;

- Type 3 – Restricted Coastal Service: Vessels engaged in operations between Indian ports, operating the maximum distance that can be covered during the 48 hours;

- Type 4 – Unrestricted Coastal Service: Vessels engaged in operations between Indian ports during all weather conditions

where the Type 1, Type 2 and Type 3 river-sea vessels are allowed to navigate up to Beaufort 4. Regarding intact stability, criteria for Type 1 and Type 2 require that:

- The $\overline{GM}$ value shall not be less than 0.3 m;

- The area under $\overline{GZ}$ curve up to the angle at which the water line reaches the top of the hatch coaming shall not be less than 0.055 mrad.

while Type 3 and Type 4 vessels should comply with the 2008 IS Code, "as far as practical and reasonable in the opinion of the Administration". Furthermore, Type 3 vessels should comply, as a minimum, with a following simplified Criteria regarding righting lever curve properties from the 2008 IS Code:

- The initial metacentric height $\overline{GM}$ shall not be less than 0.3 m;

- The righting lever $\overline{GZ}$ shall be at least 0.20 m;

- The area under the $\overline{GZ}$ shall not be less than 0.090 mrad up to an angle of flooding or 40 degrees

2.8 Conclusions

In this Chapter a brief overview of six sets of regulations intended for river-sea navigation was presented, with a focus on intact stability related requirements. It is shown that the present regulations are diverse, ranging from deterministic empirical requirements to risk-based stability assessments employing linear hydrodynamic calculations. Furthermore, most of them take into account characteristic conditions for the specified navigation area, and embed them into the regulations. Consequently, they may not be applicable to another area of navigation. Moreover, all of them contain a weather criterion as a requirement, or at least a variation of it, often with reduced wind pressure.

The Belgian and the French regulations, which share similar methodology and requirements, seem to be the most advanced. They are based on 6-degrees-of-freedom linear hydrodynamic theory, however not taking into account the effect of wind moment. Several stability failure events to which a ship can be vulnerable are detected, for which procedures are devised. However, parts of the procedures are ambiguous, making different stability assessment conclusions possible. The requirements are supplemented with the 2008 IS Code stability criteria.

Russian classification society rules deal with stability requirements in a unique and complex manner, reflecting wide varieties of navigational conditions. Although the regulations contain the "classical" Weather Criterion, its components, like heel and roll angles due to wind, and roll amplitude due to wave action, are more elaborated. Furthermore, Russian River Register has recognised excessive lateral acceleration as a dangerous condition to river-sea ships.

European and Indian regulations are primarily based on 2008 IS Code Weather Criterion, as it is. This feature seems to be conservative, in comparison with other regulations which use

reduced wind pressure. Finally, ES-TRIN is relying heavily on the international regulations, as stability requirements for container vessels are said to be the same as the current IMO resolutions, making this regulation possibly the most conservative.

Chapter 3

Review of the Second Generation Intact Stability Criteria

3.1 Introduction

The Second Generation Intact Stability Criteria (SGISC) is a new set of regulations under development by the IMO. The end of the IMO's Seventh session of the Sub-Committee on Ship Design and Construction (SDC 7, in February 2020) has marked the finalisation of the SGISC, and a testing phase is expected to be launched in the following years.

The commencement of the Second Generation Intact Stability Criteria development was set in motion when an analysis of implementation issues of the Weather Criterion on passenger ships was submitted to the IMO Sub-Committee on Stability and Load Lines and on Fishing Vessels' Safety (SLF) and when the intact stability working group within IMO was re-established, or perhaps with an actual beginning of activity on the SGISC development in September 2005 (see, for example Belenky et al., 2011; Francescutto, 2016). Nevertheless, during that period the need for performance-based criteria was expressed. It was considered that the criteria should be able to solve drawbacks recognised within the under-development Weather Criterion, foreseeing that it could be developed in a few years' time, and that the present Weather Criterion would remain as it is for only short period of time (see IMO, 2005a). Furthermore, several modes of ship stability failure was recognised: Restoring arm variation problems, Stability under Dead Ship Condition and Manoeuvring related problems in waves (IMO, 2005b). Among them, only the Dead Ship Condition failure mode is considered by the 2008 IS Code. It took several years before the 2008 IS Code was implemented (adopted in 2008, came into force in 2010), which could be considered as finalisation of the First Generation Intact Stability Criteria.

The Second Generation Intact Stability Criteria represent advanced procedures in ship stability assessment, developed by IMO. The criteria are conceived as applicable to all sea-going ships, regardless of hull form and ship particulars, taking advantage of advanced hydrodynamic models. IMO has eventually recognized five stability failure modes to which sea-going ships could be vulnerable (see Annex 3 of IMO, 2005b):

- Parametric Roll

- Pure Loss of Stability

- Surf-riding/Broaching

- Dead Ship Condition

- Excessive Accelerations

Nevertheless, these advanced hydrodynamical models can be extremely complex and sometimes impractical for everyday use, as they require numerical time-domain simulation and/or physical model tests, as well as qualified expert and experimental facilities (Umeda & Francescutto, 2016). Therefore, the SGISC is organised in multiple tiers, each being less complex and more conservative than the previous one: Direct Stability Assessment (DSA), Vulnerability Level 2 (L2), Vulnerability Level 1 (L1), plus an extra level - Operational Guidance/Operational Limitations (OG/OL). A simple scheme of the application structure of the SGISC for each stability failure mode is given in Table 3.1.

Within each stability failure mode, the Direct Stability Assessment represents the state-of-the-art procedure (see IMO, 2019a), based on realistic physical phenomena, with accurately modelled hydrodynamical forces and moments acting on a ship hull and including the effect of wind, if applicable. Moreover, it makes use of model tests and multiple-degrees-of-freedom mathematical models which are solved numerically in time-domain. Alternatively, large number of experiments may be required. Therefore, the Direct Stability Assessment may require a lot of time and resources.

IMO has foreseen the possibility of using more practical procedures (in terms of resources used) in order to assess stability, represented by Vulnerability Level 1 and Vulnerability Level 2 tiers. Nevertheless, as these simpler procedures are easier to use, they come with an increased level of conservativeness. Tiers are, usually, mutually related and lower tiers are more conservative, but they employ simplified mathematical models with reduced number of degrees of freedom.

In the next Section, all five modes of stability failure will be explained. The development, procedures and analyses of different modes of stability failure within the SGISC are well described, for example in Bulian et al. (2008); Belenky et al. (2011); Shigunov et al. (2011); Umeda & Francescutto (2016); IMO (2019a); Petacco (2019).
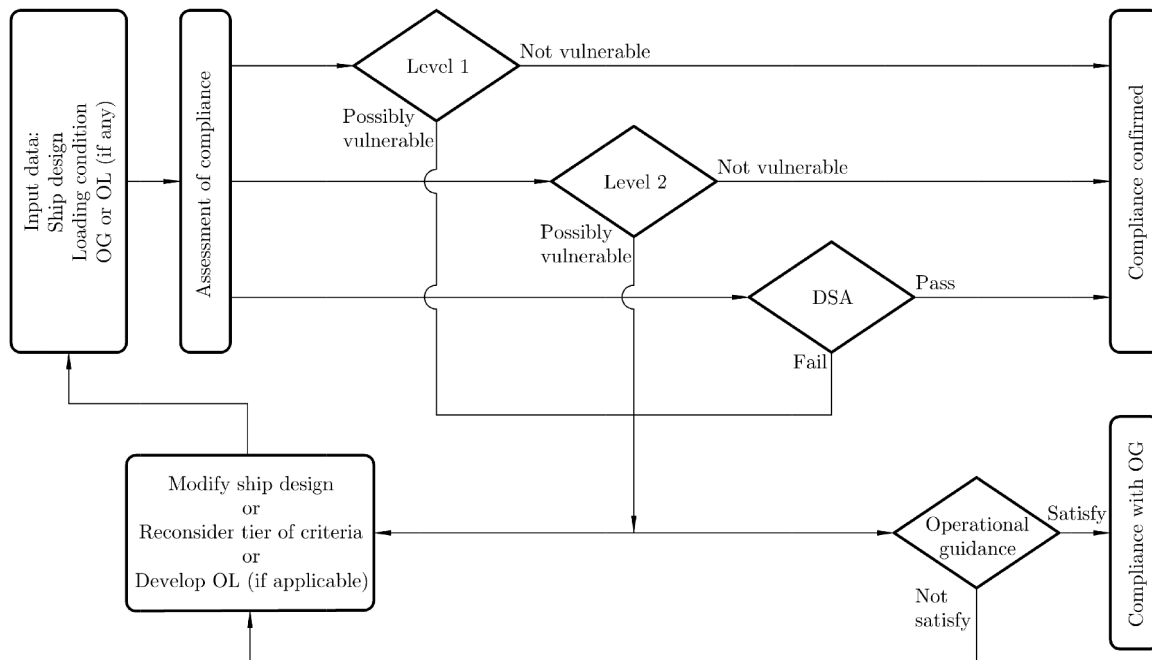

Figure 3.1: Simplified scheme of the application structure of SGISC (reconstructed from IMO (2019a)).

3.2 Brief overview of stability failure modes

3.2.1 Pure Loss of Stability

A criterion recognised as a restoring arm variation problem is the Pure Loss of Stability failure mode. A theoretical background of the criterion is well described by Belenky et al. (2011), Peters et al. (2011) or in IMO (2019b). Pure loss of stability is defined by IMO as a stability failure caused by prolonged one-time decrease of stability in waves (IMO, 2019b).

When a ship is sailing in waves, submerged volume is constantly changing, due to the hydrodynamic effects. In case when the waves are longitudinal, it is possible that a waterplane area varies significantly, depending on a ship hull shape. In general, ship sections are narrower near the bottom and flared near the deck, resulting in increase of waterplane area when the wave trough is located amidship, and in reduction of waterplane area when the crest is amidship. In an extreme case, $\overline{GZ}$ curve follows the reduction of waterplane area to such point when both initial metacentric height and significant part of $\overline{GZ}$ curve becomes negative. This endangers ship stability, risking a capsize. Of course, due to inertia of a ship, capsize does not happen instantaneously, and due to the higher celerity of longer waves resulting in the fast change of the crest position, $\overline{GZ}$ curve is, in most cases, going to be restored. However, if propulsive characteristics are such that the ship speed is high enough (close to the wave celerity), and if the ship is sailing in following waves, than it is possible that the time spent on the wave crest is prolonged, resulting in the stability failure. The phenomenon is the most prominent when wave length is close to the ship length.

However, river-sea ships are, in general, slow, which rule them out from the risk of the Pure Loss of Stability failure. Furthermore, they typically have full hull forms, with long parallel middle bodies, minimising the effect of waterplane area variation. In order to confirm this, the Vulnerability Level 1 procedure is applied to the three test vessels, described in Section 1.2.1. According to the Level 1, the vessel is considered not to be vulnerable to the Pure Loss of Stability failure mode if the minimum metacentric hight on wave $\overline{GM}_{min}$ (estimated in a rather simple way) is not less then prescribed threshold $R_{PLA} = 0.05\,\text{m}$. The results for the test vessels are given in Table 3.1. The highest realistic vertical centres of gravity $\overline{KG}$ are used (reported in the Table).

Table 3.1: Application of the Pure Loss of Stability Vulnerability Level 1 to test vessels.

	Vessel A	Vessel B	Vessel C
$\overline{KG}$ [m]	3.871	5.160	4.486
$\overline{GM}_{min}$ [m]	2.347	1.460	0.171
R_{PLA} [m]	0.050	0.050	0.050

The second requirement checks if the ship hull is narrowing when rising above the waterline (i.e tumblehome). However, the inland vessels are not expressing this characteristic, as seen on the body plans given in Section 1.2. Therefore, river-sea ships are, in general, not susceptible to the Pure Loss of Stability failure mode, and it will not be considered in the thesis.

3.2.2 Parametric Roll

The second criterion recognised as a restoring arm variation problem is the Parametric Roll stability failure mode. Detailed procedure and explanations of the phenomenon are descried by Belenky et al. (2011), Peters et al. (2011) or in IMO (2019b). Definition of the Parametric Roll, given in the SGISC explanatory notes (IMO, 2019b), is that Parametric Roll is roll motion

amplified by parametric resonance, caused by stability changes in waves or coupling with other degrees of freedom.

The physical phenomenon of the Parametric Roll has a lot in common with the Pure Loss of Stability. Both modes of stability failure happens, in general, in longitudinal waves, and are result of $\overline{GZ}$ curve variation in waves. However, in order for Parametric Roll to occur, $\overline{GZ}$ curve does not have to become negative, but it is rather triggered by the resonance of variation of $\overline{GZ}$ curve and the ship natural roll frequency, which amplifies the roll with each successive wave. This violent rolling can have significant amplitudes and can result in large accelerations, which led to accidents in the past. The amplification is greater if the wave length is close to the ship length, resulting in the most noticeable variation of waterplane area. Furthermore, it is, in general, the least favourable if the ship upright position during rolling is synchronised with the crest near amidship, reducing the stability, and when roll amplitude position is synchronised with the wave trough positioned amidship, springing the ship back upright. This corresponds to the case when the wave encounter frequency is approximately twice of the ship natural roll frequency. Moreover, it was noticed that an increase in damping can significantly reduce the occurrence of the Parametric Roll.

There are no reports of Parametric Roll in river-sea ships, to the best of the author's knowledge. Similarly to the Pure Loss of Stability failure mode, this is not surprising, as hull of typical river-sea ship is full bodied, resulting in less variation of waterplane area on waves. Nevertheless, the Vulnerability Level 1 criteria is applied to the test vessels, where, similarly to the Pure Loss of Stability, a simple test is used, checking if the change of the metacentric height on waves is larger than the prescribed threshold R_{PR} that depends on the presence of bilge keels and midship section coefficient C_M. The results of assessment are given in Table 3.2. Again, the least favourable loading conditions are used, and the bilge keels are not considered. The ship is considered not to be vulnerable if $\delta\overline{GM}/\overline{GM} \leq R_{PR}$.

Table 3.2: Application of the Pure Loss of Stability Vulnerability Level 1 to test vessels.

	Vessel A	Vessel B	Vessel C
$\overline{KG}$ [m]	3.871	5.160	4.486
$\delta\overline{GM}/\overline{GM}$	-0.510	-0.688	-0.367
R_{PR}	0.170	0.170	0.170

The second requirement is the same as for the Pure Loss of Stability, checking if the ship hull is narrowing when rising above the waterline. As there are no indications that the river-sea ships could be vulnerable to the Parametric Roll stability failure mode, it will not be further examined in the thesis.

3.2.3 Surf-riding/Broaching

A phenomenon of stability failure closely related to manoeuvrability issues and propulsion characteristics of a ship in waves is Broaching. A theoretical background and procedure of the criterion is described by Belenky et al. (2011), Peters et al. (2011) or in IMO (2019b). Broaching is defined by IMO as a phenomenon where a ship (under the wave action) cannot keep constant course despite maximum steering efforts and experiences a significant yaw motion in an uncontrolled manner (IMO, 2019b).

When a ship is sailing in following seas, with the speed close to the wave celerity, it is possible for a single wave to "capture" the ship, accelerating it to the matching speed. This phenomenon is known as Surf-riding, and it usually precedes Broaching. Because ships have tendency to be unstable in course-keeping in waves, an involuntary, uncontrollable yaw motion occurs. This

phenomenon is called Broaching, that can results in large heel angles and ultimately in capsize. It was noticed that, in order for Surf-riding to occur, the wave has to be sufficiently steep and that wave length should be between one to three times longer than the ship.

River-sea ships, in general, have low forward speeds. This is the primary check of the ship vulnerability to Surf-riding/Broaching (and alternatively, the ship has to be longer than $L \geq 200 \, \text{m}$) In order for the ship to not be considered as vulnerable, Froude number should be lower than $F_n \leq 0.3$. According to the available information presented in Table 1.2, Froude numbers of the three test vessels are calculated and given in Table 3.3.

Table 3.3: Application of the Surf-riding/Broaching Vulnerability Level 1 to test vessels.

	Vessel A	Vessel B	Vessel C
F_n [kn]	0.237	0.144	0.138

Even the shortest and fastest among the test vessels is not considered as vulnerable. In fact, the test vessel A would have to obtained the forward speed of $v = 17 \, \text{kn}$ to be considered as vulnerable. It can be concluded that river-sea ships are insusceptible to this mode of stability failure. Therefore, Surf-riding/Broaching is not considered in this thesis.

3.2.4 Dead Ship Condition

Historically the oldest dynamic stability failure phenomenon incorporated in stability regulations worldwide is the Dead Ship Condition. In a simplified way, it is incorporated within IMO as the Weather Criterion (IMO, 2008a), as a mandatory criterion. The procedure of the criterion within the Second Generation Intact Stability Criteria is given in IMO (2019b), while the development and previously proposed methods are suggested by Bulian & Francescutto (2004); Bulian et al. (2008). Dead Ship Condition is defined by IMO as a condition under which the main propulsion plant, boilers and auxiliaries are not in operation due to the absence of power (IMO, 2019b).

Without its propulsive and manoeuvring capabilities, a ship which is uncontrollably floating on water, will turn athwartship to wind and waves. From there, within a period of time, the ship is considered to roll on beam irregular waves and gusting wind. In this instant, a partial or total stability failure is possible. It should be noted that, due to the power failure, active anti-rolling devices are not functional (such as active fins or rudder roll stabilisation), and only passive devices are considered, such as bilge keels.

Taking a look at present stability regulations for river-sea ships (see Chapter 2), it may be noticed that all of them have a requirement in form of the Dead Ship Condition stability failure. Therefore, the Dead Ship Condition criterion will be tested on river-sea ships, and the justification of its applicability will be examined. However, the focus will be on the Vulnerability Level 2, as it is believed that it provides a good balance between complexity and accuracy of representation of the physical phenomenon. A detailed explanation of the Dead Ship Condition stability failure mode will be given (in Chapter 4).

3.2.5 Excessive Acceleration

Excessive Acceleration is, historically, the last mode of stability failure considered by IMO to be implemented in the SGISC, as it was not mentioned in some of the early documents and papers (for example, in IMO, 2005b; Belenky et al., 2011). However, a fatal accident of the container vessel Chicago Express (see BSU, 2009), has led to proposal of a new mode of stability failure

(Shigunov et al., 2011). The procedure of the criterion within the Second Generation Intact Stability Criteria is given in IMO (2019b).

A ship sailing in rough seas may experience significant rolling. In general, this does not pose a problem, but in a combination with the high values of metacentric height it may lead to a stability failure. Namely, high $\overline{GM}$ values correspond to the low roll periods, which in combination with large roll angles may result in dangerous lateral accelerations. As the failure mode is expected to occur at low periods (i.e. at high frequencies), the wind effects are omitted from the procedure, because the wind energy is greater at lower frequencies. The lateral accelerations generated by the roll motion are greater further away from the roll axis, and if passengers or crew are expected at such position, stability failure due to excessive accelerations should be tested. Furthermore, it is stated that ship speed is not influential in this mode of stability failure, therefore, due to simplicity, it is considered that there is no forward speed.

Lateral accelerations are included in stability criteria of Belgian, French and Russian regulations intended for river-sea ships (see Chapter 2). Therefore, the possibility of application of the Second Generation Intact Stability Criteria to this vessel type is worth analysing. Furthermore, from the point of view of the SGISC, the draft regulations for the Excessive Acceleration vulnerability assessment (see for example IMO, 2018a, 2019a) foresee that the stability of a ship should be checked with respect to this stability failure mode, in case that:

- the distance from the waterline to the highest location along the length of the ship where passengers or crew may be present exceeds 70% of the breadth of the ship; and

- the metacentric height exceeds 8% of the breadth of the ship.

These conditions are commonly satisfied for river-sea ships, making them possibly vulnerable to the Excessive Acceleration stability failure mode. Therefore, a detailed explanation of the Excessive Acceleration stability failure mode will be given (in Chapter 4).

3.3   Conclusions

The Second Generation Intact Stability Criteria is the state-of-the-art set of procedures, designed to be applicable to all sea-going ships. It makes use of advanced hydrodynamical models in order to assess the stability under various modes of stability failure. In total, five modes of stability failure are considered: Pure Loss of Stability, Parametric Roll, Surf-riding/Broaching, Dead Ship Condition and Excessive Acceleration.

In this Chapter, it is demonstrated that the river-sea ships are not vulnerable to the Pure Loss of Stability, Parametric Roll and Surf-riding/Broaching, due to the combination of full bodied hulls and low forward speed. Accordingly, the focus of the thesis will be on the two remaining modes of stability failure: Dead Ship Condition and Excessive Acceleration. Therefore, the next Chapter will be dedicated to these modes of stability failures and their application to river-sea ships.

Chapter 4

Application of the Second Generation Intact Stability Criteria to river-sea ships

4.1 Introduction

In this Chapter, a more detailed overview of the two stability failure modes, to which river-sea ships are considered to be vulnerable, is given: Dead Ship Condition and Excessive Acceleration. The focus is on the Vulnerability Level 2 procedures, as it is believed that they provide a good balance between the complexity and precision of calculations. Furthermore, Vulnerability Levels 2 will be described first, as they provide better physical representation of the phenomena, but also because Vulnerability Levels 1 are devised as a procedures derived by simplification from Vulnerability Levels 2.

At the end of this Chapter, a stability assessments of the three test vessels, based on the DSC and EA Vulnerability Level 2 procedures, will be carried out, providing the first conclusions regarding the application of the SGISC to river-sea ships.

4.2 Dead Ship Condition - Vulnerability Level 2

Dead Ship Condition Vulnerability Level 2 is governed by one-degree-of-freedom mathematical model. The roll motion is obtained by solving differential equation of roll, where excitations are described by irregular beam waves and beam gusting wind. Therefore, the pure roll motion is, in general, described by the following model:

$$(M_{44} + A_{44}) \ddot{\varphi} + M_{damp}(\dot{\varphi}) + M_{rest}(\varphi) = M_{wave}(t) + M_{wind}(t) \tag{4.1}$$

where M_{44} is the roll mass moment of inertia, A_{44} is the roll added mass moment of inertia, M_{damp} is the damping moment, M_{rest} is the restoring moment, M_{wave} is the excitation moment due to waves, M_{wind} is the excitation moment due to wind and φ is the roll angle and dots indicate time t derivatives. The equation of roll motion is non-linear. However, in order to obtain statistical parameters in a fast and practical way, the equation (4.1) is linearised.

The complete procedure of the Dead Ship Condition, as defined in the SGISC (see, for example IMO, 2013, 2019a), will be presented in this section.

4.2.1   Short-term roll motion statistics

Dead Ship Condition Vulnerability Level 2 makes use of linearised Equation (4.1), which is solved in the frequency domain. The solution is found based on the relative angle approach. It is a concept that partially compensates for the linearisation of Equation (4.1) and where, in terms of wave excitation moment, roll angle is represented relative to the wave slope angle (see Francescutto & Contento, 1998; Bulian et al., 2008; Bulian & Francescutto, 2011). However, wind excitation is considered as dependent on absolute roll angle. Furthermore, it is assumed that wind and waves are acting in the same direction, perpendicular to the ship. Therefore, a short-term motion statistics is represented by the following spectrum of (partially-)relative roll motion $S(\omega)$:

$$S(\omega) = H_{rel}^2(\omega) \cdot S_{\alpha\alpha,c}(\omega) + H^2(\omega) \cdot \frac{S_{\delta M_{wind,tot}}(\omega)}{(\Delta \cdot \overline{GM})^2} \tag{4.2}$$

where $S_{\delta M_{wind,tot}}$ is the spectrum of moment due to gusty wind action, $S_{\alpha\alpha,c}$ is the effective wave slope spectrum, H corresponds to the absolute roll transfer function, H_{rel} corresponds to the relative roll transfer function, $\Delta = mg$ is the displacement force, $\overline{GM}$ is the initial metacentric height and ω is the wave circular frequency.

The sea state is characterised by the irregular beam waves, described with the spectrum of effective wave slope $S_{\alpha\alpha,c}(\omega)$, which is calculated as follows:

$$S_{\alpha\alpha,c}(\omega) = r^2(\omega) \cdot S_{\alpha\alpha}(\omega) \tag{4.3}$$

where $r(\omega)$ is the effective wave slope coefficient and $S_{\alpha\alpha}(\omega)$ is the wave slope spectrum. The effective wave slope coefficient is an important component of the procedure, which describes complex hydrodynamic interaction between waves and a ship hull. Within the SGISC, the use of so-called standard methodology for its estimation is foreseen. The methodology for the effective wave slope coefficient calculation is described in detail in Section 4.4.2. Furthermore, the wave slope spectrum is calculated as:

$$S_{\alpha\alpha}(\omega) = \frac{\omega^2}{g^2} \cdot S_{ZZ}(\omega) \tag{4.4}$$

where $S_{ZZ}(\omega)$ is the sea elevation spectrum, and g is the gravitational acceleration. Further definition of $S_{ZZ}(\omega)$ is crucial, as it defines the environmental conditions due to waves, and largely influences the wave excitation moment estimation. The standard definition for the short-term wave characterisation in the SGISC is to use the Bretschneider (i.e. two-parameter) spectrum type for the wave elevation. Therefore, it is calculated as:

$$S_{ZZ}(\omega) = \frac{H_S^2}{4\pi} \left(\frac{2\pi}{T_Z}\right)^4 \cdot \omega^{-5} \cdot \exp\left[-\frac{1}{\pi}\left(\frac{2\pi}{T_Z}\right)^4 \cdot \omega^{-4}\right] \tag{4.5}$$

where H_S is the significant wave height and T_Z is the zero-crossing wave period; these are the characteristics of the short-term environmental condition. After defining Equations (4.5), (4.4) and (4.3), and if the values for the significant wave height and zero-crossing wave period are known, it is possible to estimate the spectrum of effective wave slope $S_{\alpha\alpha,c}(\omega)$, that defines the wave excitation moment. However, the choice of the appropriate short-term environmental condition(s), is yet to be explained.

The second excitation moment is described by the spectrum of moment due to gusting wind $S_{\delta M_{wind,tot}}$, mentioned in the Equation (4.2), which is to be calculated as:

$$S_{\delta M_{wind,tot}}(\omega) = (\rho_{air} U_w C_{whm} A_L Z)^2 \cdot \chi^2(\omega) \cdot S_v(\omega) \qquad (4.6)$$

where $S_v(\omega)$ is the spectrum of the wind gust, $\chi(\omega)$ is the aerodynamic admittance function, A_L is the lateral windage area, Z is the vertical distance from the centre of lateral windage area A_L to the centre of the underwater lateral area (or approximately to a point at one half the mean draught T), C_{whm} is the wind heeling moment coefficient which in the absence of sufficient information should be taken as $C_{whm} = 1.22$, U_w is the mean wind speed and ρ_{air} is the air density. Aerodynamic admittance function is a component that relates the mean wind speed and the induced wind pressure acting on the lateral windage area. An option for the aerodynamic admittance function estimation was proposed in earlier versions of SDC documents (see for example, IMO, 2013), which suggest the use of empirical expression given by Vickery (1968). Nevertheless, aerodynamic admittance $\chi(\omega) = 1$ is finally adopted, an option that is the simplest, but more conservative.

The spectrum of the wind gust $S_v(\omega)$ is estimated by the Davenport spectrum given by Davenport (1961), which is dependant of the mean wind speed U_w, and is calculated as:

$$S_v(\omega) = 4K \frac{U_w^2}{\omega} \cdot \frac{X_D^2}{(1 + X_D^2)^{\frac{4}{3}}}$$

with

$$K = 0.003$$

$$X_D = 600 \frac{\omega}{\pi U_w}$$

$$(4.7)$$

Here, ω corresponds to the wind speed fluctuation circular frequency and K is the drag coefficient of a surface, in this case of water waves surface. Another wind moment related simplification is that the mean wind speed is assumed to be correlated to the significant wave height H_S. This approximate wind-wave relation simplifies the definition of environmental conditions, as both wind and wave spectrum can be obtained using two parameters only - the significant wave height H_S and the zero-crossing wave period T_Z. The mean wind speed is calculated as:

$$U_w = \left(\frac{H_S}{0.06717} \right)^{\frac{1}{1.5}} \qquad (4.8)$$

The mean wind speed U_w is considered to induce the static heel angle (angle of equilibrium) φ_s, due to the constant heeling lever $l_{wind,tot}$:

$$M_{wind,tot} = \frac{1}{2} \rho_{air} U_w^2 C_{whm} A_L Z$$

$$l_{wind,tot} = \frac{M_{wind,tot}}{\Delta}$$

$$(4.9)$$

In order to estimate an appropriate roll angle spectrum, a corresponding roll transfer function has to be estimated. The squares of relative and absolute roll transfer functions are calculated as:

$$H_{rel}^2(\omega) = \frac{\omega^4 + (2\mu_e \omega)^2}{(\omega_{\varphi,e}^2(\varphi_s) - \omega^2)^2 + (2\mu_e \omega)^2}$$

$$H^2(\omega) = \frac{\omega^4}{(\omega_{\varphi,e}^2(\varphi_s) - \omega^2)^2 + (2\mu_e \omega)^2}$$

$$(4.10)$$

where μ_e is the equivalent linear roll damping coefficient and $\omega_{\varphi,e}(\varphi_s)$ is the modified natural roll frequency. The method for roll damping estimation is described in Section 4.4.1. In Equation (4.10) the natural roll frequency is modified so as to correspond to the metacentric height at the static heel angle (i.e. equilibrium angle) due to wind action with the constant speed U_w. This simple correction is calculated as:

$$\omega_{\varphi,e} = \omega_\varphi \sqrt{\frac{\overline{GM}_{res}(\varphi_s)}{\overline{GM}}} \tag{4.11}$$

where $\overline{GM}$ is the initial metacentric height corresponding to upright position, ω_φ is the natural roll frequency corresponding to $\overline{GM}$ and $\overline{GM}_{res}(\varphi_s)$ is the residual (or local) metacentric height. The modified natural roll frequency is another concept that partially compensates for the linearisation of Equation (4.1). Considering that the heel moment due to wind is constant, $\overline{GM}_{res}(\varphi_s)$ can be obtained as the first derivative of the $\overline{GZ}$ curve at the angle of equilibrium (φ_s), as:

$$\overline{GM}_{res}(\varphi_s) = \frac{\mathrm{d}\left(\overline{GZ} - l_{wind,tot}\right)}{\mathrm{d}\varphi}\bigg|_{\varphi=\varphi_s} = \frac{\mathrm{d}\overline{GZ}}{\mathrm{d}\varphi}\bigg|_{\varphi=\varphi_s} - \frac{\mathrm{d}l_{wind,tot}}{\mathrm{d}\varphi}\bigg|_{\varphi=\varphi_s} = \frac{\mathrm{d}\overline{GZ}}{\mathrm{d}\varphi}\bigg|_{\varphi=\varphi_s} \tag{4.12}$$

In the IMO documents, the exact numerical method for $\overline{GZ}$ curve differentiation is not mentioned, which is needed for solving the previous equation. In this thesis, a finite differences method was used for $\overline{GZ}$ curve differentiation. The method gives satisfying results, as the discretisation step used for the $\overline{GZ}$ curve is 1 degree.

The common method for the natural roll frequency estimation is the semi-empirical method given in 2008 IS Code (see IMO, 2008a). As the Vulnerability Level 1 is the slightly modified Weather Criterion, it seems reasonable to use the same semi-empirical method for both Level 1 and Level 2, in the absence of a more suitable method or physical experiments. Using the same method should provide better consistency between the levels. Therefore, the natural roll frequency ω_φ can be estimated from the natural roll period T_φ as:

$$\omega_\varphi = \frac{2\pi}{T_\varphi}$$
$$T_\varphi = \frac{2CB}{\sqrt{\overline{GM}}} \tag{4.13}$$
where

$$C = 0.373 + 0.023\frac{B}{d} - 0.043\frac{L_{WL}}{100}$$

Equations (4.2) $\div$ (4.13), with addition of equations given in Sections 4.4.2 and 4.4.1, provide the framework for the short-term roll motion statistics estimation. Equation (4.2) is solved numerically, with frequency ω discretised within a finite range. For the purpose of the thesis, the range and the frequency step used are the same as proposed by the showcase example in the IMO document IMO (2013): lower frequency limit $\omega_{min} = 0.000\,342\,\mathrm{rad/s}$, upper frequency limit $\omega_{max} = 3.42\,\mathrm{rad/s}$ and the frequency step $\Delta\omega = 0.000\,342\,\mathrm{rad/s}$. This ensures the sufficient accuracy of the following numerical integration, regardless of a method chosen.

4.2.2 Short-term stability failure index

In the IMO documents, short-term stability failure index $C_{DSC,s}$ is defined as the probability of the ship exceeding specified heel angles at least once in the exposure time considered, taking

into account an effective relative angle between the vessel and the waves (as defined in, for example IMO, 2019a). It is assumed that the following expression appropriately describes the short-term failure index:

$$C_{DSC,s} = 1 - \exp\left(-\lambda_{EA} \cdot T_{exp}\right) \tag{4.14}$$

In the previous Equation, T_{exp} is the exposure time adopted to be $3600\,\text{s}$, for the purpose of the stability failure estimation. This time period is the assumed short-term exposure period that the ship has to withstand in dead ship condition, regarding the short-term environmental conditions defined by H_S and T_Z. Furthermore, r_{EA} represents the intensity of the Poisson process assumed to describe the occurrence of capsize. Perhaps, a more understandable meaning has the expression $1/r_{EA}$, which represents the return period of capsize, or the average time between two capsize events (measured in seconds). Within the procedure, the r_{EA} is intended to be estimated as:

$$r_{EA} = \frac{1}{T_{Z,\varphi}} \cdot \left[\exp\left(-\frac{1}{2 \cdot RI_{EA+}^2}\right) + \exp\left(-\frac{1}{2 \cdot RI_{EA-}^2}\right)\right] \tag{4.15}$$

where $T_{Z,\varphi}$ represents the zero-crossing roll period. It is obtained from the zero-crossing roll frequency $\omega_{Z,\varphi}$, making use of the relative angle approach statistics as:

$$T_{Z,\varphi} = \frac{2\pi}{\omega_{Z,\varphi}}$$
$$\omega_{Z,\varphi} = \sqrt{\frac{m_2}{m_0}} \tag{4.16}$$

where m_0 and m_2 are, respectively, zeroth and second spectral moment of the relative roll angle spectrum $S(\omega)$. They are obtained as:

$$m_0 = \int_0^\infty S(\omega)\,\mathrm{d}\omega$$
$$m_2 = \int_0^\infty \omega^2 S(\omega)\,\mathrm{d}\omega \tag{4.17}$$

where the equations are to be solved numerically. For this purpose, the limits of integration and the frequency step are set as noted in the previous section.

In Equation (4.15), RI_{EA+} and RI_{EA-} are the risk indices to positive (leeward) and negative (windward) side. It means that failure index is estimated as the sum of two, knowing that capsize to leeward side and capsize to windward side are mutually exclusive events. Risk indices are estimated as ratios between the standard deviation of roll σ_φ and the corresponding residual range of stability $\Delta\varphi_{res,EA+}$ or $\Delta\varphi_{res,EA-}$:

$$RI_{EA+} = \frac{\sigma_\varphi}{\Delta\varphi_{res,EA+}}; \qquad \Delta\varphi_{res,EA+} = \varphi_{cap,EA+} - \varphi_s$$
$$RI_{EA-} = \frac{\sigma_\varphi}{\Delta\varphi_{res,EA-}}; \qquad \Delta\varphi_{res,EA-} = \varphi_{cap,EA-} - \varphi_s \tag{4.18}$$

where σ_φ is the standard deviation of roll, calculated as:

$$\sigma_\varphi = \sqrt{m_0} \tag{4.19}$$

and where $\varphi_{cap,EA+}$ and $\varphi_{cap,EA-}$ are called virtual capsize angles to leeward and windward side,

respectively. The concept behind the virtual capsize angles are to preserve the same residual area under the $\overline{GZ}$ curve as if non-linear restoring is being used. This way it is again possible to partially compensate for the linearisation of the roll motion equation. The virtual capsize angles are calculated using following steps, while a graphical explanation of the characteristic angles required for the DSC procedure is given in Figure 4.1:

1. Obtain the static heel angle φ_s as the equilibrium using the $\overline{GZ}$ curve and the constant heeling lever due to wind $l_{wind,tot}$ defined in Equation (4.9);

2. Identify the failure roll angles separately for leeward side $\varphi_{fail,+}$ and the windward side $\varphi_{fail,-}$ as the minimum of the following three: 1) $50°$ for leeward and $-50°$ for windward side, 2) the angle at which progressive flooding can occur both for leeward and windward side and 3) the angle of vanishing stability to leeward $\varphi_{VW,+}$ and windward side $\varphi_{VW,-}$ due to static heeling lever $l_{wind,tot}$;

3. Calculate the residual area under the $\overline{GZ}$ curve from the static heel angle φ_s to the failure angle at leeward side $\varphi_{fail,+}$ and area under the $\overline{GZ}$ curve from the failure angle at windward side $\varphi_{fail,-}$ to the static heel angle φ_s;

4. Calculate the virtual capsize angles $\varphi_{cap,EA+}$ and $\varphi_{cap,EA-}$, such that the residual areas obtained by the previous step have the same area as the corresponding areas under the linearised residual righting areas defined by the residual metacentric height $\overline{GM}_{res}$.
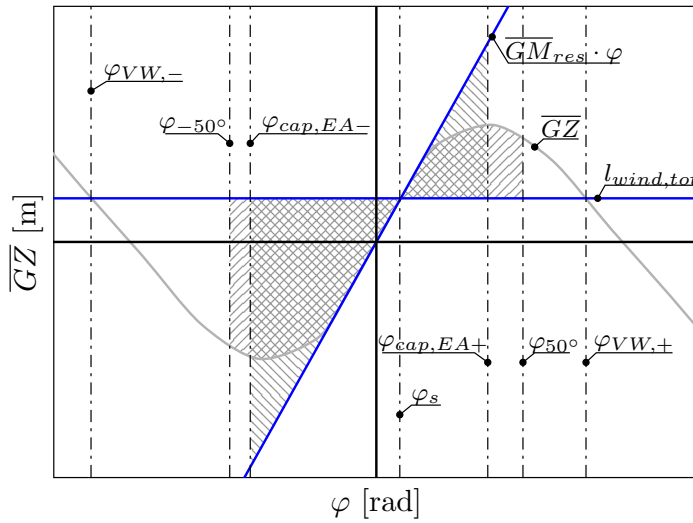

Figure 4.1: Graphical representation of the characteristic angles.

Mathematically, the described steps can be obtained as:

$$\varphi_{cap,EA+} = \varphi_s + \sqrt{\frac{2}{\overline{GM}_{res}(\varphi_s)} \cdot \int_{\varphi_{crit,+}}^{\varphi_s} \overline{GZ}_{res}(\xi)\,\mathrm{d}\xi}$$

$$\varphi_{cap,EA-} = \varphi_s - \sqrt{\frac{-2}{\overline{GM}_{res}(\varphi_s)} \cdot \int_{\varphi_s}^{\varphi_{crit,-}} \overline{GZ}_{res}(\xi)\,\mathrm{d}\xi} \tag{4.20}$$

where

$$\overline{GZ}_{res}(\xi) = \overline{GZ}(\varphi) - l_{wind,tot}$$

Table 4.1: The SGISC standard scatter table.

T_z \ H_S	3.5	4.5	5.5	6.5	7.5	8.5	9.5	10.5	11.5	12.5	13.5	14.5	15.5	16.5	17.5	18.5
0.5	1.3	133.7	865.6	1186.0	634.2	186.3	36.9	5.6	0.7	0.1	0	0	0	0	0	0
1.5	0	29.3	986.0	4976.0	7738.0	5569.7	2375.7	703.5	160.7	30.5	5.1	0.8	0.1	0	0	0
2.5	0	2.2	197.5	2158.8	6230.0	7449.5	4860.4	2066.0	644.5	160.2	33.7	6.3	1.1	0.2	0	0
3.5	0	0.2	34.9	695.5	3226.5	5675.0	5099.1	2838.0	1114.1	337.7	84.3	18.2	3.5	0.6	0.1	0
4.5	0	0	6.0	196.1	1354.3	3288.5	3857.5	2685.5	1275.2	455.1	130.9	31.9	6.9	1.3	0.2	0
5.5	0	0	1.0	51.0	498.4	1602.9	2372.7	2008.3	1126.0	463.6	150.9	41.0	9.7	2.1	0.4	0.1
6.5	0	0	0.2	12.6	167.0	690.3	1257.9	1268.6	825.9	386.8	140.8	42.2	10.9	2.5	0.5	0.1
7.5	0	0	0	3.0	52.1	270.1	594.4	703.2	524.9	276.7	111.7	36.7	10.2	2.5	0.6	0.1
8.5	0	0	0	0.7	15.4	97.9	255.9	350.6	296.9	174.6	77.6	27.7	8.4	2.2	0.5	0.1
9.5	0	0	0	0.2	4.3	33.2	101.9	159.9	152.2	99.2	48.3	18.7	6.1	1.7	0.4	0.1
10.5	0	0	0	0	1.2	10.7	37.9	67.5	71.7	51.5	27.3	11.4	4.0	1.2	0.3	0.1
11.5	0	0	0	0	0.3	3.3	13.3	26.6	31.4	24.7	14.2	6.4	2.4	0.7	0.2	0.1
12.5	0	0	0	0	0.1	1.0	4.4	9.9	12.8	11.0	6.8	3.3	1.3	0.4	0.1	0
13.5	0	0	0	0	0	0.3	1.4	3.5	5.0	4.6	3.1	1.6	0.7	0.2	0.1	0
14.5	0	0	0	0	0	0.1	0.4	1.2	1.8	1.8	1.3	0.7	0.3	0.1	0	0
15.5	0	0	0	0	0	0	0.1	0.4	0.6	0.7	0.5	0.3	0.1	0.1	0	0
16.5	0	0	0	0	0	0	0	0.1	0.2	0.2	0.2	0.1	0.1	0	0	0

Significant wave height H_S (class midpoint values)

Zero-upcrossing wave period T_z (class midpoint values)

4.2.3 Long-term stability failure index

The failure indices, both shot-term $C_{DSC,s}$ and long-term C_{DSC}, are dependant on the choice of the environmental conditions. Within the Second Generation Intact Stability Criteria the so-called standard environmental conditions are adopted. The long-term characterisation corresponds to the North Atlantic (given in the form of a scatter table in Table 4.1), while the Bretschneider spectrum is adopted to describe the short-term characterisation, as explained before. The SGISC is designed to assesses the ship stability for unrestricted operations. Therefore, the standard long-term environmental conditions are selected, as it represents the worst-case scenario. The long-term stability failure index is calculated as:

$$C_{DSC} = \sum_{i=1}^{n} C_{DSC,s,i} \cdot W_i \tag{4.21}$$

where $C_{DSC,s,i}$ is the i-th short-term stability failure index corresponding to the i-th sea state from the scatter table, and W_i is the weighting factor for the i-th sea state. The weighting factor for the i-th sea state is obtained when the reported number of occurrences from the scatter table for the sea state is divided by the total number of occurrences of the all sea states (e.g. for the standard scatter table the total number of occurrences is 100000).

Such results for the obtained long-term stability failure index C_{DSC} are to be compared to the acceptable safety level, i.e. the adopted long-term standard for the Dead Ship Condition Vulnerability Level 2. In DSC development process, several different standards were considered (see, for example IMO, 2015a), but ultimately, the long-term standard $R_{DS0} = 0.06$ was adopted. It seems that an important factor in the decision process was the matter of consistency between the Vulnerability Level 1 and the Vulnerability Level 2 results, and the adopted standard served as a counterbalance (see IMO, 2015b; Umeda & Francescutto, 2016). Nevertheless, a ship is considered not to be vulnerable to the Dead Ship Condition stability failure mode if:

$$C_{DSC} \leq R_{DS0} \tag{4.22}$$

4.3 Excessive Acceleration - Vulnerability Level 2

Excessive Acceleration Vulnerability Level 2 is governed by one-degree-of-freedom mathematical model. Statistical parameters of roll motion are obtained by solving the differential equation of roll, where excitation, unlike the DSC, is described only by irregular waves. Therefore, the roll motion is described by the following model:

$$(M_{44} + A_{44}) \ddot{\varphi} + M_{damp}(\dot{\varphi}) + M_{rest}(\varphi) = M_{wave}(t) \tag{4.23}$$

In order to have similar notation as the EA procedure, Equation (4.23) will be written in the following (linearised) form:

$$Q_{44}\ddot{\varphi} + B_{44}\dot{\varphi} + C_{44}\varphi = M_{wave} \tag{4.24}$$

where $Q_{44} = M_{44} + A_{44}$ is the sum of the roll mass moment of inertia M_{44} and the added roll mass moment of inertia A_{44}, B_{44} is the linear roll damping coefficient, $C_{44} = \Delta \cdot \overline{GM}$ is the restoring force coefficient and M_{wave} is the excitation moment due to waves only in the absence of the wind modelling. The procedure, as defined in the SGISC (see, for example IMO, 2016e, 2019a), will be presented in this Section.

4.3.1   Short-term roll motion statistics

If the solution of Equation (4.24) is assumed in a complex form as $\varphi = \varphi_a e^{i\omega_e t}$ where ω_e is the encounter wave frequency, and the wave roll moment comprises the Froude-Krylov component only, written as $M_{FK} = (a + bi)e^{i\omega_e t}$ where a and b are the real and imaginary parts of the complex excitation roll moment, then the solution for the roll amplitude φ_a can be found as:

$$\varphi_a(\omega) = \sqrt{\varphi_r^2 + \varphi_i^2}$$

with

$$\varphi_r = \frac{a\left(C_{44} - Q_{44}\omega_e^2\right) + bB_{44}\omega_e}{\left(C_{44} - Q_{44}\omega_e^2\right)^2 + \left(B_{44}\omega_e\right)}$$

$$\varphi_i = \frac{b\left(C_{44} - Q_{44}\omega_e^2\right) - aB_{44}\omega_e}{\left(C_{44} - Q_{44}\omega_e^2\right)^2 + \left(B_{44}\omega_e\right)}$$

(4.25)

where φ_r and φ_i are real and imaginary part of the complex roll amplitude, respectively. Estimation of the linear damping coefficient B_{44} regarding the Excessive Acceleration criterion, should be carried out using the same method given in Section 4.4.1, and using the following relation:

$$B_{44} = 2 \cdot \mu_e(\sigma_{\dot{x}}) \cdot Q_{44}$$

(4.26)

where $\sigma_{\dot{x}}$ is the standard deviation of roll angular velocity. If lateral symmetry of the ship hull is presumed, the excitation roll moment is simplified, with:

$$a = 0$$
$$b = r(\omega)\Delta \cdot \overline{GM}k_w$$

(4.27)

where $k_w = \omega^2/g$ is the wave number, and $r(\omega)$ is the effective wave slope coefficient given in Section 4.4.2. If the position where crew or passengers may be present is at distance h from the assumed roll axis, the transfer function of lateral acceleration $a_y^*(\omega)$ is then obtained, using the following equation, which is designed in order to take into account coupling with other motions:

$$a_y^*(\omega) = K_L\left(g\sin\varphi_a + h\omega^2\varphi_a\right)$$

(4.28)

Within the procedure, it is approximated that the roll axis is positioned at the mid height between the centre of gravity and the waterline. The factor K_L is defined as the semi-empirical non-dimensional factor taking into account vertical accelerations and yaw motion and depending on the longitudinal position of the considered location. The factor is taken form the former Germanischer Lloyd classification rules, as explained by Shigunov et al. (2011). It is to be obtained using the following expression:

$$K_L = \begin{cases} 1.125 - 0.625x/L, & \text{if } x < 0.2L \\ 1.0, & \text{if } 0.2L \le x \le 0.65L \\ 0.527 + 0.727x/L, & \text{if } x > 0.65L \end{cases}$$

(4.29)

where L is the ship length and x is longitudinal distance of the location where passengers or crew may be present from the aft end of L.

The first moment of lateral acceleration spectrum m_0 is foreseen to be calculated as:

$$m_0 = 0.75 \int_{\omega_{min}}^{\omega_{max}} \left| a_y^*(\omega) \right|^2 \cdot S_{ZZ}(\omega) \, \mathrm{d}\omega \tag{4.30}$$

where $S_{ZZ}(\omega)$ is the sea elevation spectrum, as defined in Equation (4.5), and the multiplier of 0.75 is the simplification that takes into account the influence of short-crestedness of incident waves. As it was mentioned earlier, wind is omitted from the criterion, due to the assumption that Excessive Acceleration occurs when $\overline{GM}$ values are high, which corresponds to the roll RAO peak at higher frequencies, while wind spectrum is expected at lower frequencies. Because of the same presumption, the range of frequencies is proposed (see, for example IMO, 2016e, 2019a) to be $\omega_{min} = \max\{0.5/T_\varphi; 0.2\}$, $\omega_{max} = \min\{25/T_\varphi; 2.0\}$, while the frequency step is proposed not to be larger than $(\omega_{max} - \omega_{min})/100$. However, for the purpose of the thesis, the range of frequencies from ω_{min} to ω_{max} is discretised with 10001 frequencies.

4.3.2 Short-term stability failure index

The short-term stability failure indices due to the Excessive Acceleration are calculated as:

$$C_{EA,s} = \exp\left(-\frac{R_2^2}{2\sigma_{ay}^2} \right) \tag{4.31}$$

where $R_2 = 9.81\,\mathrm{m/s^2}$ is the threshold, i.e. the limiting acceptable value of lateral acceleration. The value was adopted from the accident of the ship Chicago Express, during which the maximal attained lateral acceleration in the wheelhouse was $1g$ (see BSU, 2009). Furthermore, σ_{ay} is the standard deviation of the lateral acceleration, calculated as:

$$\sigma_{ay} = \sqrt{m_0} \tag{4.32}$$

4.3.3 Long-term stability failure index

For the Excessive Acceleration the standard environmental conditions are assumed, the same as for the Dead Ship Condition. This means that, for the purpose of the long-term environmental conditions definition, scatter table corresponding to the North Atlantic is adopted (see Table 4.1). The long-term stability failure index C_{EA} is calculated as the weighted average of short-term stability failure indices $C_{EA,s}$ defined in Equation (4.31), as:

$$C_{EA} = \sum_{i=1}^{n} C_{EA,s,i} \cdot W_i \tag{4.33}$$

where W_i is the weighting factor for the i-th sea state, as already defined in the Section 4.2.3.

Several values for the Vulnerability Level 2 long-term standard were discussed within IMO. The value which was proposed early in the process of the criterion development was based on the accident of Chicago Express, for which the calculated failure index, corresponding to the loading condition of the ship in time of the accident as $R_{EA2} = 0.0001094$, was suggested as the standard (as explained in IMO, 2016a,e). However, according to the last session of the SDC meeting (see IMO, 2019a) the standard for the Excessive Acceleration Vulnerability Level 2 criterion as $R_{EA2} = 0.00039$ has been adopted. Therefore, in order for the ship to comply with the criterion, the long-term failure index C_{EA} should be lower or equal than the long-term standard R_{EA2}:

$$C_{EA} \le R_{EA2} \tag{4.34}$$

4.4 Some methods adopted by IMO used at Vulnerability Level 2

4.4.1 Roll damping estimation method adopted by IMO

Within the SGISC, the roll damping should be estimated by means of the Simplified Ikeda's method, in the absence of either experimental data or a more suitable method. It is developed by Kawahara et al. (2009), based on well-known Ikeda's method (see Himeno, 1981). The method itself will not be described in detail, due to its extensiveness, and because thorough procedure is readily available (see Kawahara et al., 2009). Nevertheless, the possibility of implementation of the Simplified Ikeda's method to river-sea ships is examined in Chapter 6 of the thesis, where additional properties of the method will be mentioned. At first glance, shortcomings of the Simplified Ikeda's method implementation to river-sea ships can be the somewhat limited applicability range and the fact that the method was not developed for hull forms with geometric properties typical for river-sea ships. Nevertheless, if applicability range is exceeded the appropriate limiting value of the method should be adopted.

The outcome of the Simplified Ikeda's method is the equivalent linear roll damping coefficient as a function of roll amplitude $B_{44}(\varphi_a)$, composing of friction B_F, wave making B_W, eddy making B_E and bilge keel B_{BK} damping components (as given by Kawahara et al., 2009). In accordance with Dead Ship Condition and Excessive Acceleration scenarios, a ship is assumed to have zero forward speed (IMO, 2019a), therefore the lift damping component B_L is not considered. After the equivalent linear roll damping coefficient as a function of roll amplitude $B_{44}(\varphi_a)$ is estimated, the results are fitted in order to obtain the roll damping coefficients μ, β and δ in the following form:

$$\frac{B_{44}(\varphi_a)\omega_\varphi^2}{2\Delta \cdot \overline{GM}} \rightarrow \mu + \beta\frac{4}{4\pi}\omega_\varphi\varphi_a + \delta\frac{3}{8}\omega_\varphi^2\varphi_a^2 \tag{4.35}$$

Which is graphically shown in Figure 4.2, where the procedure defined by Equation (4.35) is applied on the three test vessels (presented in Section 1.2.1).

This gives the possibility to estimate roll velocity dependant linear damping coefficient, provided that the standard deviation of roll angular velocity $\sigma_{\dot{x}}$ is known. Moreover, $\sigma_{\dot{x}}$ can be calculated from the appropriate spectrum of roll motion as:

$$\sigma_{\dot{x}} = \sqrt{\int_0^\infty \omega^2 S_x(\omega)\,\mathrm{d}\omega} \tag{4.36}$$

where $S_x(\omega)$ is the spectrum of absolute roll angle:

$$S_x(\omega) = H^2(\omega) \cdot S_m(\omega) = H^2(\omega) \cdot \frac{S_M(\omega)}{(\Delta \cdot \overline{GM})^2}$$

with

$$S_M(\omega) = S_{M,wave}(\omega) + S_{\delta M_{wind,tot}}(\omega)$$
$$S_{M,wave}(\omega) = (\Delta \cdot \overline{GM})^2 \cdot S_{\alpha\alpha,c}(\omega)$$

$$\tag{4.37}$$

An issue arises because a corresponding value for the roll standard deviation of roll velocity is needed in order to use the adequate equivalent linear roll damping coefficient, however, the one cannot be obtained unless the Equation (4.2) is solved, for which damping has to be known (as a component of the roll transfer function). Therefore, the following iterative procedure (given in IMO, 2013) may be used:
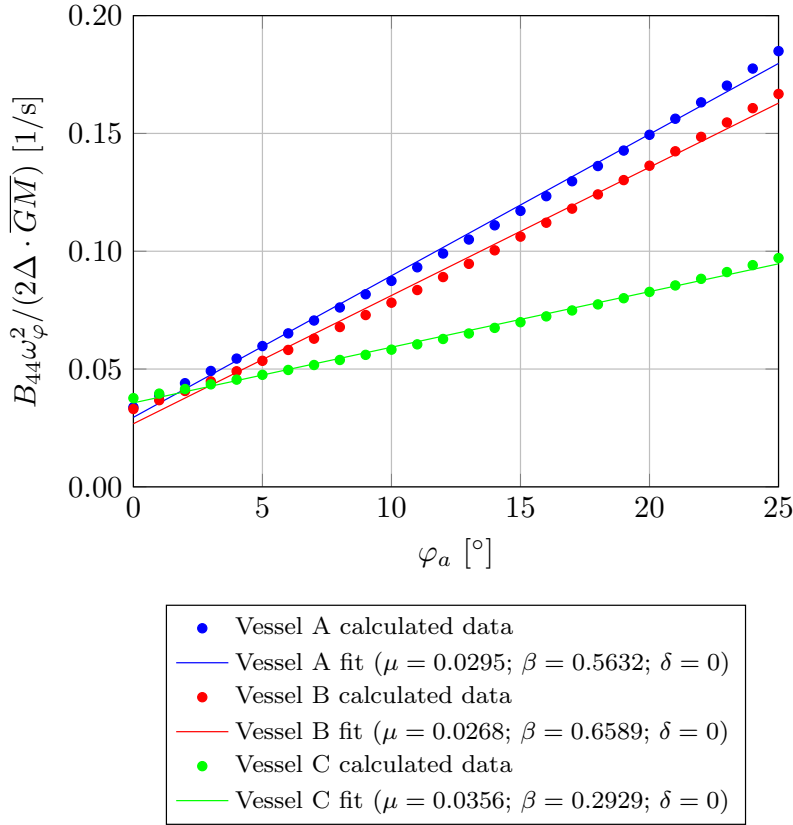
Figure 4.2: Example of damping coefficients fit. For all vessels $\overline{OG}/T = 0$ is used and presence of the bilge keels is assumed (according to Table 4.2)

1. For a given ship, loading condition and short-term environmental conditions an initial guess for the standard deviation of roll angular velocity $\sigma_{\dot{x},j}$ is made. As the iteration is expected to converge rather fast, it is sufficient and acceptable to assume $\sigma_{\dot{x},j} = 0 \, \mathrm{rad/s}$ for the first iteration (see IMO, 2013);

2. The equivalent linear roll damping coefficient $\mu_e(\sigma_{\dot{x}})$ is estimated using the following equation:

$$\mu_e(\sigma_{\dot{x}}) = \mu + \beta\sqrt{\frac{2}{\pi}}\sigma_{\dot{x}} + \delta\frac{3}{2}\sigma_{\dot{x}}^2 \tag{4.38}$$

3. With the $\mu_e(\sigma_{\dot{x},j})$ known, the absolute roll angle spectrum $S_x(\omega)$ can be calculated using the Equation (4.37);

4. After the differential equation of roll motion is solved, it is possible to obtain the new standard deviation of roll angular velocity $\sigma_{\dot{x},j+1}$ according to the Equation (4.36), with an improved precision;

5. The two standard deviation of roll angular velocity: $\sigma_{\dot{x},j}$ and $\sigma_{\dot{x},j+1}$ are now compared, and if the absolute difference between the two is larger than some prescribed tolerance (in this thesis the tolerance $|\sigma_{\dot{x},j} - \sigma_{\dot{x},j+1}| \leq 0.00001$ is set), the value $\sigma_{\dot{x},j+1}$ is assigned to $\sigma_{\dot{x},j}$ and the loop is continued back from the step 2. However, if the tolerance is reached, the loop is stopped and the value of $\sigma_{\dot{x},j+1}$ is assigned to the standard deviation of roll angular velocity $\sigma_{\dot{x}}$;
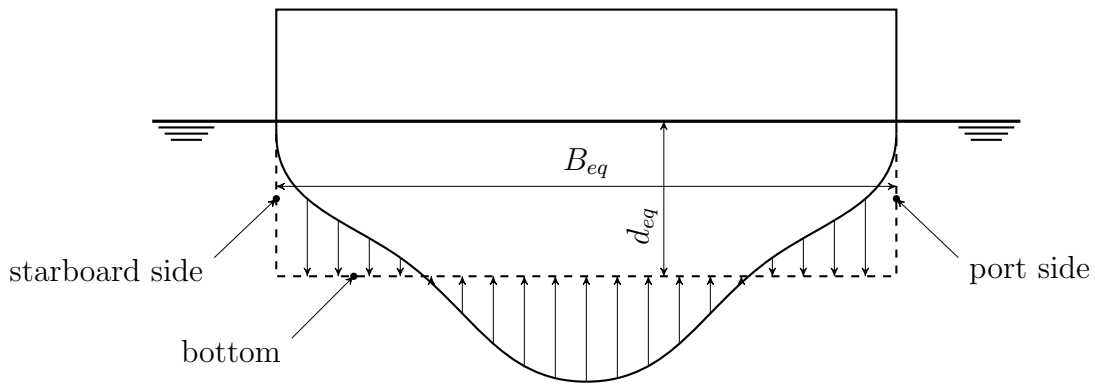
Figure 4.3: Example of section transformation - IMO methodology.

6. The final value for the equivalent linear roll damping coefficient $\mu_e(\sigma_{\dot{x}})$ can be estimated, according to Equation (4.38).

The range of roll amplitudes should be as large as possible (see IMO, 2013), so that future extrapolations of the fitted polynomial defined in Equation (4.35) could be avoided. In this thesis, the used range is from $0°$ to $25°$, with a step of $1°$, where the actual value for $0°$ is replaced with an approximation (i.e. $0 \approx 1 \cdot 10^{-16}$), in order to avoid a numerical problem. Furthermore, it was assumed that cubic damping coefficient δ is negligible, and only linear μ and quadratic β roll damping coefficients are used.

4.4.2 Effective wave slope coefficient estimation method adopted by IMO

Within the Second Generation Intact Stability Criteria, the so-called standard method (IMO method) was proposed (see, for example IMO, 2013). The principle of the method is to transform each cross-section of the ship hull into a rectangular shape, keeping dimensions of a section as same as possible (as shown in Figure 4.3), and afterwards estimating the sectional Froude-Krylov roll moments. This transformation provides analytical solution for the sectional wave moment, and total wave moment is obtained by integration over the ship length. The total roll moment is an intermediate step in effective wave slope coefficient estimation.

The IMO method is based on the following assumptions and approximations (the corresponding algorithm is shown in Figure 4.4):

1. The underwater part of each transverse section of the ship is substituted by the "equivalent underwater section" having, in general, the same breadth at the waterline and the same underwater area of the original section, however:

   (a) sections heaving zero breadth at the waterline, such as those in the region of the bulbous bow, are neglected;

   (b) the draught of the "equivalent underwater section" is limited to the ship sectional draught;

2. The effective wave slope coefficient for each wave frequency is determined by using the "equivalent underwater sections" considering only the undisturbed linear wave pressure.

3. For each section, a formula is applied which is the exact analytical solution for the rectangle.

$$A(x) > 0 \wedge B(x) > 0$$

no / yes

$$A_{eq}(x) = 0$$
$$B_{eq}(x) = 0$$
$$T_{eq}(x) = 0$$

$$A(x)/B(x) \le T(x)$$

no / yes

$$T_{eq}(x) = T(x)$$
$$B_{eq}(x) = B(x)$$
$$A_{eq}(x) = B_{eq}(x)T_{eq}(x)$$

$$A_{eq}(x) = A(x)$$
$$B_{eq}(x) = B(x)$$
$$T_{eq}(x) = A_{eq}(x)/B_{eq}(x)$$
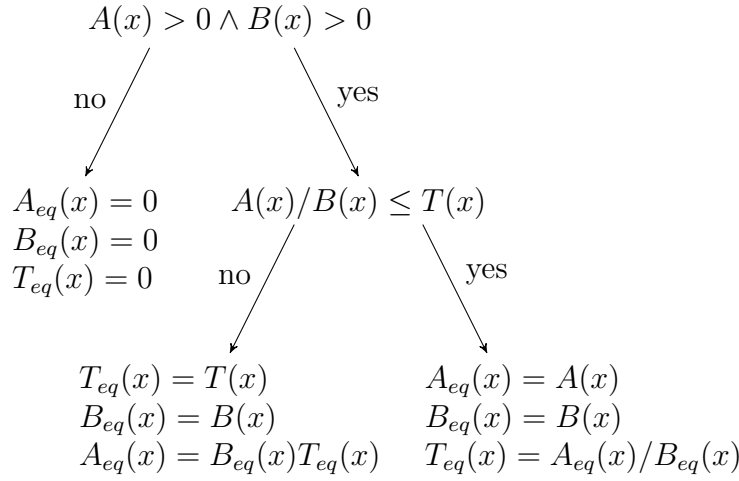
Figure 4.4: Section transformation algorithm - IMO methodology.

Due to the changes in the sections shape, vessel particulars can also be changed, therefore particulars of the "equivalent vessel" should be determined as:

$$
\begin{aligned}
V_{eq} &= \int_L A_{eq}(x)dx \\
\overline{BM}_{eq} &= \frac{1}{V_{eq}} \int_L \frac{1}{12} B_{eq}{}^3(x)dx \\
\overline{KB}_{eq} &= T + \frac{1}{V_{eq}} \int_L \frac{-T_{eq}(x)}{2} A_{eq}(x)dx \\
\overline{KG}_{eq} &= \overline{KB}_{eq} + \overline{BM}_{eq} - \overline{GM} \\
\overline{OG}_{eq} &= \overline{KG}_{eq} - T
\end{aligned}
\tag{4.39}
$$

The standard method for effective wave slope coefficient estimation is as follows:

$$
r(\omega) = \left| \frac{\int_L C(x)dx}{V_{eq}\overline{GM}} \right|
$$

where

$$
C(x) = \begin{cases} 0, & \text{if } A_{eq}(x) = 0 \text{ and } B_{eq}(x) = 0 \\ A_{eq}(x)\left[K_1(x) + K_2(x) + F_1(x)\overline{OG}_{eq}\right], & \text{otherwise} \end{cases}
$$

and where

$$
K_1(x) = \frac{\sin\left(k_w \dfrac{B_{eq}(x)}{2}\right)}{\left(\dfrac{k_w B_{eq}(x)}{2}\right)} \cdot \frac{\left(1 + k_w T_{eq}(x)\right)e^{-k_w T_{eq}(x)} - 1}{k_w{}^2 T_{eq}}
\tag{4.40}
$$

$$
K_2(x) = -\frac{e^{-k_w T_{eq}(x)}}{k_w{}^2 T_{eq}(x)} \cdot \left[\cos\left(k_w \frac{B_{eq}(x)}{2}\right) - \frac{\sin\left(k_w \dfrac{B_{eq}(x)}{2}\right)}{\left(\dfrac{k_w B_{eq}(x)}{2}\right)}\right]
$$

$$
F_1(x) = -\frac{1 - e^{-k_w T_{eq}(x)}}{k_w{}^2 T_{eq}(x)} \cdot \frac{\sin\left(k_w \dfrac{B_{eq}(x)}{2}\right)}{\left(\dfrac{k_w B_{eq}(x)}{2}\right)}
$$

For the purpose of the thesis, and in order to estimate Frude-Krylov roll moment based on the IMO methodology, hulls of river-sea ships are described with 21 equidistant cross-section, and numerical integration is performed by means of Simpson's I rule. The number of cross-sections used is proved to be sufficient for accurate results in case of inland vessels and river-sea ships.

IMO methodology is a simple method to use, and it is the exact analytical solution of dynamic pressure integration over the wetted surface for rectangular section shaped hull, in order to obtain Froude-Krylov roll moment. Drawback of this method is that standard hull sections are in general never rectangular, not even those corresponding to midship part of a hull. Therefore, simple algorithm of transforming sections into rectangles is introduced within IMO methodology, trying to keep sectional breadth the same, as well as the area of the section, whenever it was possible. It means that a point on the hull $P(x, y, z)$ would have to change only z coordinate in order to fulfill this task (see Figure 4.3, indicated by the arrows). Nevertheless, in case that sectional area $A(x)$ divided by the sectional breadth $B(x)$ is larger than its draught $T(x)$, transformation procedure suggests to keep both breadth and draught the same, and to change sectional area (see Figure 4.4). Therefore, differences in ship particulars can be introduced, and thus particulars have to be recalculated, using the Equation (4.39). Considering aforementioned, and the fact that global result of roll moment is obtained by integration over the ship length, IMO methodology should have better results for full hull forms, heaving high vertical prismatic coefficient C_{VP} (which accounts for fullness of sections), and high prismatic coefficient C_P (which accounts for hull slenderness). Since river-sea ships tend to have full hull forms (e.g. $C_B \approx 0.9$ and $C_{VP} \approx 0.85$), good results of Froude-Krylov force may be expected for this vessel type.

4.5 Dead Ship Condition - Vulnerability Level 1

The Dead Ship Condition Vulnerability Level 1 criterion is the Severe wind and rolling criterion (Weather Criterion) as given in Part A/2.3 of the IS Code (IMO, 2008a), with an extension of the wave steepness factor s. However, the application of the Weather Criterion (without any modification) to river-sea ships seems to be questionable. This is mostly due to severe environmental conditions foreseen, that are not expected in coastal areas, but also due to semi-empirical expressions that estimate some of important parameters, such as the effective wave slope, the roll damping, the natural roll period, etc. which are tuned considering a population of sea-going ships at the time. Therefore, national regulations for river-sea ships often modify the Weather Criterion in order to take into account more realistic environmental conditions (as explained in Chapter 2). This is most practically done by reducing the wind pressure. However, according to Bačkalov (2017) it is a question how this should be done, as the original wind pressure of $P = 504\,\text{Pa}$ (corresponding to the wind speed of $v = 26\,\text{m/s}$) comes from an analysis of stability of Japanese vessels, rather than from an actual measurements of severe weather conditions. Nevertheless, such modification of the wind pressure is foreseen by the SGISC (IMO, 2019a), as well as modification of the wave steepness factor s and the angle of roll φ_1.

Moreover, in case of the Dead Ship Condition, the Vulnerability Level 1 is neither directly derived from a more advanced tier, nor there are clear mathematical connections, although both levels consider the same physical phenomenon. The Level 1 estimates the minimum acceptable metacentric height only, while the Level 2 criterion can provide both the minimum and maximum limits of metacentric heights.

Therefore, the main focus of the thesis is going to be on the Vulnerability Level 2 as it considers more realistic environmental conditions and more advanced hydrodynamics, which could be adapted to the river-sea operational conditions and design characteristics of river-sea ships. Furthermore, an effort will be me made to derive a novel simple method for stability

assessment of river-sea ships which would be suitable for use at Vulnerability Level 1. Instead of modifying the Weather Criterion, the proposed Vulnerability Level 1 is going to be based on results of stability calculations done at Vulnerability Level 2.

4.6 Excessive Acceleration - Vulnerability Level 1

The Excessive Acceleration Vulnerability Level 1 criterion was derived based on the Vulnerability Level 2 procedure (explained in Section 4.3). It is assumed that the predominant contribution to the first moment of lateral acceleration spectrum m_0 (described by Equation (4.30)) comes from the region in proximity of the natural roll frequency (IMO, 2016e). Therefore, by assuming that $\omega = \omega_\varphi$, then by introducing the wave steepness factor s (the same as in the DSC Level 1) and by reducing the estimation process of the effective wave slope coefficient and roll damping, the procedure could be significantly simplified. A procedure like this is simple to use, and is in line with the idea of multi-tiered approach within the SGISC. However, the procedure is tuned for sea-going ships and corresponding environmental conditions. In order to adapt it for this ship type, the complete derivation process should be redone, having in mind characteristics of river-sea ships and their operational and environmental conditions. Therefore, the same as concluded for the Dead Ship Condition, the focus of the thesis will be on the Vulnerability level 2.

4.7 Application of the stability criteria to river-sea ships

The Second Generation Intact Stability Criteria is generally considered to be applicable to all sea-going ship types, regardless of their design properties. This implies that the SGISC should be applicable to unconventional ships as well and, consequently, to river-sea ships too.

With the test vessels chosen and particulars defined in Table 1.2, and with Dead Ship Condition and Excessive Acceleration criteria procedure defined, it should be possible to apply the criteria to the test vessels. However, the calculations returned no results. A closer examination showed that calculations were unable to carry out convergence of the standard deviation of roll velocity, as explained in Section 4.4.1.

Interestingly, the results are possible to obtain, if it is assumed that the bilge keels are installed. The dimensions of the bilge keels are given in Table 4.2. The lengths of the considered bilge keels correspond to the maximal values foreseen by the Simplified Ikeda's method. Results for stability assessment of the vessels A, B and C with bilge keels added, are given in Figures 4.5, 4.6, 4.7, respectively, where the left subfigures, Subfigures (a) show the Dead Ship Condition failure index C_{DSC} as a function of the metacentric height $\overline{GM}$ and the right subfigures, Subfigures (b) show the Excessive Acceleration failure index C_{EA} as a function of the metacentric height $\overline{GM}$. A ship is considered as safe, from the intact stability point of view, if both of the criteria are satisfied, expressed with conditions (4.22) and (4.34). In the Figures, the red shaded areas represent corresponding unacceptable safety levels (i.e. values of the failure indices higher than the long-term standards) as given by the SGISC. The results show that all test vessels would be practically unable to operate, considering the Second Generation Intact

Table 4.2: Information regarding bilge keels of the test vessels.

	Vessel A Tanker	Vessel B Container vessel	Vessel C Container vessel
l_{BK} [m]	$0.4 L_{PP}$	$0.4 L_{PP}$	$0.4 L_{PP}$
b_{BK} [m]	0.22	0.175	0.15

Stability Criteria requirements. Only the test vessel A, as seen in Figure 4.5, has a narrow range of acceptable metacentric heights, corresponding approximately to $\overline{GM} = 0.1\,\mathrm{m} \div 0.4\,\mathrm{m}$, which is unattainable by this ship.


(a) DSC failure index as a function of $\overline{GM}$.

(b) EA failure index as a function of $\overline{GM}$.
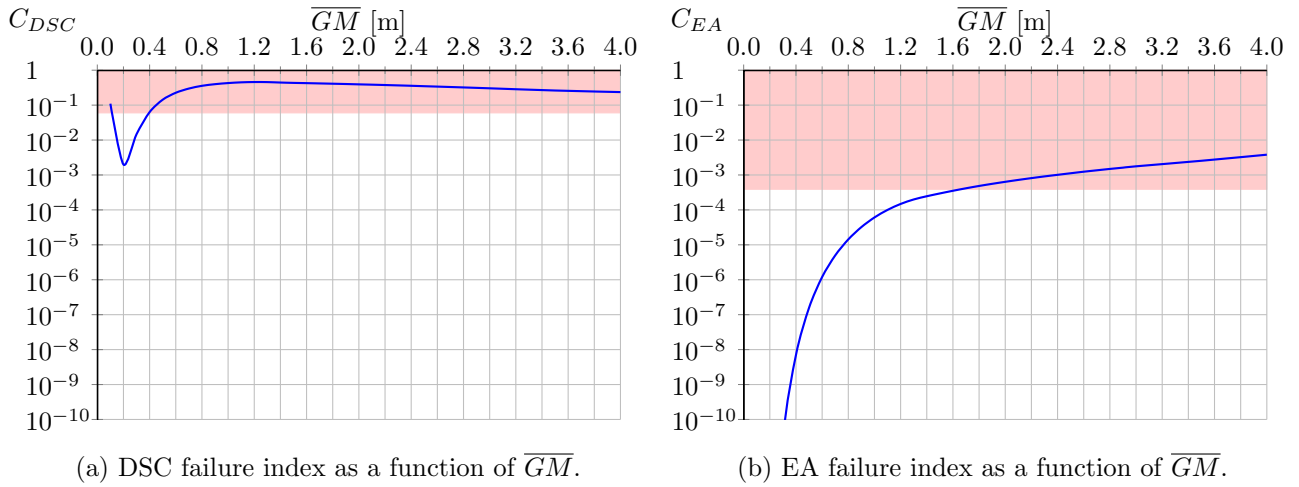
Figure 4.5: Stability assessment - vessel A with bilge keels. The SGISC unmodified procedure.

(a) DSC failure index as a function of $\overline{GM}$.

(b) EA failure index as a function of $\overline{GM}$.
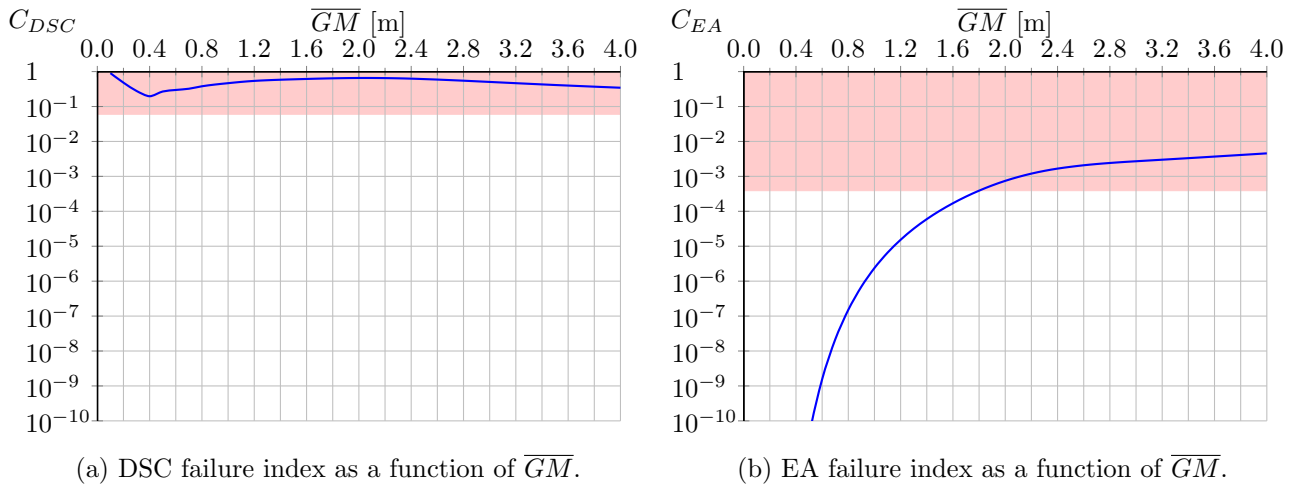
Figure 4.6: Stability assessment - vessel B with bilge keels. The SGISC unmodified procedure.

(a) DSC failure index as a function of $\overline{GM}$.

(b) EA failure index as a function of $\overline{GM}$.
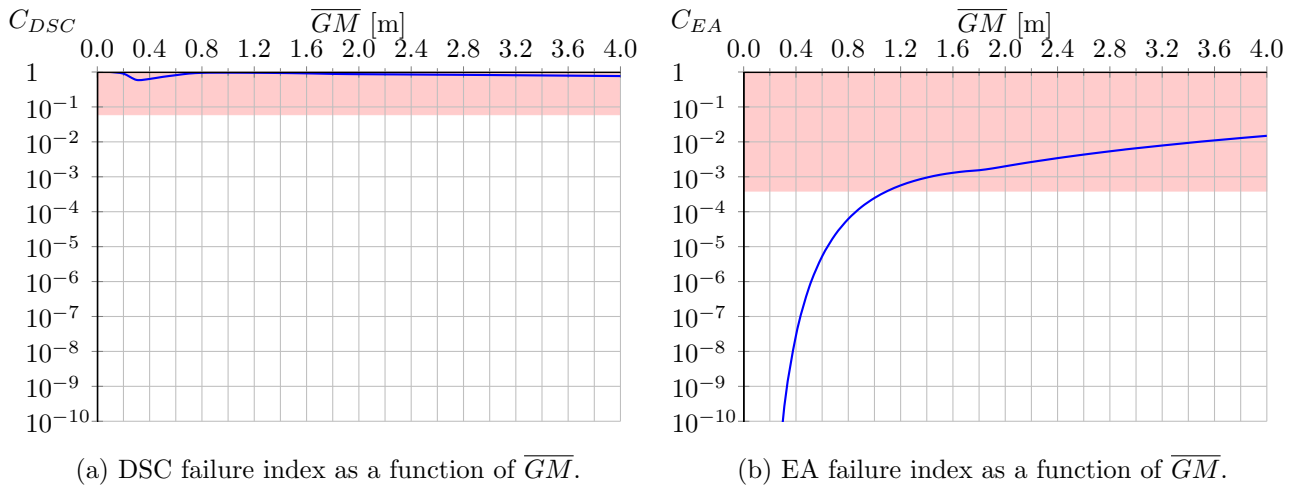
Figure 4.7: Stability assessment - vessel C with bilge keels. The SGISC unmodified procedure.

4.8 Conclusions

The Second Generation Intact Stability Criteria makes use of advanced hydrodynamic models, which should be applicable regardless of hull geometry and ship type, in order to assess the stability under various modes of stability failure. Therefore, it is reasonable to assume that the same procedures may be applied to river-sea ships. This thesis is focused on two modes of stability failure - Dead Ship Condition and Excessive Acceleration, as river-sea ships are found not to be vulnerable to other modes, due to the combination of full hull shapes and low service speeds. Vulnerability Level 2 was identified as the most appropriate tier to be applied on river-sea ships, due to a favourable combination of accuracy of representation of physical phenomena and a relative simplicity of application, and thus is thoroughly examined. Finally, Level 2 of DSC and EA criteria were applied to three river-sea ships, designated as the test vessels.

In IMO (2019b), non-conventional ships are defined as ships that are vulnerable to stability failures and which are neither explicitly nor properly covered by the existing stability regulations. However, it seems that the two described procedures are unsuitable for application to river-sea ships, which designate these vessels as non-conventional ships by the IMO definition. It was noticed that, under certain conditions, it was unable to obtain the failure indices, due to ineffectual convergence of standard deviation of roll angular velocity (as explained in Section 4.4.1). It was concluded that damping plays an important role in determining whether results are possible to be obtain or not, and if the presence of the bilge keels is assumed, which results in higher damping estimated, calculations were possible to carry out, as shown in Figures 4.5, 4.6, 4.7. Therefore, the Simplified Ikeda's method will be more closely examined in one of the following chapters. It should be noted that whenever particulars of a river-sea ship are outside of the range of the Simplified Ikeda's method applicability, the limiting value was used, thus excluding the potential source of error. Therefore, in order to successfully apply the Second Generation Intact Stability Criteria to river-sea ships it is of paramount importance that damping estimation suitable to river-sea ships is adopted. However, the test vessels are unable to operate even with the bilge keels instaled, due to high values of failure indices. Therefore, another important aspect in stability assessment of river-sea ships is to consider an appropriate environmental conditions. Namely, river-sea ships are not designed to operate in an extreme environment, such as North Atlantic (the environmental conditions considered as the standard within SGISC). Therefore, the next chapter will examine the possibility to adapt the environmental conditions more suitable to river-sea operations.

Chapter 5

Consideration of appropriate environmental conditions

5.1 Introduction

River-sea ships are intended for inland navigation and short coastal voyages. This characteristic should be reflected in stability assessment of these ships. Failing to do so, will result in underestimated stability and reduced operability.

On the other hand, the Second Generation Intact Stability Criteria have foreseen the possibility to substitute the environmental conditions, "to the satisfaction of administration" (see IMO, 2019a). Furthermore, modification of the standard environmental conditions (as defined in Section 4.2) is regarded as the operational limitation in IMO (2019a), as it permits operations in a specific area only, to which that particular environmental conditions correspond to. Although the modification of the environmental conditions is straightforward, provided the new environmental conditions are given, to the best of the author's knowledge there are no studies showing such implementation.

In this Chapter, a principle of adopting new environmental conditions is shown. As an example for the purpose of the thesis, a new scatter table is chosen. It is followed by the change of the wave spectrum, and the introduction of a new wind-wave relation. Finally, the influence of the new environmental condition on the DSC and EA failure indices is analysed. However, it should be noted that such long-term environmental conditions, as well as the wind-wave relation, are location-specific and most certainly they are inapplicable to other regions.

The present Chapter is a result of a study already published by Rudaković & Bačkalov (2019).

5.2 Adopting new wind and wave climate

The SGISC define the "standard" or "reference environmental conditions" that ought to be applied in stability assessment, but make provisions for using "alternative environmental conditions", that is, other data that are deemed to be more appropriate in the case of restricted navigation or operational limitations (see IMO, 2016c, 2018a, 2019b). For the purposes of the present analysis, the use was made of the available wind and wave measurements in the Belgian coastal zone (see Chatelier et al., 2017). The wave scatter table is given in Table 5.1. Furthermore, for the purposes of the thesis, the following relation between the mean wind speed U_w and significant wave height H_S was established, based on the measurements given by Chatelier et al. (2017):

$$U_w = 11.75 \cdot H_S^{0.375} \tag{5.1}$$

In Figure 5.1, Equation (5.1) is compared to the wind-wave relation as given in the draft vulnerability criteria of Level 2 for the Dead Ship Condition stability failure mode (see, for example IMO, 2015b). It may be noticed that the same significant wave height in the coastal zone is associated with stronger winds than in the open sea.
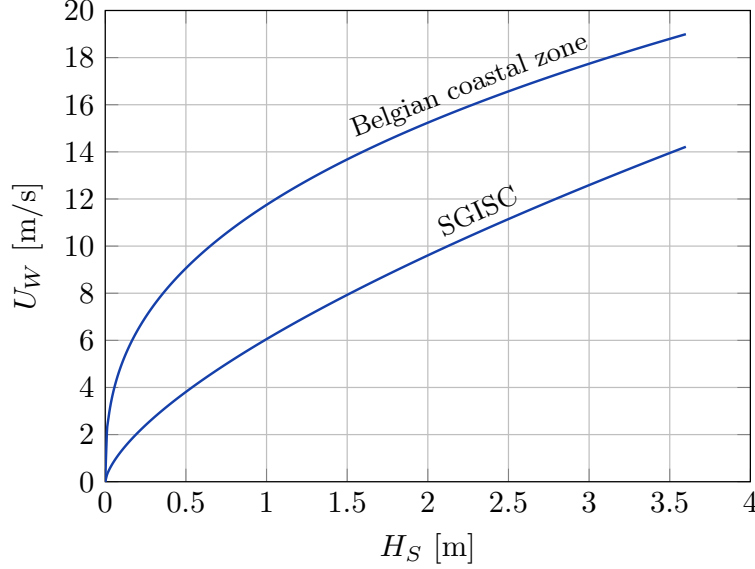

Figure 5.1: Adopted relation between mean wind speed and significant wave height in the Belgian coastal zone, and comparison with the relation used within the SGISC.

The Mean JONSWAP wave spectrum was adopted as the alternative to the standard spectrum foreseen by vulnerability criteria IMO (2015b). The use of JONSWAP spectrum has proved to be successful when addressing the North Sea coastal environment (see Verwaest et al., 2008; van Essen & Peters, 2017; Chatelier et al., 2017). Therefore, the sea elevation spectrum is to be calculated as:

$$S_{ZZ}(\omega) = A\gamma^B \cdot \frac{5}{16} \frac{H_S^2}{\omega_m} \left(\frac{\omega_m}{\omega}\right)^5 \cdot \exp\left[-\frac{5}{4}\left(\frac{\omega_m}{\omega}\right)^4\right]$$

where

$A = 0.658$

$B = \exp\left[-\frac{1}{2\sigma^2}\left(\frac{\omega}{\omega_m} - 1\right)\right]$

$\gamma = 3.3$

$\sigma = \begin{cases} 0.07, & \text{for } \omega < \omega_m \\ 0.09, & \text{for } \omega > \omega_m \end{cases}$

and where

$\omega_m = \dfrac{2\pi}{T_m}$

$$\tag{5.2}$$

where ω_m is the modal wave frequency, T_m is the modal wave period and γ is the peakedness factor.

Table 5.1: Wave scatter diagram of the Belgian coastal zone (H_S is the significant wave height, T_m is the modal wave period).

Significant wave height H_S [m] (class midpoint values are assumed)	Modal wave period T_m [s] (class midpoint values)														$\sum T_m$
	3.25	3.75	4.25	4.75	5.25	5.75	6.25	6.75	7.25	7.75	8.25	8.75	9.25	9.75	
3.6	0	0	0	0	0	0	0	0	0	0	0	0	0.01	0	0.01
3.5	0	0	0	0	0	0	0	0	0	0	0	0.03	0	0	0.03
3.4	0	0	0	0	0	0	0	0	0	0	0	0.01	0.01	0	0.02
3.3	0	0	0	0	0	0	0	0	0	0	0	0.01	0.01	0	0.02
3.2	0	0	0	0	0	0	0	0	0	0	0.01	0.03	0.01	0	0.05
3.1	0	0	0	0	0	0	0	0	0	0	0.04	0.05	0	0	0.09
3.0	0	0	0	0	0	0	0	0	0	0	0.04	0.10	0	0	0.14
2.9	0	0	0	0	0	0	0	0	0.01	0.02	0.04	0.10	0.01	0	0.18
2.8	0	0	0	0	0	0	0	0.01	0.03	0.02	0.09	0.07	0	0	0.22
2.7	0	0	0	0	0	0	0	0.03	0.01	0.07	0.09	0.03	0	0	0.23
2.6	0	0	0	0	0	0	0	0.02	0.04	0.15	0.11	0.01	0	0	0.33
2.5	0	0	0	0	0	0	0	0.07	0.10	0.08	0.07	0.01	0.01	0	0.34
2.4	0	0	0	0	0	0	0	0.07	0.07	0.21	0.10	0	0.01	0	0.46
2.3	0	0	0	0	0	0	0.04	0.06	0.14	0.18	0.07	0.02	0	0	0.51
2.2	0	0	0	0	0	0	0.04	0.05	0.15	0.12	0.02	0.01	0	0	0.39
2.1	0	0	0	0	0	0	0.10	0.12	0.17	0.14	0.01		0	0	0.54
2.0	0	0	0	0	0	0.02	0.07	0.17	0.13	0.10	0.02		0	0	0.51
1.9	0	0	0	0	0	0.03	0.26	0.22	0.20	0.07	0.01		0	0	0.79
1.8	0	0	0	0	0.01	0.13	0.33	0.33	0.27	0.09	0		0	0	1.16
1.7	0	0	0	0	0.01	0.18	0.44	0.53	0.30	0.07	0		0	0	1.53
1.6	0	0	0	0	0.01	0.42	0.70	0.63	0.22	0.01	0.01		0	0	2.00
1.5	0	0	0	0	0.11	0.58	0.79	0.57	0.14	0.01	0		0	0	2.20
1.4	0	0	0	0	0.24	0.61	0.87	0.36	0.15	0.02	0		0	0	2.25
1.3	0	0	0	0.01	0.41	0.84	1.11	0.45	0.18	0.06	0.01		0	0	3.07
1.2	0	0	0	0.07	0.93	1.38	1.16	0.42	0.16	0.05	0.04		0	0	4.21
1.1	0	0	0	0.24	1.31	1.65	1.12	0.41	0.11	0.03	0.03		0	0	4.90
1.0	0	0	0.02	0.62	1.93	1.85	0.92	0.26	0.02	0.03	0		0	0	5.65
0.9	0	0	0.08	0.98	2.53	1.72	0.72	0.15	0.09	0.01	0		0	0	6.28
0.8	0	0	0.25	1.56	3.36	1.90	0.63	0.18	0.10	0.02	0		0	0	8.00
0.7	0	0	0.60	2.29	3.42	2.12	0.55	0.33	0.18	0.04	0.01	0.01	0	0	9.54
0.6	0	0.03	1.16	2.68	3.18	1.56	0.77	0.33	0.24	0.07	0.01	0.01	0	0	10.04
0.5	0	0.27	1.32	3.36	3.10	2.03	1.15	0.80	0.32	0.10	0.01		0	0	12.46
0.4	0.01	0.35	1.45	3.13	3.76	2.21	1.31	0.65	0.3	0.04	0		0	0	13.21
0.3	0	0.05	0.85	2.02	3.30	1.35	0.75	0.27	0.04	0.02	0		0	0	8.65

5.3 Application of the stability criteria to river-sea ships considering modification of environmental conditions

Following the change in environmental conditions, the stability of the test vessels was reassessed. The results are presented in form of figures in the similar manner as in Section 4.7, and the failure indices for the test vessels A, B and C with the bilge keels are given in Figures 5.2, 5.3 and 5.4.

The results show significant reduction in the failure indices. This could have been expected as the wave climate of the North Sea is certainly milder in comparison to the navigation conditions on the North Atlantic which are implemented in the Second Generation Intact Stability Criteria. After the modification of environmental conditions, it can be seen that the acceptable range of the metacentric heights is significantly expanded, for all of the vessels. However, the failure indices for the test vessels without the bilge keels are still not possible to obtain. Such result could be somewhat unexpected, considering that the examined vessels are even formally intended for sailing in navigation zone 3 (up to $H_S = 0.6\,\text{m}$ for inland vessels sailing in inland waterways). This may signal an inadequacy of methodology used within

(a) DSC failure index as a function of $\overline{GM}$.　　　(b) EA failure index as a function of $\overline{GM}$.
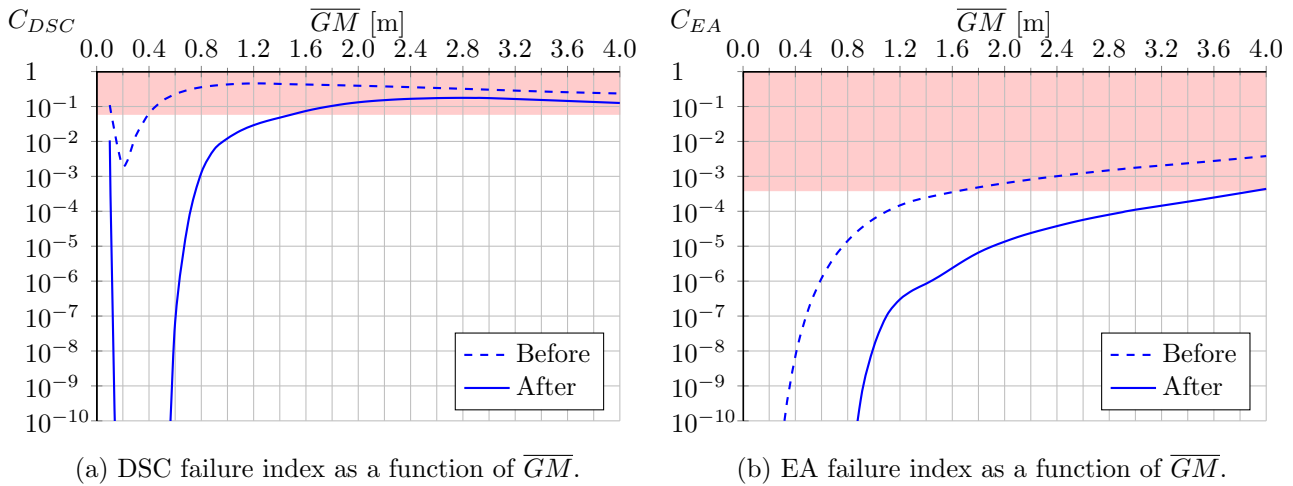
Figure 5.2: Stability assessment - vessel A with bilge keels. The results following the adoption of the new environmental conditions.

(a) DSC failure index as a function of $\overline{GM}$.　　　(b) EA failure index as a function of $\overline{GM}$.
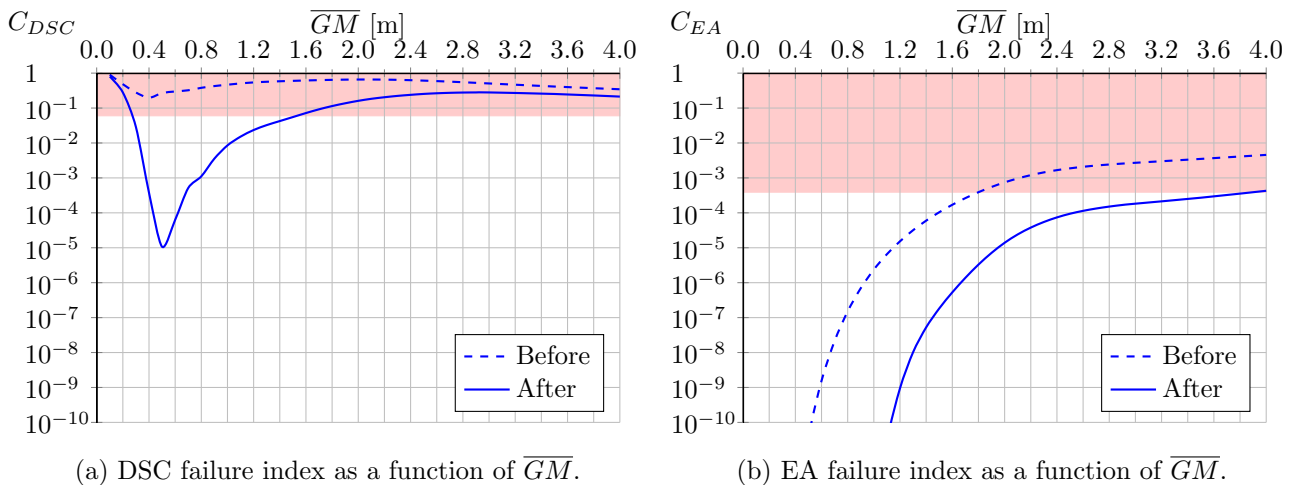
Figure 5.3: Stability assessment - vessel B with bilge keels. The results following the adoption of the new environmental conditions.

(a) DSC failure index as a function of $\overline{GM}$.

(b) EA failure index as a function of $\overline{GM}$.
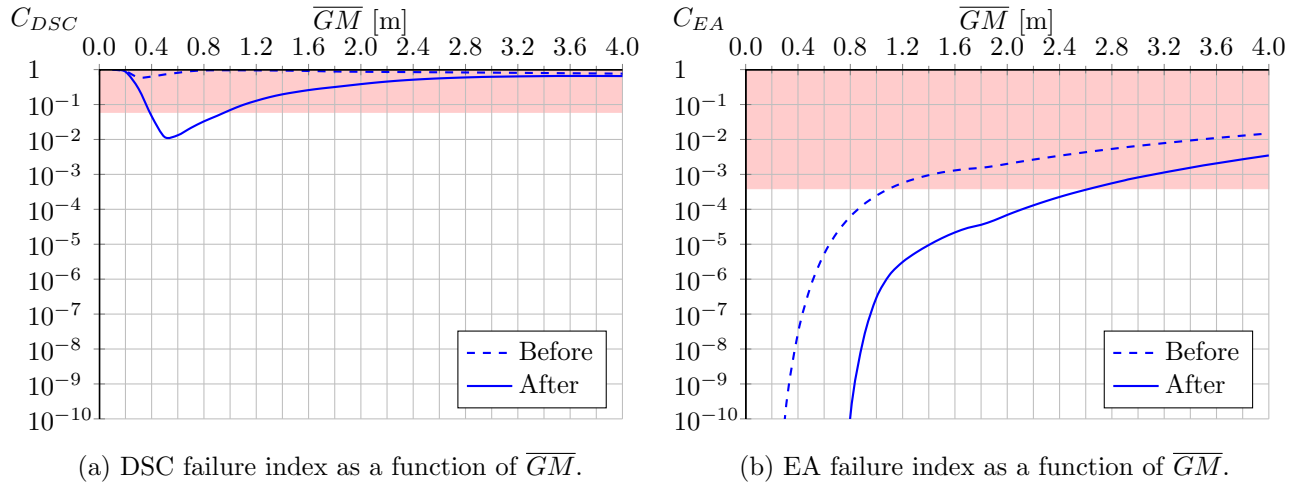
Figure 5.4: Stability assessment - vessel C with bilge keels. The results following the adoption of the new environmental conditions.

SGISC. In fact, the calculations have shown that it is impossible to obtain the proper roll damping coefficients, unless the ship has bilge keels. This raises suspicion over the applicability of the method for roll damping estimation, proposed within SGISC. Therefore, the applicability of the Simplified Ikeda's method on river-sea ships is going to be the subject of the next Chapter.

Interestingly, based on the presented stability assessments, it seems that river-sea ships are more vulnerable to the Dead Ship Condition than to the Excessive Acceleration failure mode. The attainable ranges of metacentric heights of the vessels A and B (as described in Section 1.2.1) are not affected by the Excessive Acceleration failure mode, and the vessel C is affected just marginally.

5.4   Conclusions

In this Chapter, environmental conditions are reconsidered. As river-sea ships sail in coastal waters, it was concluded that the "standard" scatter table that describes the North Atlantic, foreseen by the Second Generation Intact Stability Criteria, would be too demanding to be applied to stability assessment of this type of ships. It is therefore considered that a proper wave scatter table, as well as an appropriate wind-wave relation, describing the environmental conditions in the specific operational area should be used in stability assessment of river-sea ships. However, if corresponding scatter table is not available, stability assessment could not be possible. In some cases when a local authority is already regulating the river-sea navigation, a corresponding scatter table has already been developed. In this thesis, an example is made with the environmental conditions corresponding to Belgian coast.

Adopting new environmental conditions is simple, yet an important step. It was shown that the failure indices are significantly reduced after these changes, providing the river-sea ships with wider range of acceptable metacentric heights, in terms of intact stability. Moreover, the Dead Ship Condition failure mode has proved to be predominant mode of stability failure for river-sea ships.

Chapter 6

Roll damping estimation of river-sea ships

6.1 Introduction

A proper mathematical modelling of ship dynamics was indicated by Bačkalov et al. (2016) as one of the most important tasks of future research on stability of inland vessels. In this respect, it is well-known that the outcome of the analysis of roll motion and, consequently, assessment of ship stability, considerably depend on the roll damping. However, experimental data on roll damping of inland vessels are scarce and unreliable. In such case, a possible solution could be to use some of the existing semi-empirical methods in order to estimate roll damping coefficients.

Nevertheless, the viability of such approach is questionable knowing that the available methods are primarily intended for conventional sea-going ships. This concerns the well-established Ikeda's method (Himeno, 1981) and its "simplified" version (Kawahara et al., 2009) based on regression analysis of data generated by applying the classic method on a series of ships developed from the Taylor series. The question of applicability of the Simplified method is particularly relevant as it was recommended for use within the Second Generation Intact Stability Criteria framework (see e.g. IMO, 2016d), in the absence of either experimental data or another, more suitable method. However, in the Section 4.7 and Section 5.3, a possible issue with roll damping of river-sea ship was indicated.

In order to examine the relevance of the classic and Simplified Ikeda's method for inland vessels and river-sea ships, roll damping coefficients were calculated, using both methods, for several sample ships. The preliminary results were quite unexpected: for some ships, the roll damping coefficients estimated by the Simplified Ikeda's method were found to be negative. Such results triggered further investigation with even more surprising findings that could concern safety assessment of sea-going ships as well. It is therefore believed that the outcome of the present chapter is not relevant for inland vessels and river-sea ships only, but could have an impact on ship stability analysis in general. Finally, stability of the three test vessels is assessed based on the Second Generation Intact Stability Criteria, following the modification of the Simplified Ikeda's method.

The present Chapter is the result of a study already published by Rudaković & Bačkalov (2017).

6.2 Application of the methods to sample inland vessels

Inland vessels and river-sea ship hulls often have high breadth-to-draught ratios (i.e. $B/T > 4$), while geometry of some of the aft cross-sections may yield as much as $B/T \approx 10$. In

addition, hull form coefficients of these vessels are typically $C_B = 0.82 \div 0.94$ and $C_M \geq 0.99$. Several vessels from the database (given in Section 1.2) are selected to be used in the present investigation. In addition, four more vessels outside of the database are used (noted T34, T35, C36 and T37), which are considered to be suitable for the following analysis. The geometric properties of all vessels and river-sea ships used in the present Chapter, are given in Table 6.1.

Table 6.1: Sample vessels - Simplified Ikeda's method.

Vessel	L_{WL} [m]	B [m]	T [m]	C_B [-]	C_M [-]	B/T [-]
T1	66.83	10.50	3.45	0.8212	0.9959	3.04
T2	84.30	9.56	3.60	0.9226	0.9987	2.66
Vessel A (T4)	85.20	11.40	4.30	0.8514	0.9969	2.65
T5	85.77	10.95	2.80	0.8535	0.9982	3.91
Vessel B (C14)	108.40	11.40	2.46	0.8683	0.9964	4.40
C21	109.81	11.45	2.60	0.8783	0.9986	4.63
T25	124.33	11.40	4.50	0.8992	0.9988	2.53
C26	133.75	14.50	3.60	0.9031	0.9957	4.03
C27	134.27	11.45	2.68	0.9088	0.9974	4.27
C28	134.30	14.50	4.00	0.9123	0.9978	3.63
C30	134.79	11.45	3.33	0.9101	0.9974	3.44
T34	81.82	9.40	3.07	0.8497	0.9967	3.06
T35	105.76	11.40	2.80	0.8806	0.9964	4.07
C36	111.25	14.50	3.30	0.8336	0.9886	4.39
T37	121.10	11.40	4.30	0.8976	0.9965	2.65

6.2.1 Simplified Ikeda's method

Due to the aforementioned specific features, most of the vessels used are clearly out of range of applicability of Ikeda's method. According to Kawahara et al. (2009), the simplified method may be applied to ships having:

$$0.5 \leq C_B \leq 0.85, \quad 2.5 \leq B/T \leq 4.5, \quad \hat{\omega} \leq 1,$$
$$-1.5 \leq \overline{OG}/T \leq 0.2, \quad 0.9 \leq C_M \leq 0.99 \tag{6.1}$$

Symbol $\hat{\omega}$ stands for non-dimensional frequency:

$$\hat{\omega} = \omega\sqrt{\frac{B}{2g}} \tag{6.2}$$

while the distance $\overline{OG}$ of the centre of gravity from the calm water level from is downwards positive. It should be noted that $\overline{OG}$ in the Second Generation Intact Stability Criteria is defined as upwards positive.

Nevertheless, the roll damping coefficients were calculated for all sample ships, whereby the total roll damping was considered to consist of:

$$B_{44} = B_F + B_W + B_E \tag{6.3}$$

where B_F is the friction damping, B_W is the wave damping and B_E is the eddy damping. For the time being, the bilge keel damping B_{BK} is omitted from the calculations, since inland vessels

normally do not have bilge keels. The lift damping component B_L is also excluded, since it is considered that the vessel speed is $v = 0$. This is also in line with the Dead Ship Condition and Excessive Acceleration Criteria assumptions. Furthermore, it should be noted that whenever the limits of applicability range were exceeded, maximal values of B/T, C_B and C_M were used in the calculations. Furthermore, $\overline{GM}$ values used for this purpose were estimated, based on the usual loading conditions for this vessel type. Consequently, since the use of the simplified method does not require knowledge of any details of hull geometry that would distinguish an inland vessel from a sea-going one, the calculated B_{44} coefficients could formally correspond to a Taylor standard series ship of the same characteristics.

Figure 6.1 shows the non-dimensional equivalent linear total roll damping:

$$\hat{B}_{44} = \frac{B_{44}}{\rho V B^2} \sqrt{\frac{B}{2g}} \tag{6.4}$$

as a function of roll amplitude for the all ships examined. It can be noticed that, except for the sample vessels T1 and C36, the total roll damping of the examined ships decreases with the increase of the roll amplitude. Surprisingly, some ships (T2 and T37) may even reach negative roll damping at large enough rolling amplitudes. This is recognised as the cause of errors mentioned in Section 4.7 and Section 5.3, where it was impossible for the standard deviation of roll angular velocity $\sigma_{\dot{x},j}$ to converge, due to decreasing trend of the roll damping.
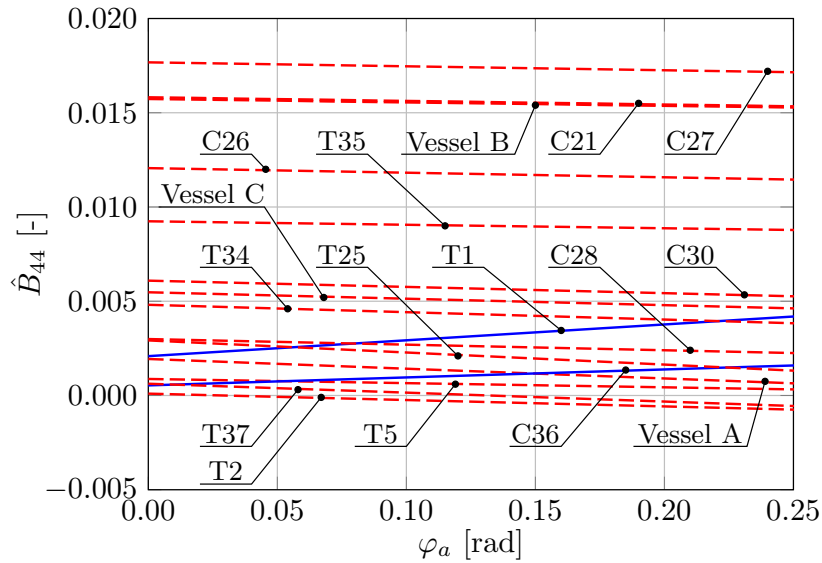
Figure 6.1: Total roll damping $\hat{B}_{44}$ of the examined ships as a function of roll amplitude φ_a, according to the Simplified Ikeda's method.

A closer examination of components revealed that in all the cases analysed (again, except for sample vessels T1 and C36), the eddy making component was negative. The focus of investigation thus turned to the eddy damping.

The eddy damping is calculated as follows:

$$\hat{B}_E = \frac{4\hat{\omega}\varphi_a}{3\pi x_2 x_1^3} C_R \tag{6.5}$$

where:

$$C_R = A_E \exp\left(B_{E1} + B_{E2} x_3^{B_{E3}}\right) \tag{6.6}$$

and

$$A_E = f(x_1, x_2), \quad B_{E1} = f(x_1, x_2, x_3),$$
$$B_{E2} = f(x_2, x_4), \quad B_{E3} = f(x_1, x_2) \tag{6.7}$$

while $x_1 = B/T$, $x_2 = C_B$, $x_3 = C_M$ and $x_4 = \overline{OG}/T$.

From Equation (6.5) it may be concluded that eddy damping could be negative only if C_R becomes negative. Furthermore, C_R given by Equation (6.6) could be negative only if A_E becomes negative. Therefore, it would be interesting to examine the structure of the formula for the computation of A_E:

$$A_E = A_{E1} + A_{E2} = \underbrace{(-0.0182x_2 + 0.0155)(x_1 - 1.8)}_{A_{E1}} -$$
$$\underbrace{-79.414x_2^4 + 215.695x_2^3 - 215.883x_2^2 + 93.894x_2 - 14.848}_{A_{E2}} \tag{6.8}$$

If the geometric properties of an examined ship i.e. B/T and C_B remain within the boundaries of the method applicability, A_{E1} cannot become negative. However, A_{E2} may become both negative and larger than A_{E1} in case $C_B > 0.84$, whereby the exact value of this "critical" block coefficient depends on B/T ratio. A_E as a function of B/T and C_B is given in Figure 6.2. Now it is possible to explain the principal difference in the eddy making component (and, consequently, the total roll damping) between ships T1 and C36 and the rest of the sample vessels: T1 and C36 are the only ships with $C_B < 0.84$.
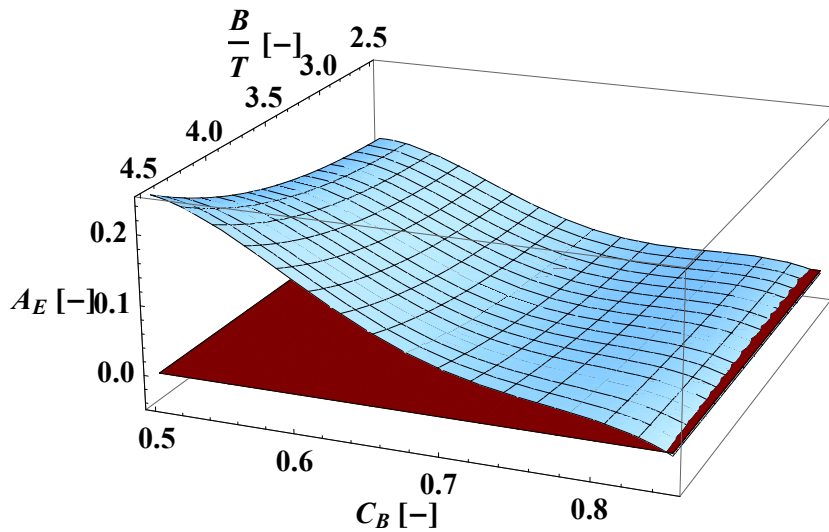
Figure 6.2: A_E as a function of B/T and C_B.

The factor C_R computed over the complete domain of applicability of the Simplified Ikeda's method is given in Figure 6.3. In line with the analysis of Equations (6.6) and (6.8), C_R is negative for high values of C_B regardless of B/T, $\overline{OG}/T$ and C_M. Another interesting feature is noticeable: the sign of the partial derivative of the Equation (6.6) with respect to C_B changes when block coefficient attains sufficiently high value. This happens at $C_B = 0.74 \div 0.81$ (depending on $\overline{OG}/T$ and C_M values) and becomes particularly evident for the high midship coefficients C_M.

Therefore, while the eddy making component of damping and, consequently, the total roll damping corresponding to $C_B > 0.84$ are obviously incorrect, it is also questionable whether B_{44} calculated with the Simplified Ikeda's method could be considered reliable in a much wider

range of block coefficients, i.e. $0.74 < C_B < 0.84$. Thus, the issue of accuracy of the Simplified Ikeda's method is not limited to inland vessels and river-sea ships only, but may also concern sea-going ships with high block coefficients, otherwise believed to be covered by the method.

(a) $\overline{OG}/d = 0.2$, $C_M = 0.9$.

(b) $\overline{OG}/d = 0.2$, $C_M = 0.99$.

(c) $\overline{OG}/d = -1.5$, $C_M = 0.9$.

(d) $\overline{OG}/d = -1.5$, $C_M = 0.99$.
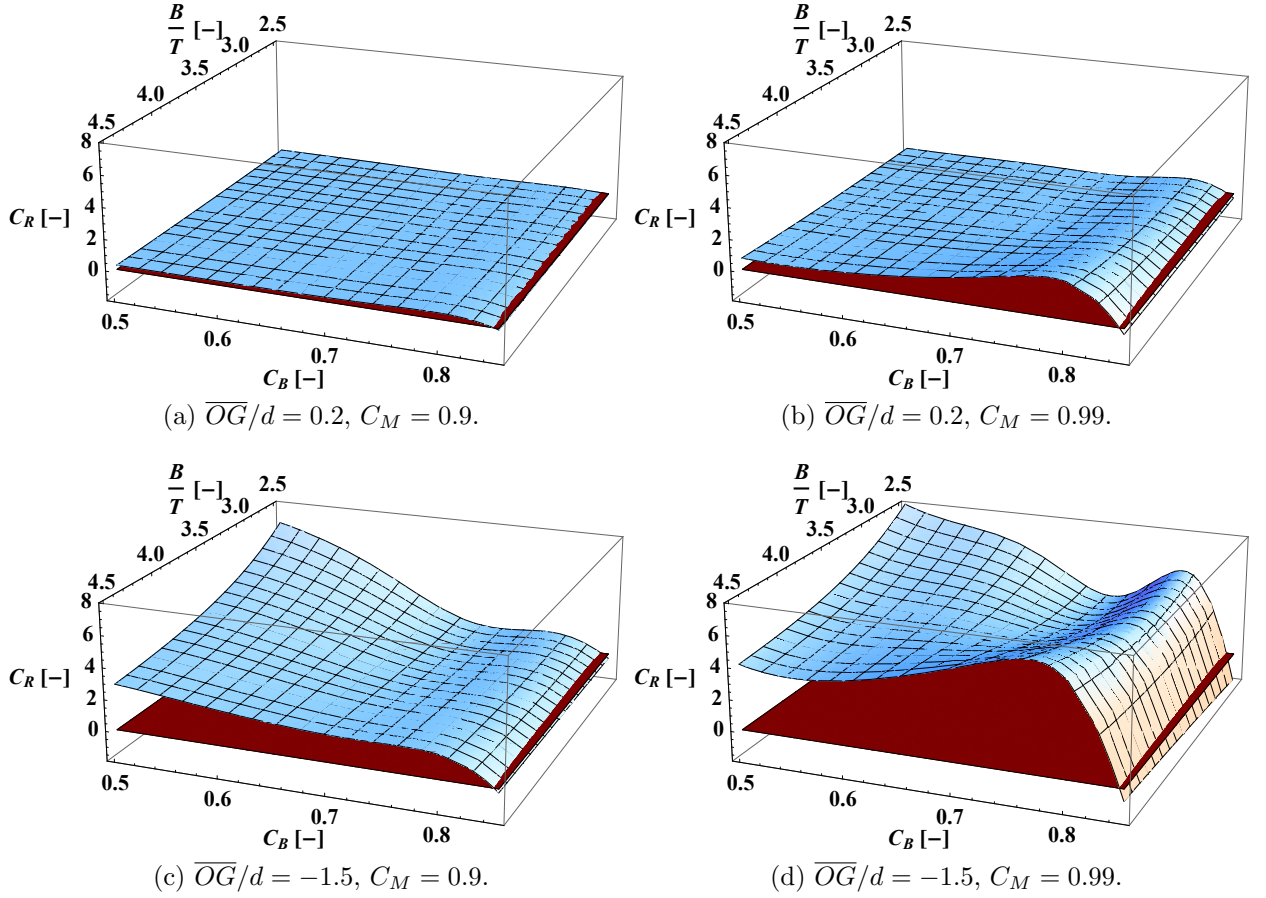
Figure 6.3: C_R computed over the applicability domain of the Simplified Ikeda's method.

6.2.2 Classic Ikeda's method

It would be interesting to examine the possibility to amend the Simplified Ikeda's method, so as to get more reliable prediction of the eddy making damping component for ships with high C_B, and ultimately for inland vessels and river-sea ships.

A_{E2} as defined by Equation (6.8) as well as some possible modifications are shown in Figure 6.4. Obviously, there is an array of possibilities for adjustment of the function in the examined range of block coefficients.

In absence of experimental data, the appropriate modification of function A_{E2} could be sought by calculating the eddy damping using the classic Ikeda's method and comparing it to the results obtained by a proposed amendment.

Unlike its simplified version, the classic Ikeda's method requires the knowledge of detailed hull geometry, that is, geometric particulars of cross sections: sectional breadth B_s and draught d_s, sectional area coefficient σ, bilge radius r_b, and the local maximal distance between the roll axis and hull surface r_{max}. For this purpose, four vessels were selected from Table 6.1 – T1, A, T34 and C36. Two seagoing tankers with high block coefficients (Table 6.2) were considered as well. Eddy making component computations were performed using 51 equidistant cross-sections. The block coefficients of the selected ships are in the range $C_B = 0.798 \div 0.851$.
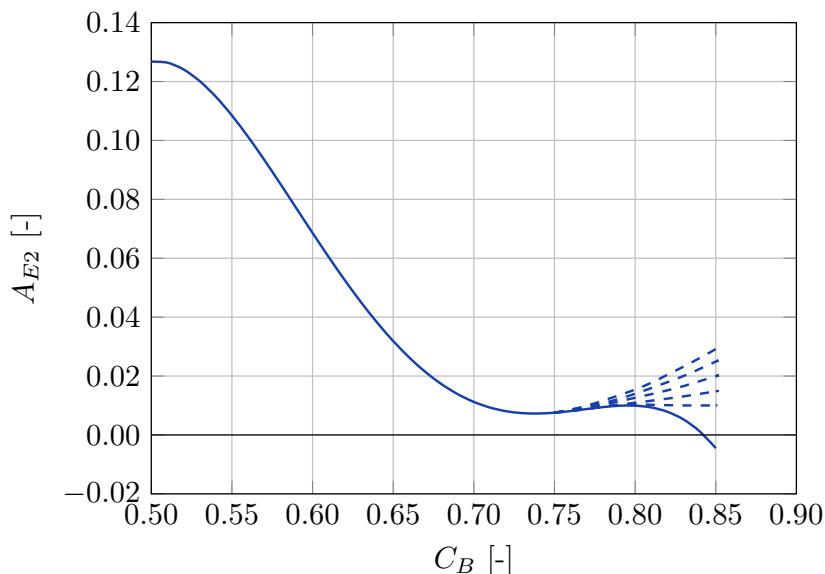
Figure 6.4: A_{E2} calculated by Equation (6.8) (full line) and possible corrections (dashed lines).

It should be noted that in the classic method, the pressure distribution on the hull surface is obtained assuming the cross-sections are approximated by Lewis forms. Clearly, this is not a proper approximation for a number of aft cross-sections of examined inland vessels and river-sea ships. Therefore, although the proposed procedure seems to be simple, it is not free from challenges.

With respect to that, it should be noted that for cross-sections of certain geometric characteristics, (typically for combinations of high beam-to-draught ratios and relatively low area coefficients) the sectional eddy damping calculated by the classic Ikeda's method could also be negative. This is often the case with forward- and aft-most cross-sections of inland vessels. A trivial solution (and it seems, the usual remedy, see Kawahara et al., 2009) for this deficiency is
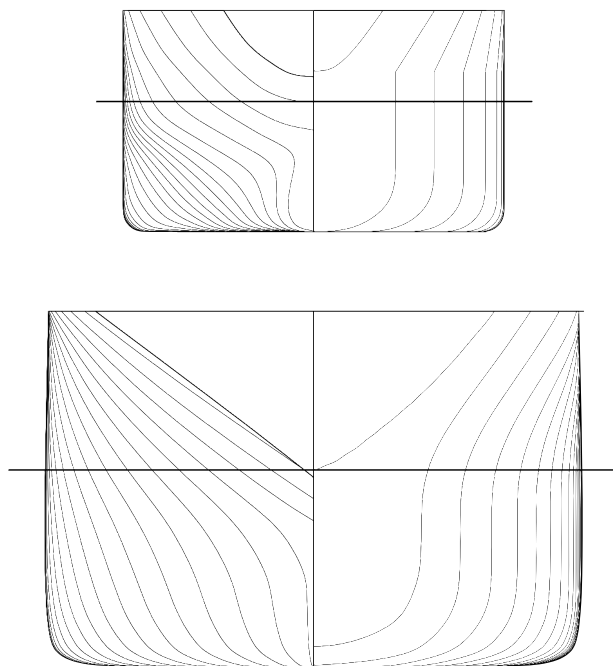
Figure 6.5: Sea-going tankers used in computation of the eddy making component according to the classic Ikeda's method (Panamax above, Suezmax below).

Table 6.2: Sample sea-going tankers.

Vessel	L [m]	B [m]	T [m]	C_B [-]	B/d [-]
Panamax	287.78	32.2	11	0.843	2.927
Suezmax	230.07	45.52	16.6	0.7982	2.742

to take the damping of a "problematic" cross-section as zero. Having no possibility to estimate a correct value of the eddy damping corresponding to such cross-sections, the same approach was used in this thesis.

6.3   A possible adjustment of simplified formula for the eddy making component of damping

In order to find an appropriate adjustment of Equation (6.8), the following procedure is proposed. Assuming that, for each ship, it may be established:

$$B_{E(s)} \approx B_{E(c)} \tag{6.9}$$

(where "s" stands for the simplified and "c" stands for the classic method) it would be possible to extract the "correct" value of A_{E2} corresponding to a given (high) block coefficient, provided that $B_{E(c)}$ is calculated beforehand.

$B_{E(c)}$ is obtained by numerical integration of the sectional eddy damping over the ship length:

$$B_{E(c)} = \int_L B'_{E(c)} \, \mathrm{d}x \tag{6.10}$$

where

$$B'_{E(c)} = \frac{4\omega\varphi_a}{3\pi} \rho T_s^4 C_{R(c)} \tag{6.11}$$

The sectional $C_{R(c)}$ depends on B_s and T_s, σ, r_b, r_{max}, $\overline{OG}$ as well as pressure coefficient C_P. More precisely:

$$C_{R(c)} = \left(\frac{r_{max}}{T_s} \right)^2 f \left(\frac{r_b}{T_s}, \frac{B_s}{2T_s}, \sigma, \frac{\overline{OG}}{T_s} \right) C_P \tag{6.12}$$

Given the complexity of the procedure for the calculation of r_b, r_{max} and C_P, the respective expressions are omitted, but may be found in e.g. Falzarano et al. (2015), who presented the consolidated formulae of the classic method. On the other hand, the eddy damping of a ship, according to the simplified method, is:

$$B_{E(s)} = \frac{4\omega\varphi_a}{3\pi} \rho T^4 L C_{R(c)} \tag{6.13}$$

where $C_{R(c)}$ is defined by Equation (6.6). From Equations (6.9) to (6.11) and (6.13) it follows:

$$C_{R(s)} = \frac{1}{d^4 L} \int_L T_s^4 C_{R(c)} \, \mathrm{d}x \tag{6.14}$$

Then, using Equations (6.6), (6.8) and (6.14), an estimate of A_{E2} may be obtained for a given ship.

Finally, using the described procedure, A_{E2} values were calculated for the selected vessels (see Figure 6.6).
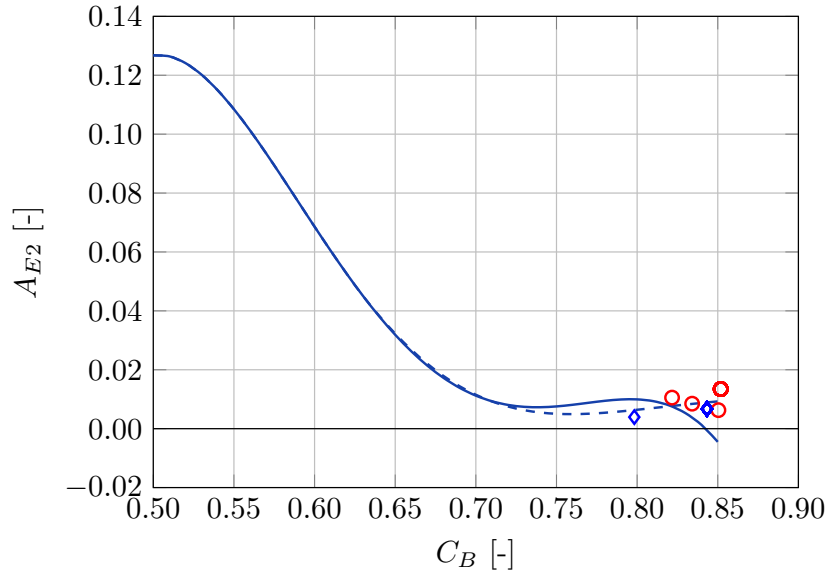
Figure 6.6: A_{E2} calculated by Equation (6.8) (full line) and the proposed correction given by Equation (6.15) (dashed line). Circles represent the values calculated for the inland vessels, while diamonds correspond to the sea-going tankers.

Based on these results, a new expression for A_E, valid in the whole range of applicability of the Simplified Ikeda's method, is proposed:

$$A_{E-new} = A_{E1} + A_{E2-new} = \underbrace{(-0.0182x_2 + 0.0155)(x_1 - 1.8)}_{A_{E1}} -$$
$$\underbrace{+151.48x_2^5 - 567.603x_2^4 + 840.297x_2^3 - 612.498x_2^2 + 218.904x_2 - 30.497}_{A_{E2-new}} \tag{6.15}$$

A_{E-new} as a function of B/T and C_B is given in Figure 6.7. The factor C_R adjusted by
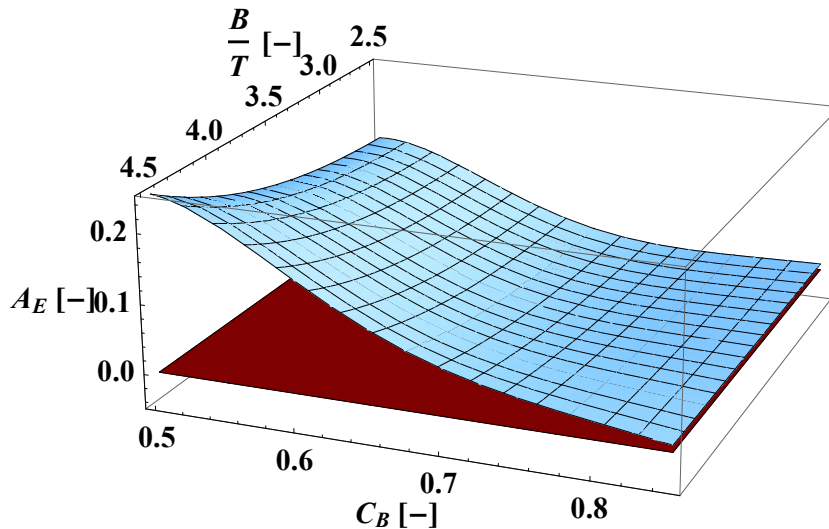
Figure 6.7: A_{E-new} as a function of B/T and C_B.

(a) $\overline{OG}/d = 0.2$, $C_M = 0.99$.   (b) $\overline{OG}/d = -1.5$, $C_M = 0.99$.
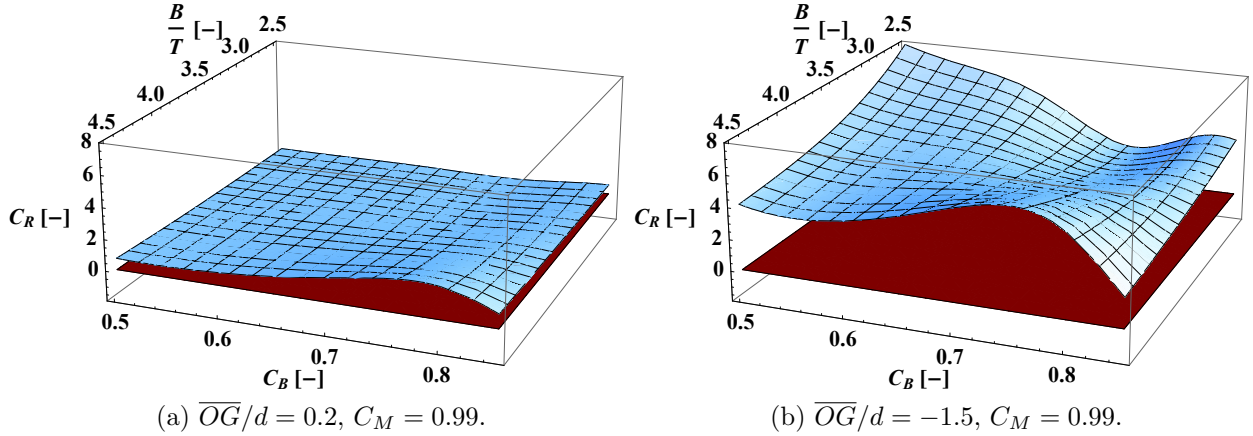
Figure 6.8: Factor C_R adjusted by Equation (6.15) computed over the applicability domain of the Simplified Ikeda's method.

Equation (6.15) is computed within the range of applicability of the Simplified Ikeda's method and given in Figure 6.8. Finally, the non-dimensional equivalent linear total roll damping of the sample ships given in Table 6.1 is computed using the adjusted simplified formula for eddy damping, see Figure 6.9. Whenever the block coefficient exceeded the applicability range, the calculations were carried out with $C_B = 0.85$. As it can be seen in Figure 6.9, the total roll damping attains an increasing trend with respect to roll amplitude, as it should be normally expected.
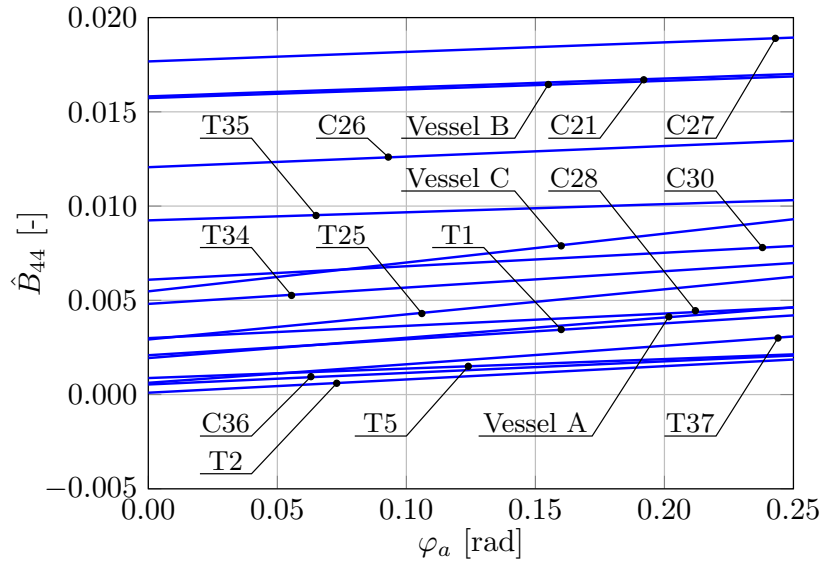
Figure 6.9: Total roll damping $\hat{B}_{44}$ of examined ships as a function of roll amplitude φ_a, according to the Simplified Ikeda's method, taking into account proposed adjustment of the eddy damping component.

6.4 Further extension of simplified formula for the eddy damping to inland vessels

It was already pointed out that most of the sample vessels given in Table 6.1, and most of inland vessels in general, fall out of the range of applicability of the Simplified Ikeda's method

with respect to B/T and C_B. For instance, the beam-to-draught ratios (for scantling draught) of typical European river cruisers are in the range of $5.5 \div 8.5$. Therefore, without model tests, it appears difficult to adjust the Simplified Ikeda's method so as to extend its applicability to just any inland vessel.

For the sake of comparison, for some sample vessels having $C_B > 0.85$ (see Table 6.2), $C_{R(s)}$ was calculated by using Equation (6.14), based on classic Ikeda's method, taking into account actual hull form geometry (corresponding to real C_B) in the computation of $C_{R(c)}$. These figures are subsequently compared to data obtained by applying the simplified formula (6.6) using both expression (6.8) for A_E and the proposed adjustment of A_E given by (6.15); in these two latter cases, $C_B = 0.85$ is always used, instead of the actual block coefficients.

Table 6.3: Discrepancies in estimation of the eddy making component using different formulae and limitations. All calculations were carried out for $\overline{OG} = 0\,\mathrm{m}$.

Vessel	C_B [-]	$C_{R(s)}$ [-]		
		(6.6) + (6.8)	(6.6) + (6.15)	(6.14)
T2	0.9226	-0.3773	0.7846	4.6228
T4	0.8535	-0.3876	0.8808	6.3669
Vessel B (C14)	0.8664	-0.3744	0.9480	3.5575
C26	0.9031	-0.3862	0.8927	2.6430
C30	0.9101	-0.3884	0.8386	3.5152

Significant discrepancies between the values of C_R obtained using different approaches indicate that an accurate estimation of the eddy making component of such full-bodied vessels remains a task for the future. For the time being, however, if the Simplified Ikeda's method is employed, it is suggested to use the adjusted eddy damping formula (proposed in the thesis and based on (6.15)) applying the method limitations whenever the geometric properties of the analysed hull exceed the applicability range.

6.5 Application of the stability criteria to river-sea ships following modification of roll damping method

In order to further examine the proposed modification of the Simplified Ikeda's method, the stability assessment according to the Dead Ship Codition and Excessive Acceleration, explained in Section 4.7, will be re-evaluated, using the same test vessels. The only difference is the use of the new formula for the eddy making component (6.7), as given in Section 6.3. Furthermore, in order to examine influence of bilge keels on stability assessment, both results with and without the presence of the bilge keels will be presented throughout the thesis.

The failure indices for the test vessels A, B and C with the presence of the bilge keels are given in Figures 6.10, 6.11 and 6.12, respectively. Comparing these results with the results obtained before the eddy damping component modification, it can be seen that the differences are noticeable. The general trend, according to the three Figures, is the reduction of indices C_{DSC} and C_{EA} over the whole range of $\overline{GM}$. Although the new expression for A_{E-new} can estimate smaller roll damping (which occurs for $C_B \approx 0.75 \div 0.82$, as shown in Figure 6.7), in case of river-sea ships it usually does not occur due to high block coefficient of river-sea ships. Moreover, the differences are negligible for the test vessels B and C for the Dead Ship Condition. However, the change is the most noticeable in Figure 6.10(b), where the upper limit of the allowable $\overline{GM}$, according to the Excessive Acceleration, has significantly increased.

(a) DSC failure index as a function of $\overline{GM}$.

(b) EA failure index as a function of $\overline{GM}$.
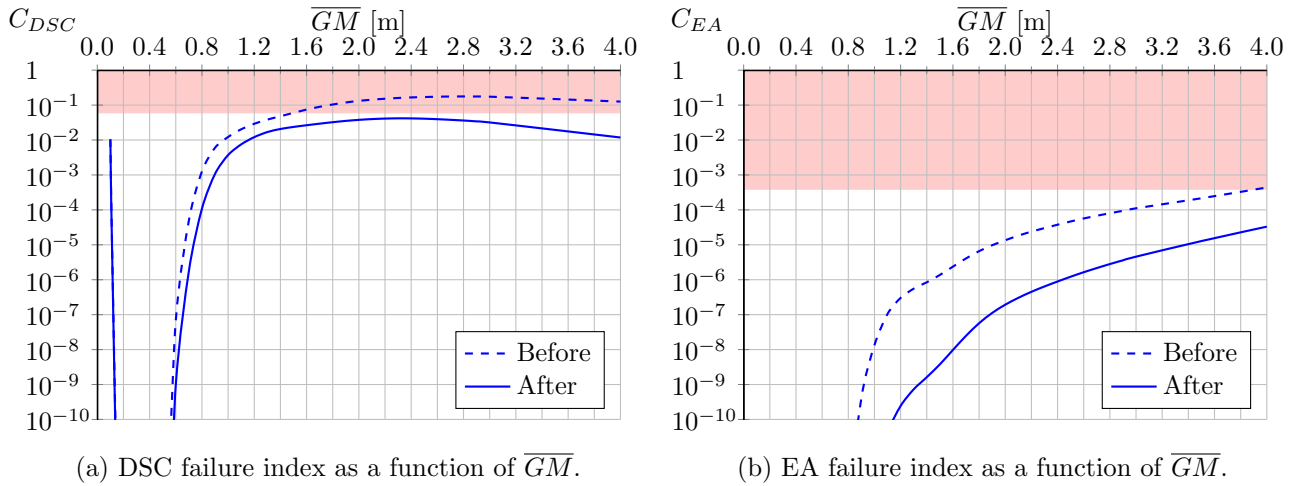
Figure 6.10: Stability assessment - vessel A with bilge keels. The results following the modification of the Simplified Ikeda's method.


(a) DSC failure index as a function of $\overline{GM}$.

(b) EA failure index as a function of $\overline{GM}$.
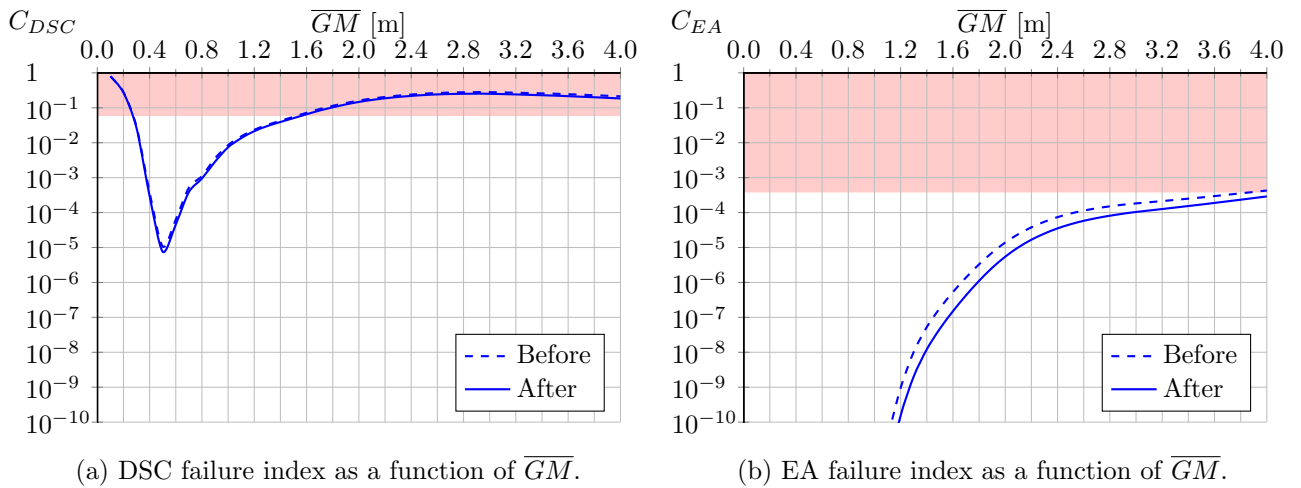
Figure 6.11: Stability assessment - vessel B with bilge keels. The results following the modification of the Simplified Ikeda's method.

(a) DSC failure index as a function of $\overline{GM}$.

(b) EA failure index as a function of $\overline{GM}$.
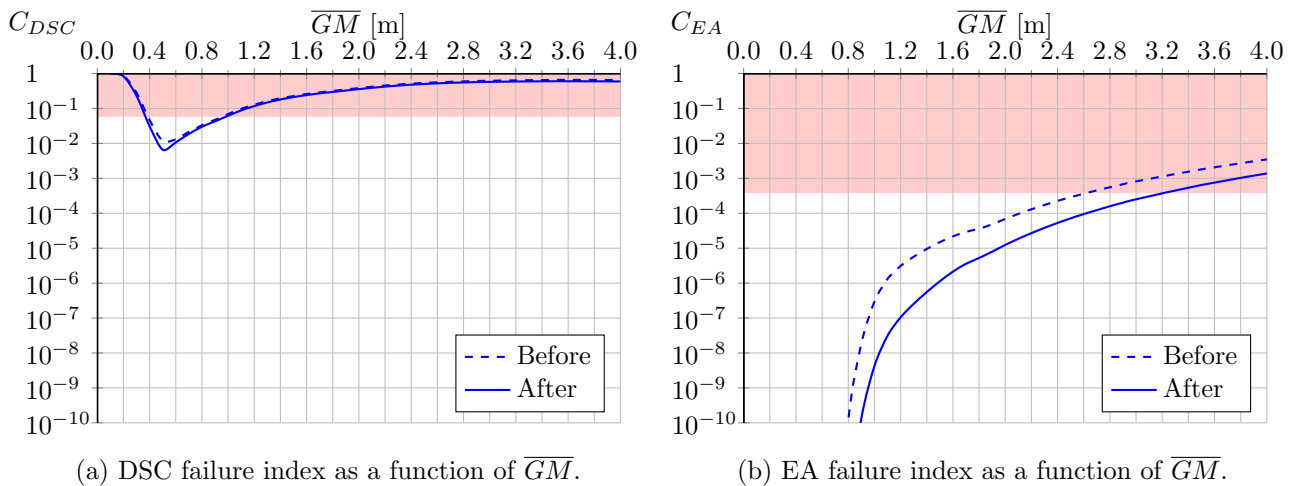
Figure 6.12: Stability assessment - vessel C with bilge keels. The results following the modification of the Simplified Ikeda's method.

Due to the fact that now roll damping is always positive and also have an increasing trend as a function of roll amplitude, the results are possible to obtain, regardless of the bilge keel presence. The failure indices for the test vessels A, B and C without the bilge keels are given in Figures 6.13, 6.14 and 6.15, respectively. The failure indices curves follow the expected shape, without unusual behaviour. However, the corners on the graphs can be seen, the most noticeable one is in Figure 6.15(b), at $\overline{GM} = 1.8\,\text{m}$, but also in Figure 6.13(b), at $\overline{GM} = 1.4\,\text{m}$. In both cases it occurs when the limiting value of $\overline{OG}/T \leq 0.2$ is reached. As the result $\overline{OG}/T$ remains fixed at its maximal value, even though this does not correspond to actual values attained at higher metacentric heights. This is one more parameter of the Simplified Ikeda's method, for which the applicability range is often narrower than river-sea ship particulars.

(a) DSC failure index as a function of $\overline{GM}$.

(b) EA failure index as a function of $\overline{GM}$.
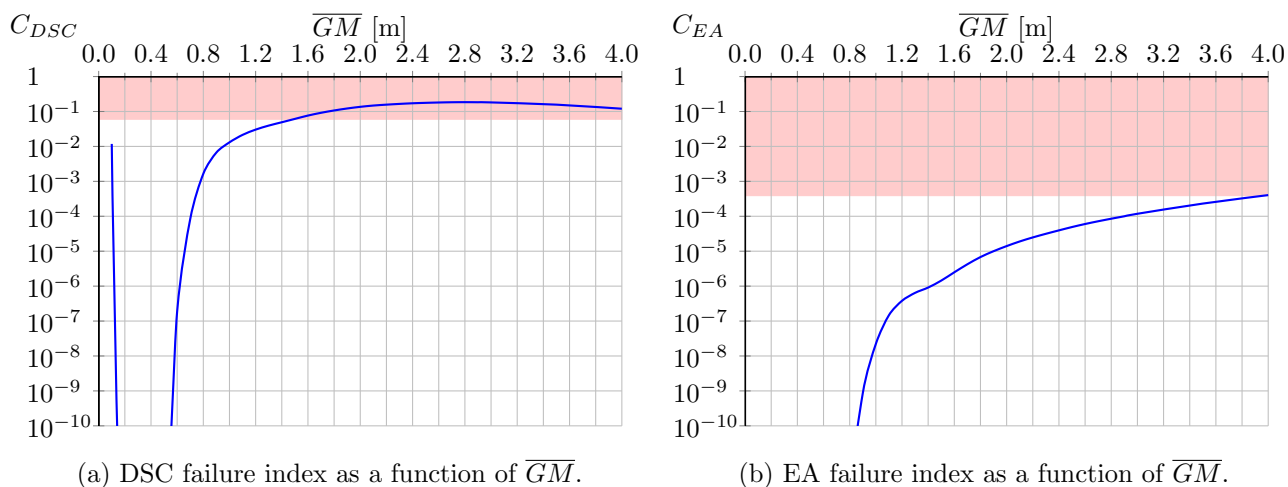
Figure 6.13: Stability assessment - vessel A without bilge keels. The results following the modification of the Simplified Ikeda's method.

(a) DSC failure index as a function of $\overline{GM}$.

(b) EA failure index as a function of $\overline{GM}$.
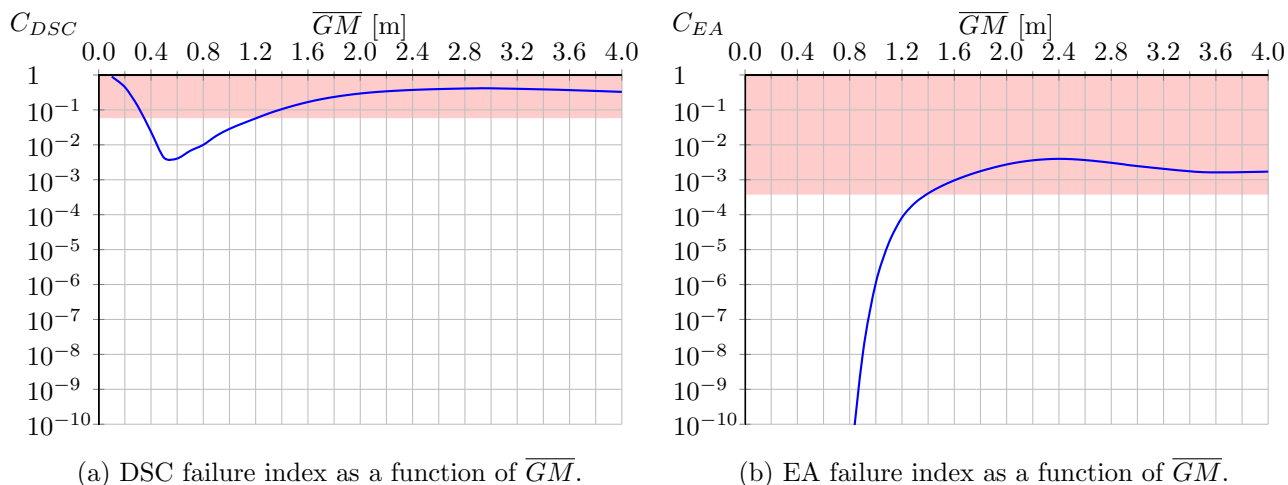
Figure 6.14: Stability assessment - vessel B without bilge keels. The results following the modification of the Simplified Ikeda's method.

(a) DSC failure index as a function of $\overline{GM}$.

(b) EA failure index as a function of $\overline{GM}$.
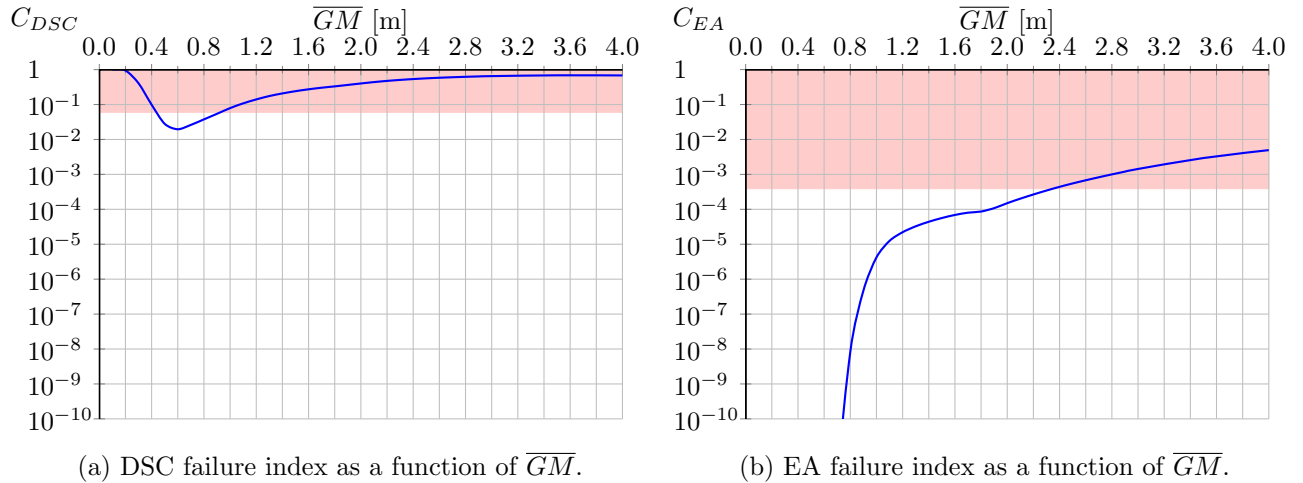
Figure 6.15: Stability assessment - vessel C without bilge keels. The results following the modification of the Simplified Ikeda's method.

Furthermore, comparing Figures 6.13, 6.14 and 6.15, with the Figures 6.10, 6.11 and 6.12, the influence of the bilge keels can be noticed. However, in order to have a better insight into the effect of the bilge keels on intact stability of river-sea ships, comparative plots between failure indices with and without bilge keels are given as a function of metacentric height, in Figure 6.16. It can be seen that the presence of bilge keels, as expected, has a positive effect on stability, over the whole range of metacentric heights. Due to their impact on stability on the one hand, and due to simplicity and low cost on the other, it is advised to consider the installation of the bilge keels on river-sea ships.

(a) Dead Ship Condition.

(b) Excesive Acceleration.
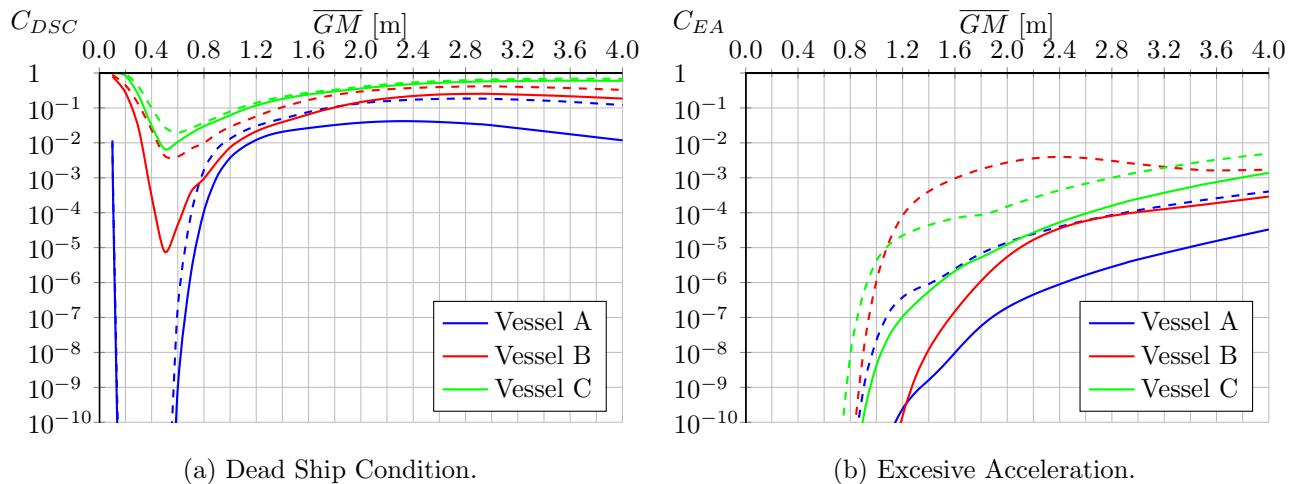
Figure 6.16: Comparative plots between failure indices with bilge keels (full lines) and without bilge keels (dashed lines) as a function of $\overline{GM}$.

6.6 Conclusions

In the course of investigation of applicability of the Simplified Ikeda's method for the roll damping prediction to European inland vessels and river-sea ships, it was found that the eddy damping formula fails to properly predict the corresponding damping component if the block

coefficient of the vessel is sufficiently large, i.e. $C_B > 0.8$. This deficiency is particularly striking for $C_B > 0.84$, when the eddy making component of damping becomes negative.

Therefore, an adjustment of the simplified formula for the eddy making component prediction is proposed, based on calculations performed using the classic Ikeda's method. The method was applied to several typical inland hulls with high block coefficients ($C_B = 0.82 \div 0.85$) and high midship coefficients ($C_M \geq 0.99$), covering a complete range of applicability of the simplified method with respect to beam-to-draught ratios ($B/T = 2.6 \div 4.4$). Two typical sea-going tankers (having $C_B \approx 0.8$ and $C_B \approx 0.84$) were included in the calculations as well. It is expected that the derived expression could extend the applicability of the Simplified Ikeda's method to inland ships, in absence of adequate experimental data. Furthermore, the adapted formula provides a better estimation of the eddy damping component not only for inland vessels but also for sea-going ships with full hull forms.

The latter stability assessment of the test vessels showed significant improvement, as there are no evident errors in the calculation procedure. Furthermore, the benefits of presence of the bilge keels on stability has been recognised. Therefore, it is recommended that the bilge keels are installed on river-sea ships as, on the one hand, they positively affect the stability, and on the other, they are cost-effective and simple to install. However, motivated by the results of modification of the method for roll damping estimation, it is reasonable to thoroughly examine other methods foreseen by the SGISC also (e.i. method for effective wave slope coefficient and natural roll period estimation), and to adapt them for the application to river-sea ships, if possible.

Chapter 7

Effective wave slope coefficient of river-sea ships

7.1 Introduction

An important step in the assessment of ship safety in rough weather in intact condition is to properly account for roll excitation moment induced by waves. As the fluid-ship interaction is complex, the concept of effective wave slope coefficient was developed as a practical tool for 1DOF roll motion prediction. In the past, the effective wave slope coefficient was usually considered only at natural roll frequency (e.g. Blume, 1979; Fujino et al., 1993; IMO, 2008a,b; Yamagata, 1959) or in regions of frequency close to the roll natural frequency (e.g. Francescutto et al., 2001; Francescutto & Serra, 2002). However, in the SGISC framework, a frequency-dependent effective wave slope coefficient is necessary in a wide range of frequencies when applying the Level 2 vulnerability assessment approach for Dead Ship Condition (IMO, 2016d, 2017). To this end, a simplified approach was proposed within SGISC (IMO method, described in Section 4.4.2), which accounts for Froude-Krylov roll moment only, and where ship sections at different longitudinal positions, as an approximation, are substituted by rectangles (IMO, 2016d, 2017). At the same time, other approaches based on Froude-Krylov assumption which are able to more accurately account for the exact hull shape by direct pressure integration, are also readily available and simple to implement. Such approaches are either based on a 3D panelling of the hull surface, or on a "strip-theory" approximation. It is also noted that direct Froude-Krylov pressure integration for the determination of the effective wave slope coefficient is presently considered as a possible calculation option within the draft SGISC framework (IMO, 2017). In this context, Umeda et al. (2007) suggested that the simplified Froude-Krylov approach based on rectangular approximation of ship sections could provide acceptable results in terms of capsizing probability predictions when compared with other methods. However, due to the importance of the effective wave slope coefficient, it is reasonable to consider also more advanced and more precise methods, possibly based on linear seakeeping hydrodynamic. In this respect, Mizuno (1973, 1975) formulated the frequency dependent effective wave slope coefficient from the coupled linear roll-sway dynamical system taking into account all mechanic and hydrodynamic terms in the 2DOF dynamical system. The results reported by Mizuno (1973, 1975), considering both calculations and experiments, appear to indicate that the effective wave slope calculated according to the Froude-Krylov approximation tends to be conservative, leading to overestimation of roll motion when used in numerical predictions. At the same time, results by Mizuno (1973, 1975) indicate that the Froude-Krylov approximation for the effective wave slope is appropriate in the region of low frequencies, i.e. for long waves, and this is in line with the indications from Umeda & Tsukamoto (2008) who made reference, for the same purpose, to the study by Tasai (1965). An approach for the determination of frequency de-

pendent effective wave slope coefficient accounting for the 3-DOF linear sway-roll-yaw coupling was presented by (Bulian et al., 2008; Bulian & Francescutto, 2009; Míguez González & Bulian, 2018). This latter approach, which is one of the approaches that are going to be used in the thesis, accounts for the coupling of roll with both sway and yaw, but it is an approximate method because it neglects the effect of damping. Nevertheless, experimental results reported by Bulian & Francescutto (2009) and Bulian et al. (2009) indicate that the approach is capable of providing the effective wave slope with sufficient accuracy for the prediction of roll amplitude in beam waves.

The focus of this chapter will be on the determination of the effective wave slope for inland/river-sea ships, which are characterised by full hull forms, long parallel middle bodies and large breadth-to-draught ratios. In addition, such ships may have high position of centre of gravity above the waterline compared to the ship draught. To the author's best knowledge, there seems to be no studies on effective wave slope of river-sea ships. Nevertheless, in the past, studies were carried out for other type of vessels sharing some of the characteristics of the ships considered herein. Fujino et al. (1993) investigated the effective wave slope in case of small craft with large breadth and shallow draught. They determined the effective wave slope coefficient from experiments (by means of measurement of wave exciting roll moment, or resonant roll angle in regular beam waves) and from calculations based on Froude-Krylov approximation, and they compared the results with the predictions from the formula in the present Weather Criterion (IMO, 2008a). They found that the formula from the Weather Criterion significantly overestimated both the results obtained from experiments and also the results obtained from Froude-Krylov calculations, particularly for conditions with high position of centre of gravity above the waterline. Fujino et al. (1993) also noticed that the effective wave slope coefficient from the Froude-Krylov approach had a tendency to overestimate the values obtained from experimental measurement of wave exciting roll moment with models fixed in roll and with unconstrained sway and heave in beam waves. On the completely opposite side of the spectrum of vessels' size, Francescutto et al. (2001) and Francescutto & Serra (2002) studied the effective wave slope coefficient for the case of large passenger ships, which are also characterised by large breadth-to-draught ratios and high position of centre of gravity above the waterline in proportion to the draught. They determined the effective wave slope coefficient from the analysis of experimental resonant roll motion in regular beam waves, and they also found that the formula from the Weather Criterion (IMO, 2008a) systematically overestimated the effective wave slope coefficient obtained from the analysis of experiments. The overestimation tendency of Weather Criterion formula was also confirmed by the experimental tests on two-dimensional models by Sato et al. (2008).

With specific reference to inland vessels and river-sea ships, the overall goal of this chapter is to provide a better insight into some of the existing methods for effective wave slope coefficient prediction, and to identify what type of approach may be considered more suitable for intact stability assessment of river-sea ships based on the modified SGISC framework in the thesis. Therefore, first, the methods considered in this study are described in Section 7.2. Then, Section 7.3 and the associated Appendix B provide an overview of the loading conditions of the vessels from the database (presented in Section 1.2), which are used in Section 7.4 for the systematic comparisons among different effective wave slope coefficient prediction methods. The three test vessels are used in Section 7.4 for reporting more in-depth analyses and comparisons. Finally, a summary of the obtained results, a series of concluding remarks are provided in Section 7.5.

The present Chapter is a result of a study already published by Rudaković et al. (2019) and contained in the report Rudaković (2018).

7.2 Effective wave slope coefficient: definition and prediction methods

In general, the effective wave slope coefficient at a wave frequency ω, can be defined as

$$r(\omega) = \frac{M_{wave}}{\Delta \cdot \overline{GM} k_w a_w} \qquad (7.1)$$

where here M_{wave} is the amplitude of a properly defined wave induced roll moment and a_w is the wave amplitude. The specific definition of M_{wave} depends on the method used for the determination of the effective wave slope coefficient, as discussed in the following sections.

Irrespective of the calculation method, the effective wave slope function $r(\omega)$ shows some characteristic properties. The low frequency limit is $\lim_{\omega \to 0} r(\omega) = 1$, whereas the high frequency limit is $\lim_{\omega \to \infty} r(\omega) = 0$. Usually, $r(\omega)$ can be expected to be in the range between 0 and 1. However, in some cases, the effective wave slope function may also exceed 1 in some ranges of frequencies, as it can happen for small metacentric heights at relatively high frequencies. According to (7.1), the frequencies where $r(\omega) = 0$ correspond to the frequencies where $M_{wave} = 0$. For conventional hull shapes and loading conditions, the natural frequency is typically between $\omega = 0$ and the first minimum (or first zero) of $r(\omega)$.

From Equation (7.1), it can be seen that the problem of prediction of the effective wave slope coefficient comes down to the problem of calculation of the amplitude of a properly defined roll moment M_{wave}. The Chapter, therefore, addresses the determination of the effective wave slope coefficient considering a series of different methods, namely:

- Predictions using direct calculations based on linear seakeeping hydrodynamics (hereinafter, shortly, "reduced 3DOF" approach);

- Predictions based on linear Froude-Krylov approximation;

- Predictions using semi-empirical methods.

The considered methods are described in detail in the following sections.

7.2.1 Direct calculation based on linear seakeeping hydrodynamics - Reduced 3DOF approach

Direct calculation in this chapter is carried out by means of a linear hydrodynamic approach, following Bulian et al. (2008) and Bulian & Francescutto (2009, 2011). The starting point is the classical linear seakeeping, frequency domain, 3-DOF model for sway-roll-yaw:

$$(\mathbf{M} + \mathbf{A}(\omega))\ddot{\mathbf{x}} + \mathbf{B}(\omega)\dot{\mathbf{x}} + \mathbf{C}\mathbf{x} = \widehat{\mathbf{F}}(\omega) \qquad (7.2)$$

where, $\mathbf{M}$ is the mass matrix, $\mathbf{A}$ is the added mass matrix, $\mathbf{B}$ is the damping matrix, $\mathbf{C}$ is the restoring matrix, $\hat{\mathbf{F}}$ is the vector of complex generalised forces, ω is the wave frequency, $\mathbf{x}$ is the complex state vector and dots indicate time derivatives. The method is based on the derivation of a single 1DOF equation for roll, implicitly embedding the coupling with sway and yaw, but omitting the effect of damping. This approximation was used in the past, although for different purposes, by Hutchison (1991) and by Naciri & Lledo (2001), who considered the case of coupled sway-roll dynamics, neglecting also the coupling with yaw. By removing the damping matrix $\mathbf{B}$, equation (7.2) becomes:

$$\begin{cases} \mathbf{Q}(\omega)\ddot{\mathbf{x}} + \mathbf{C}\mathbf{x} = \widehat{\mathbf{F}}(\omega) \\ \text{with } \mathbf{Q}(\omega) = \mathbf{M} + \mathbf{A}(\omega) \end{cases} \tag{7.3}$$

The system (7.3) corresponds to the following set of three equations:

$$\begin{cases} Q_{22}\ddot{y} + Q_{24}\ddot{\varphi} + Q_{26}\ddot{\psi} = \widehat{F}_2 \\ Q_{42}\ddot{y} + Q_{44}\ddot{\varphi} + Q_{46}\ddot{\psi} + C_{44}\varphi = \widehat{F}_4 \\ Q_{62}\ddot{y} + Q_{64}\ddot{\varphi} + Q_{66}\ddot{\psi} = \widehat{F}_6 \end{cases} \tag{7.4}$$

where subscript indices refer to the standard 6DOF linear seakeeping nomenclature for anti-symmetric motions (2: sway, 4: roll, 6: yaw). The roll degree of freedom in system (7.4) can be virtually "decoupled" by variables' substitutions, in order to obtain a single equation, containing only roll as explicit state variables, but still preserving the effects of coupling with sway and yaw motion.

The resulting 1-DOF roll equation has the following familiar form:

$$I_{44,c}(\omega)\ddot{\varphi} + C_{44}\varphi = \widehat{F}_{4,c}(\omega) \tag{7.5}$$

where the roll moment, in complex notation, is (Bulian et al., 2008; Bulian & Francescutto, 2009, 2011):

$$\widehat{F}_{4,c} = \widehat{F}_4 + \frac{\widehat{F}_2\left(Q_{42}Q_{66} - Q_{46}Q_{62}\right) - \widehat{F}_6\left(Q_{42}Q_{26} - Q_{46}Q_{22}\right)}{Q_{26}Q_{62} - Q_{66}Q_{22}} \tag{7.6}$$

The effective wave slope coefficient $r(\omega)$ can eventually be obtained by substituting the modulus of $\widehat{F}_{4,c}$ for M_{wave} in (7.1). It is important to highlight that the result is independent from the arbitrarily chosen centre of reference system used for the seakeeping computations.

The model (7.5) can also be used to estimate the undamped natural roll frequency of the ship ω_φ (which will be elaborated in more details in Chapter 8), as the solution of the following equation:

$$\begin{cases} \omega_\varphi = \sqrt{\dfrac{C_{44}}{I_{44,c}(\omega)}} \\ \text{with } I_{44,C}(\omega_\varphi) = Q_{44} - \dfrac{Q_{42}\left(Q_{24}Q_{66} - Q_{64}Q_{26}\right) - Q_{46}\left(Q_{24}Q_{62} - Q_{64}Q_{22}\right)}{Q_{22}Q_{66} - Q_{26}Q_{62}} \\ \text{where } Q_{ij} = Q_{ij}(\omega_\varphi) \ i,j = 2,4,6 \end{cases} \tag{7.7}$$

It is noted at this point, that also Tasai (1971) addressed the problem of the determination of the undamped natural roll frequency of the coupled sway-roll-yaw linear model, and he also used the approximation of neglecting the effect of damping. Although the derivation procedures herein and by Tasai (1971) are different, the final results are equivalent, and the undamped natural roll frequencies coincide.

7.2.2 Linear Froude-Krylov approach(es)

This approach, in line with the linear approximation, determines the roll moment by direct integration of undisturbed wave pressure on the wetted surface (i.e. Froude-Krylov roll moment) of a fixed hull considering beam regular waves. The moment is calculated with respect to the centre of gravity G, and it can be formally written as follows:

$$M_{FK} = \int_S \vec{r} \times (-p\vec{n}) \, \mathrm{d}S \tag{7.8}$$

where $\vec{r}$ is the radius vector from the centre of gravity G to the generic point on the hull surface S, p is the undisturbed wave pressure, and $\vec{n}$ is unitary normal vector of S pointing to the fluid. As the approach is linear, the integration is carried out on the wetted hull surface in calm water. In time domain, M_{FK} is a sinusoidal function of time for an incident regular wave. For the determination of the effective wave slope coefficient, the amplitude of M_{FK} is substituted for M_{wave} in (7.1). In case the calculation is carried out, equivalently, in frequency domain, M_{FK} in (7.8) corresponds to the phasor of the Froude-Krylov moment, and its modulus is substituted for M_{wave} in (7.1).

The distinctive positive characteristic of this method is that it is very simple to be implemented. The main drawback is associated with the fact that this approach totally neglects diffraction effects and effects associated with coupling from other relevant motions (sway and yaw).

The linear Froude-Krylov method can be implemented using various approaches, which in practice differ in the way of describing the hull shape for carrying out the integration in (7.1). The methods used in the present work are explained in the following.

The most precise Froude-Krylov method is based on the accounting for the exact three-dimensional shape of the hull. The hull is then discretised by a finite number of polygonal (in this thesis triangular) panels, allowing to accurately describe also complex hull shapes (see Figure 7.1). Each panel is associated to a relevant set of particulars (area, centroid position and unitary normal vector), which are used to determine the Froude-Krylov roll moment using the discretisation of (7.8). This method provides an accurate estimation of the Froude-Krylov excitation.
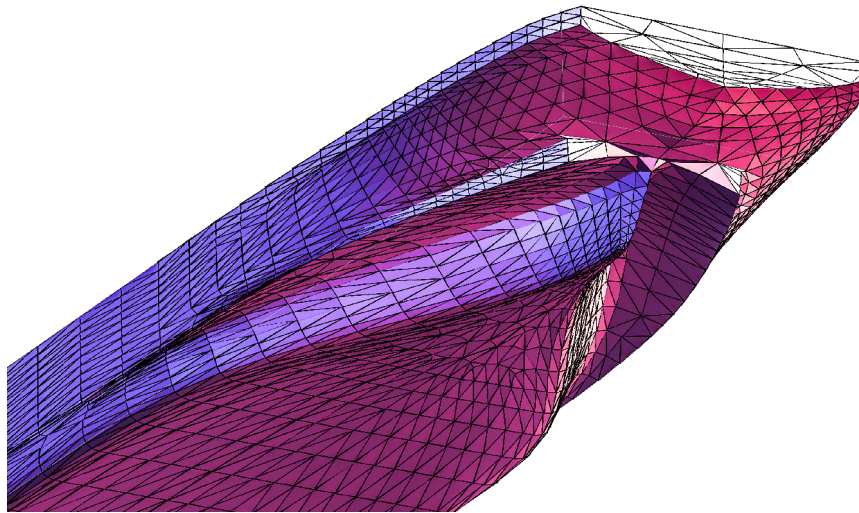
Figure 7.1: Example of hull panelisation - 3D panel method. Aft part of the test vessel B.

A less precise method is based on the strip-theory approximation, which, however, can make effective use of the classical simplified representation of vessels through sections. In this approach, as usual, the integral (7.8) is approximated by an integration of roll moments calculated for 2D sections along the hull. To determine the sectional roll moment, each hull section is discretised with a finite number of 2D linear panels (see Figure 7.2), which are then used for determining Froude-Krylov forces and moments acting on each panel. Each panel is defined with a set of particulars (length, centroid position and unit normal vector). The summation of contributions from each panel in the section provides the sectional roll moment.

The drawback of this method is that it does not account for the exact three-dimensional hull shape, but rather uses the strip-theory approximation to obtain the total Froude-Krylov roll moment. Nevertheless, the strip-method can be expected to provide results that are close to those obtained from the 3D panel method for hull shapes having high values of longitudinal prismatic coefficient C_P.
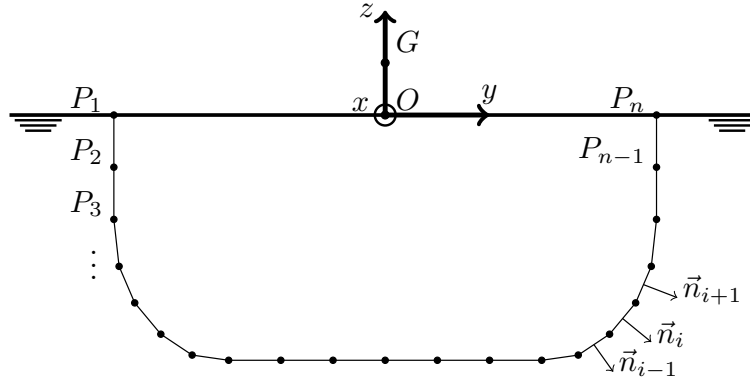
Figure 7.2: Example of section panelisation - 2D panel method (strip-theory).

For the purpose of the thesis, a code for 2D panel and 3D panel Froude-Krylov effective wave slope coefficient was developed.

A further simplification is applied in the method proposed by IMO ("IMO method", described in Section 4.4.2) in the framework of Second Generation Intact Stability Criteria for Level 2 vulnerability assessment for Dead Ship Condition (IMO, 2017). The principle of the method is to transform each true hull section into an "equivalent" rectangular section, keeping, as far as possible, the section breadth at waterline and the sectional underwater area (see Figure 7.3, where shaded area represents the "equivalent" rectangular section). This transformation allows using the exact analytical solution for the sectional Froude-Krylov wave moment of rectangular sections, instead of requiring the panelisation of the true section. The "total" wave moment is then obtained following the strip-theory approach by integration of sectional wave moments over the ship length. A first version of this simplified methodology was presented by Umeda & Tsukamoto (2008). However, since ship sections are, in general, not rectangular, in some cases the IMO methodology may provide poor approximations of the true Froude-Krylov roll moment. Conversely, the "IMO method" can be expected to provide better approximations for full hull forms, having high vertical prismatic coefficient C_{VP} as well as high longitudinal prismatic coefficient C_P.
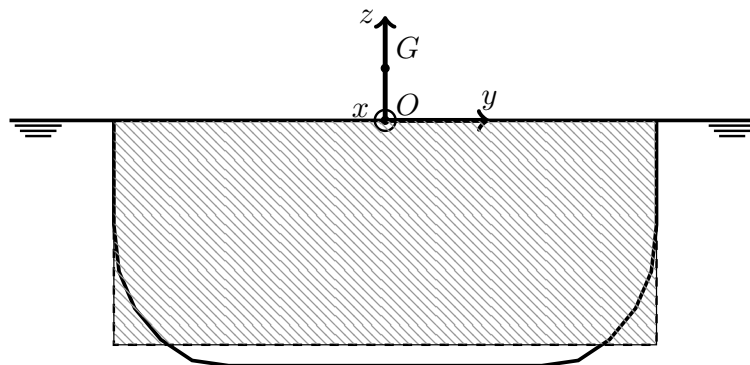
Figure 7.3: Example of section transformation to a rectangular shape with the same area and breadth - IMO methodology.

7.2.3 Semi-empirical methods

In general, semi-empirical methods for effective wave slope coefficient estimation are easy to use, but, strictly speaking, their prediction accuracy is limited to hull forms which do not significantly differ from those used in the development of the method. Such methods are based on some form of regression of the effective wave slope coefficient and can be developed, in principle, from experimental data or from calculations of higher complexity and accuracy. Moreover, in such methods, the effective wave slope coefficient is typically provided at natural frequency only. There is a limited number of semi-empirical methods available in literature (e.g. Blume, 1979; IMO, 2008a,b; Watanabe, 1938; Yamagata, 1959), and none of them, to the author's best knowledge, is intended to cover river-sea ships.

The semi-empirical prediction method proposed by Blume (1979) provides the effective wave slope coefficient only at natural roll frequency. The effective wave slope coefficient as a function of the non-dimensional natural roll period according to Blume (1979) is reconstructed in Figure 7.4. In the figure, the full line is the mean prediction curve corresponding to conventional (at the time of development) hull shapes and $\overline{GM}$ values, and the dashed lines provide an indication of the prediction intervals. On the horizontal axis of Figure 7.4, T_φ is the roll natural period, B is the ship breadth, and g is the gravitational acceleration.
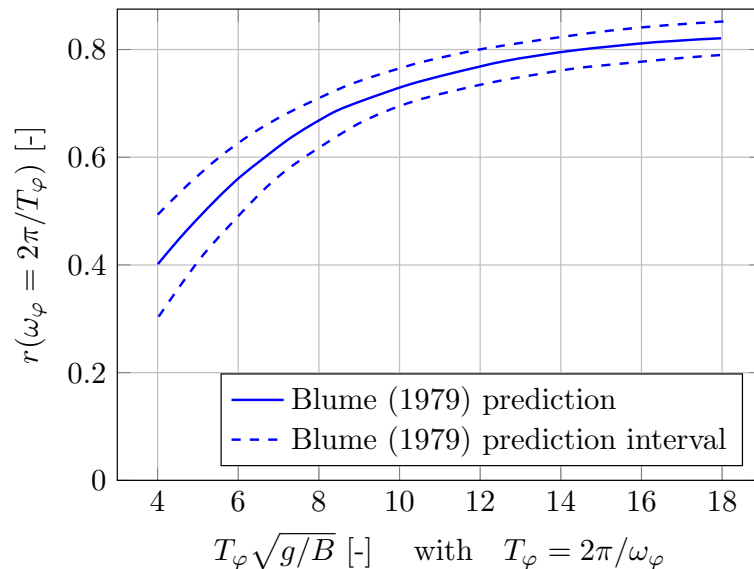
Figure 7.4: Effective wave slope coefficient at natural roll frequency. The Figure is reconstructed from Blume (1979).

Another semi-empirical method is given in the 2008 IS Code within the Weather Criterion (IMO, 2008a). As the Weather Criterion is designed to assess the ability of the ship to withstand the combined effect of wind gust and beam waves at resonance, the effective wave slope coefficient for this purpose is estimated, as in case of Blume (1979), only at natural roll frequency. As indicated in MSC.1/Circ.1281 (IMO, 2008b), the method derives from the work of Watanabe (1938) with subsequent simplifications from Yamagata (1959). More precisely, Watanabe (1938) developed an approximate formula, based on Froude-Krylov calculations assuming trochoidal waves for simplified hull shapes, with the effective wave slope coefficient formula depending on a set of influential parameters: wave length, vertical position of centre of gravity, metacentric height, breadth, draught, block coefficient and water plane area coefficient. A further simplification was then reported by Yamagata (1959), having the following form:

$$r = 0.73 + 0.6\overline{OG}/T \tag{7.9}$$

which is the form presently used within the IMO Weather Criterion. In the expression (7.9), $\overline{OG} = \overline{KG} - T$ is the vertical position of centre of gravity above the waterline, and T is the ship draught. Yamagata (1959) reported a good agreement between formula (7.9) and results calculated for 60 actual ships using the approach by Watanabe (1938), as reconstructed in Figure 7.5. Conversely, results from Fujino et al. (1993), Francescutto et al. (2001) and Francescutto & Serra (2002) indicate that the semi-empirical formula (7.9) can be conservative compared to experimental results or Froude-Krylov calculations for vessels with large values of B/T and/or $\overline{OG}/T$.
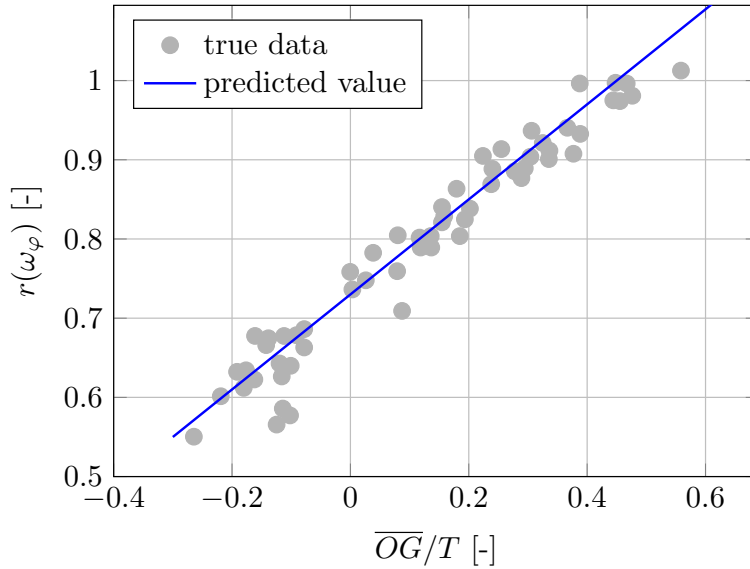
Figure 7.5: Effective wave slope coefficient at natural roll frequency, according to IMO Weather Criterion formulation, reconstructed from Yamagata (1959).

7.3 Vessel database and loading conditions

For the purpose of the present analysis, vessels from the database (given in Section 1.2, not including the validation vessels from Section 1.2.2) are selected for systematic calculation of effective wave slope coefficient as a function of frequency, as well as at natural roll frequency, using different methodologies. For each vessel, a range of operational conditions was considered in order to have a broad range of characteristic parameters. An overview of the vessels' particulars and principal dimensionless coefficients is given in Appendix B.

For the purpose of the study, three draughts were used for each vessel: a maximum draught corresponding to the scantling draught, a draught corresponding to the minimum draught enabling full immersion of the tunnels, and an intermediate draught conventionally set as the average between the previous two. All calculations were carried out for even keel condition (i.e. zero trim). Regarding the loading conditions, a wide range of tested $\overline{KG}$ was chosen so as to cover realistic loading conditions. The minimum $\overline{KG}$ was taken about half of the scantling draught, whereas the maximum $\overline{KG}$ corresponds to metacentric heights around $0.3\,\text{m} \div 0.5\,\text{m}$, depending on the vessel and draught. For simplicity, the range of $\overline{KG}$ was kept constant when varying the calculation draught. The considered database eventually comprises a total of 567 vessel-draught-$\overline{KG}$ combinations. For each vessel and loading condition in the database, different dry roll radii of inertia k_{xx} were considered, corresponding to $0.25B$, $0.30B$, $0.35B$, $0.40B$ and $0.45B$. The dry yaw radius of inertia k_{zz} was kept constant and equal to $0.25L_{WL}$. Therefore, a total of 2835 vessel-draught-$\overline{KG}$-k_{xx} combinations were considered. Furthermore, for each vessel and condition, the natural roll frequency ω_φ was calculated according to (7.7).

Furthermore, more detailed calculation results are provided for the three test vessels A, B, and C. Their particulars, and body lines and considered loading conditions are given in Section 4.7. Additionally, considered loading conditions together with the roll natural frequency ω_φ (according to (7.7)) and the corresponding roll natural period $T_\varphi = 2\pi/\omega_\varphi$ used for this purpose, are given in Table 7.1.

Table 7.1: Particulars and loading conditions of the test vessels.

	Vessel A	Vessel B	Vessel C
Type	Tanker	Container vessel	Container vessel
Draught description	maximum	minimum	intermediate
T [m]	4.3	2.0	2.5
$\overline{KG}$ [m]	3.5	2.5	4.0
$\overline{GM}$ [m]	1.37	4.02	1.71
k_{xx} [m]	$0.35B$	$0.30B$	$0.40B$
k_{zz} [m]	$0.25L_{WL}$	$0.25L_{WL}$	$0.25L_{WL}$
ω_φ [rad/s]	0.816	1.382	0.771
T_φ [s]	7.700	4.546	8.150

7.4 Comparison of effective wave slope coefficient calculation methods

In this section, the methods described in Section 7.2 are applied to the database of vessels described in Section 7.3, and results of the predictions are compared. The "reduced 3DOF" method (Section 7.2.1) is assumed to be the most accurate among the considered methods, because it better represents hydrodynamic effects, within the limit of the considered approximations. For this reasons, it will therefore be used as reference in the comparisons.

Hydrodynamic coefficients for the reduced 3DOF method (Section 7.2.1) were determined for the vessels in the database by the strip-theory code ShipmoPC Version 3.5.8, with sectional calculations based on Boundary Element Method (McTaggart, 1997). The 3D panel method (Section 7.2.2) was applied using in-house code designed for the purpose of this thesis, by discretising the actual hull surface into approximately $5000 \div 43000$ panels, depending on the size and complexity of a hull. Afterwards, to increase the accuracy of numerical integration of (7.8), the mesh was refined through three sequential applications of regular refinement (splitting of each triangle in four triangles using mid points of edges). The IMO method (Section 7.2.2) was applied by using a total of 21 sections for each vessel, according to the procedure described in Section 4.4.2.

Representative examples of effective wave slope coefficients calculated with the three methods for the test vessels A, B and C and associated loading condition given in Table 7.1, are shown in Figures 7.6, 7.7 and 7.8, respectively.

It can be noticed that, for all three vessels, the 3D panel method and the IMO method, which are both based on the Froude-Krylov approximation, provide very close results, particularly for vessels B and C which have larger C_B and C_P (see Table 1.2). The effective wave slope coefficient calculated by the reduced 3DOF method tends to be smaller than that obtained by the other two methods, for all three vessels. As discussed hereinafter, the tendencies observed for the three samples vessels will be confirmed by the behaviour observed for the whole database.

Furthermore, it is noted that qualitatively similar results were obtained in the past by Mizuno (1973, 1975), when he compared the effective wave slope coefficient based on linear Froude Krylov assumption, and the effective wave slope coefficient calculated by using a coupled roll-sway model based on linear hydrodynamics, neglecting yaw, but taking into accound the effect of linear damping. His findings were also supported by experimental results. Figures 7.6, 7.7 and 7.8, also show that the effective wave slope coefficient calculated with the exact Froude-Krylov approach ("3D panel") and by considering hydrodynamic effects ("reduced 3DOF"), while being noticeably different at the roll natural frequency, tend to converge in the region of low frequencies. This confirms the considerations of Umeda & Tsukamoto (2008) based on the work by Tasai (1965), regarding the suitability of the Froude-Krylov approximation in the range of long waves.
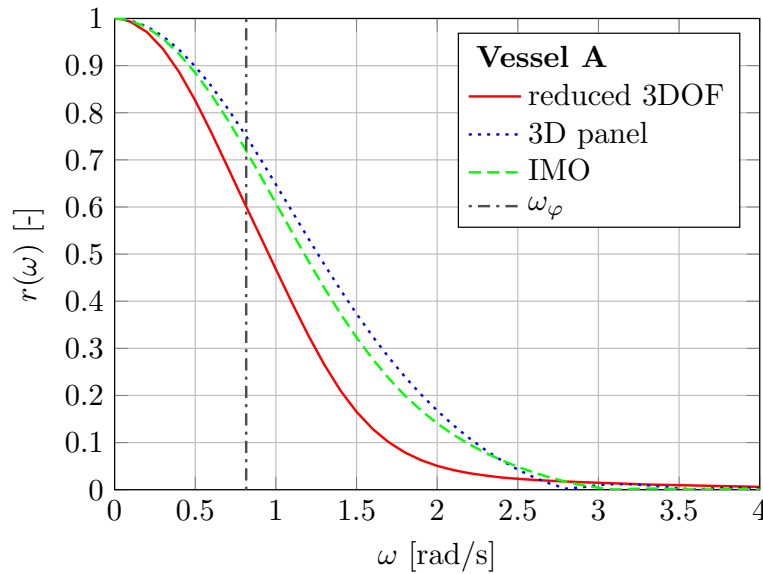
Figure 7.6: Frequency dependent effective wave slope coefficients, as determined by different methods, for sample vessel A. The figure also reports the calculated roll natural frequency.
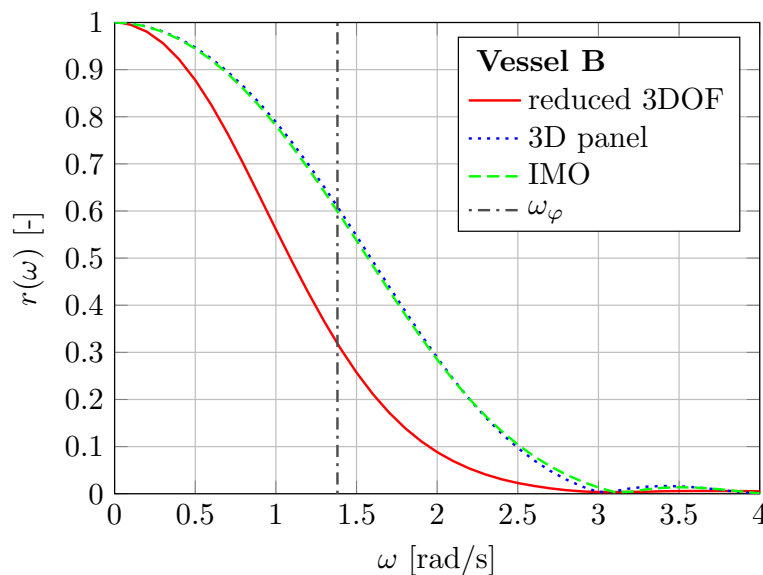
Figure 7.7: Frequency dependent effective wave slope coefficients, as determined by different methods, for sample vessel B. The figure also reports the calculated roll natural frequency.
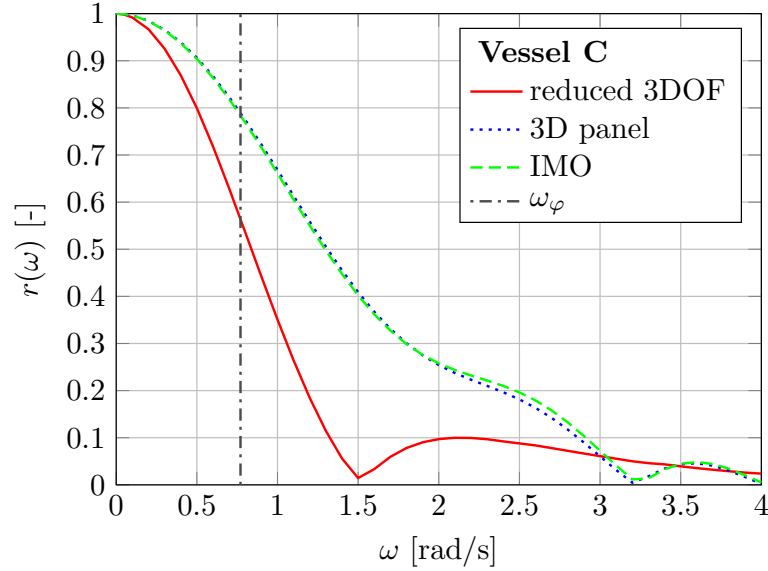
Figure 7.8: Frequency dependent effective wave slope coefficients, as determined by different methods, for sample vessel C. The figure also reports the calculated roll natural frequency.

In order to represent the large dataset, the first set of results will be presented herein in terms of percentile levels as obtained from the distribution of data. In particular, the data will be represented through 25%, 50% (median) and 75% percentiles. In addition, minimum and maximum values will also be reported to give an indication of the extremes. The range between the 25% and the 75% percentiles is the interquartile range and it contains 50% of the data.

The original effective wave slope coefficient data were calculated as a function of the dimensional wave frequency ω. The same set of calculation frequencies was used for all vessels, from $0.1\,\text{rad/s}$ up to $4.0\,\text{rad/s}$, with constant steps of $0.1\,\text{rad/s}$. To better cover the low frequency range, an additional calculation frequency was also considered at $0.05\,\text{rad/s}$. However, in order to combine results from different vessels, data have been eventually analysed as a function of the non-dimensional wave number, defined as follows:

$$\hat{k} = k_w B = \omega^2 B / g \tag{7.10}$$

As a result of the quadratic transformation from ω to $\hat{k}$, the available data are not uniformly distributed in terms of non-dimensional wave number $\hat{k}$. Moreover, non-dimensional wave numbers for which data are available do not coincide among different vessels, unless the vessels have the same breadth. Therefore, the distribution of data, and the associated percentile levels, were calculated using a "sliding window" technique, where subsets of data are analysed for different intervals (i.e. "windows") of $\hat{k}$, similar to what was done, in a different context, by Bulian & Francescutto (2005). In this study, the "windows" specified for the analysis are non-overlapping and have adaptive widths, which try to follow the distribution of data points with the aim of keeping a similar number of samples in each window. Figure 7.9 shows the number of data points within each window, as a function of the centre of the window, and the widths of the bins in the figure correspond to the widths of the corresponding window used in the analysis. It is underlined that the number of points in each window can exceed the total number of combinations vessel-draught-$\overline{KG}$-k_{xx} (i.e. 2835 - see Section 7.3) as data from multiple calculation frequencies can fall in the same window of analysis.

First, Figure 7.10 shows the analysis of data in terms of effective wave slope coeffcient as estimated by the reduced 3DOF method as a function of $\hat{k}$. Then, the reduced 3DOF approach is compared to two linear Froude-Krylov methods: the IMO method and the 3D panel method,
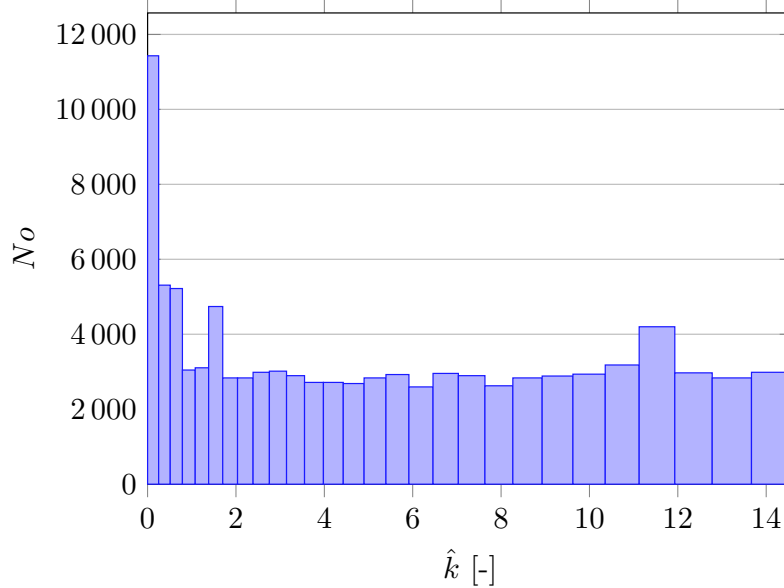
Figure 7.9: Number of samples in each analysis window. The centre and width of each bin correspond, respectively, to the centre and width of the corresponding window as used in the analysis.

both discussed in Section 7.2. These analyses were carried out for all the vessel-loading condition combinations (2835 in total) described in Section 7.3.

The comparison is carried out by analysing:

- Differences, as a function of $\hat{k}$, between IMO method and reduced 3DOF method, calculated as $\Delta r(\hat{k}) = r_{IMO}(\hat{k}) - r_{3DOF}(\hat{k})$, with results shown in Figure 7.11; and

- Differences, as a function of $\hat{k}$, between 3D panel method and reduced 3DOF method, calculated as $\Delta r(\hat{k}) = r_{3Dpanel}(\hat{k}) - r_{3DOF}(\hat{k})$, with results shown in Figure 7.12.

It is noted that all considered methods in the present comparison are such that the effective wave slope coefficient tends to 1.0 as the frequency ω tends to zero. Therefore, differences among methods for $\hat{k} \to 0$ always tend to zero. Although calculations could not be numerically performed for exactly zero frequency for numerical reasons, such theoretical limit was used in the reporting of results.

From the results in Figure 7.11 and Figure 7.12, it can be seen that, in general, the IMO method and the 3D panel method (i.e. methods based on the Froude-Krylov approximation) can be considered to be more conservative than the reduced 3DOF method, having a tendency to a positive median in the difference, with a maximum median difference of about 0.3. Nevertheless, there is a minor number of conditions where the IMO and the 3D panel methods can estimate significantly smaller values of effective wave slope coefficient at some frequencies. This can occur for low metacentric heights, for frequencies significantly higher than typically realistic natural roll frequencies. It can also occur for higher metacentric heights, in the high frequency region, as a result of the humps and hollows of the effective wave slope coefficient based on Froude-Krylov approximation compared to the smoother behaviour of the effective wave slope coefficient based on the reduced 3DOF method. However, these latter cases are generally associated with small effective wave slope coefficients.

The results of the difference between IMO method and reduced 3DOF method (Figure 7.11), are apparently similar to the corresponding results for the 3D panel method (Figure 7.12). Therefore, a comparison of results between 3D panel method and IMO method has been performed for the overall database and the corresponding statistical analysis is shown in Figure
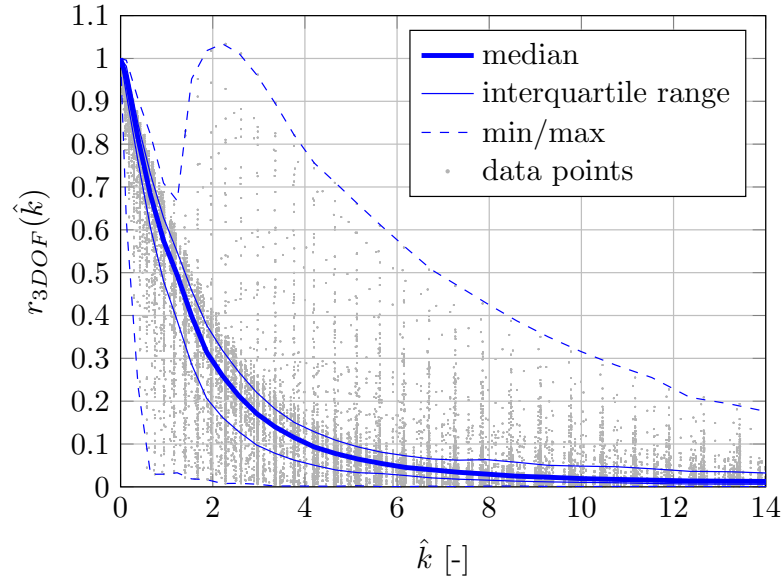
Figure 7.10: Statistical analysis of frequency dependent effective wave slope coefficient as estimated by the reduced 3DOF method.
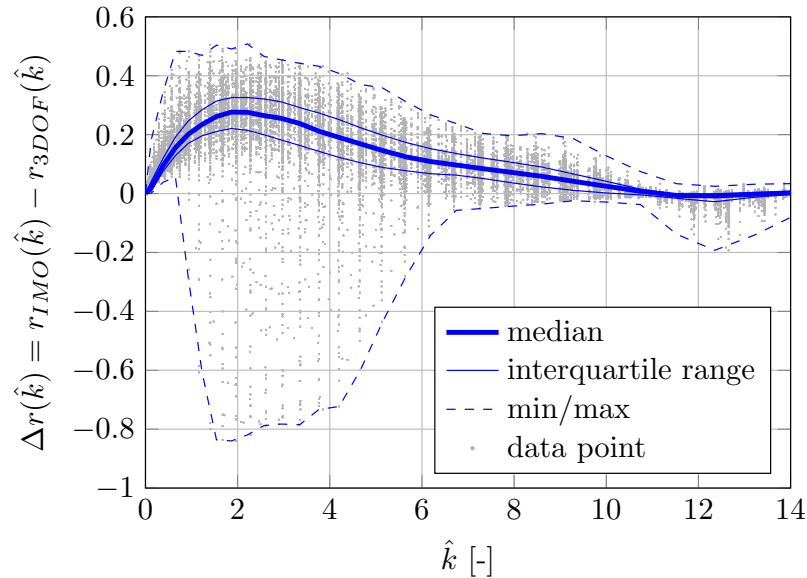

Figure 7.11: Statistical analysis of frequency dependent effective wave slope coefficient difference between IMO method and reference reduced 3DOF method.

7.13. The outcomes indicate that, for the considered database of vessels and loading conditions, these two methods provide a very close estimation of the frequency dependent effective wave slope coefficient, having maximum absolute value of median difference of about 0.015, and maximum interquartile range of about 0.025. Moreover, the overall bias difference between these two methods is very small, with a tendency for the 3D panel method to predict slightly larger effective wave slope coefficients than the IMO method in the range of low dimensionless wave numbers, and with the opposite occurring in the range of high wave numbers. The overall good matching between these two methods is a consequence of the full hull forms of river-sea ships, with long parallel middle bodies and high midship coefficients. With vessels having such characteristics, the sectional transformation performed by the IMO methodology, where actual sections are substituted by "equivalent rectangles", still provides a good matching between original and transformed sections. These outcomes are actually in line with the example results
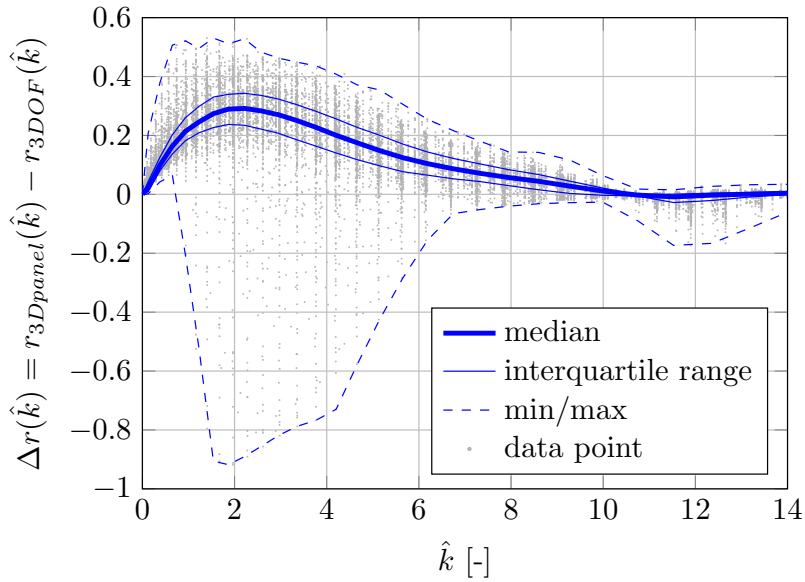
Figure 7.12: Statistical analysis of frequency dependent effective wave slope coefficient difference between 3D panel method and reference reduced 3DOF method.
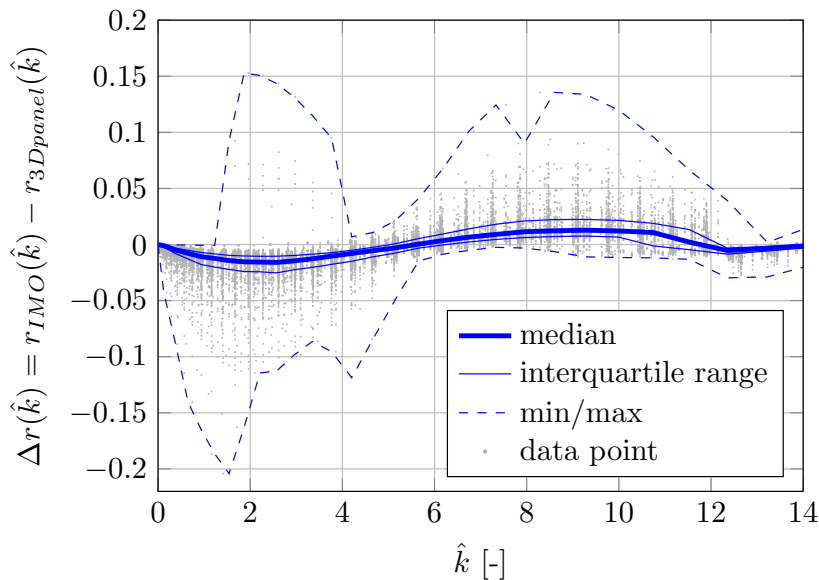
Figure 7.13: Statistical analysis of frequency dependent effective wave slope coefficient difference between IMO method and 3D panel method.

obtained for the three sample vessels (Figures 7.6, 7.7 and 7.8), where the 3D panel method and the IMO method provide very close results for all vessels. Overall, this implies that the IMO method and the 3D panel method, both of which are based on the linear Froude-Krylov approach for the estimation of the effective wave coefficient, can be expected to provide close results when applied to river-sea ships.

Further comparisons are carried out between the effective wave slope coefficient at natural roll frequency as estimated by the reduced 3DOF method and by the two semi-empirical methods discussed in Section 7.2.3 ("Blume method" and "IMO Weather Criterion method").

In Figures 7.14 and 7.15, the effective wave slope coefficients obtained by the reduced 3DOF method at natural roll frequency are compared to the Blume's curve. The figures report information for the overall database and, in addition, they report also curves of effective wave slope coefficient for different dimensionless roll natural periods $T_\varphi \sqrt{g/B}$, for the test vessels

A, B and C. In the plotting of the curves for the three vessels in Figure 7.14 the dry radius of inertia was kept constant for each vessel (see Table 7.1), whereas $\overline{KG}$ was varied for each vessel (Vessel A: $2.5\,\text{m} \leq \overline{KG} \leq 4.5\,\text{m}$; Vessel B: $2.5\,\text{m} \leq \overline{KG} \leq 5.0\,\text{m}$; Vessel C: $2.0\,\text{m} \leq \overline{KG} \leq 4.0\,\text{m}$; variation step $\delta\overline{KG} = 0.5\,\text{m}$ for all vessels). Instead, in Figure 7.15, the $\overline{KG}$ of each vessel was kept constant (see Table 7.1) and the dry radius of inertia was varied for each vessel in the range $0.25 \leq k_{xx}/B \leq 0.45$ with a variation step $\delta k_{xx}/B = 0.05$ for all vessels (in accordance with the variation of k_{xx}/B for all the vessels in the database, as discussed in Section 7.3).
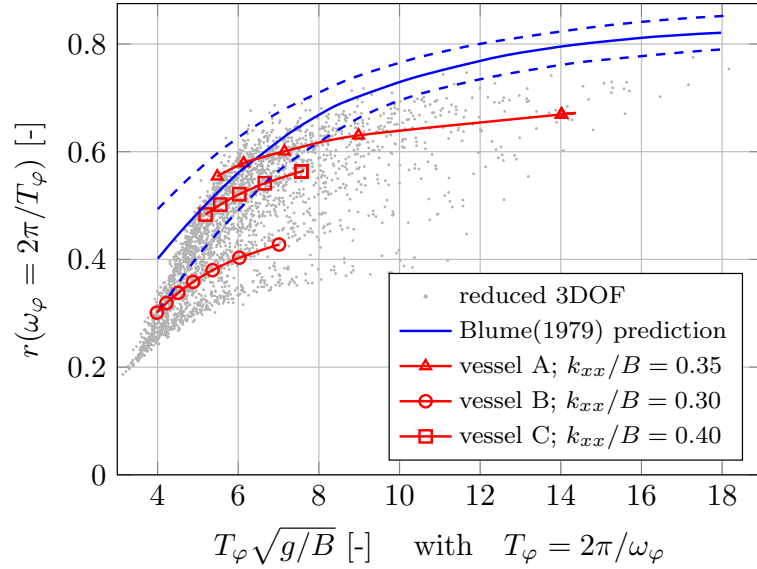
Figure 7.14: Comparison between effective wave slope coefficient at natural roll frequency according to Blume (1979) and according to reduced 3DOF method. Highlighted curves correspond to the sample vessels A, B and C, with fixed k_{xx}/B and variable $\overline{KG}$ (Vessel A: $2.5\,\text{m} \leq \overline{KG} \leq 4.5\,\text{m}$; Vessel B: $2.5\,\text{m} \leq \overline{KG} \leq 5.0\,\text{m}$; Vessel C: $2.0\,\text{m} \leq \overline{KG} \leq 4.0\,\text{m}$; variation step $\delta\overline{KG} = 0.5\,\text{m}$ for all vessels).
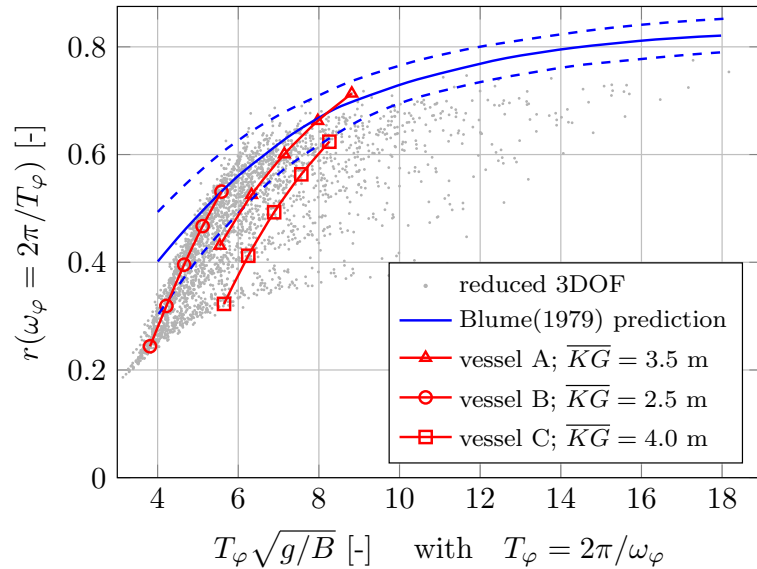
Figure 7.15: Comparison between effective wave slope coefficient at natural roll frequency according to Blume (1979) and according to reduced 3DOF method. Highlighted curves correspond to the sample vessels A, B and C, with fixed $\overline{KG}$ and variable k_{xx}/B ($0.25 \leq k_{xx}/B \leq 0.45$ and variation step $\delta k_{xx}/B = 0.05$ for all vessels).

Results for the whole database in Figure 7.14 and Figure 7.15 indicate that the effective wave slope coefficient predicted by the Blume's approach tends to be larger, and, thus conservative, in comparison to results by the reduced 3DOF method. However, the overall trends of the Blume's method and the reduced 3DOF method appears to be similar. This is particularly well exemplified by the curves associated with the three sample vessels. By considering both the results in Figure 7.14 and in Figure 7.15 for the three sample vessels, it seems that the Blume's trend better represents results from the reduced 3DOF if it is assumed that k_{xx}/B increases when increasing $\overline{KG}$.

In Figure 7.16, a similar comparison for the overall database is presented, but this time between the results obtained with the reduced 3DOF method and with the IMO Weather Criterion method (see (7.9)). It can be seen that the effective wave slope coefficient of river-sea ships at natural roll frequency predicted by the IMO Weather Criterion formula significantly differs from the results obtained by the reduced 3DOF method. The comparisons appear to be worse than those reported in Figures 7.14 and 7.15 for the Blume method. River-sea ships have higher B/T ratios than standard sea-going ships, and for high $\overline{KG}$, the ratio $\overline{OG}/T$ can be significantly higher than the indicated applicability range of the IMO Weather Criterion formula. In fact, the indicated ranges of applicability of IMO Weather Criterion are $B/T < 3.5$, $-0.3 \leq \overline{OG}/T \leq 0.5$ and roll period smaller than $20\,\mathrm{s}$ (IMO, 2008a). Having in mind the typical parameters of river-sea ships (see Appendix B), the disagreement between the results obtained by the IMO Weather Criterion formula and the reduced 3DOF method could have been expected. Moreover, the effective wave slope coefficients predicted by the IMO Weather Criterion formula appear to be unrealistic in the range of large $\overline{OG}/T$ ratios. These outcomes confirm the results obtained in the past for sea-going vessels, and also simplified two-dimensional sections, characterised by large values of B/T and/or $\overline{OG}/T$ (Fujino et al., 1993; Francescutto et al., 2001; Francescutto & Serra, 2002; IMO, 2002; Sato et al., 2008).

Similar to Figure 7.14 and Figure 7.15, Figure 7.17 (constant k_{xx}/B, variable $\overline{KG}$) and Figure 7.18 (variable k_{xx}/B, constant $\overline{KG}$) compare the effective wave slope coefficient at natural roll frequency obtained using the 3DOF method for the three sample vessels as a function of $\overline{OG}/T$ with predictions from IMO Weather Criterion. In Figure 7.17, an almost linear increase of $r(\omega_\varphi)$ is observed with the increase of $\overline{OG}/T$ for constant k_{xx}/B, and this is in line with the Weather Criterion, at least in terms of general qualitative trend. Considering
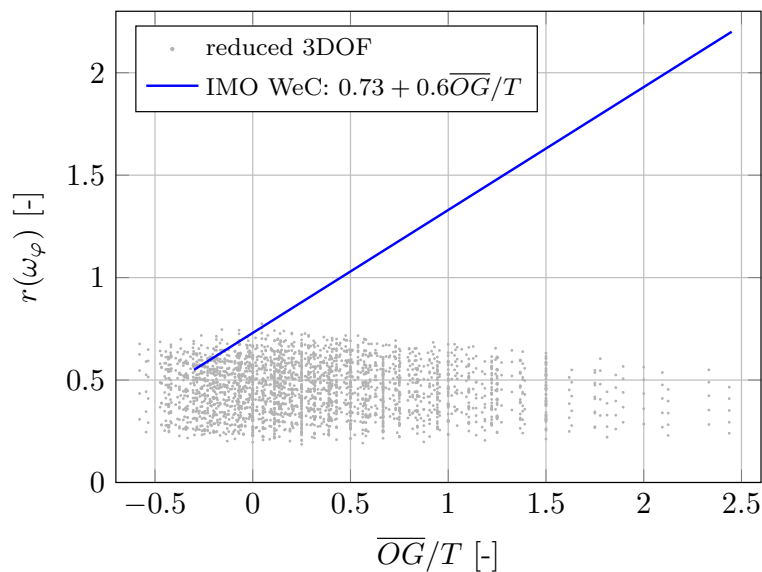

Figure 7.16: Comparison between effective wave slope coefficient at natural roll frequency according to IMO Weather Criterion (IMO, 2008a) and according to reduced 3DOF method.

both results from Figure 7.17 and Figure 7.18, it seems that also in this case the alignment may be improved if an increase of $\overline{KG}$ is assumed to be associated also with an increase of k_{xx}/B. Among the three sample vessels, vessel A, which is the one with the smallest B/T ratio and the smallest C_B and C_P coefficients, shows the best agreement with the IMO Weather Criterion formula. However, considering the other two vessels and the overall database, it appears that predictions of effective wave slope coefficient at the roll natural frequency according to IMO Weather Criterion are unsuitable for river-sea ships.
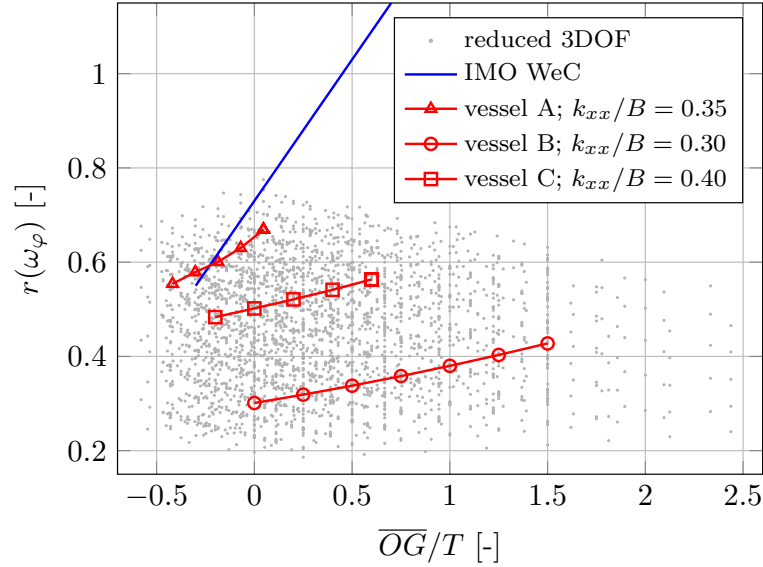
Figure 7.17: Comparison between effective wave slope coefficient at natural roll frequency according to IMO Weather Criterion (IMO, 2008a) and according to reduced 3DOF method. Highlighted curves correspond to the sample vessels A, B and C, with fixed k_{xx}/B and variable $\overline{KG}$ (Vessel A: $2.5\,\mathrm{m} \leq \overline{KG} \leq 4.5\,\mathrm{m}$; Vessel B: $2.5\,\mathrm{m} \leq \overline{KG} \leq 5.0\,\mathrm{m}$; Vessel C: $2.0\,\mathrm{m} \leq \overline{KG} \leq 4.0\,\mathrm{m}$; variation step $\delta\overline{KG} = 0.5\,\mathrm{m}$ for all vessels).
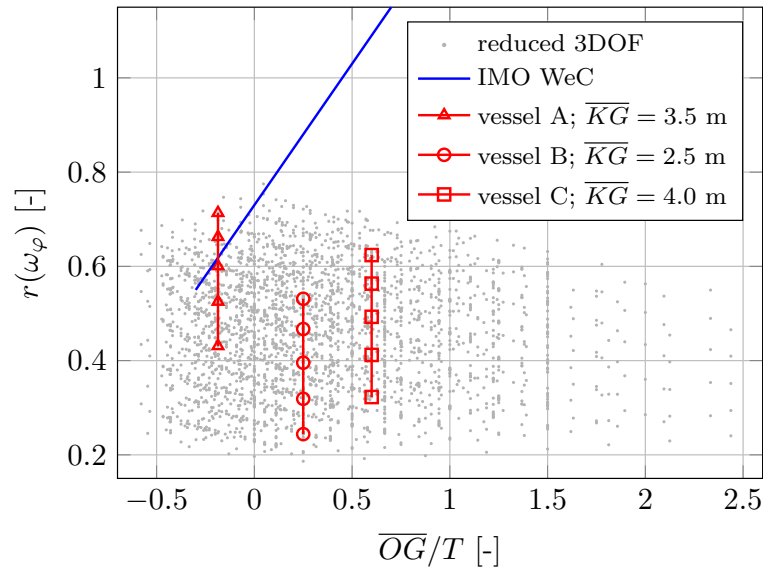
Figure 7.18: Comparison between effective wave slope coefficient at natural roll frequency according to IMO Weather Criterion (IMO, 2008a) and according to reduced 3DOF method. Highlighted curves correspond to the sample vessels A, B and C, with fixed $\overline{KG}$ and variable k_{xx}/B ($0.25 \leq k_{xx}/B \leq 0.45$ and variation step $\delta k_{xx}/B = 0.05$ for all vessels).

Interestingly, within Russian River Register (2015) the same formula (7.9) for effective wave slope coefficent estimation is foreseen to be applied to inland vessels and river-sea ships, but with additional limitation that $r \leq 1$. Presumably, r is limited in order to cope with the issue shown in Figure 7.16, where (7.9) tends to significantly overestimate effective wave slope coefficient at natural frequency, for high $\overline{OG}/T$.

7.5   Conclusions

This study presented an investigation on the applicability of different methods for the effective wave slope coefficient prediction to river-sea ships. A proper determination of the effective wave slope coefficient is, indeed, of particular importance in intact stability assessment when roll motion is to be predicted on the basis of simplified 1DOF approaches. This section provides a summary of the approach used in the study and the main conclusions drawn from the analysis.

Several methods for prediction of effective wave slope coefficient either over a range of wave frequencies or at the natural roll frequency, have been presented and compared, in the typical beam waves condition:

- A 3DOF approach based on linear hydrodynamics, which considers the coupling of sway and yaw with roll motion, under the approximation of neglecting the effect of damping, and provides a frequency-dependent effective wave slope coefficient ("reduced 3DOF method", Section 7.2.1);

- Two linear approaches taking into account Froude-Krylov roll moment only, one based on a direct 3D-panelization of the hull and one based on a strip-theory approach where the hull sections are approximated by rectangular sections, both providing a frequency-dependent effective wave slope coefficient ("3D panel method" and "IMO method", respectively, Section 7.2.2);

- Two semi-empirical methods, both estimating the effective wave slope coefficient at natural roll frequency only ("Blume method" and "IMO Weather Criterion method", Section 7.2.3).

The methods are characterised by different levels of complexity and accuracy in addressing the underlying hydrodynamics. The study was carried out on 31 self-propelled inland or river-sea vessels, considering different loading conditions and mechanical characteristics, which resulted in a total of 2835 examined vessel-draught-$\overline{KG}$-k_{xx} combinations. In addition, more detailed results have been reported and discussed for the three test vessels. In the study, the reduced 3DOF method was considered as the most accurate one, and it was therefore used as reference in the comparisons.

The two tested Froude-Krylov methods (3D panel method and IMO method) provide very similar results in the examined range of frequencies. This indicates that the two methods may be considered basically equivalent for the purpose of determination of effective wave slope coefficients of river-sea ships (see Figures 7.6, 7.7, 7.8, 7.11, 7.12 and, in particular, Figure 7.13). This result can be explained by the full hull forms typical of river-sea ships, which are characterised by long parallel middle bodies and high midship section coefficients. Consequently, the use of strip-theory and the approximation of ship sections with rectangles, as done in the IMO method, provide a sufficiently good approximation of the Froude-Krylov effective wave slope coefficient based on the exact hull form (3D panel method). Larger differences were observed, in fact, for the slenderer vessels (compare Figure 7.6 with Figures 7.7 and 7.8). Therefore, since the agreement between the two tested methods based on Froude-Krylov assumption is a result of the specific typical hull geometry of river-sea ships, the outcomes of the analysis

should not be considered as valid for conventional sea-going ships, which are usually featuring lower longitudinal and vertical prismatic coefficients.

The two tested semi-empirical methods for the estimation of effective wave slope coefficient at the natural roll frequency are targeting standard sea-going ships. Due to differences in design between river-sea ships and standard sea-going ships, the two examined approaches appeared to be unsuitable for application to river-sea ships (see Figures 7.14, 7.15, 7.16, 7.17 and 7.18). Furthermore, when applied to river-sea ships, the two semi empirical methods exhibit a general tendency to overestimate the effective wave slope coefficients at the natural roll frequency when compared to the results obtained by the reduced 3DOF method. This particularly applies to the predictions obtained by the method embedded in the IMO Weather Criterion. Such results should have been, however, expected, as the characteristics of river-sea ships are for the most part outside of the ranges of parameters used in the development of the IMO Weather Criterion.

According to the obtained results, the approaches based on Froude-Krylov assumption (3D panel method and IMO method) appear to be conservative in comparison to the reduced 3DOF method. In the vast majority of cases the effective wave slope coefficients from the 3D panel method and from the IMO method are greater than those from the reduced 3DOF method in the tested range of frequencies (see Figures 7.6, 7.7, 7.8, 7.11 and 7.12), particularly in the vicinity of realistic values of the roll natural frequency. The level of conservativeness, in some cases, was very large. Such results are also supported by the available literature. The opposite was found to be possible in case of high frequencies for metacentric heights towards the lower bound of tested interval of $\overline{GM}$. For larger metacentric heights this may happen in regions of high frequencies where the effective wave slope is, in general, small.

Therefore, for the purposes of intact stability assessment of river-sea ships on the basis of simplified roll models, wave excitation could be accounted for by one of the following methods:

a) A method based on the Froude-Krylov assumption, e.g. a direct pressure integration method or the simplified so-called IMO method, which is simple to implement, but comes at the cost of conservativeness and limited accuracy;

b) The herein presented reduced 3DOF method, or another, similar method considering dynamic and hydrodynamic coupling of roll with sway and yaw, which provides for a more accurate representation of dynamic and hydrodynamic effects, but requires the use of a seakeeping software.

While option b) may be more computationally challenging, the cost of its use could be offset by the benefits of a more appropriate stability assessment of river-sea ships.

It should be noted that semi-empirical methods for predicting the effective wave slope coefficient at natural roll frequency with sufficient accuracy, are not available for river-sea ships. A possible way of addressing this problem could be to develop a new semi-empirical model based on systematic analysis of directly calculated frequency-dependent effective wave slope coefficients for river-sea ships.

With the introduction of 3DOF method for the effective wave slope coefficient estimation it is reasonable to apply the same method to the natural roll period estimation. Although the exact procedure is already described briefly and the formula is given in (7.7), more detailed analysis will be carried out in the next chapter.

Chapter 8

Natural roll period of river-sea ships

8.1   Introduction

The natural roll period T_φ (or alternatively the natural roll frequency ω_φ) is one of the basic parameters in stability assessment in rough weather due to the phenomenon of resonant frequency, and is thus subject of research in this thesis. The resonant frequency in beam waves was thoroughly examined in the past, and was considered as the most important (if not the only important) for stability assessment (Blume, 1979; IMO, 2008b; Yamagata, 1959), and even maritime regulation currently in force consider only this dynamic condition (IMO, 2008a). Furthermore, the Second Generation Intact Stability Criteria also considers the natural roll period as a basic parameter, for which the formula given in the 2008 IS Code was suggested as the estimation method (IMO, 2019a).

In this Chapter, a detailed overview of some of the existing methods for the natural roll frequency estimation is presented, the methods are compared and further discussed, pointing out their advantages and disadvantages. The main focus was given to the possibility of applying the direct calculation of the natural roll period based on linear seakeeping hydrodynamics, following the conclusions of Chapter 7. The possibility of improving the IMO method for the natural roll frequency estimation was considered and an alternative formula was proposed. For this purpose, the same vessel database and loading conditions described in Section 7.3 are used.

The present Chapter is a result of a study contained in the report Rudaković (2018).

8.2   Natural roll frequency estimation

Although the natural roll frequency has been studied for a long time (see, for example Froude, 1861), it seems that the estimation methods have not been significantly improved ever since. Therefore, in order to single out the most appropriate method for application to river-sea ships, the following natural roll period estimation methods are considered:

- Predictions using 3-degrees-of-freedom direct calculations based on linear seakeeping hydrodynamics ("reduced 3DOF" approach, mentioned earlier in Chapter 7);

- Predictions using 1-degree-of-freedom direct calculations based on linear seakeeping hydrodynamics ("1DOF" approach);

- Predictions using semi-empirical methods.

8.2.1 Direct calculation based on linear seakeeping hydrodynamics - Reduced 3DOF approach

The natural roll frequency is influenced by sway and yaw motions. Therefore, using the three-degree-of-freedom model could improve results. By neglecting the damping (following the principle explained in Section 7.2.1), the Equation (7.5) was obtained and written as follows:

$$I_{44,c}(\omega)\ddot{\varphi} + C_{44}\varphi = \widehat{F}_{4,c}(\omega)$$

The same equation can be rewritten in the following form:

$$\ddot{\varphi} + \frac{C_{44}}{I_{44,c}(\omega)}\varphi = \frac{\widehat{F}_{4,c}(\omega)}{I_{44,c}(\omega)} \tag{8.1}$$

where natural roll frequency is

$$\omega_\varphi = \sqrt{\frac{C_{44}}{I_{44,c}(\omega)}} \tag{8.2}$$

which in expanded form is (based on the principle given by Bulian et al., 2008; Bulian & Francescutto, 2009, 2011):

$$\omega_\varphi = \sqrt{\frac{C_{44}\left(Q_{22}Q_{66} - Q_{26}Q_{62}\right)}{Q_{22}Q_{44}Q_{66} - Q_{22}Q_{46}Q_{64} - Q_{24}Q_{42}Q_{66} + Q_{24}Q_{46}Q_{62} + Q_{26}Q_{42}Q_{64} - Q_{26}Q_{44}Q_{62}}} \tag{8.3}$$

Note that natural roll frequency should be found for $\omega = \omega_\varphi$. This procedure of finding a characteristic root (see, for example Fossen, 2011), is graphically described in Figure 8.1:
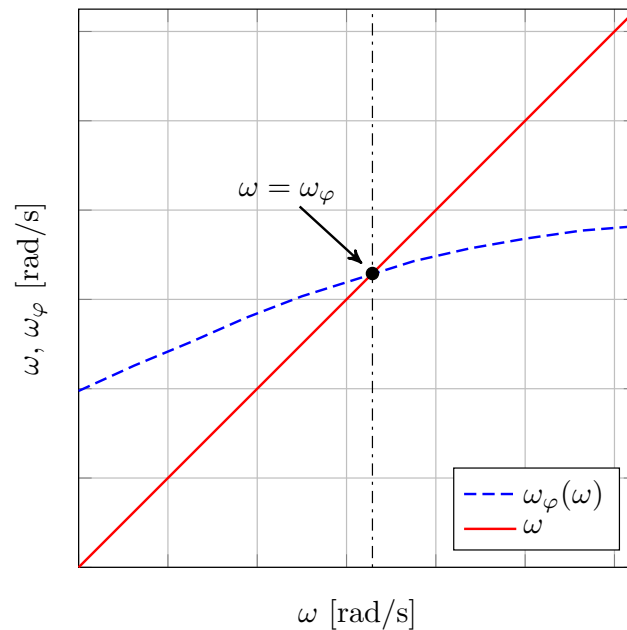
Figure 8.1: Characteristic root finding of natural roll frequency.

8.2.2   Direct calculation based on linear seakeeping hydrodynamics - 1DOF approach

A simple method for deriving natural roll frequency is by using one-degree-of-freedom linear model:

$$(M_{44} + A_{44}(\omega)) \ddot{\varphi} + B_{44}(\omega)\dot{\varphi} + C_{44}\varphi = F_4 \tag{8.4}$$

which can be written in the following form:

$$\ddot{\varphi} + \frac{B_{44}(\omega)}{M_{44} + A_{44}(\omega)}\dot{\varphi} + \frac{C_{44}}{M_{44} + A_{44}(\omega)}\varphi = \frac{F_4}{M_{44} + A_{44}(\omega)} \tag{8.5}$$

where the natural roll frequency is as follows:

$$\omega_\varphi = \sqrt{\frac{C_{44}}{M_{44} + A_{44}(\omega)}} = \sqrt{\frac{\Delta \cdot \overline{GM}}{M_{44} + A_{44}(\omega)}} = \sqrt{\frac{g\overline{GM}}{k_{xx}^2 \left(1 + \kappa_{44}(\omega)\right)}} \tag{8.6}$$

and κ_{44} is non-dimensional added roll mass moment of inertia coefficient. Similar procedure for obtaining characteristic root shown in Figure 8.1, should be also applied to the 1DOF for obtaining natural roll frequency.

Using the 1DOF model for obtaining the natural roll frequency is a simple approach, which seems to be widely used in seakeeping calculations. Nevertheless, as roll motion is coupled with sway and yaw, and for both the 1DOF and 3DOF estimations seakeeping calculations are necessary thus the complexity of calculations are similar, it is reasonable to use the more advanced 3DOF model. Therefore, only the 3DOF will be considered from now on.

8.2.3   Semi-empirical formulae

Usual way for natural roll period estimation is derived from the assumption of one-degree-of-freedom roll oscillations, as described in Section 8.2.2. If mass moment of inertia and added mass moment of inertia are, for the sake of simplicity, considered together, Equation (8.6) can be written as follows:

$$\omega_\varphi = \sqrt{\frac{g\overline{GM}}{k_{xx}'^2}} = \frac{\sqrt{g\overline{GM}}}{k_{xx}'} \tag{8.7}$$

where k_{xx}' is considered to be "wet" roll radius of inertia (in contrast to the "dry" roll radius of inertia k_{xx}). The natural roll period and the natural roll frequency are connected by the equation (4.13):

$$\omega_\varphi = \frac{2\pi}{T_\varphi}$$

while usually, in semi-empirical formulae it is common to express natural roll period in the following form:

$$T_\varphi = \frac{2\pi k_{xx}'}{\sqrt{g\overline{GM}}} \tag{8.8}$$

where the "wet" roll radius of inertia k_{xx}', is often written as $k_{xx}' = K = CB$, where C is the coefficient of roll radius of inertia, representing a percentage of ship breadth.

Solution proposed in similar form as given in (8.8) can be seen, for example, in Munro-Smith formula (Munro-Smith, 1973):

$$T_\varphi = \frac{2\pi \frac{1}{3} B}{\sqrt{g\overline{GM}}} \tag{8.9}$$

Moreover, as the ratio of $\pi/\sqrt{g} \approx 1$, some formulae made use of this approximations. It is a case for current IMO regulation formula within the Weather Criterion (IMO, 2008a), where coefficient C is defined as follows:

$$T_\varphi = \frac{2CB}{\sqrt{\overline{GM}}} \tag{8.10}$$
$$C = 0.373 + [0.023\,(B/d)] - [0.043\,(L/100)]$$

Even more simple form can be seen in formula given by Benford (1991):

$$T_\varphi = \frac{0.76B}{\sqrt{\overline{GM}}} \tag{8.11}$$

and formula by George (1983):

$$T_\varphi = \frac{0.8B}{\sqrt{\overline{GM}}} \tag{8.12}$$

or formula given by Bureau Veritas (2014), rules for inland navigation:

$$T_\varphi = 2.2\frac{0.35B}{\sqrt{\overline{GM}}} \tag{8.13}$$

It can be noticed that all of aforementioned formulae have the same form and the only difference is in "wet" roll radius of inertia. Moreover, another semi-empirical formulae obtain mass moment of inertia in more complex form, and make use of Equation (8.8) to estimate the natural roll period. It is the case with the formula of Peach & Brook (1987), where:

$$K = 0.3\sqrt{(B^2 + D^2)} \tag{8.14}$$

or another formula of Bureau Veritas (see Peach & Brook, 1987):

$$K = 0.289B\sqrt{1 + 4(\overline{KG}/B)^2} \tag{8.15}$$

A formula given by Kato (1956), which was used in the Japanese stability standard (see Yamagata, 1959), was proposed for use within the Weather Criterion. However, the procedure was considered to be tedious (see IMO, 2008b). Moreover, the formula was consider within the SGISC as an alternative for the mass moment of inertia estimation (see IMO, 2016b). Formula takes into account several ship particulars:

$$(K/B)^2 = F\left[C_B C_U + 1.1C_U(1 - C_B)(H_e/T - 2.2) + (H_e/B)^2\right] \tag{8.16}$$

where C_U is the upper deck area coefficient determined as deck area divided by $L_{PP} \cdot B$, H_e is effective depth calculated as $H_e = T + A_w/L_{PP}$, A_w is profile projected areas of erections and deck houses and F is a constant value depending on the ship type (e.g. 0.125 for passenger and/or cargo ships, 0.133 for tankers and 0.177 for whalers).

8.3 Vessel database and loading conditions

For the purpose of the natural roll period analysis, the database described in Section 1.2 and the loading conditions described in Section 1.2 are used. Therefore, total of 31 self-propelled vessels were used, taking into account different dry roll radii of inertia k_{xx}, three different draughts T and different vertical centre of gravities $\overline{KG}$. In total 2835 vessel-draught-$\overline{KG}$-k_{xx} combinations were considered, for which natural roll periods T_φ were estimated. These combinations and ranges are selected in order to cover all possible realistic loading conditions, which will be used for the direct calculation of the natural roll period. However, there is not a method specifically developed for inland vessels, that can estimate the dry roll radius of inertia. Therefore, at this instance, it will be assumed in the mentioned range, while the proper method for the dry roll radius of inertia estimation will remain an open question. The supplementary data for the database is given in Appendix B.

8.4 Comparison of different methodologies

The natural roll frequency was estimated using the 3DOF linear hydrodynamic approach, together with some of the semi-empirical methods, for all variations of vessels and loading conditions in the database. Nevertheless, problem of adequate comparison arises because experimental results the of natural roll frequency for river-sea ships are not readily available. Therefore, in this report, results obtained by the 3DOF linear hydrodynamic approach will be deemed as the benchmark data.

In Figure 8.2 the natural roll frequency estimated by the 3DOF method (see Section 8.2.1) as a function of natural roll frequency estimated by the IMO method (see Equation (8.10)) is plotted. Because the IMO method considers the dry roll radius of inertia empirically, significant scattering around ideal value can be seen. Five groups of data can be noticed in the plot, corresponding to the five different dry roll radii of gyration used for the 3DOF method estimation. Furthermore, in the IMO method it is not clear how the dry roll radius of inertia
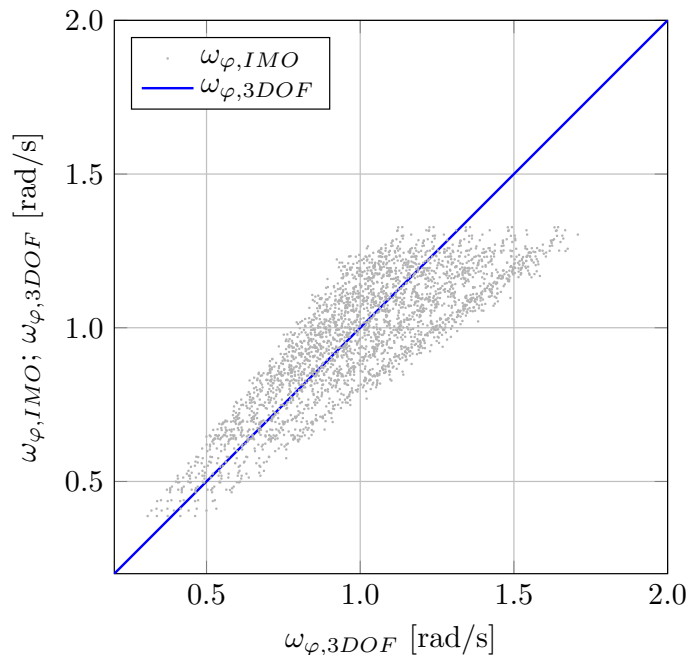
Figure 8.2: Comparative plot of estimated natural roll frequency - 3DOF method vs IMO method.

is taken into account. Most likely, only the "wet" roll radius is considered as a whole – the similar case as for other semi-empirical methods, because they all use Equation (8.8) as the starting point. Nevertheless, it seems that there is a certain value of dry roll radius of inertia, that corresponds, with sufficient precision, to the values estimated by the IMO method.

In Figure 8.3 the similar plot was made, but this time showing the natural roll frequency estimated by the 3DOF method as a function of natural roll frequency estimated by Bureau Veritas rules formula for inland navigation vessels (see Equation (8.13)). The specific semi-empirical formula is selected as it is the only one designated for application to inland vessels. The results are apparently similar to the ones estimated by the IMO method, nevertheless, it seems that the natural frequency estimated by the BV formula (8.13) tends to return values which are generally higher than the ones obtained by the 3DOF method. Other semi-empirical formulae, which estimate the "wet" roll radius of inertia simply as percentage of ship's breadth, generally have similar estimation tendency, with different accuracy.

Moreover, a comparison of the natural roll frequencies as a function of metacentric height for the three test vessels are given in Figure 8.4. It can be seen that difference can be significant, particularly for higher metacentric height.

As these semi-empirical methods are simple methods for the natural roll frequency estimation, it would be interesting to improve them in simple way, in order to make them more flexible. For that purpose, the IMO method was selected as a good candidate, having the most similar trends, to the results obtained by the 3DOF method. It seems that separating the dry from the additional roll radius of inertia could lead to better estimation results. Therefore, it is considered that the natural roll frequency is:

$$\omega_\varphi = \sqrt{\frac{g\overline{GM}}{k_{xx}^2 + \delta k_{xx}^2}} \tag{8.17}$$

where k_{xx} is the "dry" roll radius of inertia and δk_{xx} is the additional roll radius of inertia, such that $k'_{xx} = \sqrt{k_{xx}^2 + \delta k_{xx}^2}$.
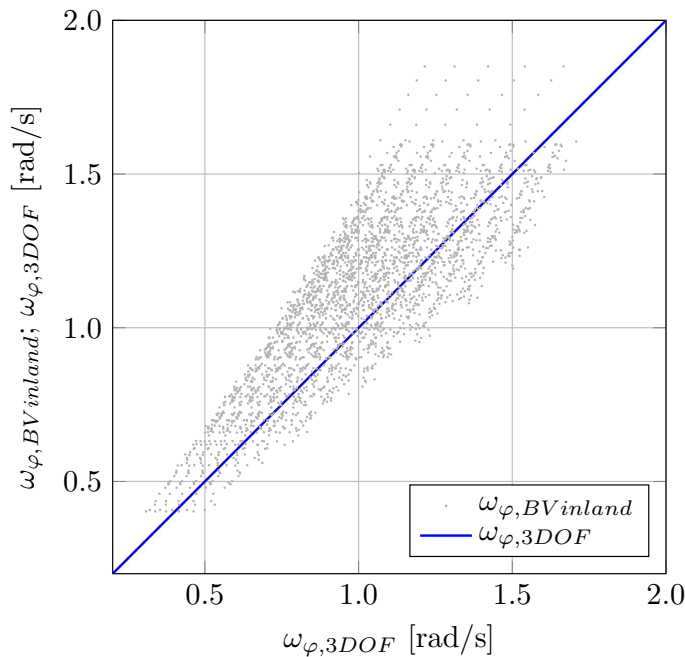
Figure 8.3: Comparative plot of estimated natural roll frequency - 3DOF method vs BV inland method.

The first step is to find values of the "wet" roll radius of inertia which if used instead of coefficient C in the IMO formula, will correspond to the values obtained by using the 3DOF method (see Figure 8.2), for all combination of vessels and all loading conditions in the database. Then, the average of all values can be found, which can be used as the correction factor. This value was found to be $0.362B$ for the presented database of river-sea ships. Therefore, the following formula was developed, which is more versatile for the natural roll frequency estimation, provided that the value of dry roll radius of inertia is known:

$$\omega_\varphi = \sqrt{\frac{g\overline{GM}}{k_{xx}^2 + \delta k_{xx}^2}}$$

where

$$\delta k_{xx}^2 = \left(\frac{CB\sqrt{g}}{\pi}\right)^2 - (0.362B)^2$$

(8.18)

and where C is coefficient defined in the Weather Criterion, shown in Equation (8.10). The benefit of the modified IMO formula is shown in Figure 8.5, where the natural roll frequency estimated by 3DOF method as a function of natural roll frequency estimated by the newly improved IMO formula was plotted, similarly to the previous plots. It can be seen that the estimation is now more in line with the values estimated by the 3DOF method, with a tendency of more significant scattering as the natural frequency increases. Nevertheless, with the rather simple modification, the standard IMO formula can be more flexible, and more precise. The only but crucial problem is the persistent lack of dry roll radius of inertia estimation procedure, with which natural roll period estimation precision would be significantly improved. Therefore, the proposed procedure only improves the added mass moment of inertia. It should be noted that the correction factor of $0.362B$ is obtained using the database of river-sea ships, and that the improved IMO formula may only be valid for this ship type.
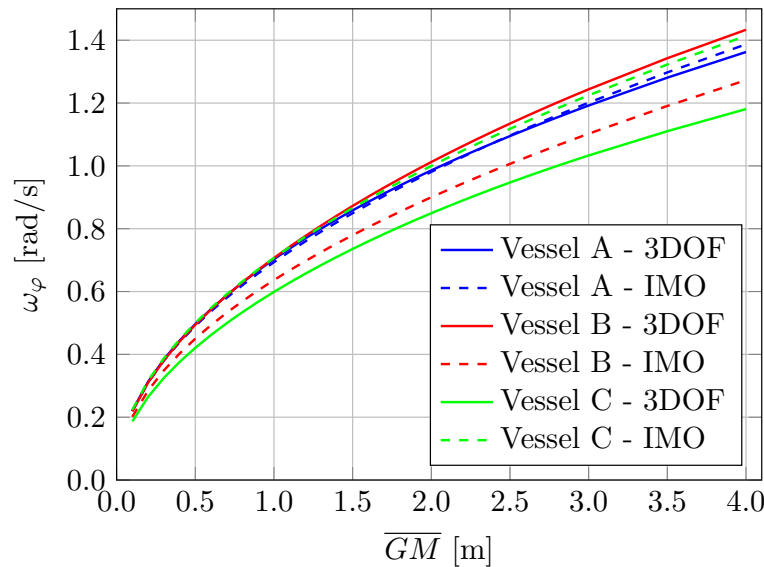
Figure 8.4: Natural roll frequency as a function of metacentric height of the test vessels - 3DOF method and IMO method.
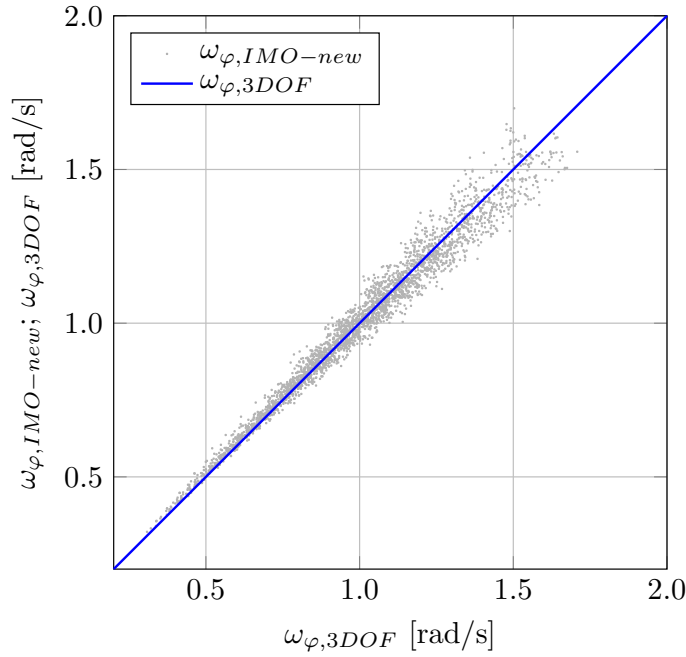
Figure 8.5: Comparative plot of estimated natural roll frequency - 3DOF method vs improved IMO method.

8.5 Application of the stability criteria to river-sea ships considering the modifications of the effective wave slope coefficient and the natural roll period

Following the introduction of the reduced 3DOF method for the effective wave slope coefficient and natural roll frequency estimation, the stability of the test vessels is reassessed, again with and without the presence of bilge keels in order to further assess their efficiency. The failure indices as a function of the metacentric height, for the test vessels A, B and C with the bilge keels installed are given in Figures 8.6, Figures 8.7 and Figures 8.8, respectively. The results of stability assessment obtained before the modification of the effective wave slope coefficient and natural roll period (dashed line) are reported as well, for the reference purpose.

(a) DSC failure index as a function of $\overline{GM}$.

(b) EA failure index as a function of $\overline{GM}$.
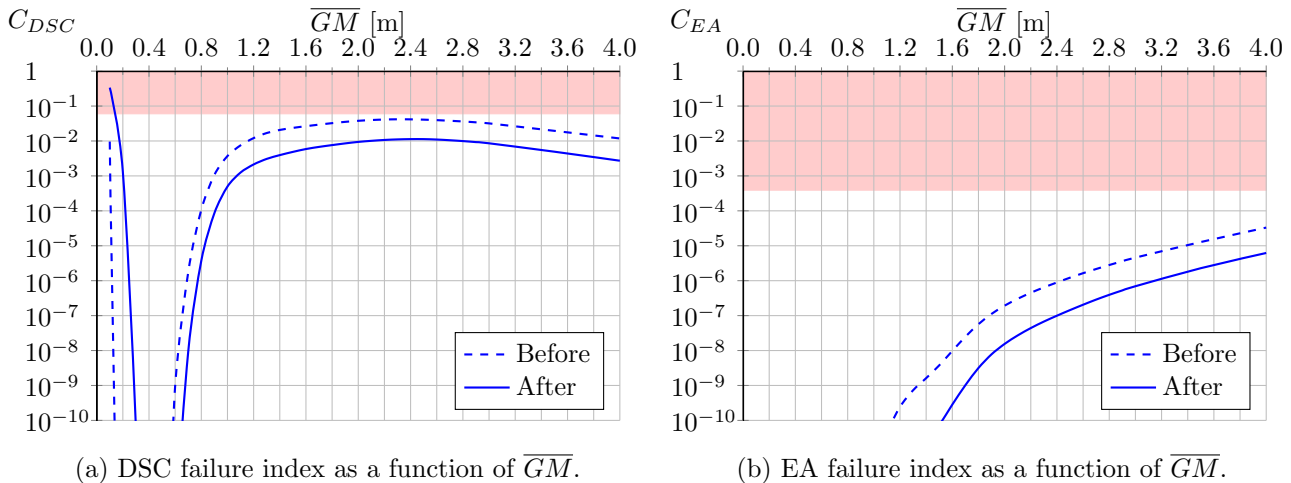
Figure 8.6: Stability assessment - vessel A with bilge keels. The results following the modification of the effective wave slope coefficient and natural roll frequency.

(a) DSC failure index as a function of $\overline{GM}$.

(b) EA failure index as a function of $\overline{GM}$.
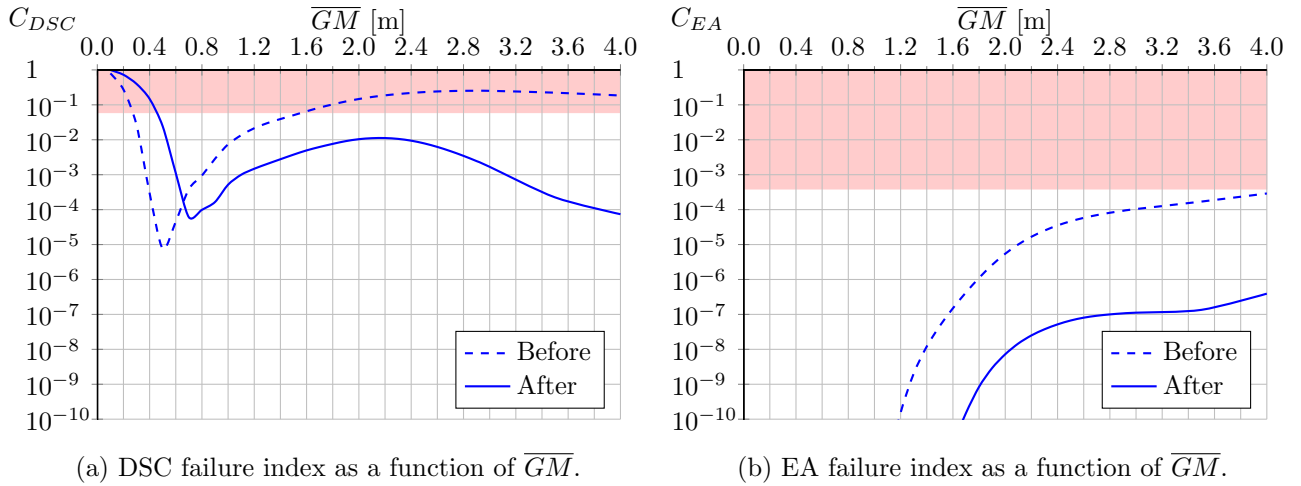
Figure 8.7: Stability assessment - vessel B with bilge keels. The results following the modification of the effective wave slope coefficient and natural roll frequency.

(a) DSC failure index as a function of $\overline{GM}$.

(b) EA failure index as a function of $\overline{GM}$.
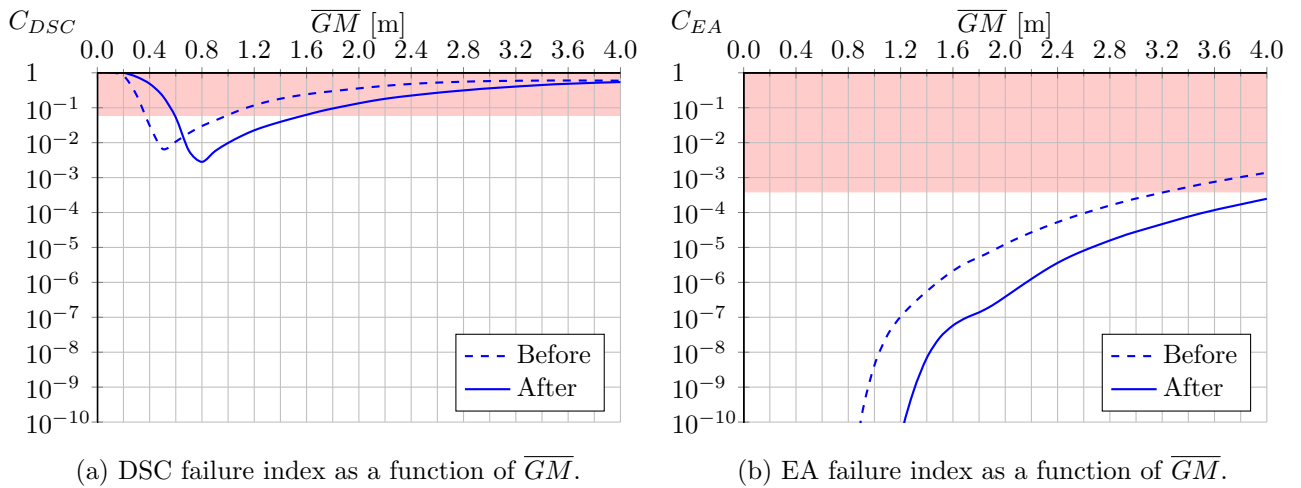
Figure 8.8: Stability assessment - vessel C with bilge keels. The results following the modification of the effective wave slope coefficient and natural roll frequency.

Additionally, the failure indices for the test vessels without the bilge keels are presented in Figures 8.9, 8.10, 8.11.

The differences shown are significant. On the other hand, for the first time in these graphs differences are not only quantitative, but also qualitative, as the values are both reduced and shifted toward the higher metacentric heights. Due to better physical models used for the effective wave slope coefficient and the natural roll period estimation, the results are believed to be more accurate.

(a) DSC failure index as a function of $\overline{GM}$.

(b) EA failure index as a function of $\overline{GM}$.
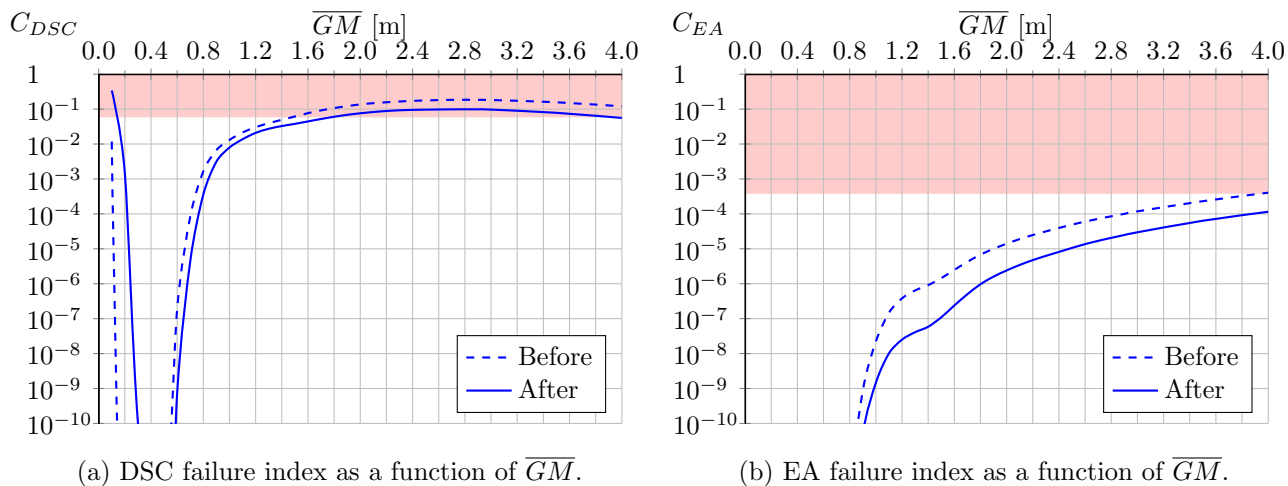
Figure 8.9: Stability assessment - vessel A without bilge keels. The results following the modification of the effective wave slope coefficient and natural roll frequency.

(a) DSC failure index as a function of $\overline{GM}$.

(b) EA failure index as a function of $\overline{GM}$.
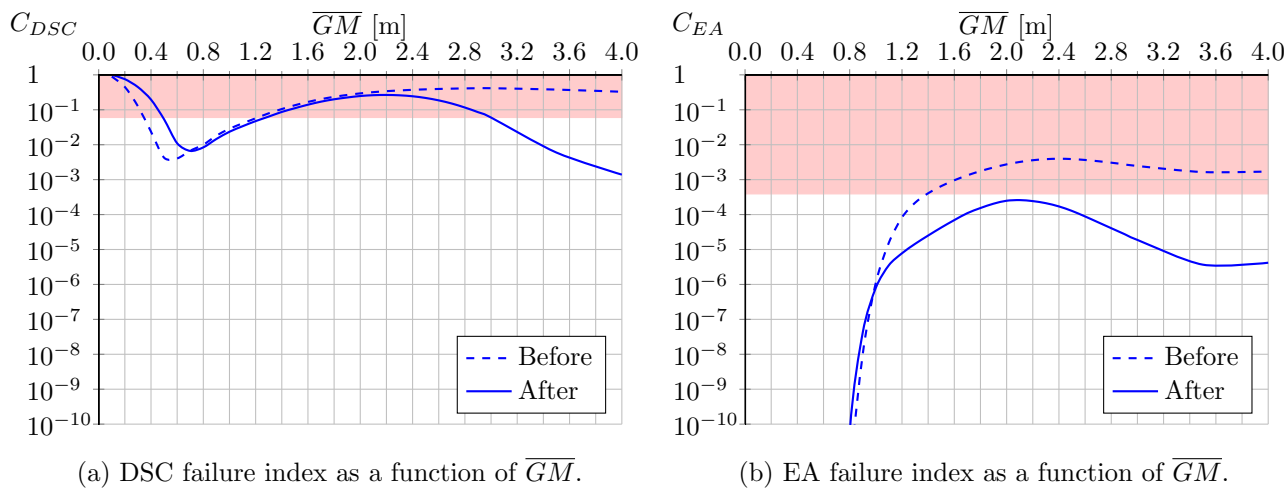
Figure 8.10: Stability assessment - vessel B without bilge keels. The results following the modification of the effective wave slope coefficient and natural roll frequency.

(a) DSC failure index as a function of $\overline{GM}$.

(b) EA failure index as a function of $\overline{GM}$.
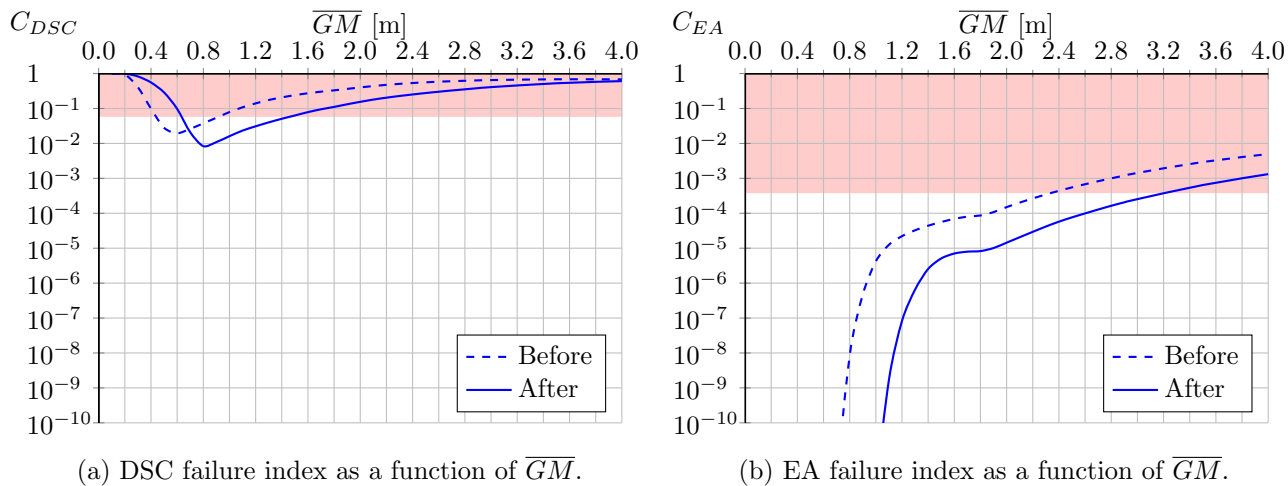
Figure 8.11: Stability assessment - vessel C without bilge keels. The results following the modification of the effective wave slope coefficient and natural roll frequency.

8.6   Conclusions

The natural roll period is an important parameter in stability assessment. Two approaches to natural roll period estimation were considered and discussed in this thesis – the semi-empirical approach and the approach based on linear hydrodynamics. It was shown that the semi-empirical methods can have good estimation precision with not so good accuracy, but the main drawback is lack of separate dry roll radius of inertia consideration. Therefore, simple improvement of the IMO formula for the natural roll frequency estimation was proposed (see Equation (8.17)). However, the 3DOF method has the potential to estimate the added mass moment of inertia more precisely than existing semi-empirical methods, with the complexity of estimation as the only drawback.

Unfortunately, the 3DOF method improves only a part of the estimated natural roll period of river-sea ships. On the other hand, the "dry" roll radius of inertia k_{xx} is an important part of the estimation process, for which, to the best of the author's knowledge, there is no procedure for estimation for inland vessels or river-sea ships corresponding to different loading conditions.

Although, the more precise estimation method of k_{xx} is not available and its development is out of the scope of the thesis, k_{xx} and δk_{xx} will be considered to be separate for the purpose of this research. However, it will be once again emphasised that k_{xx} is a missing link in stability assessment of not only inland vessels and river-sea ships, but also sea-going ships.

The stability of the test vessels is reassessed, showing the influence of the reduced 3DOF method implementation for the estimation of the effective wave slope and natural roll frequency. It is believed that the better representation of the physical model has increased the accuracy of the assessment.

Chapter 9

Regression models for natural period and effective wave slope coefficient

9.1   Introduction

In the thesis, the analysis of existing methods for estimation of the effective wave slope coefficient are presented and sorted into three approaches – semi-empirical, linear Froude-Krylov and linear hydrodynamic approach (Chapter 7). Furthermore, the semi-empirical and the linear hydrodynamic approaches for the natural roll period are analysed as well (Chapter 8). Advantages and disadvantages of particular methods are discussed, concluding that the 3DOF linear hydrodynamic method enables for the most complex and precise method among the all considered. Therefore, the method is recommended for estimation of effective wave slope coefficient and natural roll period of river-sea ships. However, complexity of calculation, primarily the need for seakeeping calculations, makes the whole procedure cumbersome and too complex for everyday engineering practice. The development of simple regression models are seen as a practical solution to the problem.

Results show that using the 3DOF coupled model for determination of the natural roll frequency and effective wave slope are significantly different from the results obtained by other methods. This is due to more realistic representation of ship hydrodynamics and, hence, of roll motion, but also due to the coupling effect of sway and yaw. Therefore, the goal of this chapter is to develop simplified regression formulae using results from systematic calculations based on the 3DOF method. To this end, the following considerations should be addressed along the process:

- Formulae should represent a balance between simplicity, accuracy and precision;

- Formulae should be robust with respect to applicability range, giving reasonable results, even when applied (slightly) outside of the basic applicability range;

- To accommodate vessels of different main dimensions, formulae should be based on the non-dimensional quantities;

- Consistency should be maintained among different regression formulae, when applicable;

- For the purpose of regression, a database of representative inland vessels and river-sea ships should be considered, for which the database presented in Section 7.3 will be used.

The present Chapter is a result of a study contained in the report Rudaković (2018).

9.2 Regression formula for natural roll frequency

In order to develop a regression formula for the natural roll frequency, and considering afore-mentioned statements, and observations given in Section 8, it is reasonable to assume the regression model in the following from:

$$\omega_\varphi = \sqrt{\frac{g\overline{GM}}{k_{xx}^2 + \delta k_{xx}^2}} \tag{9.1}$$

where δk_{xx} is the added roll radius of inertia, such that $\sqrt{k_{xx}^2 + \delta k_{xx}^2}$ corresponds to the "wet" roll radius of inertia k'_{xx}. If significant parameters that define loading condition: $\overline{GM}$ and k_{xx} are deemed as known variables, the regression of natural roll frequency comes down to the regression of added roll radius of inertia δk_{xx}. Therefore:

$$\delta k_{xx} = \sqrt{\frac{g\overline{GM}}{\omega_\varphi^2} - k_{xx}^2} \tag{9.2}$$

and in order to make this regression non-dimensional, previous expression can be written in a form of non-dimensional radius of added mass for which the regression will be done:

$$\frac{\delta k_{xx}}{B} = \sqrt{\frac{g\overline{GM}}{(B\omega_\varphi)^2} - \left(\frac{k_{xx}}{B}\right)^2} \tag{9.3}$$

In order to use the most influential parameters and, at the same time, have as simple model as possible, an analysis of correlation between the non-dimensional added roll radius and different other parameters was performed. To facilitate the choice of parameters, a correlation coefficient plot was made, given in Appendix C. After thorough examination and tests, three non-dimensional parameters were taken, which are presumed to make the best regression: B/T, C_B and C_{WL}.

With aforementioned parameters, a linear regression model was used. Furthermore, in order to make values grouped in proximity of ideal regression model predominant, and at the same time to dampen the effect of distant values and make them less influential, robust regression with iteratively re-weighted least squares using Huber weighting function and using median absolute deviation (MAD) scaling of residuals was used (as explained, for example, in Pardoe, 2020). As a result, the following regression formula is proposed:

$$\frac{\delta k_{xx}}{B} = K_0 + K_1 + K_2 + K_3$$

$$K_0 = \begin{cases} 0.6048, & \text{for the upper limit of 95\% prediction interval} \\ 0.5909, & \text{for the predicted value} \\ 0.5804, & \text{for the lower limit of 95\% prediction interval} \end{cases}$$

$$K_1 = 0.05516\frac{B}{T} - 0.001876\left(\frac{B}{T}\right)^2 + 0.05674\frac{B}{T}C_{WL}$$

$$K_2 = 3.332C_B + 3.215C_B{}^2 - 0.07211C_B\frac{B}{T}$$

$$K_3 = -4.556C_{WL} + 6.8603C_{WL}{}^2 - 9.328C_{WL}C_B \tag{9.4}$$

In order to have a possibility to account for the dispersion of calculated data, the coefficient K_0 was presented with three values, showing the modelled value, together with upper and

lower limits of 95% prediction interval. Graphically, it is shown in Figure 9.1, where directly calculated values (using the 3DOF method) are plotted as a function of values obtained using the regression formula (RF). In Figure, full blue line is the regression line and dashed blue lines are the upper and lower boundaries of approximated 95% prediction interval, obtained after removing 2.5% of the largest positive errors, and 2.5% of the largest negative errors.
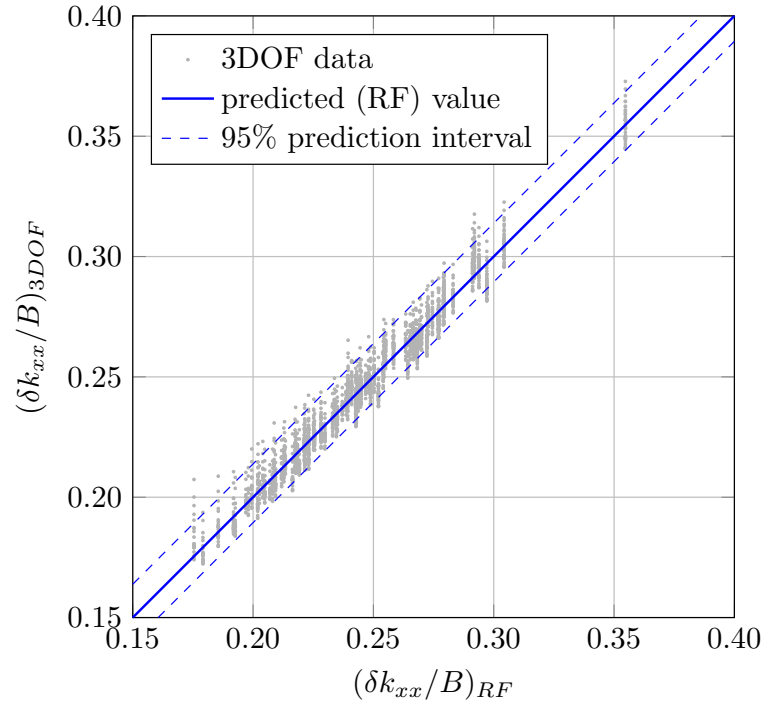

Figure 9.1: Calculated value of $\delta k_{xx}/B$ (3DOF method) versus predicted values (regression formula).
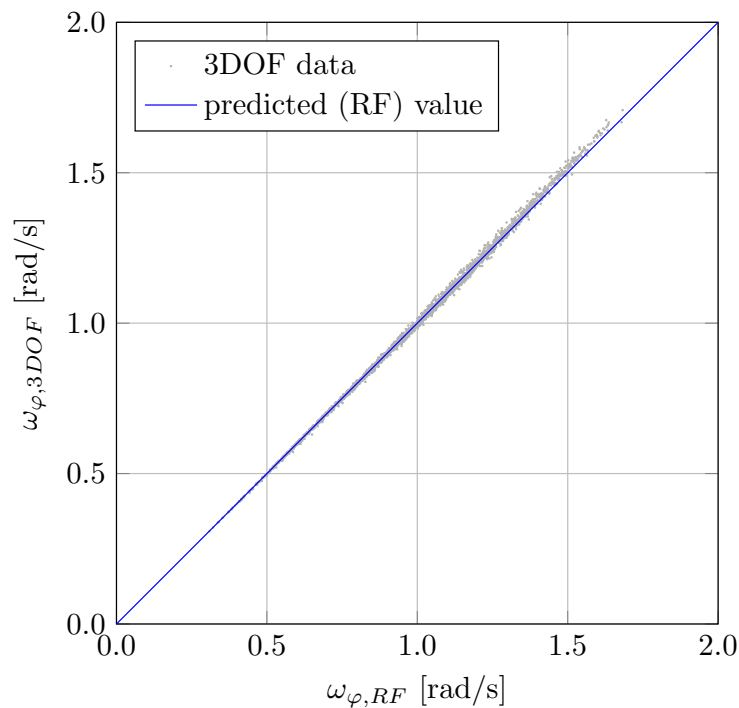
Figure 9.2: Calculated value of natural roll frequency (3DOF method) versus predicted values (regression formula).

However, regression model of non-dimensional added roll radius of inertia $\delta k_{xx}/B$ is not of an interest per se. Therefore, the values of natural roll period of inland vessels and river-sea ships, estimated by the newly proposed regression formula (RF) are shown in Figure 9.2, where directly calculated values of the natural frequency (using the 3DOF method described in Section 8.2.1) are plotted as a function of values estimated by the developed regression formula (9.4). The prediction errors as a function of predicted natural roll frequency is given in Figure 9.3. Some bias for the larger frequencies can be observed on the plot, which, if one looks carefully, can be seen also in Figure 9.1, corresponding to the lower values of $\delta k_{xx}/B$.
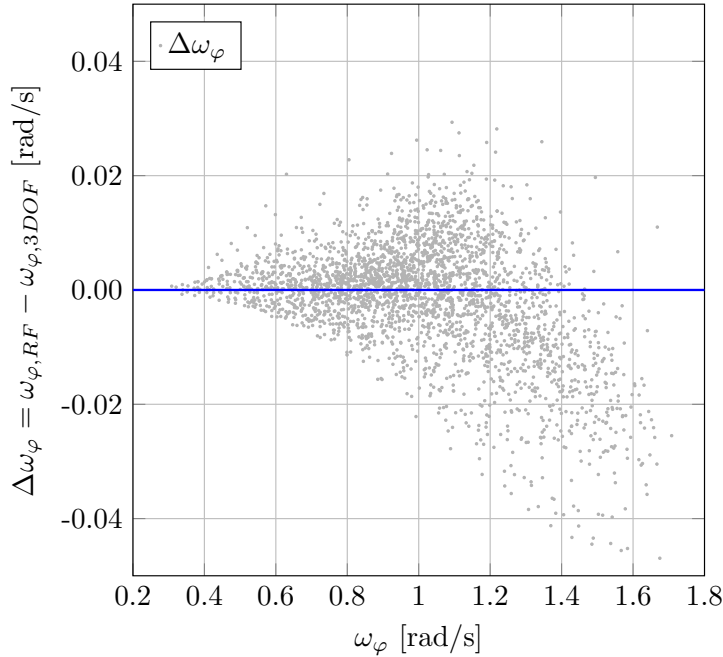
Figure 9.3: Prediction errors of ω_φ.

9.3   Regression formula for effective wave slope coefficient at natural roll frequency

Development of a simplified regression formula for the effective wave slope at natural roll frequency seemed like a reasonable next step. This parameter is widely used in stability assessment, and it is believed that it could be an important step in defining influential parameters for the subsequent development of a regression formula for the frequency dependent effective wave slope coefficient.

The first step is to obtain values for the effective wave slope coefficient at natural roll frequency using the 3DOF method (described in Section 7.2.1) together with the estimated values for the natural roll frequency, again using the 3DOF method (see Section 8.2.1), for all sets of variations within the database. In order to make a regression, analyses of influential non-dimensional parameters is performed, again, relying on the correlation coefficient plot (see Appendix C). Among all, four influential parameters were selected as parameters for further regression: k_{xx}/B, B/T, C_B and $\overline{GM}/B$.

With aforementioned parameters, once again, robust regression with iteratively re-weighted least squares using Huber weighting function and using median absolute deviation (MAD) scaling of residuals was used (see Pardoe, 2020). From there, the following regression formula is obtained:

$$r(\omega_\varphi) = R_0 + R_1 + R_2 + R_3 + R_4$$

$$R_0 = \begin{cases} \text{-0.5813,} & \text{for the upper limit of 95\% prediction interval} \\ \text{-0.5969,} & \text{for the predicted value} \\ \text{-0.6068,} & \text{for the lower limit of 95\% prediction interval} \end{cases}$$

$$R_1 = 3.416\frac{k_{xx}}{B} - 0.5722\left(\frac{k_{xx}}{B}\right)^2 - 2.814\left(\frac{k_{xx}}{B}\right)^3 + 7.543\left(\frac{k_{xx}}{B}\right)^2\frac{\overline{GM}}{B}$$

$$R_2 = -0.02502\frac{B}{T} + 0.002894\left(\frac{B}{T}\right)^2 + 0.04164\frac{B}{T}\frac{\overline{GM}}{B} - 0.06073\frac{B}{T}\frac{k_{xx}}{B}$$

$$R_3 = 1.198C_B - 0.8308C_B{}^2 - 0.1989C_B\frac{k_{xx}}{B} - 0.006306C_B\frac{B}{T}$$

$$R_4 = -0.2855\frac{\overline{GM}}{B} - 5.276\frac{\overline{GM}}{B}\frac{k_{xx}}{B} + 0.5694\frac{\overline{GM}}{B}C_B$$

(9.5)

where, similarly to the previous regression, the first coefficient R_0 is presented with the three values, showing modelled value, together with upper and lower limits of 95% prediction interval. Once again, the goodness of the regression formula is graphically showed in Figure 9.4, where the 3DOF calculated values are plotted as a function of predicted values, together with the predicted value and limits of 95% prediction interval. In addition, Figure 9.5 was given, showing the prediction error as a function of predicted value.
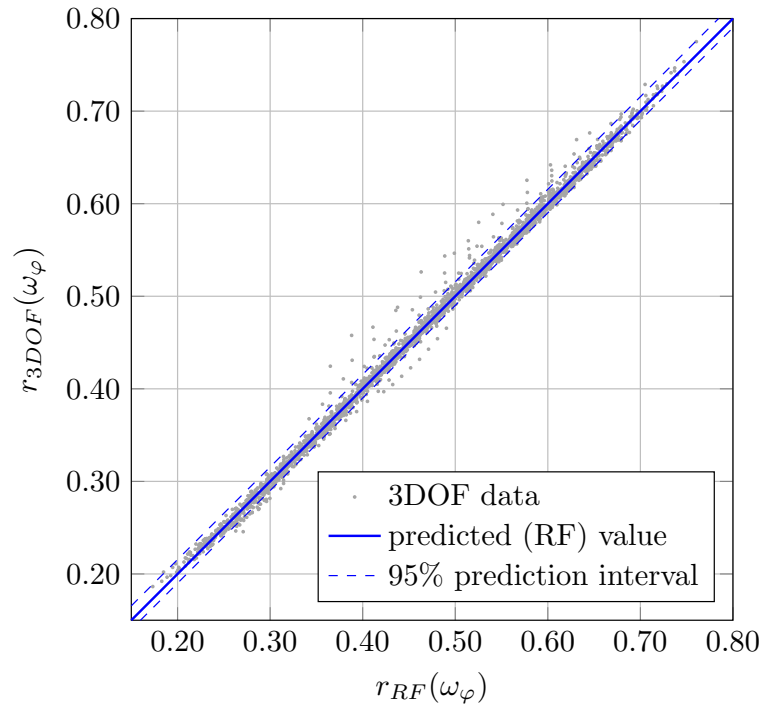
Figure 9.4: Calculated value of $r(\omega_\varphi)$ (3DOF method) versus predicted values (regression formula).
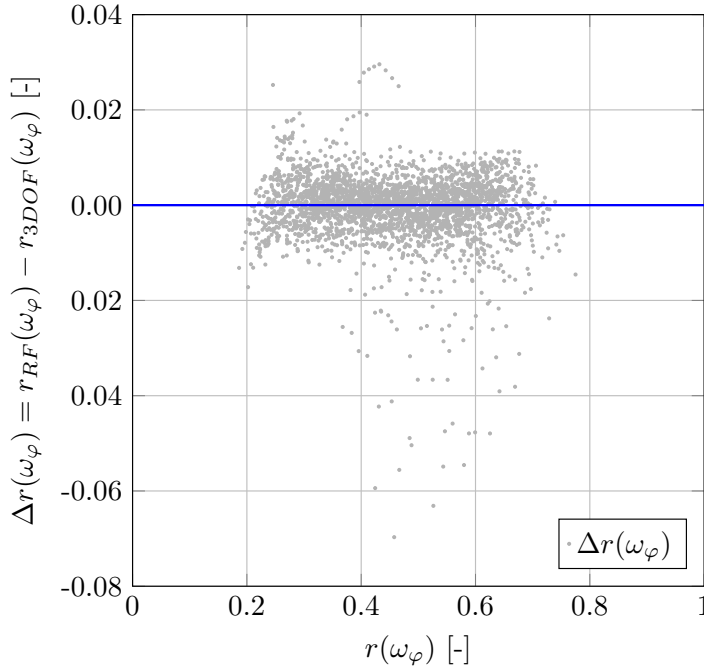
Figure 9.5: Prediction errors of $r(\omega_\varphi)$.

9.4 Regression formula for frequency dependent effective wave slope coefficient

It was assumed that the effective wave slope coefficient directly calculated using linear hydrodynamic approach provides better results than the linear Froude-Krylov approaches, due to accounting for coupling with other motions and diffraction forces (see Chapter 7). Therefore, a proper regression of the effective wave slope coefficient could qualitatively improve the stability assessment, while providing simple and quick estimation procedure.

Due to complexity of regression of the frequency dependent effective wave slope coefficient, and increasing number of parameters needed, it was decided to use a non-linear regression model, able to describe the effective wave slope function for each individual case of combinations of vessels and loading conditions in the database. Solution was found in a non-linear regression model assumed in a shape of following rational function:

$$r\left(\omega\right) = \left| \frac{1 + a\hat{k}}{1 + b\hat{k} + c\hat{k}^3} \right|$$
(9.6)

where $\hat{k}$ is non-dimensional wave number defined as $\hat{k} = k_w B = \omega^2 B/g$ and a, b and c are fitted coefficients that define effective wave slope function for each case from the database. This shape of assumed model is quite robust, enabling regression formula to follow the properties of $r(\omega)$ explained in Chapter 7, such as $\lim_{\omega \to 0} r(\omega) = 1$ and $\lim_{\omega \to \infty} r(\omega) = 0$, while properly describing the shape of the function. Furthermore, with the selected order of the numerator and of the denominator polynomials in Equation (9.6), derivative of $r(\omega \to 0)$ with respect to frequency well describes starting slope of the function.

Last step is to define coefficients a, b and c. It was observed that better results and further simplification of regression model can be made if the regression model is forced to pass through the point of the effective wave slope at natural frequency $r(\omega_\varphi)$, which in following equations, for the sake of simplicity, will be written as r_φ. Furthermore, this ensures consistency between

the present regression model and the regression model in Section 9.3 for the effective wave slope coefficient at natural roll frequency. Therefore, in order to satisfy aforementioned, coefficient a becomes:

$$a = \frac{r_\varphi \left(1 + b\hat{k}_\varphi + c\hat{k}_\varphi^3\right) - 1}{\hat{k}_\varphi} \tag{9.7}$$

where $\hat{k}_\varphi = \omega_\varphi^2 B/g$, furthermore ω_φ is the roll natural frequency as obtained from the regression formula presented in Section 9.2 using Equations (9.1) - (9.4), r_φ is the effective wave slope coefficient at natural roll frequency as obtained from the regression formula presented in Section 9.3 using Equation (9.5) and coefficient b and c are yet to be defined.

It was noticed that for the proposed regression model, the results are not very sensitive to variations of the coefficients b and c. With all aforementioned properties of regression model, shape of a resulting function is greatly restrained, even if coefficients b and c are changed significantly. Therefore, for a significant part of the effective wave slope, from $\omega = 0$ through $\omega = \omega_\varphi$ and up until around the first zero crossing, function is well estimated regardless of coefficients b and c, for all combinations of input parameters. This will be pointed out and further explained in the following section.

Considering all these statements, it was decided to keep prediction of remaining parameters as simple as possible. Therefore, a very simple regression models has been developed, taking fitted coefficients from regressions of all cases from the database, and taking into account only parameter $\overline{OG}/B$ for the further regressions of coefficients b and c. Obtained formulae are as follows:

$$b = 0.5438 - 1.270\frac{\overline{OG}}{B} + 3.600 \left(\frac{\overline{OG}}{B}\right)^2$$
$$c = 0.08857 - 0.4127\frac{\overline{OG}}{B} + 0.6709 \left(\frac{\overline{OG}}{B}\right)^2 \tag{9.8}$$
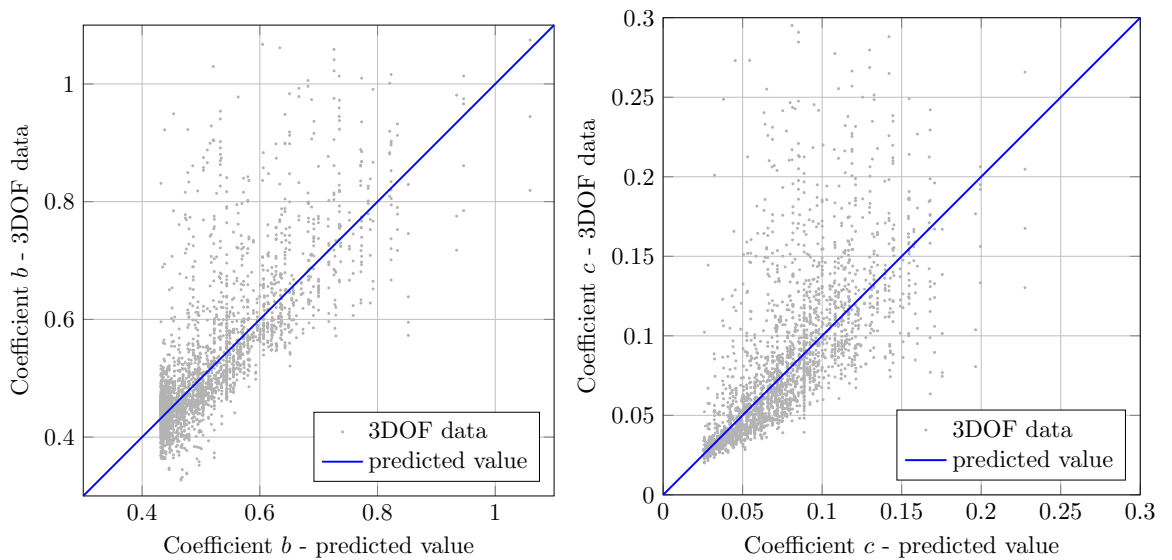
(a) Prediction errors of coefficients b.

(b) Prediction errors of coefficients c.

Figure 9.6: Analysis of regression formula coefficients for frequency dependant effective wave slope coefficient.

In Figure 9.6, the calculated values (3DOF method) are plotted as a function of the predicted (RF) value. Although the 3DOF values are scattered around the predicted value, it can be said that majority of data are in near proximity of the ideal value, especially considering the previous statement that predicted value for effective wave slope function is not sensitive to variations in the coefficients b and c. Any further attempt to make a better regression of the coefficients resulted in significantly more complex models, without a considerable improvement in estimation accuracy and precision.

In order to evaluate errors of proposed regression model, Figure 9.7 is reported in similar manner as Figures 7.11, 7.12 and 7.13. Here, absolute differences $\Delta r(\hat{k})$ between values predicted by the regression and predicted by the 3DOF method for all cases in the database are plotted through their median value, interquartile range (as $\pm 25\%$ from median value) and values of minimum and maximum errors, all as a function of non-dimensional frequency $\hat{k}$. Figure shows that the interquartile range (i.e. 50% of all data) is within the range of ± 0.01 of the 3DOF values. Although min/max error range can go up to almost 0.2, it can occur in minority of cases, and it was noticed that it comes from the combination of low metacentric heights and high frequencies. This will be analysed in more details in the next section.
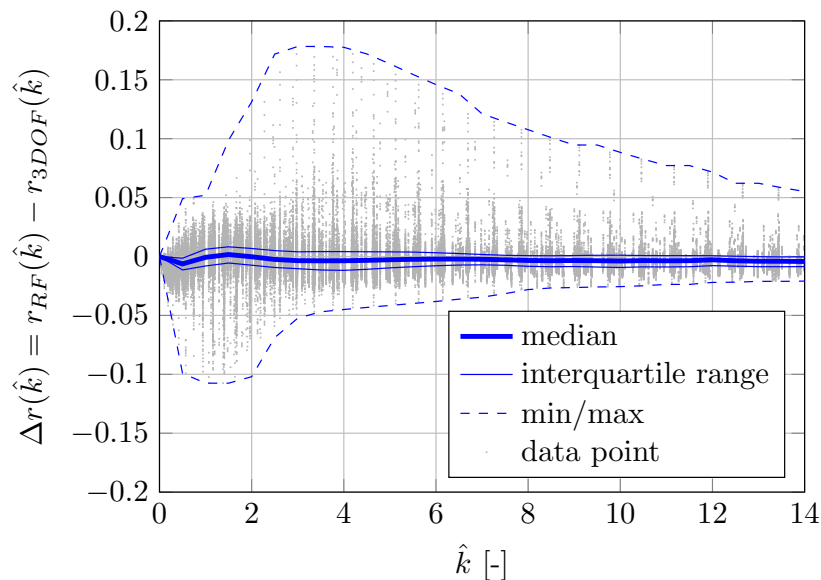
Figure 9.7: Statistical analysis of frequency dependent effective wave slope coefficient difference between proposed developed regression method and reference reduced 3DOF method.

9.5 Validation of regression models

For the validation, different sets of loading conditions were used for each vessel - three different draughts (scantling, low and an intermediate taken as an average between scantling and low) and three metacentric heights (low $\overline{GM} = 0.15$ m, the highest realistic for a given condition and an intermediate). The values of the natural roll frequency ω_φ, the effective wave slope at natural frequency $r(\omega_\varphi)$, and the effective wave slope function $r(\omega)$ were directly calculated using the 3DOF method (see Sections 7.2.1 and 8.2.1) and compared to values obtained by the presented regression formulae (see Equations (9.1) - (9.4), Equation (9.5) and Equations - (9.8), respectively). In total, 18 sets of data are obtained.

Comparisons of ω_φ and $r(\omega_\varphi)$ are shown in Table 9.1, where the columns "3DOF" correspond to the directly calculated values using the 3DOF method, the columns "RF" correspond to the developed regression formulae, and $\delta\omega_\varphi$ or $\delta r(\omega_\varphi)$ are the relative errors of natural roll frequency

Table 9.1: Validation of ω_φ and $r(\omega_\varphi)$.

vessel	T [m]	k_{xx}/B [-]	$\overline{GM}$ [m]	ω_φ [rad/s]		$r(\omega_\varphi)$ [-]		C_{DSC} [-]		C_{EA} [-]	
				3DOF	RF	3DOF	RF	3DOF	RF	3DOF	RF
Vessel V1	3.350	0.35	2.15	1.193	1.188	0.5190	0.5020	$5.81 \cdot 10^{-4}$	$3.64 \cdot 10^{-4}$	$6.78 \cdot 10^{-8}$	$3.94 \cdot 10^{-8}$
			1.15	0.8827	0.8688	0.5760	0.5635	$1.55 \cdot 10^{-3}$	$1.23 \cdot 10^{-3}$	$3.43 \cdot 10^{-11}$	$1.56 \cdot 10^{-11}$
			0.15	0.3169	0.3138	0.6605	0.6249	$5.39 \cdot 10^{-1}$	$6.38 \cdot 10^{-1}$	≈ 0	≈ 0
	2.625	0.30	2.55	1.428	1.404	0.3773	0.3803	$3.80 \cdot 10^{-15}$	$1.03 \cdot 10^{-14}$	$1.95 \cdot 10^{-9}$	$1.78 \cdot 10^{-9}$
			1.35	1.0454	1.0219	0.4528	0.4488	$6.74 \cdot 10^{-11}$	$1.47 \cdot 10^{-10}$	$8.09 \cdot 10^{-12}$	$7.37 \cdot 10^{-12}$
			0.15	0.3427	0.3406	0.5310	0.5173	$2.11 \cdot 10^{-2}$	$6.72 \cdot 10^{-2}$	≈ 0	≈ 0
	1.900	0.40	3.15	1.233	1.228	0.4908	0.4843	$4.90 \cdot 10^{-9}$	$3.07 \cdot 10^{-9}$	$2.59 \cdot 10^{-7}$	$1.96 \cdot 10^{-7}$
			1.65	0.9022	0.8884	0.5668	0.5621	$5.16 \cdot 10^{-8}$	$4.07 \cdot 10^{-8}$	$3.31 \cdot 10^{-10}$	$2.05 \cdot 10^{-10}$
			0.15	0.2671	0.2679	0.6573	0.6398	$2.42 \cdot 10^{-1}$	$3.23 \cdot 10^{-1}$	≈ 0	≈ 0
Vessel V2	3.210	0.35	3.15	1.177	1.179	0.4572	0.4516	$9.08 \cdot 10^{-2}$	$8.50 \cdot 10^{-2}$	$5.90 \cdot 10^{-6}$	$5.26 \cdot 10^{-6}$
			1.65	0.8574	0.8530	0.5227	0.5233	$5.61 \cdot 10^{-2}$	$5.53 \cdot 10^{-2}$	$1.45 \cdot 10^{-8}$	$1.45 \cdot 10^{-8}$
			0.15	0.2541	0.2572	0.6091	0.5950	$9.83 \cdot 10^{-1}$	$9.91 \cdot 10^{-1}$	≈ 0	≈ 0
	2.655	0.40	3.65	1.117	1.125	0.4968	0.4917	$1.50 \cdot 10^{-2}$	$2.10 \cdot 10^{-2}$	$1.71 \cdot 10^{-5}$	$1.56 \cdot 10^{-5}$
			1.90	0.8141	0.8118	0.5662	0.5684	$2.55 \cdot 10^{-2}$	$2.58 \cdot 10^{-2}$	$1.48 \cdot 10^{-7}$	$1.54 \cdot 10^{-7}$
			0.15	0.2244	0.2281	0.6587	0.6451	$6.81 \cdot 10^{-1}$	$7.26 \cdot 10^{-1}$	≈ 0	≈ 0
	2.100	0.30	4.45	1.459	1.443	0.3037	0.2987	$5.36 \cdot 10^{-9}$	$3.95 \cdot 10^{-9}$	$5.02 \cdot 10^{-6}$	$3.62 \cdot 10^{-6}$
			2.30	1.0438	1.0372	0.3902	0.3846	$1.27 \cdot 10^{-6}$	$1.15 \cdot 10^{-6}$	$9.25 \cdot 10^{-9}$	$7.04 \cdot 10^{-9}$
			0.15	0.2557	0.2649	0.4986	0.4706	$7.45 \cdot 10^{-1}$	$7.14 \cdot 10^{-1}$	≈ 0	≈ 0

and effective wave slope coefficient at the natural frequency, between the calculated values and the regression, respectively. In Table 9.1 all combinations of loading conditions used for the validation are reported. With variations in draught, wide range of parameter B/T is used, and furthermore, metacentric height and mass moment of inertia are varied, so in general, significant range of applicability of proposed regressions was tested. It is shown that predicted values of effective wave slope at natural frequency and of natural roll frequency are very good representation of calculated values. It is shown that proposed models for ω_φ and $r(\omega_\varphi)$ are capable to estimate proper values over the range of different draughts, metacentric heights and mass moments of inertia, with acceptable level of accuracy.

Comparison of the calculated and predicted effective wave slope as a function of frequency is shown in Appendix D. Data reported in the Appendix indicate that, in general, the regression formula can estimate proper values with very good precision. Significant errors occur for low $\overline{GM}$ values in combination with relatively high frequencies. Fortunately, for these cases, natural frequency is expected at much lower frequencies than the region of errors, therefore roll RAO primary peak should be outside of this part, nevertheless in these cases, higher frequency region can have impact to the results of stability assessment. This was tested by calculating the Dead Ship Condition and Excessive Acceleration failure indices. Accordingly, the failure indices are reported in Table 9.1.

9.6 Application of the stability criteria to river-sea ships using developed regression formulae

Similarly to the previous chapters, the modified stability assessment procedure, based on the Second Generation Intact Stability Criteria is applied to river-sea ships. Following the two previous Chapters (see Chapters 7 and 8), the 3DOF method is examined, for the purpose of the estimation of the two parameters of paramount importance, in order to be implemented to the novel stability procedure. However, in this Chapter, a regression models are derived, in order to simplify the estimation process. The influence of the implementation of the regression models with respect to the 3DOF method, is shown in Figure 9.8, Figure 9.9 and Figure 9.10, where indices C_{DSC} and C_{EA} as a function of $\overline{GM}$ obtained for the test vessels A, B and C with bilge keels are given, respectively.

(a) DSC failure index as a function of $\overline{GM}$. (b) EA failure index as a function of $\overline{GM}$.
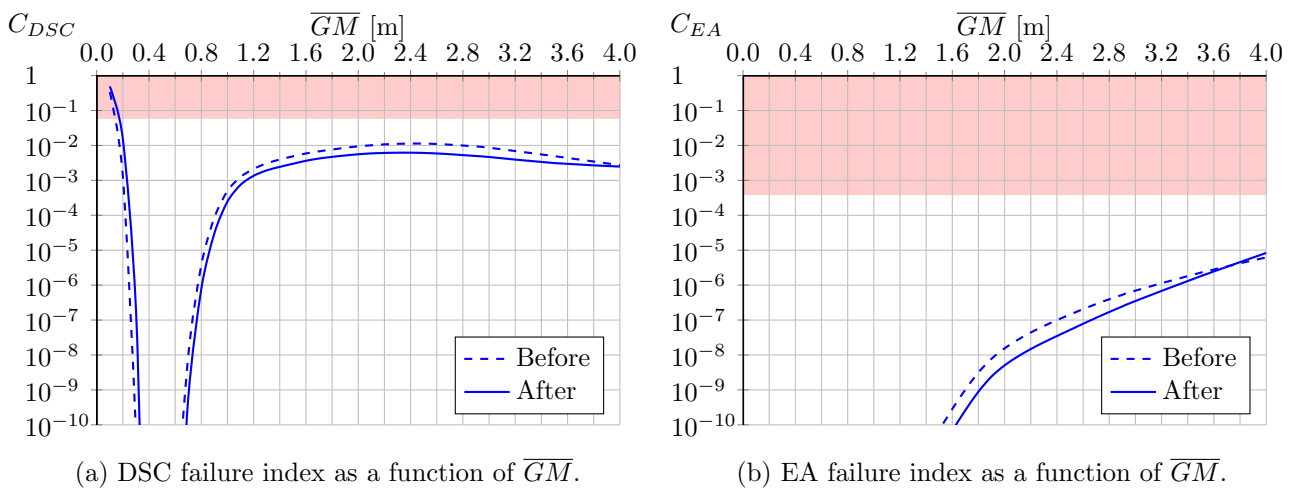
Figure 9.8: Stability assessment - vessel A with bilge keels. The results following the introduction of the reduced 3DOF method regression models.

(a) DSC failure index as a function of $\overline{GM}$.

(b) EA failure index as a function of $\overline{GM}$.
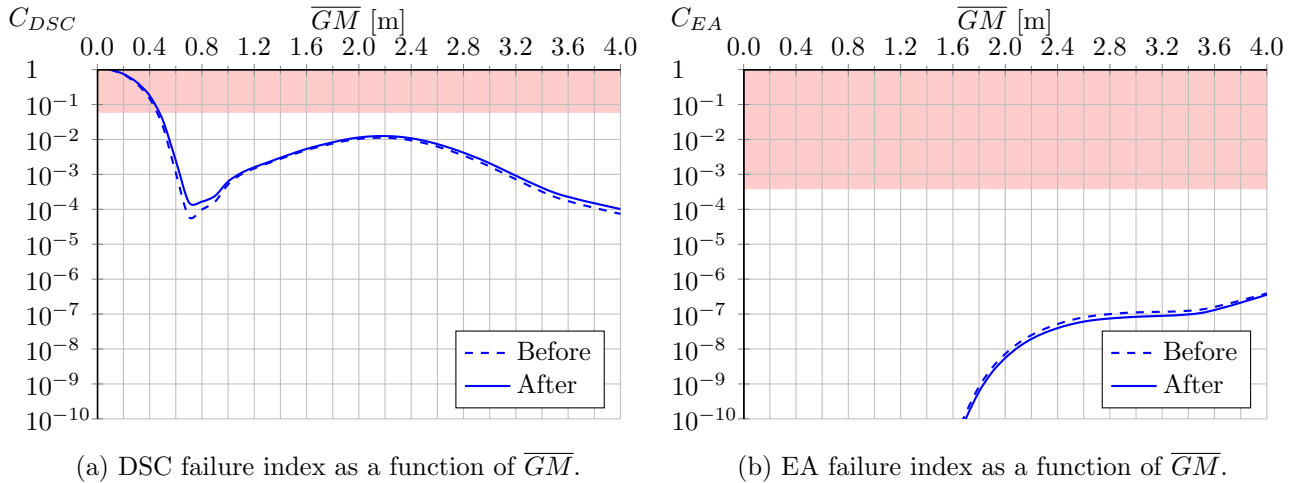
Figure 9.9: Stability assessment - vessel B with bilge keels. The results following the introduction of the reduced 3DOF method regression models.

(a) DSC failure index as a function of $\overline{GM}$.

(b) EA failure index as a function of $\overline{GM}$.
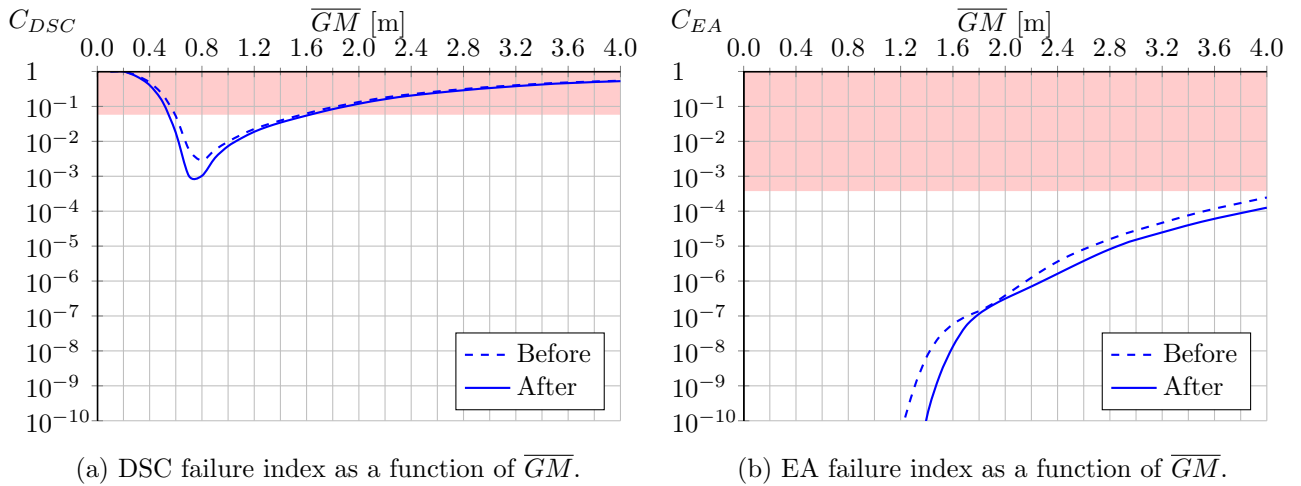
Figure 9.10: Stability assessment - vessel C with bilge keels. The results following the introduction of the reduced 3DOF method regression models.

The results for the test vessels A, B and C without the bilge keels are given in Figures 9.11, 9.12 and 9.13, respectively.

The differences caused by the introduction of the regression models are somewhat noticeable. The differences are more noticeable for the Excessive Acceleration than for the Dead Ship Condition. Nevertheless, in proximity to the long-term standards, differences are always within one order of magnitude. Therefore, it is considered that benefits of its simplicity, in comparison to the reduced 3DOF method, surpass disadvantages caused by inaccuracy.
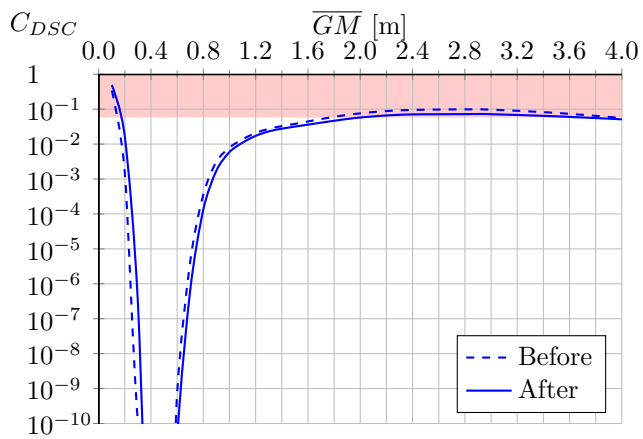
(a) DSC failure index as a function of $\overline{GM}$.
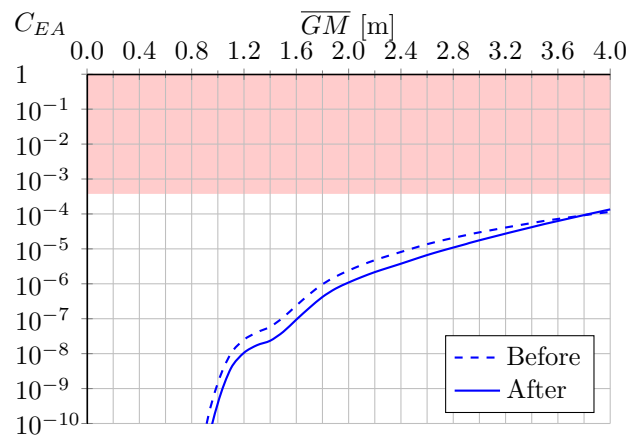
(b) EA failure index as a function of $\overline{GM}$.

Figure 9.11: Stability assessment - vessel A without bilge keels. The results following the introduction of the reduced 3DOF method regression models.
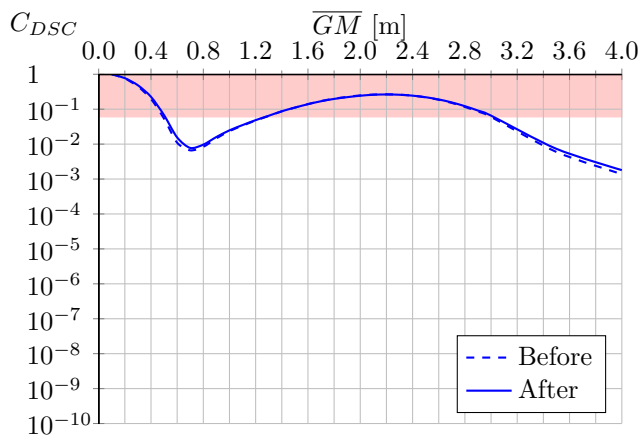
(a) DSC failure index as a function of $\overline{GM}$.
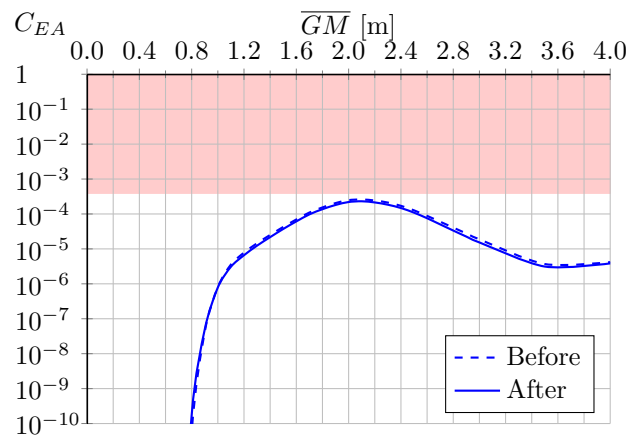
(b) EA failure index as a function of $\overline{GM}$.

Figure 9.12: Stability assessment - vessel B without bilge keels. The results following the introduction of the reduced 3DOF method regression models.
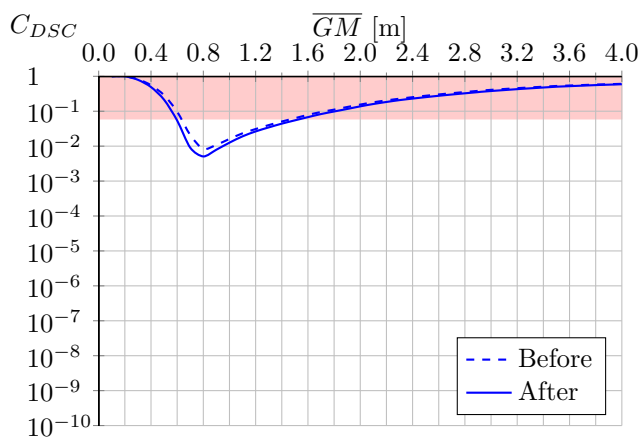
(a) DSC failure index as a function of $\overline{GM}$.
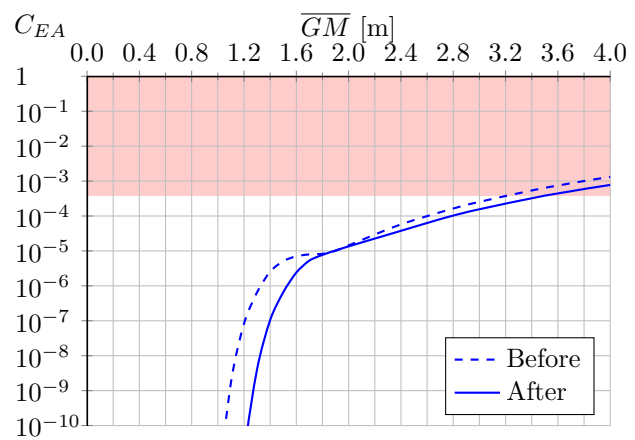
(b) EA failure index as a function of $\overline{GM}$.

Figure 9.13: Stability assessment - vessel C without bilge keels. The results following of the introduction of the reduced 3DOF method regression models.

9.7 Conclusions

In this Chapter regression formulae for estimation of the natural roll frequency (Section 9.2), the effective wave slope at natural frequency (Section 9.3) and the frequency dependant effective wave slope coefficient (Section 9.4), are given in Equations (9.4), (9.5) and (9.6), respectively. Furthermore, validation (given in Section 9.5) showed that the developed formulae provide a very good representation of the parameters, provided that several basic vessel particulars and loading condition are known. Larger errors occur for the effective wave slope function for combination of low metacentric heights and high frequency – a combination that should be less influential for stability assessment. For all other combinations of particulars and loading conditions, proposed regressions for $r(\omega)$ estimate well the expected values. Nevertheless, a missing link is that, apparently, there are no adequate methodologies for the estimation of the mass moment of inertia for inland vessels and river-sea ships.

Because the regressions are designed using representative database of inland vessels and river-sea ships, the newly developed formulae are considered to be applicable to all vessels of the same type. Nevertheless, it is recommended to consult the coefficient correlation plot given in Appendix C to confirm that vessel particulars correspond to the particulars used for the regressions design.

Chapter 10

Introducing OL of river-sea ships with respect to maximum significant wave height

10.1   Introduction

The Second Generation Intact Stability Criteria framework foresees the use of operational limitations (OL) which are regarded as limitations on the overall operability of the vessel in specific loading conditions (Bačkalov et al., 2016). Detailed definitions and procedures are introduced in IMO (2018a,b), and the updated information are given in IMO (2019a). In this Chapter, a possibility for application of the operational limitations related to maximum significant wave height for river-sea ships will be examined.

The SGISC foresees the limitation of the maximum significant wave hight to all modes of stability failure except one – the Dead Ship Condition (see IMO, 2019a). It is considered that due to power failure, the ship would not be able to avoid heavy weather. However, as river-sea ships are designed for short voyages in a coastal areas, it is considered that crew would be able to assess if the weather will be favourable during the course of the voyage, providing that an appropriate weather forecast is accessible. Furthermore, the principle is already used in Belgium (since 1962), France and Russian Federation, where the operational limitations are successfully implemented (see Chapter 2).

Some parts of the present Chapter were published in Rudaković & Bačkalov (2019).

10.2   Application of the stability criteria to river-sea ships considering the operational limitations

The calculations are carried out for the complete scatter table given in Table 5.1 (up to $H_{S,max} = 3.6\,\text{m}$) as well as for the scatter table limited by the following wave heights: $3.5\,\text{m}$, $3.0\,\text{m}$, $2.5\,\text{m}$, $2.0\,\text{m}$, $1.5\,\text{m}$, $1.0\,\text{m}$ and $0.5\,\text{m}$. According to IMO (2019a), the scatter table should be limited corresponding to the maximum significant wave height considered, however, it is not specified whether the limited scatter table should be re-normalised or not. Nevertheless, in this theses, whenever the wave height limitation is introduced, the wave scatter table is re-normalised in such way that the total probability of occurrence of the all sea states used is equal to 1. Both C_{DSC} and C_{EA} are calculated for series of metacentric heights as in the previous chapters. The goal is to determine a range of loading conditions for which both C_{DSC} and C_{EA} are below the limiting values in navigation up to a given significant wave height. For instance, if indices C_{DSC} and C_{EA} calculated for an examined ship in a given loading condition did not exceed

critical levels in waves up to $H_{S,max} = 3.6$ m, then the navigation in the designated area would be unrestricted in the loading case considered. On the other hand, if either C_{DSC} or C_{EA} are above the threshold values in e.g. waves up to $H_{S,max} = 2.0$ m, the navigation should not be permitted in the given loading condition if this significant wave height is exceeded.

The results of calculations are organised in a familiar way. Indices C_{DSC} and C_{EA} for the test vessels A, B and C with bilge keels installed are given in the Figure 10.1, Figure 10.2 and Figure 10.3, respectively.

(a) DSC failure index as a function of $\overline{GM}$. (b) EA failure index as a function of $\overline{GM}$.
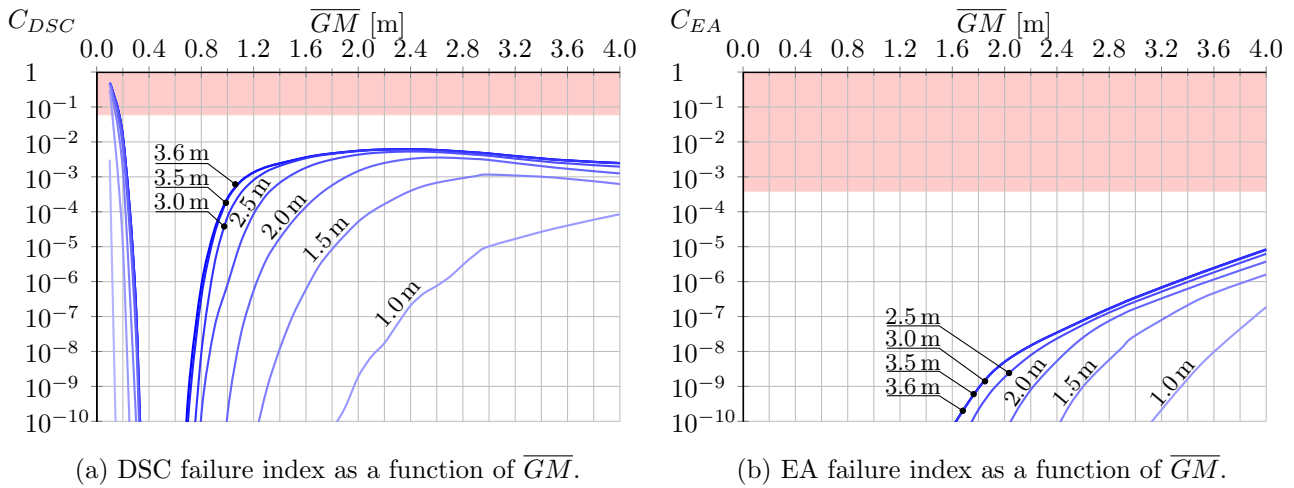
Figure 10.1: Stability assessment - vessel A with bilge keels. The results following the introduction of the operational limitations with respect to maximum significant wave height.


(a) DSC failure index as a function of $\overline{GM}$. (b) EA failure index as a function of $\overline{GM}$.
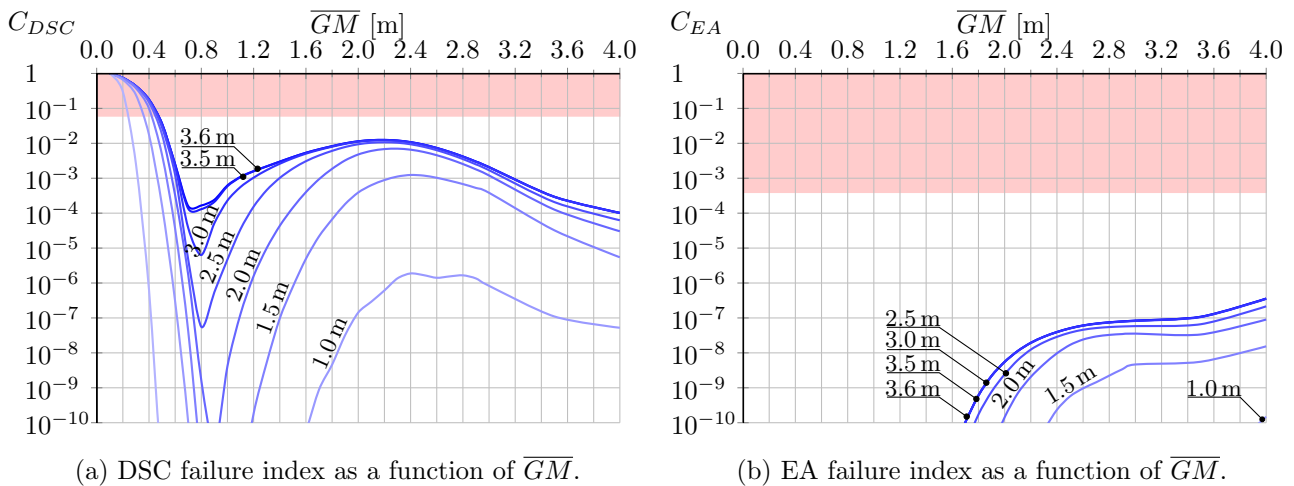
Figure 10.2: Stability assessment - vessel B with bilge keels. The results following the introduction of the operational limitations with respect to maximum significant wave height.

(a) DSC failure index as a function of $\overline{GM}$.

(b) EA failure index as a function of $\overline{GM}$.
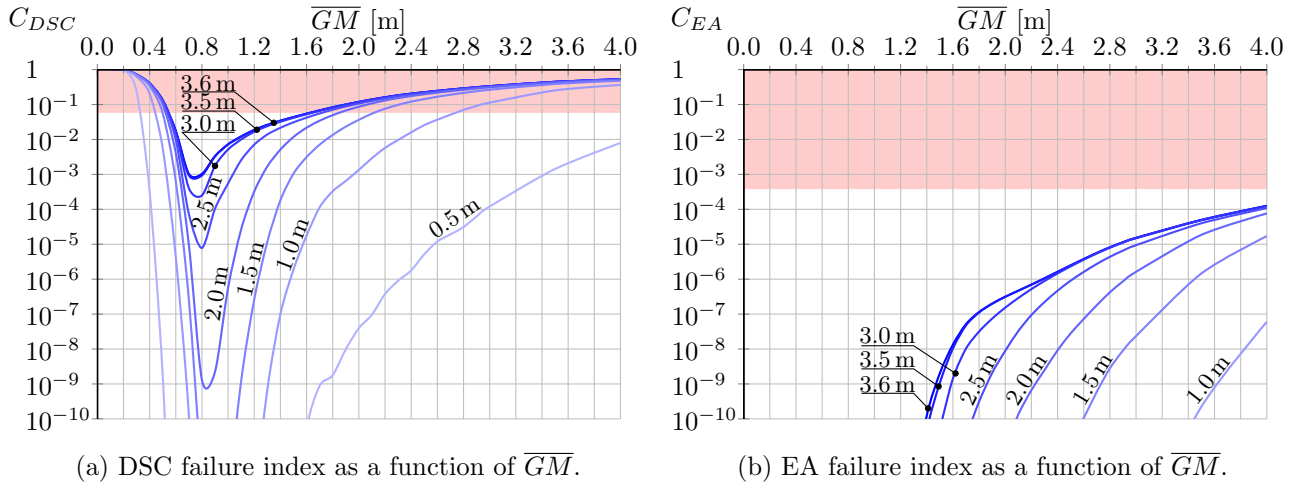
Figure 10.3: Stability assessment - vessel C with bilge keels. The results following the introduction of the operational limitations with respect to maximum significant wave height.

Additionally, results for the test vessels A, B and C without the bilge keels are given in Figures 10.4, 10.5 and 10.6, respectively.

As expected, the introduction of the operational limitations with respect to maximum significant wave height $H_{S,max}$ have a global effect on the results (with respect to $\overline{GM}$), reducing the indices C_{DSC} and C_{EA}. Each successive reduction of $H_{S,max}$ results in gradually lower C_{DSC} and C_{EA}. Results for $H_{S,max} = 3.6$ m and $H_{S,max} = 3.5$ m have similar values due to a small difference in the input scatter table used (see Table 5.1), and the corresponding curves are usually overlapping. Moreover, it seems that the differences between all $H_{S,max}$ curves are smaller for higher metacentric heights.

In this Chapter, the long-term standards, i.e. acceptable level of C_{DSC} and C_{EA} values, are considered to be the ones provided by the SGISC. If, for example, attention is paid to Figure 10.3(a), it can be noticed that the range of acceptable $\overline{GM}$ is significantly increased with the reduction of $H_{S,max}$; for $H_{S,max} = 3.6$ m the range is $\overline{GM} = 0.545$ m $\div$ 1.642 m, for $H_{S,max} = 2.5$ m the range is $\overline{GM} = 0.536$ m $\div$ 1.731 m, for $H_{S,max} = 1.0$ m the range is $\overline{GM} = 0.444$ m $\div$ 2.749 m and so on.

(a) DSC failure index as a function of $\overline{GM}$.

(b) EA failure index as a function of $\overline{GM}$.
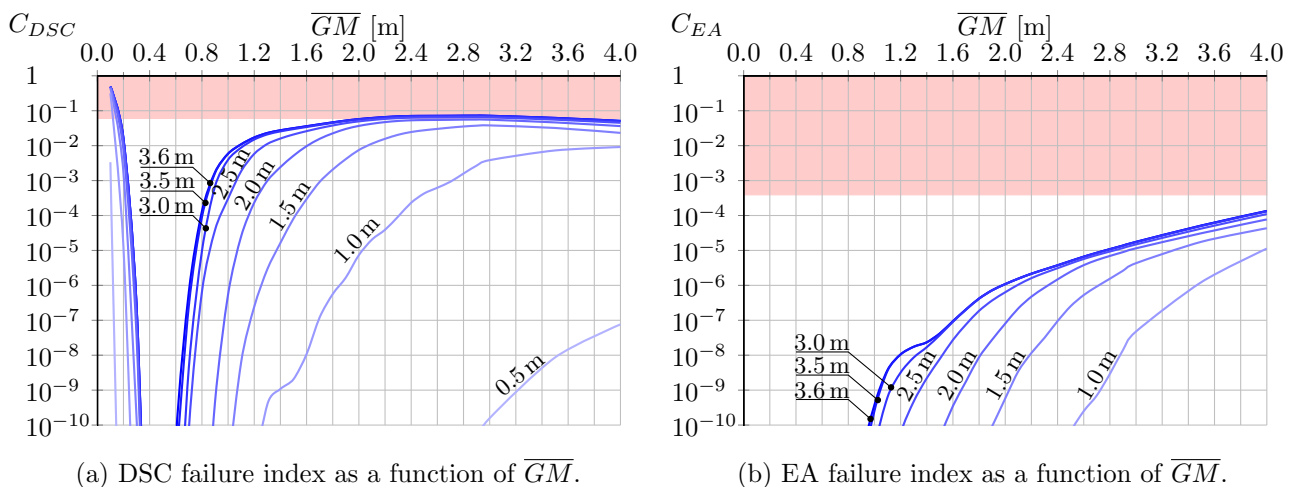
Figure 10.4: Stability assessment - vessel A without bilge keels. The results following the introduction of the operational limitations with respect to maximum significant wave height.

(a) DSC failure index as a function of $\overline{GM}$.

(b) EA failure index as a function of $\overline{GM}$.
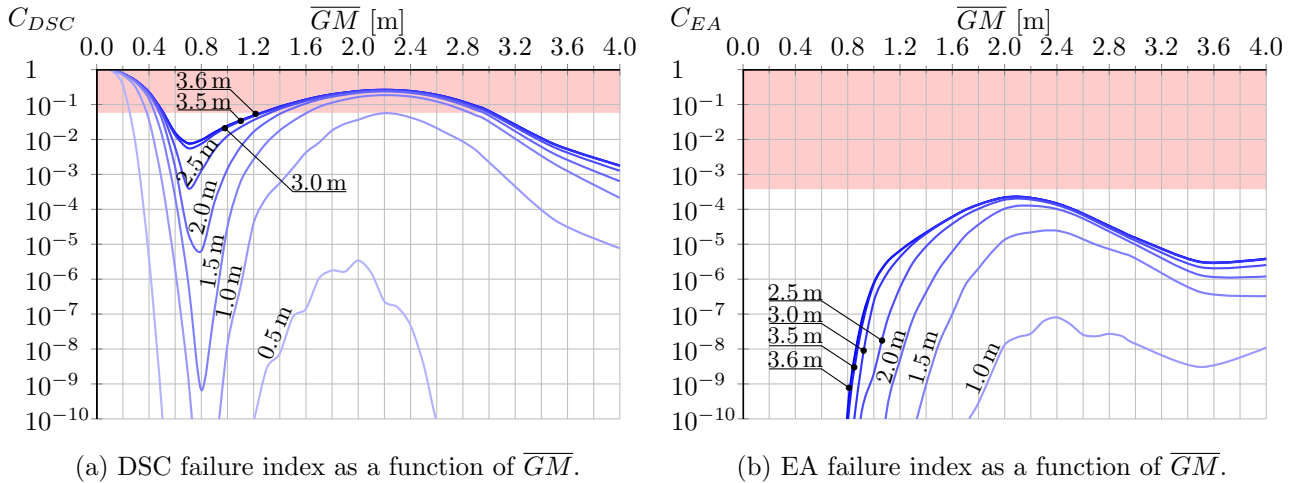
Figure 10.5: Stability assessment - vessel B without bilge keels. The results following the introduction of the operational limitations with respect to maximum significant wave height.

(a) DSC failure index as a function of $\overline{GM}$.

(b) EA failure index as a function of $\overline{GM}$.
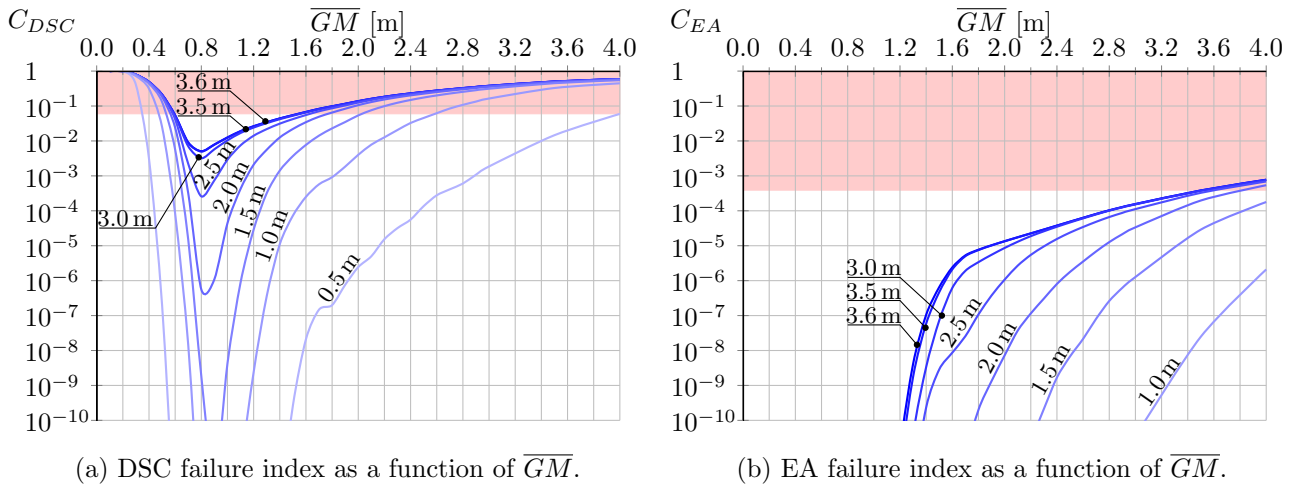
Figure 10.6: Stability assessment - vessel C without bilge keels. The results following the introduction of the operational limitations with respect to maximum significant wave height.

However, reading out the Figures in this form is not practical. Therefore, it is more practical to plot a graph of operational limitations, as shown in Figures 10.7, 10.8 and 10.9, for the test vessels A, B and C, respectively. The hatched area in Figures represents the range of acceptable metacentric heights (for which both C_{DSC} and C_{EA} are below the standards) plotted as a function of $H_{S,max}$. The area is bounded by the obtained acceptable ranges of $\overline{GM}$, but also by the range of expected loading conditions for a vessel (see explanation in Section 1.2.1). Therefore, using only two values: forecast for the significant wave height $H_{S,max}$ and metacentric height of the ship $\overline{GM}$ it is possible to assess intact stability in expected weather conditions based on the previously calculated operational limitations. Furthermore, while in Figure 10.3 discrete values of $H_{S,max}$ were used, the figure of operational limitation provides a continuous interpolated values.

In order to quantify the effectiveness of a design and operational measures, some indicators could be introduced. The vessel operational limitations index OLI_1 could be defined as the ratio of the calculated operational limitations (the hatched areas in Figures 10.7, 10.8 and 10.9) and the theoretical maximum of operational limitations (see Table 10.1). Thus, it would be $OLI_{1,max} = 1$ in case that the unrestricted service in the specified coastal area would be possible

with any technically viable vertical cargo distribution at a given draught.

The position of the centroid of the hatched area with respect to the abscissa of the OL chart could be used as an additional information on the vessel operational limitations (see Table 10.1). Therefore, the operational limitation index OLI_2 is introduced, which is obtained when the centroid of the hatched area is normalised with the half of the maximal significant wave height in the wave scatter table. The greater the value of OLI_2, the wider are the limits of operation which correspond to the higher maximum significant wave heights. Consequently, in case of unrestricted service in a specified coastal area it would be $OLI_{2,max} = 1$.

Although increase in OLI_1 is followed by increase in OLI_2 in these examples, it may not always be the case. By changing the loading conditions (i.e. by changing draught), different combinations of operational limitation indices are possible, providing additional insight into the effectiveness of a design (see Rudaković & Bačkalov, 2019).


(a) With bilge keels.   (b) Without bilge keels.
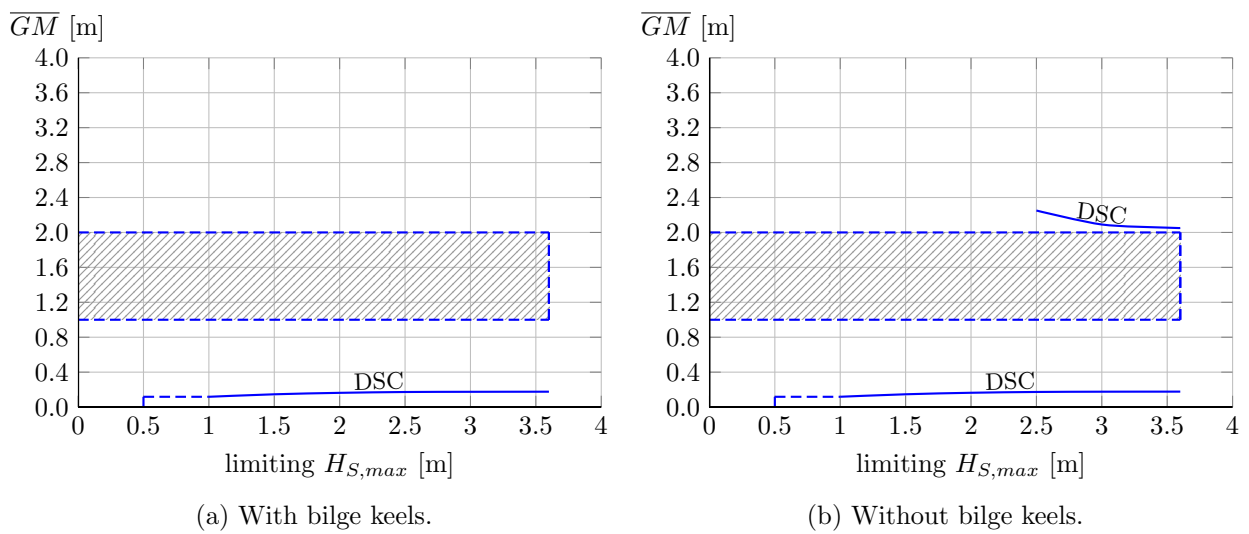
Figure 10.7: Operational limitations graph for the test vessel A.

(a) With bilge keels.   (b) Without bilge keels.
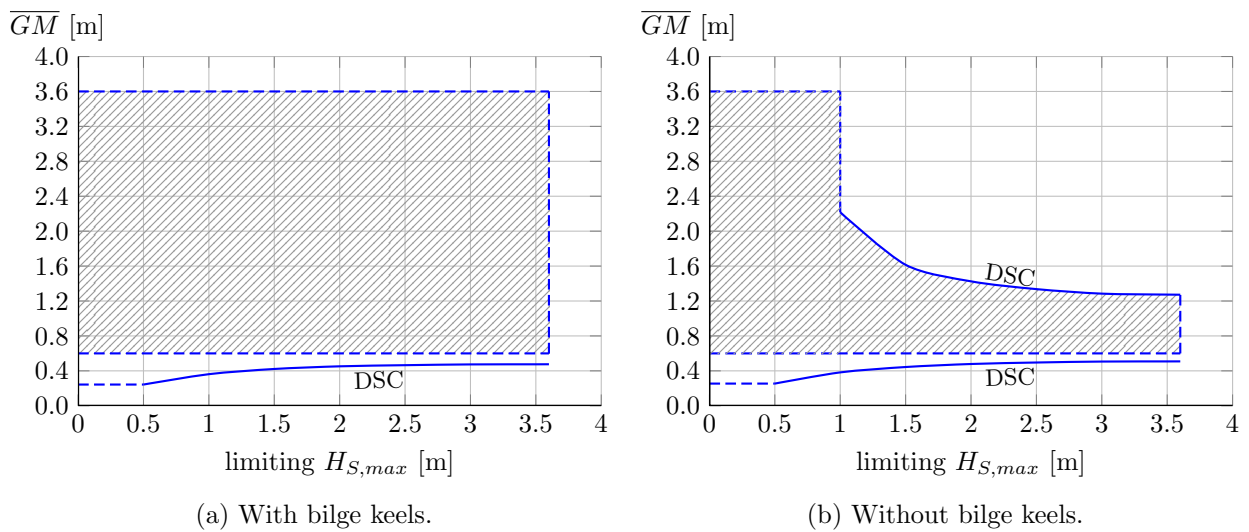
Figure 10.8: Operational limitations graph for the test vessel B.

(a) With bilge keels.

(b) Without bilge keels.
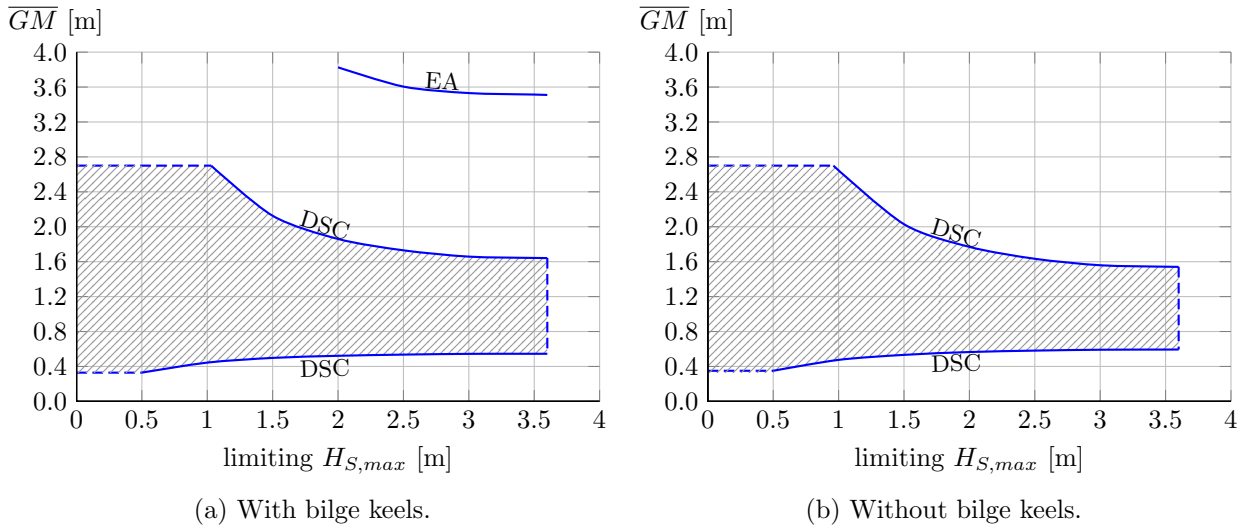
Figure 10.9: Operational limitations graph for the test vessel C.

Table 10.1: Operation limitation indices for the test vessels.

	Vessel A		Vessel B		Vessel C	
bilge keels	yes	no	yes	no	yes	no
OLI_1	1.00	1.00	1.00	0.48	0.70	0.65
OLI_2	1.00	1.00	1.00	0.66	0.83	0.80

10.3   Conclusions

This Chapter investigated the application of the operational limitations with respect to maximum significant wave height to river-sea ships. By setting the maximum significant wave height, river-sea ships may extent the range of metacentric heights or even be provided with a possibility to operate in coastal water, in condition that are considered to be safe from the stability point of view. It is a concept that is foreseen for use within the SGISC, and it is, in a similar way, already implemented to river-sea ships in Belgium and France.

Operational limitation graphs are presented in this Chapter, which make it more practical to obtain pre-calculated data of acceptable combinations of maximum allowable significant wave height and metacentric height. These graphs are supplemented with the introduction of the operational limitation indices OLI_1 and OLI_2. It is a concept that could serve as a tool for comparing vessels in order to assess the effectiveness of a design in terms of operability.

Chapter 11

Development of Vulnerability Level 1 of Dead Ship Condition for river-sea ships

11.1 Introduction

Several crucial modifications and improvements of the Dead Ship Condition and Excessive Acceleration criteria have been suggested in the previous chapters. Implementation of the criteria to river-sea ships is now possible, with an improved physical model that more accurately describes ship roll motion in beam waves (and wind). Although the novel procedure can be utilized according to the previous chapters, the consolidated procedures are given in Appendix E. However, the final step in stability assessment is missing, since the long-term standards for the Dead Ship Condition and the Excessive Acceleration Vulnerability Level 2 are not defined.

The presented procedures for the DSC and EA criteria are a reliable way of stability assessment. However, sometimes they can lead to an unnecessary work, for example, for a ship that is considered not to be vulnerable to a mode of stability failure. Therefore, the possibility of developing simple and consistent Dead Ship Condition Vulnerability Level 1 procedure, directly derived from the Vulnerability Level 2, will be tested as well in this Chapter. Similarly to the logic behind the SGISC, a multi-tiered approach will be provided, giving a user the possibility to choose an appropriate level of complexity, but conservativeness, too.

The goal of the Chapter is to provide the unified procedure for the novel approach to stability assessment of river-sea ships, following the research presented in the previous chapters. First, the procedures based on the modified Dead Ship Condition and Excessive Acceleration criteria from the SGISC framework are given in Appendix E. Then, the final part required for the complete stability assessment, the standards for the Vulnerability Level 2, are discussed in Section 11.2. Based on the provided procedures, the stability assessments of the vessels from the database are obtained, which are then used in Section 11.3 for the development of the Vulnerability Level 1 procedures for the Dead Ship Condition. Finally, the summary of the Chapter and concluding remarks are given in Section 11.4.

11.2 Discussion on long-term standards for Vulnerability Level 2

Setting the appropriate intact stability long-term standard is a delicate process. During the SGISC development, standards for various stability failure modes were set, changed and modified, in order to achieve two main requirements: the consistency between the tiers of stability assessment, and an adequate balance of safety achieved by the novel methodology and the cost-effectiveness of its use. The consistency between the tiers implies that the more com-

plex assessment levels should return less conservative results. On the other hand, the safety achieved by the newly-introduced standards should not come at a too high cost, i.e. it should not be over-restrictive for the existing fleet. Ultimately, the standards were adopted and the test phase of SGISC is expected to start, when soundness of the procedures will be analysed and possibly corrected, if needed. The corrections, perhaps, would most easily be done by fine-tuning the standards. A similar approach was already used in the development phase, when the relationship between the DSC Vulnerability Level 1 and Level 2 was tested (see IMO, 2015b; Umeda & Francescutto, 2016) using an interesting concept: the results of the calculation of the failure index C_{DSC} (obtained with the DSC L2) were presented as function of the relation b/a (from the DSC L1), for a population of existing ships. It was then possible to set the standard for Level 2, based on the condition that the calculated C_{DSC} values are below the standard if $b/a > 1$. Although it served as a good starting point, this was proved to be insufficient, as further inconsistencies between the levels were noticed (see IMO, 2019a). Another option would be to form the long-term standard based on the appropriate statistical data on frequency of accidents (per ship per year). Such approach was discussed in IMO (2019c) where average frequency of accidents of container ships due to heavy weather (originating from the Formal Safety Assessment study IMO, 2007) was used as a basis for the development of safety levels. It is worth noting that Hofman & Bačkalov (2005) discussed the appropriate standard by comparing the probabilities of stability failures corresponding to the minimal metacentric heights (calculated based on the Weather Criterion requirements) of several existing ships. The appropriate standard was adopted as a trade-off between safety and potential effects on the existing fleet.

For the purpose of the thesis, it is maybe pragmatic to set the same standards for river-sea ships as the ones within the SGISC. However, analysing the figures of stability assessments after each modification of the procedure, a general tendency of failure index reduction can be noticed. In some cases, those modifications are the result of improved physical model implementation of a phenomenon (e.g. the introduction of the reduced 3DOF method), which can significantly change the result of stability assessment. Therefore, the long-term standards should be re-examined. As a starting point, it would be interesting to perform the similar analysis as in IMO (2015b) or Hofman & Bačkalov (2005), however, there is no method, alike the Weather Criterion, that can reflect neither the condition in which river-sea ships operate, nor the ship particulars. Neither there are available appropriate data on frequency of accidents of river-sea ships. The second option could be to take the loading conditions of vessels and environmental conditions in which existing river-sea ships sailed without an incident. Those vessels and loading conditions could be than considered as safe, for which failure indices could be obtained based on criteria. Finally, the obtained indices should be used to set new standards or at least to get a rough notion of it. Unfortunately, such information is not available for this research. Therefore, in this instance, provisional long-term standards will be used.

For the purpose of derivation of the Vulnerability Level 1 of Dead Ship Condition, the same standard as in SGISC $R_{DS0} = 0.006$, will be used. The proposed standard is subjected to discussion, and as it was case with the standards from the SGISC, there is a need for its optimisation. Ideally, the soundness of the procedure, as well as the adopted standards should be tested in practice, by monitoring the performance of a river-sea fleet in realistic conditions. However, one should have in mind that the goal is to optimise the long-term standards, while providing the acceptable level of safety and minimal restrictions of navigation.

11.3   Development of Vulnerability Level 1 for DSC

Within the SGISC, the Vulnerability Level 1 is usually derived from the more complex procedure (i.e. from Vulnerability Level 2), applying further simplification of the mathematical model.

However, so far this was not the case with the Dead Ship Condition, where Vulnerability Level 1 and Level 2 are developed independently. To be more precise, the Weather Criterion was implemented within the SGISC as the Vulnerability Level 1, with a modification of the wave steepness coefficient s. Although both Level 1 and Level 2 represent the same physical phenomenon, there is no simplification process that connects the two levels. Consequently, it is known that sometimes DSC Level 1 and Level 2 criteria can provide inconsistent results (as pointed out in IMO, 2019a). Therefore, the idea of this Section is to provide a new procedure for Vulnerability Level 1 derived directly from the results of the Vulnerability Level 2 assessment, and developed with the specific design and operational features of river-sea ships in mind. Although not impossible, it is definitely a challenging task to come up with simple, yet robust enough procedure suitable for the Vulnerability Level 1 criteria. An example of the derivation of DSC Vulnerability Level 1 procedure will be given in this Section.

A possible solution for the Vulnerability Level 1 derivation could be found in development of a simple regression model. As the long-term environmental characterisation, the scatter table of the Belgian coastal zone (given in 5.1) is used for this purpose. In order to develop a regression, the database (presented in Section 7.3) is extended by two additional hulls, generated for this purpose, in order to have a representative of container vessel of CEMT IV and CEMT III classes (as defined in CEMT, 1992). With the database defined, the Vulnerability Level 2 criteria, as defined in this Chapter, is applied, varying the loading conditions that are considered influential for the future regressions. Therefore, the range of metacentric heights $\overline{GM} = 0.1\,\text{m} \div 3.0\,\text{m}$ with the step of $\Delta\overline{GM} = 0.1\,\text{m}$ is used, with two additional values of 3.5 m and 4.0 m, in order to further extend the range. Furthermore, three different values of the bilge keels length are used – the maximum allowable by the Simplified Ikeda's method of $0.4L$, then $0.2L$, and no bilge keels. Regarding the Dead Ship Condition, two additional parameters are varied. The first is the windage lateral area A_L, which is varied in case of container vessels by changing the maximum number of container tiers (which consequentially also changed the wind lever Z). The second is the flooding angle, used in the range of $\varphi_{flood} = 5° \div 50°$ with the step of $\Delta\varphi_{flood} = 5°$. Additionally, in order to introduce the operational limitation with respect to maximum significant wave height, the values as defined in Chapter 10 are used – $H_{S,max} = 3.6\,\text{m}, 3.5\,\text{m}, 3.0\,\text{m}, 2.5\,\text{m}, 2.0\,\text{m}, 1.5\,\text{m}, 1.0\,\text{m}$ and 0.5 m. Only the design draught and even keel are considered, and the value for the dry roll radius of inertia is kept constant as $k_{xx} = 0.40B$. Therefore, this example will be limited to these loading conditions only. The combinations of $\overline{GM}\text{-}H_{S,max}\text{-}l_{BK}\text{-}\varphi_{flood}\text{-}A_L(Z)$ resulted in 422400 stability assessments in total in case of the Dead Ship Condition (taking also into account the calculations for the validation vessels, given in Section 1.2.2, which are not used for the regression model development, but will be used later on for the validation of the formulae).

With the results obtained, and based on the long-term standards suggested in the previous section, it is possible to obtain the:

- Minimal acceptable value of metacentric height – $\overline{GM}_{DSC,min}$

- Maximal acceptable value of metacentric height – $\overline{GM}_{DSC,max}$

The obtained data will be used as input for two regression models. Furthermore, the corresponding vessel particulars and loading conditions will be tested in order to select the influential parameters for the regressions. The regression models are conceived as simple polynomials, taking into account as few parameters as possible. An important consideration is to achieve the consistency between the Level 1 and Level 2 (i.e. the Level 1 must always be more conservative than the Level 2). Therefore, even though the proposed Vulnerability Level 1 is derived from the Vulnerability Level 2 it is not a performance-based, but a parametric criterion.

11.3.1 Dead Ship Condition - Vulnerability Level 1 regression

After analysis and tests, three parameters were selected as the most influential for the regression: the position of metacentre $\overline{KM}$, the angle of flooding φ_{flood} and a coefficient adopted from the 2008 IS Code that takes into account the dimensions of bilge keels, noted here, due to simplicity, as C_{BK}, where:

$$C_{BK} = \frac{A_K \cdot 100}{L_{WL} \cdot B} \tag{11.1}$$

and where A_K is the total area of the bilge keels.

Several more parameters were thoroughly considered, such as windage area, wind moment lever and various non-dimensional parameters. However, selecting the three parameters showed an optimal balance between goodness and simplicity of regression model, while an additional parameter would improve the prediction only moderately. Better results were obtained if the separate regressions were made for each maximum significant wave height used for the calculations, in comparison if $H_{S,max}$ is used as a parameter in the regression. Furthermore, it was noticed that better regression model was obtained if only CEMT Va and CEMT VIb vessels are used, corresponding to vessels length $L = 95\,\mathrm{m} \div 140\,\mathrm{m}$. The shorter vessels produced larger scattering of data, making the regression significantly inaccurate.

Both for $\overline{GM}_{DSC,min}$ and $\overline{GM}_{DSC,max}$ the same model was conceived regardless of the maximum significant wave height, changing the coefficient only. With aforementioned parameters, the model is proposed:

$$
\begin{aligned}
\overline{GM}_{DSC,min} = \overline{GM}_{DSC,max} = {}& a_0 + a_1 \cdot C_{BK} + a_2 \cdot C_{BK}^2 + a_3 \cdot \overline{KM} + a_4 \cdot \overline{KM}^2 + a_5 \cdot \varphi_{flood} \\
& + a_6 \cdot \varphi_{flood}^2 + a_7 \cdot C_{BK} \cdot \overline{KM} + a_8 \cdot C_{BK} \cdot \varphi_{flood} + a_9 \cdot \overline{KM} \cdot \varphi_{flood}
\end{aligned} \tag{11.2}
$$

In Figure 11.1, the values obtained using the Vulnerability Level 2 procedure (given in Section E.1) for the complete database are plotted as a function of newly developed regressions, for different maximum significant wave heights. The full line shows the regression formulae values. Because the Level 1 should always be more conservative than the Level 2, all data points should be below the full line (which is currently not the case with regression formulae). Therefore, the formulae are modified by simply increasing the interval by the most extreme difference between the values calculated by the Level 2 and the formulae. By doing this, the Vulnerability Level 1 is somewhat less precise, but always more conservative than the Level 2.

The obtained coefficients a_0, a_1, a_2, ..., a_9 for the regression model of the minimal acceptable value of metacentric height for the Dead Ship Condition $\overline{GM}_{DSC,min}$, are given in Table 11.1. The first column represent the maximum significant wave height $H_{S,max}$, for which the corresponding coefficients should be used within Equation (11.2). Four different $H_{S,max}$ were used only, in order to provide consistency between each regression.

Table 11.1: Regression coefficients for the $\overline{GM}_{DSC,min}$.

$H_{S,max}$	a_0	a_1	a_2	a_3	a_4	a_5	a_6	a_7	a_8	a_9
1.0	2.075	0.045	-0.0050	-0.414	0.0467	-0.0215	0.00046	-0.0078	0.00000	-0.00219
2.0	2.308	0.063	-0.0058	-0.473	0.0538	-0.0196	0.00045	-0.0096	-0.00027	-0.00244
3.0	2.273	0.049	-0.0046	-0.478	0.0548	-0.0184	0.00045	-0.0065	-0.00042	-0.00263
3.6	2.245	0.058	-0.0055	-0.471	0.0544	-0.0181	0.00044	-0.0074	-0.00051	-0.00268
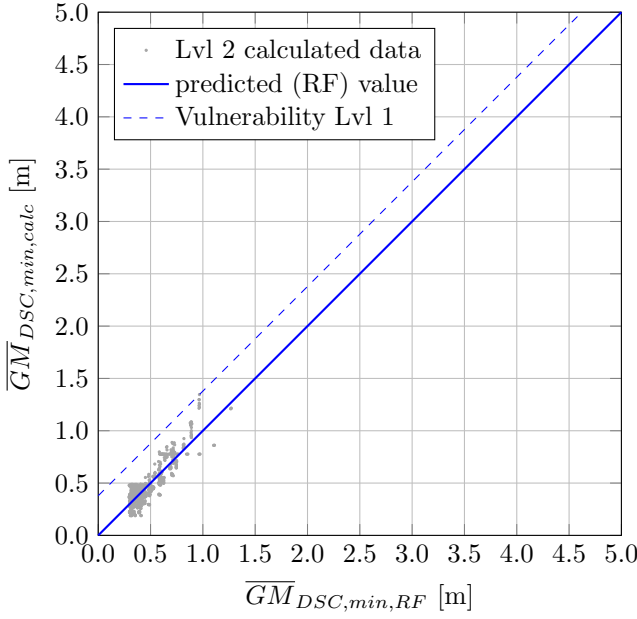
(a) Maximum significant wave height $H_{S,max} = 3.6\,\text{m}$.
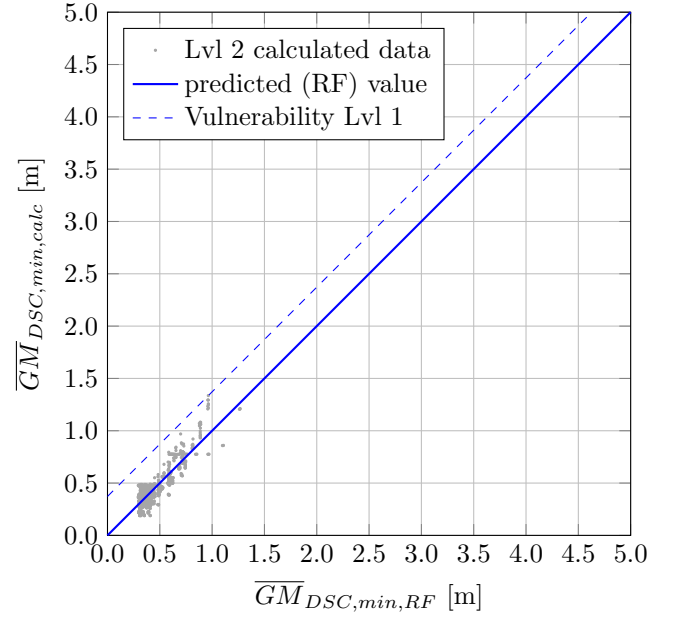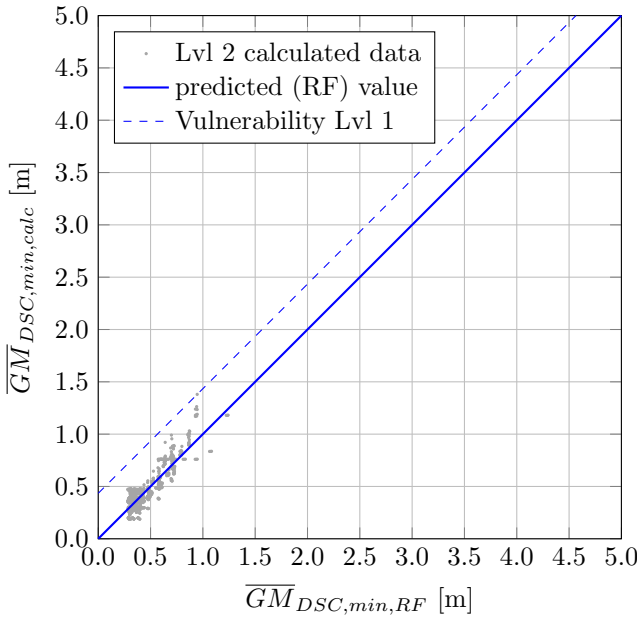
(b) Maximum significant wave height $H_{S,max} = 3.0\,\text{m}$.

(c) Maximum significant wave height $H_{S,max} = 2.0\,\text{m}$.
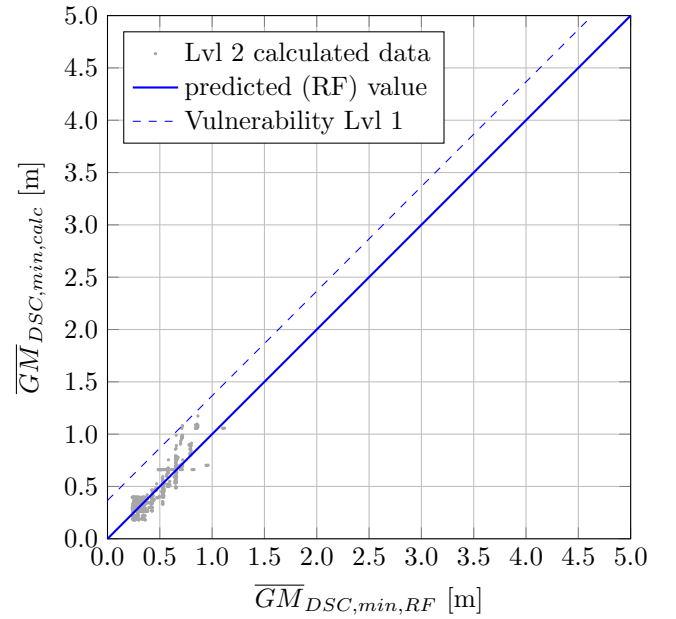
(d) Maximum significant wave height $H_{S,max} = 1.0\,\text{m}$.

Figure 11.1: Calculated values of $\overline{GM}_{DSC,min}$ (DSC L2) versus predicted values (regression formula).

The formulae for $\overline{GM}_{DSC,max}$ are obtained employing the similar principle. In Figure 11.2, the values obtained using the Vulnerability Level 2 procedure are plotted as a function of newly developed regressions, for different maximum significant wave heights. The same problem of conservativeness applies here, however, now the data points corresponding to the Vulnerability Level 2 have to be above the Vulnerability Level 1. The dashed lines correspond to the newly proposed regression formulae for $\overline{GM}_{DSC,max}$ estimation.

The regression model for the maximal acceptable value of metacentric height for the Dead Ship Condition $\overline{GM}_{DSC,max}$ takes the same form as the previous model given by Equation (11.2). The only difference is in the coefficients a_0, a_1, a_2, ..., a_9, which are given in the Table 11.2.
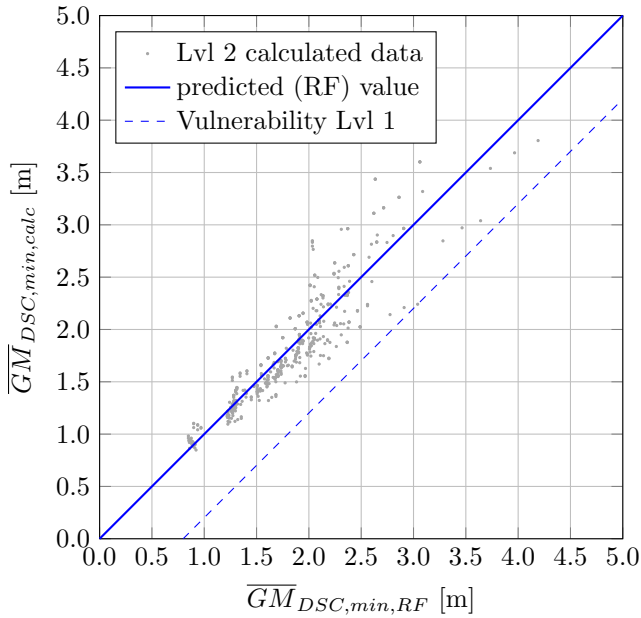
(a) Maximum significant wave height $H_{S,max} = 3.6\,\text{m}$.
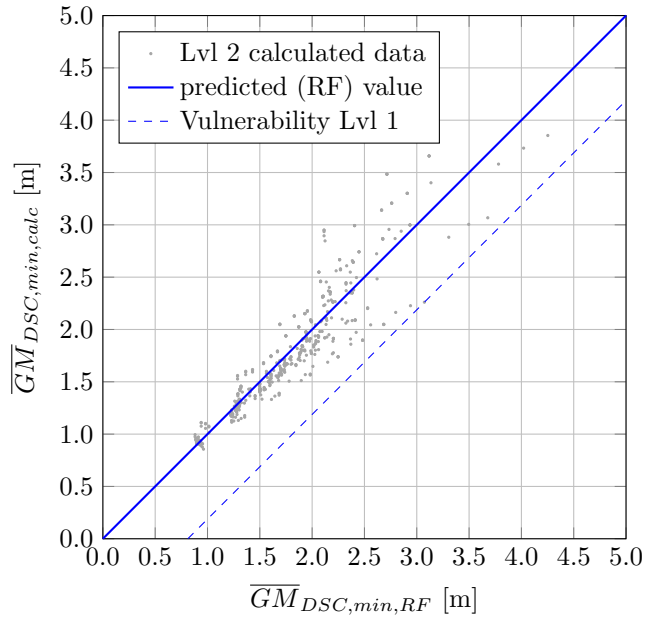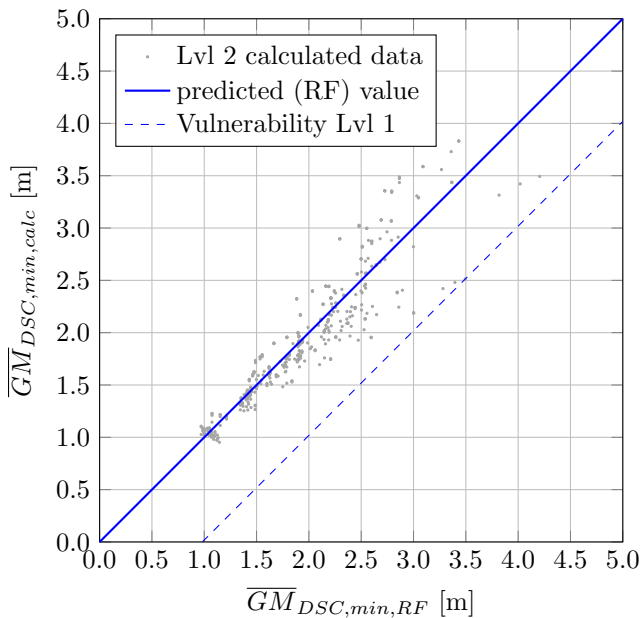
(b) Maximum significant wave height $H_{S,max} = 3.0\,\text{m}$.

(c) Maximum significant wave height $H_{S,max} = 2.0\,\text{m}$.
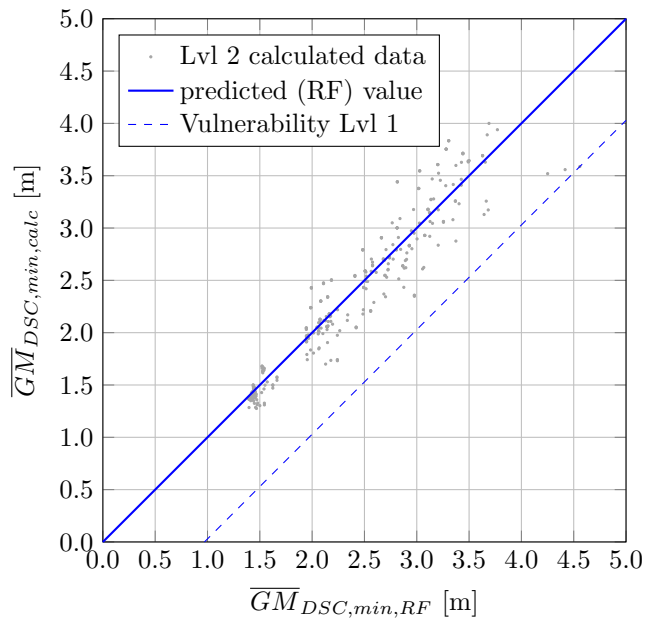
(d) Maximum significant wave height $H_{S,max} = 1.0\,\text{m}$.

Figure 11.2: Calculated values of $\overline{GM}_{DSC,max}$ (DSC L2) versus predicted values (regression formula).

Table 11.2: Regression coefficients for the $\overline{GM}_{DSC,max}$.

$H_{S,max}$	a_0	a_1	a_2	a_3	a_4	a_5	a_6	a_7	a_8	a_9
1.0	12.964	-0.602	-0.0575	-4.833	0.4457	-0.1172	0.00076	0.1052	0.03315	0.04259
2.0	10.677	-0.821	-0.0339	-4.018	0.3714	-0.0578	0.00036	0.1157	0.03651	0.02068
3.0	8.412	-0.694	-0.0182	-3.267	0.3055	-0.0044	-0.00063	0.1159	0.02045	0.01496
3.6	8.000	-0.672	-0.0122	-3.175	0.2995	0.0199	-0.00104	0.1113	0.01992	0.01256

The presented formulae are considered to be applicable to vessels with the similar characteristics as the vessels from the database (given in Section 1.2 and further described in Appendix A) used for the development of the formulae. In general, formulae are considered to be applicable for the range of particulars:

$$4.0\,\mathrm{m} \leq \overline{KM} \leq 7.7\,\mathrm{m}$$
$$0 \leq C_{BK} \leq 1.77$$
$$5° \leq \varphi_{flood} \leq 50° \qquad (11.3)$$
$$95\,\mathrm{m} \leq L \leq 140\,\mathrm{m}$$
$$k_{xx} = 0.40B$$

11.3.2 Validation of regression models

The vessel V2 (described in Section 1.2.2), which was not used for the development of the regression formulae, fits in the applicability criteria of $\overline{GM}_{DSC,min}$ and $\overline{GM}_{DSC,max}$ regression formulae, given in Section 11.3.1. Therefore, it will be used for the validation of the formulae, given by Equation (11.2) and Table 11.1 and 11.2.

Because the vessel is a container vessel, four different loading conditions are considered, corresponding to the four lateral windage areas. The flooding angle is systematically varied from $\varphi_{flood} = 5°$ up to $\varphi_{flood} = 50°$. Three combinations of the bilge keels length are used: $0.4L$, $0.2L$ and no bilge keels. After the calculations of the Dead Ship Condition Vulnerability Level 2 were performed, the corresponding values for $\overline{GM}_{DSC,min}$ and $\overline{GM}_{DSC,max}$ based on the calculations and based on the regression formulae are obtained. In Figure 11.3, the values of $\overline{GM}_{DSC,min}$ and $\overline{GM}_{DSC,max}$ based on the Vulnerability Level 2 are plotted as a function of predicted values based on the regression formulae for the all maximum significant wave heights. It is shown that for all combinations of the loading conditions and the flooding angles, the derived Level 1 procedure returns results which are always more conservative than the Level 2.

Furthermore, the comparison of the values obtained by the Level 2 and by the newly developed Level 1 procedures for the vessel B and vessel C (vessel A is not taken into account because it is out of the applicability range for the Level 1 formulae), are given in Table 11.3. It can be seen that Level 1 results are always more conservative then the Level 2 results, although the Level 1 results have somewhat reduced range of acceptable metacentric heights. The influence of the bilge keels is also noticeable.

According to the derived Level 1, the vessel C has limited operability range, and can operate in the coastal area up to $H_{S,max} = 2\,\mathrm{m}$ if the bilge keels are installed. On the other hand, the vessels B and T19 have significantly larger operability range. However, if Figures 10.3(a) and 10.6(a) are observed and compared to Figures 10.2(a) and 10.5(a), it can be seen the vessel C is a more vulnerable vessel than the vessel B, even if Vulnerability Level 2 is employed, due to larger windage area and smaller angle of flooding. This is, to some extent, recognised by the Vulnerability Level 1 formulae.

Table 11.3: Comparison of the results for the Vulnerability Level 1 and Level 2 procedures for the vessels B, C and T19.

vessel	bilge keels	$H_{S,max}$	$\overline{GM}_{DSC,min}$		$\overline{GM}_{DSC,max}$	
			DSC L2	DSC L1	DSC L2	DSC L1
Vessel B	no	1.0	0.457	0.823	2.025	1.960
		2.0	0.575	0.857	1.383	0.862
		3.0	0.630	0.950	1.012	0.548
		3.6	0.643	0.961	0.967	0.517
	yes	1.0	0.425	0.821	unrestricted	2.783
		2.0	0.526	0.864	1.876	1.329
		3.0	0.560	0.944	1.402	0.837
		3.6	0.562	0.958	1.342	0.790
Vessel C	no	1.0	0.531	0.912	2.058	0.600
		2.0	0.638	0.926	1.308	0.389
		3.0	0.712	1.014	0.905	0.084
		3.6	0.747	1.019	0.855	0.045
	yes	1.0	0.498	0.923	2.209	0.853
		2.0	0.591	0.952	1.418	0.426
		3.0	0.627	1.018	1.018	0.184
		3.6	0.636	1.031	0.971	0.142
Vessel T19	no	1.0	0.402	0.780	unrestricted	4.410
		2.0	0.484	0.835	2.458	1.470
		3.0	0.502	0.938	1.654	0.942
		3.6	0.503	0.951	1.578	0.881
	yes	1.0	0.402	0.770	unrestricted	5.625
		2.0	0.482	0.830	unrestricted	2.244
		3.0	0.501	0.926	2.314	1.340
		3.6	0.502	0.941	2.145	1.251
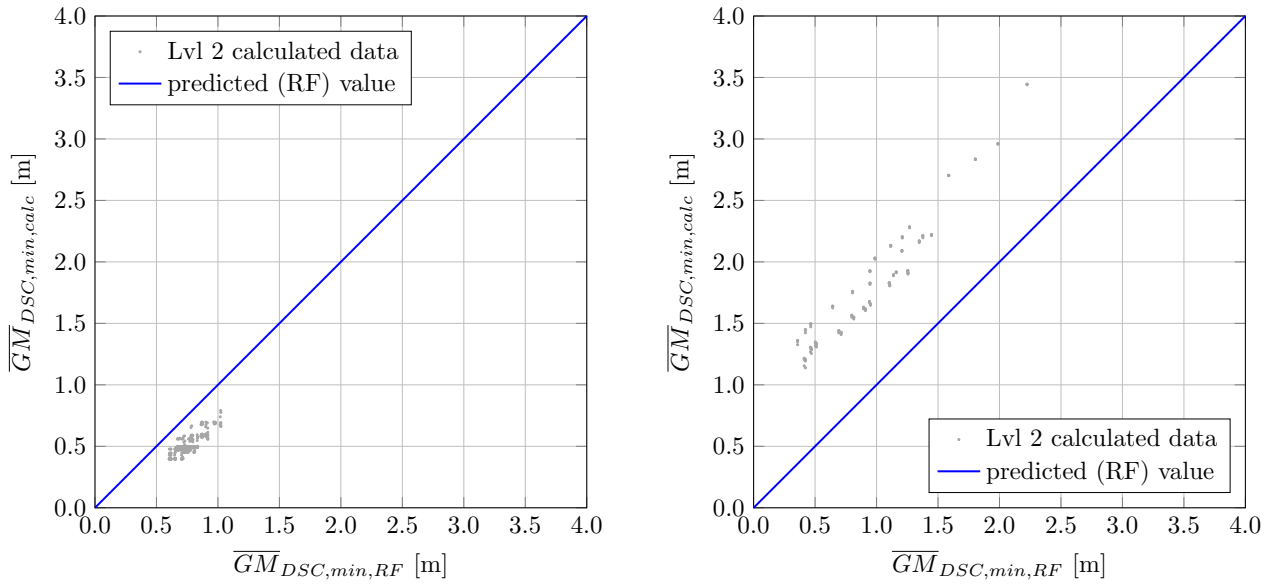
(a) Calculated values of $\overline{GM}_{DSC,min}$ (DSC L2) versus predicted values (regression formula).

(b) Calculated values of $\overline{GM}_{DSC,max}$ (DSC L2) versus predicted values (regression formula).

Figure 11.3: Validation of the DSC Vulnerability Level 1 regression formulae.

11.4 Conclusions

In the previous Chapters, the newly developed procedures for the Dead Ship Condition and Excessive Acceleration Vulnerability Level 2 are presented. The procedures were tested in the previous chapters, by applying them to the three river-sea test vessels. The part that was not examined, up until this Chapter, is the selection of the appropriate long-term standards for the developed Vulnerability Level 2 procedures. However, it was concluded that the adoption of the proper standards is too demanding at the moment, and that the developed procedures should be first tested in practice, in order to gather more information. For the time being, a set of provisional standards are adopted, following a brief discussion.

Although the procedure for the Dead Ship Condition, corresponding to the Vulnerability Level 2 criteria, provides a framework for the stability assessment of river-sea ships, the need for a simpler and faster estimation method was expressed, which would correspond to the Vulnerability Level 1 criteria. These Level 1 procedures would have to be more conservative than the Level 2, but should provide a quick result to be applied in an early ship design stage or on ships that are not considered vulnerable to a mode of stability failure.

Based on stability assessment of river-sea ships performed at Vulnerability Level 2, it would be possible to derive the Vulnerability Level 1 procedures, by applying the regression analysis. Following this approach, the regression models for ranges of acceptable metacentric heights according to the Dead Ship Condition (defined by the minimum $\overline{GM}_{DSC,min}$ and maximum $\overline{GM}_{DSC,max}$ metacentric heights) are obtained. The separate models for four different maximum significant wave heights were derived – $H_{S,max} = 3.6\,\mathrm{m}, 3.0\,\mathrm{m}, 2.0\,\mathrm{m}$ and $1.0\,\mathrm{m}$. The developed models showed good consistent relation with the Vulnerability Level 2 results. However, an advantage of this type of procedure, in contrast to the DSC Vulnerability Level 1 within the SGISC, is that both lower and upper limits of metacentric height can be estimated.

The analysis of the possible Vulnerability Level 1 regression model developed from the results based on Vulnerability Level 2 is just a case study of the principle. The regression model obtained in this way would be location-specific, as it requires the selection of environmental conditions corresponding to the observed area. Furthermore, the model is applicable to the

similar vessels to those used for its development, while the larger database of vessels, and even more calculations performed, would results in more precise and consistent formulae. The larger database would possibly extend the applicability range of such formulae.

Chapter 12

Conclusion

The thesis examines the stability of river-sea ships in light of contemporary progress of stability assessment of sea-going ships and proposes a novel approach to intact stability analysis of this type of ships, applicable in both design phase and operation. Even though the proposed approach is based on the Second Generation Intact Stability Criteria framework, it introduces a range of modifications which concern the practical aspects (i.e. the calculation procedures) as well as the conceptual side of the framework.

River-sea ships are primarily inland navigation vessels that are allowed to operate in coastal areas, if certain technical requirements are met and environmental conditions are favourable. River-sea ships currently operate worldwide, which resulted in development of various different regulations. Thus, the regulations are inevitably location-specific, valid only for the operational area for which they are conceived. Therefore, the current stability regulations for river-sea ships are examined in Chapter 2. It was concluded that the regulations are diverse, ranging from the deterministic empirical requirements to risk-based stability assessment, but always employing certain assumptions and simplifications. Therefore, the focus of the research was put on the Second Generation Intact Stability Criteria and the possibility of its implementation to river-sea ships.

The Second Generation Intact Stability Criteria (SGISC) is a new set of regulations that is currently in the final stage of development, put forward by International Maritime Organisation. SGISC are conceived as the state-of-the-art procedures applicable to all sea-going ships, considering five modes of stability failures to which ships could be vulnerable: Pure Loss of Stability, Parametric Roll, Surf-riding/Broaching, Dead Ship Condition and Excessive Acceleration. As these advanced hydrodynamical models may be too complex for everyday use, which requires qualified experts and specialised experimental facilities, a multi-tiered approach was adopted. Each successive tier is less complex but more conservative then the previous one: Direct Stability Assessment, Vulnerability Level 2, Vulnerability Level 1, plus an extra level – Operational Guidance/Operational Limitations. However, due to distinctive particulars of river-sea ships (long parallel middle bodies resulting in full bodied hulls, and low forward speeds) these vessels are not vulnerable to the Pure Loss of Stability, Parametric Roll and Surf-riding/Broaching. Nevertheless, they are vulnerable to the Dead Ship Condition and Excessive Acceleration failure modes, which made the roll motion due to beam wind and waves the focus of the research. These conclusions were presented in Chapter 3.

The possibility of implementing the Dead Ship Condition and Excessive Acceleration criteria to river-sea ships is examined in Chapter 4, for which the suitable computer codes were developed for the purpose of the research for the thesis. However, it was noticed that, unless the test vessels were equipped with bilge keels, it was not possible to obtain long-term indices of stability failures. Nonetheless, the results with the bilge keels installed are possible, but the results indicated that the test vessels could not comply with the Dead Ship Condition and

Excessive Accelerations criteria. This could have been the consequence of the environmental conditions prescribed by the SGISC, which correspond to the North Atlantic, and as such cannot be considered as an appropriate representation of weather conditions in coastal areas in which river-sea ships are expected to operate.

Therefore, in Chapter 5, a possibility of adopting more appropriate environmental conditions are examined. Modification of the environmental conditions is foreseen within the SGISC, which is considered as the operational limitation with respect to environmental conditions. In accordance to the SGISC, it is suggested that environmental conditions should be adapted based on corresponding area of operations of a specific river-sea ship. An example of scatter table, wave spectrum and wind-wave relation modification was given, corresponding to the Belgian coast. The stability assessment of the test vessels showed that a proper representation of the environmental conditions is of paramount importance in stability assessment, because, in this particular case, it resulted in significant reduction of failure indices. However, the failure indices for the test vessels were still unable to obtain, unless they were equipped with bilge keels, suggesting that they are unable to comply with the SGISC requirements. Such results raised the suspicion, as they seemed to be in disagreement with the operational practice with river-sea ships in the North Sea as well as with the expected outcome of the SGISC procedures. This triggered the analysis of applicability of methods used for estimation of roll damping and wave excitation moments.

Therefore, the roll damping estimation method proposed for the use within the SGISC (i.e. the Simplified Ikeda's method) was analysed in Chapter 6. The analysis demonstrated that the total roll damping of examined ships decreased with the increase of the roll amplitude. In extreme cases, some ships would have even reach negative roll damping at large roll amplitudes. After further investigation, it was revealed that a component of the total roll damping, the eddy damping, may become negative for the block coefficients corresponding to $C_B > 0.84$ (which is the case for the most river-sea ships). As a result, a modification of eddy making component was proposed, which eliminated the issue. Consequently, the reassessment of stability of river-sea ships confirmed that even the vessels without bilge keels could comply with the Dead Ship Condition and Excessive Acceleration criteria (with modified environmental conditions). It should be noted that the problem of negative eddy making component is not limited to inland vessels, but affects sea-going ships with high block coefficient, too. Moreover, the clear benefits of the presence of bilge keels are recognised, as their presence resulted in the significant increase of the acceptable ranges of metacentric heights, both according to the Dead Ship Condition and Excessive Acceleration criteria. Therefore, it is recommended to install bilge keels on river-sea ships, as this is both inexpensive and effective method for intact stability improvement.

An important aspect in stability assessment in beam waves is to properly account for the wave excitation moment. Therefore, an analysis of the most suitable method for the effective wave slope coefficient estimation is examined in Chapter 7. Several methods based on three different approaches were examined: a method based on linear hydrodynamic (reduced 3DOF), two methods based on linear Froud-Krylov (3D panel and IMO method prescribed for use within the SGISC) and two semi-empirical methods. The research was carried out on the database of vessels in order to perform a comparative study. It was shown that, if applied to river-sea ships, the two Froude-Krylov methods provide very similar results, due to long parallel middle bodies and high midship section coefficients. However, the two Froude-Krylov methods are more conservative than the reduced 3DOF method, which is based on more advanced hydrodynamics and coupling of roll with sway and yaw. Therefore, it was concluded that the effective wave slope coefficient of river-sea ships could be estimated either by a method based on the Froude-Krylov approach, which is simpler to use, but also more conservative, or by the reduced 3DOF method which accounts for more accurate dynamic and hydrodynamic effects, but requires the use of a seakeeping software.

The similar principle was employed in the study of the natural roll period of river-sea ships, presented in Chapter 8. Several semi-empirical methods were considered, together with the reduced 3DOF method. It was concluded that the implementation of reduced 3DOF method may improve the natural roll period estimation, as it is based on more advanced hydrodynamics. However, the same as for the effective wave slope coefficient, it requires the use of a seakeeping software. Nevertheless, the stability of the test vessels are reassessed, following the modification of the effective wave slope coefficient and natural roll frequency according to the reduced 3DOF method. The results showed significant qualitative change, with a general tendency of failure index reduction.

Although the reduced 3DOF method is a promising method for the effective wave slope coefficient and natural roll period estimation, it may be too impractical for engineering practice. Therefore, corresponding approximate prediction methods based on regression analysis were developed in Chapter 9. In total, three regression models were proposed: a model for the natural roll frequency, a model for the effective wave slope coefficient at natural roll frequency and a model for the frequency dependant effective wave slope coefficient. The predictions obtained using the models show very good agreement with the results obtained with the reduced 3DOF method. Thus, another stability assessment of the test vessels was performed, but this time employing the regression formulae for the natural roll period and effective wave slope coefficient as a replacement for the reduced 3DOF method, in order to additionally validate the formulae. The differences between failure indices using the reduced 3DOF method and using the regression formulae are within the same order of magnitude, and therefore are considered to be acceptable. It was concluded that the benefits of the simplicity of employing the regression formulae by far surpass the inaccuracies that may arise in stability assessment. The consolidated procedures for stability assessment of river-sea ships considering all the modifications of the SGISC Vulnerability Level 2 for Dead Ship Condition and Excessive Accelerations presented in the thesis, are given in Appendix E.

Even with all the modifications of the Dead Ship Condition and Excessive Acceleration criteria, operations of the river-sea ships may still be limited to narrow ranges of loading conditions. Therefore, a possibility of applying operational limitation with respect to maximum significant wave height to the river-sea ships was analysed in Chapter 10. This is the concept that would allow the river-sea ships to operate in coastal area, if short-term environmental conditions (i.e. the significant wave height) is up to a certain value. Additionally, a concept of operational limitation indices OLI_1 and OLI_2 is introduced, which quantify the acceptable operability range represented by maximum significant wave height and metacentric height. It may serve as a useful tool for comparing vessels in order to assess the effectiveness of a design in terms of operability.

In Chapter 11, a brief discussion on adoption of the long-term standards (i.e. acceptable safety levels) was given. Moreover, a need for a simple procedure for stability assessment of river-sea ships, which could be used at Vulnerability Level 1 instead of Weather Criterion, was expressed. Therefore, after a systematic stability assessment of vessels from the database, a parametric criterion suitable for use at Vulnerability Level 1 of Dead Ship Condition, based on the regression analysis of results of stability assessment done at Vulnerability Level 2 was proposed. The proposal comprises a simple yet reliable formula which can be used in order to estimate the required minimal and maximal metacentric height based on few basic parameters only. Moreover, the validation of the proposed Vulnerability Level 1 showed that the consistency between the levels is achieved, as the Level 1 outcome is always more conservative than the Level 2.

Although the procedures for the Dead Ship Condition and Excessive Acceleration criteria for river-sea ships are developed, they are not quite completed. The question of the appropriate long-term standards remains open. Testing of the proposed criteria in actual operational

conditions could contribute to fine-tuning of standards. Furthermore, the modified eddy damping component is an important improvement, which helps in accurate modelling of the roll motion. Therefore, the possibility of improvement of the other damping components is worth a research. However, the Simplified Ikeda's method is based on the original Ikeda's research, which is carried out on a database of ship forms which are now considered as obsolete, and certainly different from the river-sea ship hulls. Therefore, a novel experimental model test (perhaps, similarly as it is done and explained in some recent researches, for example Oliva-Remola, 2018; Rodríguez et al., 2020), having in mind hull forms of river-sea ships, would be extremely beneficial for the accurate roll motion modelling. Although the regression models for the natural roll period and effective wave slope coefficients of river-sea ships are developed in this thesis, they are dependant of properly assumed roll radius of inertia of the ship, for which an accurate estimation method for inland vessels or river-sea ships does not exist. Therefore, it remained an opened issue in this thesis. Another aspect characteristic for river-sea ships, which is not considered in the thesis, is the influence of the low freeboard height, which can significantly influence the ship hydrodynamics in case of large roll angles (see e.g. Belenky et al., 2011; IMO, 2019a). Moreover, a research of the wind effects could be a rewarding step, as the influence of wind profile is not taken into account, as well as the influence of other motion (especially sway) on the wind force. Furthermore, the Excessive Acceleration criterion implements few empirical approximations, that should be examined. It is the case with, for example, the factor K_L which semi-empirically takes into account vertical accelerations and yaw motion depending on the longitudinal position, or with the multiplier of 0.75 which takes into account the influence of short-crestedness. These possible improvements would be beneficial for the accuracy of stability assessment, but would inevitably increase the complexity of the calculations. As a consequence, this would only emphasise the need for reliable Vulnerability Level 1 procedures, which could possible be derived directly form the Level 2, preserving the physical meaning of the criteria (as far as practical) while making them independent from a specific area of operation.

Bibliography

Bačkalov, I. (2012). A probabilistic analysis of stability regulations for river-sea ships. In *Proceedings of the 11th International Conference on the Stability of Ships and Ocean Vehicles (STAB 2012)*, (pp. 67–77)., Athens.

Bačkalov, I. (2017). *International maritime regulations: Ship safety.* Belgrade: University of Belgrade, Faculty of Mechanical Engineering. in Serbian.

Bačkalov, I. (2019). A probabilistic analysis of stability regulations for river-sea ships. In *Contemporary Ideas on Ship Stability* (pp. 707–723). Springer.

Bačkalov, I., Bulian, G., Cichowicz, J., Eliopoulou, E., Konovessis, D., Leguen, J. F., Rosén, A., & Themelis, N. (2016). Ship stability, dynamics and safety: Status and perspectives from a review of recent STAB conferences and ISSW events. *Ocean Engineering*, *116*, 312–349.

Bačkalov, I., Bulian, G., Rosén, A., Shigunov, V., & Themelis, N. (2016). Improvement of ship stability and safety in intact condition through operational measures: challenges and opportunities. *Ocean engineering*, *120*, 353–361.

Belenky, V., Bassler, C. G., & Spyrou, K. J. (2011). Development of second generation intact stability criteria. Technical report, Naval Surface Warfare Centre Carderock Division.

Benford, H. (1991). *Naval architecture for non-naval architects.* Society of Naval Architects.

Blume, P. (1979). Experimentell bestimmung von koeffizienten der wirksamen rolldämpfung und ihre anwedung zur abschätzung extremer rollwinkel. *Schiffstechnik*, *26*, 3–23.

BS (2007). Royal Decree concerning inland vessels also used for non-international sea voyages (In Flemish and French). N. 2007 - 1187.

BSI (1962). Dienstnorm nr. 8 - Motorvrachtschepen voor estuaire vaart. Technical report, Belgian Shipping Inspectorate, Belgian Ministry of Transport.

BSU (2009). Very serious marine casualty: Fatal accident on board of CMV Chicago Express during typhoon 'Hagupit' on 24 September 2008 off the coast of Hong Kong. Accident investigation report, Hamburg.

Bulian, G. & Francescutto, A. (2004). A simplified modular approach for the prediction of the roll motion due to the combined action of wind and waves. *Proceedings of the Institution of Mechanical Engineers, Part M: Journal of Engineering for the Maritime Environment*, *218*(3), 189–212.

Bulian, G. & Francescutto, A. (2005). Some considerations on the probability distributions for the damage length and damage penetration based on a re-analysis of recorded ship collisions data. *International shipbuilding progress*, *52*(4), 325–356.

Bulian, G. & Francescutto, A. (2009). Experimental results and numerical simulations on strongly non-linear rolling of multihulls in moderate beam seas. *Proceedings of the Institution of Mechanical Engineers, Part M: Journal of Engineering for the Maritime Environment*, *223*(2), 189–210.

Bulian, G. & Francescutto, A. (2011). Effect of roll modelling in beam waves under multi-frequency excitation. *Ocean engineering*, *38*(13), 1448–1463.

Bulian, G., Francescutto, A., & Fucile, F. (2009). Project HYD-III-CEH-5: Determination of relevant parameters for the alternative assessment of intact stability Weather Criterion on experimental basis. HYDRALAB project.

Bulian, G., Francescutto, A., & Maccari, A. (2008). Possible simplified mathematical models for roll motion in the development of performance-based intact stability criteria – extended and revised version. Quaderno di dipartimento no. 46, Department of Naval Architecture, Ocean and Environmental Engineering, University of Trieste, Trieste.

Bureau Veritas (2014). Rules for the classification of inland navigation vessel. NR 217.B1 DNI R04 E, Antwerpen.

CEMT (1992). Resolution No. 92/2 on New Classification of Inland Waterways. CEMT/CM(92)6/FINAL, Conférence Européenne des Ministres des Transports, Athens.

CESNI (2019). European Standard laying down Technical Requirements for Inland Navigation vessels (ES-TRIN). Edition 2019/1, European Committee for drawing up Standards in the field of Inland Navigation.

Chatelier, J. M., Nzengu, W. N., & Cocito, R. (2017). Stability and seakeeping of river-sea vessels – classification rules. In *Proceedings of the 16th International Ship Stability Workshop (ISSW 2017)*, (pp. 149–158)., Belgrade.

Davenport, A. G. (1961). The spectrum of horizontal gustiness near the ground in high winds. *Quarterly Journal of the Royal Meteorological Society*, *87*(372), 194–211.

Directorate General of Shipping (2013). River-sea vessel (RSV) notification 2013 - Annex to DG shipping Order 18 of 2013. Technical report, Mumbai.

Falzarano, J., Somayajula, A., & Seah, R. (2015). An overview of the prediction methods for roll damping of ships. *Ocean Systems Engineering*, *5*(2), 55–76.

Fossen, T. (2011). *Handbook of marine craft hydrodynamics and motion control*. John Wiley & Sons.

Francescutto, A. (2016). Intact stability criteria of ships – past, present and future. *Ocean engineering*, *120*, 312–317.

Francescutto, A. & Contento, G. (1998). The modeling of the excitation of large amplitude rolling in beam waves. In *Proceedings of the 4th International Ship Stability Workshop*, St. John's, Newfoundland.

Francescutto, A. & Serra, A. (2002). Experimental tests on ships with large values of B/T, OG/T and roll period. In *Proceedings of the 6th International Workshop on Ship Stability*, New York. Webb Institute.

Francescutto, A., Serra, A., & Scarpa, S. (2001). A critical analysis of weather criterion for intact stability of large passenger vessels. In *Proceedings of 20th International Conference on Offshore Mechanics and Arctic Engineering (OMAE'01)*, Rio de Janeiro, Brazil.

Froude, W. (1861). On the rolling of ships. *Transaction of The Institution of Naval Architects*, *2*, 180–227.

Fujino, M., Fuji, I., Hamamoto, M., Ikeda, Y., Ishida, S., Morita, T., Tanai, K., & Umeda, N. (1993). Examination of roll damping coefficients and effective wave slope coefficients for small passenger craft. In *Proceedings of the U.S. Coast Guard Vessel Stability Symposium*, (pp. 60–78).

George, W. E. (Ed.). (1983). *Stability and Trim for the Ship's Officer*. Cornell Maritime Press.

Himeno, Y. (1981). Prediction of ship roll damping a state of the art. Technical report, University of Michigan.

Hofman, M. & Bačkalov, I. (2005). Weather criterion for seagoing and inland vessels – some new proposals. In *Proceedings of International Conference on Marine Research and Transportation, ICMRT '05, University of Naples "Federico II"*, (pp. 53–62).

Hutchison, B. L. (1991). The transverse plane motion of ships. *Marine Technology*, *28*(2), 55–72.

IMO (2002). SLF 45/6/5: Weather criterion for large passenger ships. Submitted by Italy, International Maritime Organisation, London.

IMO (2005a). SLF 48/21: Report to the maritime safety committee. Revision 2, International Maritime Organisation, London.

IMO (2005b). SLF 48/4/1: Review of the Intact Stability Code. Submitted by Germany, International Maritime Organisation, London.

IMO (2007). MSC 83/INF.8: Formal Safety Assessment. Submitted by Denmark, International Maritime Organisation, London.

IMO (2008a). Adoption of The International Code on Intact Stability, 2008 (2008 IS Code). Technical report, International Maritime Organisation, London.

IMO (2008b). MSC.1/Circ.1281: Explanatory Notes to the International Code on Intact Stability, 2008. Technical report, International Maritime Organisation, London.

IMO (2013). SDC 1/INF.6: Vulnerability assessment for dead-ship stability failure mode. Submitted by Italy and Japan, International Maritime Organisation, London.

IMO (2015a). SDC 3/6/1: Report of the Correspondence Group on Intact Stability regarding second-generation intact stability criteria. Submitted by Japan, International Maritime Organisation, London.

IMO (2015b). SDC 3/INF.10: Information collected by the Correspondence Group on Intact Stability regarding second generation intact stability criteria. Submitted by Japan, International Maritime Organisation, London.

IMO (2016a). SDC 3/WP.5: Finalization of Second Generation Intact Stability Criteria, Amendments to Part B of the 2008 IS Code on Towing, Lifting and Anchor Handling Operations. Technical report, International Maritime Organisation, London.

IMO (2016b). SDC 4/5/1/Add.1: Draft Explanatory Notes on the vulnerability of ships to the dead ship stability failure mode. Submitted by Japan, International Maritime Organisation, London.

IMO (2016c). SDC 4/5/1/Add.3: Draft Explanatory Notes on the vulnerability of ships to the dead ship stability failure mode. Submitted by Japan, International Maritime Organisation, London.

IMO (2016d). SDC 4/5/1/Add.3: Draft Explanatory Notes on the vulnerability of ships to the dead ship stability failure mode. Submitted by Japan, International Maritime Organisation, London.

IMO (2016e). SDC 4/5/1/Add.4: Draft Explanatory Notes on the vulnerability of ships to the excessive acceleration stability failure mode. Submitted by Japan, International Maritime Organisation, London.

IMO (2017). SDC 5/6/9: Finalization of the draft guidelines for the specification of direct stability assessment, and for the preparation and approval of operational limitations and operational guidance. Submitted by Germany, International Maritime Organisation, London.

IMO (2018a). SDC 6/5: Report of the Correspondence Group (part 1). Submitted by Japan, International Maritime Organisation, London.

IMO (2018b). SDC 6/5/1: Report of the Correspondence Group (part 2). Submitted by Japan, International Maritime Organisation, London.

IMO (2019a). SDC 7/5: Report of the Correspondence Group (Part 1). Submitted by Japan, International Maritime Organisation, London.

IMO (2019b). SDC 7/INF.2: Finalization of Second Generation Intact Stability Criteria - Information collected by the Correspondence Group on Intact Stability (part A). Submitted by Japan, International Maritime Organisation, London.

IMO (2019c). SDC 7/INF.2/Add.2: Finalization of Second Generation Intact Stability Criteria - Information collected by the Correspondence Group on Intact Stability (part C). Submitted by Japan, International Maritime Organisation, London.

Journal officiel de la République Française (2014). Arrêté du 15 décembre 2014 relatif à la navigation de bateaux porte-conteneurs fluviaux en mer pour la desserte de Port 2000 et des quais en Seine à Honfleur. Texte 18 sur 122.

Kato, H. (1956). Approximate methods of calculating the period of roll of ships. *Journal of Zosen Kiokai*, *1956*(89), 59–64. in Japanese.

Kawahara, Y., Meakawa, K., & Ikeda, Y. (2009). A simple prediction formula of roll damping of conventional cargo ships on the basis of Ikeda's method and its limitation. (pp. 387–398).

Lamb, T. (Ed.). (2004). *Ship Design and Construction*. Number vol. 2. Society of Naval Architects and Marine Engineers.

McTaggart, K. A. (1997). SHIPMO7: An Updated Strip Theory Program for Predicting Ship Motions and Sea Loads in Waves. Technical memorandum 96/243, Defence Research Establishment Atlantic (DREA).

Míguez González, M. & Bulian, G. (2018). Influence of ship dynamics modelling on the prediction of fishing vessels roll response in beam and longitudinal waves. *Ocean Engineering*, *148*, 312–330.

Mizuno, T. (1973). On the effective wave slope in the rolling motion of a ship among waves. *Journal of the Society of Naval Architects of Japan*, *1973*(134), 85–102. in Japanese.

Mizuno, T. (1975). On the effective wave slope in the rolling motion of a ship among waves (the second report). *Journal of the Society of Naval Architects of Japan*, *1975*(137), 120–131. in Japanese.

Munro-Smith, R. (1973). *Ships and naval architecture*. Institute of Marine Engineers.

Naciri, M. & Lledo, N. (2001). Non-linear low frequency roll excitation of a rectangular barge. In *Proceedings of 20th International Conference on Offshore Mechanics and Arctic Engineering (OMAE'01)*, Rio de Janeiro, Brazil.

Oliva-Remola, A. (2018). *On ship roll damping: analysis and contributions on experimental techniques*. PhD thesis, Universidad Politécnica de Madrid.

Pardoe, I. (2020). STAT501 – Regression Methods – Online Notes. https://online.stat.psu.edu/stat501/lesson/welcome-stat-501, last accessed on 2020/05/13, (see, in particular, "13.3 - Robust Regression Methods" from https://online.stat.psu.edu/stat501/lesson/13/13.3).

Peach, R. & Brook, A. (1987). The radii of gyration of merchant ships. *North East Coast Institution of Engineers & Shipbuilders Transactions*, *103*(3), 115–117.

Petacco, N. (2019). *Second Generation Intact Stability criteria: Analysis, Implementation and Applications to significant ship typologies*. PhD thesis, University of Genoa, Genoa, Italy.

Peters, W., Belenky, V., Bassler, C., Spyrou, K., Umeda, N., Bulian, G., & Altmayer, B. (2011). The second generation intact stability criteria: an overview of development.

Rodríguez, C. A., Ramos, I. S., Esperança, P. T., & Oliveira, M. C. (2020). Realistic estimation of roll damping coefficients in waves based on model tests and numerical simulations. *Ocean engineering*, *213*.

Rudaković, S. (2018). Effective wave slope and natural roll frequency for river-sea ships: direct calculation and development of simplified regression formulae. Erasmus+ mobility project: 2017-1-IT02-KA107-035527, University of Trieste, Trieste, Italy.

Rudaković, S. & Bačkalov, I. (2017). On application of standard methods for roll damping prediction to inland vessels. (pp. 159–166).

Rudaković, S. & Bačkalov, I. (2019). Operational limitations of a river-sea container vessel in the framework of the second generation intact stability criteria. *Ocean Engineering*, *183*, 409–418.

Rudaković, S., Bulian, G., & Bačkalov, I. (2019). Effective wave slope coefficient of river-sea ships. *Ocean Engineering*, *192*.

Russian River Register (2015). Rules for classification and construction of ships (RCCS). Technical report, Moscow.

Sato, Y., Taguchi, H., Ueno, M., & Sawada, H. (2008). An experimental study of effective wave slope coefficient for two-dimensional model. In *Proceedings of the 6th Osaka Colloquium on Sekeeping and Stability of Ships*, (pp. 298–304).

Shigunov, V., Rathje, H., El Moctar, O., & Altmayer, B. (2011). On the consideration of lateral accelerations in ship design rules. In *Proceedings of the 12th International Ship Stability Workshop (ISSW 2017), Washington*.

Tasai, F. (1965). On the equation of rolling motion of a ship. Technical report, Reports of Research Institute for Applied mechanics, Kyusyu University. in Japanese.

Tasai, F. (1971). On the sway, yaw and roll motions of a ship in short crested waves. Technical report.

Truijens, P., Vantorre, M., & Vanderwerff, T. (2006). On the design of ships for estuary service. *The Transactions of the RINA: International Journal of Maritime Engineering*, (A2), 25–39.

Umeda, N. & Francescutto, A. (2016). Current state of the second generation intact stability criteria-achievements and remaining issues. In *Proceedings of the 15th International Ship Stability Workshop (ISSW 2016)*, (pp. 3–9)., Stockholm.

Umeda, N., Koga, S., Ueda, J., Maeda, E., Tsukamoto, I., & Paroka, D. (2007). Methodology for calculating capsizing probability for a ship under dead ship condition. In *Proceedings of the 9th International Ship Stability Workshop (ISSW 2007)*, Hamburg, Germany.

Umeda, N. & Tsukamoto, I. (2008). Simplified formula for calculating effective wave slope coefficient and its impact on ship stability assessment. In *Proceedings of the 6th Osaka Colloquium on Seakeeping and Stability of Ships*, (pp. 293–297)., Osaka, Japan.

UNECE (2016). Resolution No. 61, Recommendations on Europe-Wide Technical Requirements for Inland Navigation Vessels. Technical report, New York and Geneva.

UNECE (2019). Resolution No. 61, Recommendations on Europe-Wide Technical Requirements for Inland Navigation Vessels. Revision 2, New York and Geneva.

van Essen, S. & Peters, H. (2017). Choosing the safest wave. *The Naval Architect*, 49–53. October issue.

Vantorre, M., Eloot, K., & Delefortrie, G. (2012). Probabilistic regulation for inland vessels operating at sea as an alternative hinterland connection for coastal harbours. *European Journal of Transport and Infrastructure Research*, *12*(1), 111–131.

Verwaest, T., Doorme, S., Verelst, K., & Trouw, K. (2008). The wave climate in the Belgian coastal zone. In *Proceedings of the 9th International Conference LITTORAL 2008, A Changing Coast: Challenge for the Environmental Policie*, (pp. 1–8).

Vickery, B. (1968). Load fluctuations in turbulent flow. *Journal of the Engineering Mechanics Division*, *94*(1), 31–46.

Watanabe, Y. (1938). Some contributions to the theory of rolling. *Transaction of the Institution of Naval Architects*, *80*, 408–432.

Watson, D. G. (1998). *Practical ship design*, volume 1. Elsevier.

Yamagata, M. (1959). Standard of stability adopted in Japan. *Transaction of the Institution of Naval Architects*, *101*, 417–443.

Appendix A

Details of vessels in the database

This appendix provides an overview of the main characteristics of the vessels in the database described in Section 1.2. The database consists of 31 self-propelled vessels, comprising 23 tankers, 4 general cargo vessels, 3 container vessels and 1 LPG tanker.

Figure A.1 shows the distributions of main ships' particulars at maximum calculations draught: length at waterline L_{WL}, breadth B, draught T, displaced volume V, and maximum considered vertical position of centre of gravity $\overline{KG}_{max}$.

Figure A.2 provides the distribution of the main hull form coefficients and of some other relevant geometric dimensionless parameters for the vessels in the database, considering the maximum draught. The figure reports distributions for the following quantities: block coefficient C_B, waterplane area coefficient C_{WL}, midship section coefficient C_M, longitudinal prismatic coefficient C_P, vertical prismatic coefficient C_{VP}, ratio L_{WL}/B, ratio B/T, and ratio $\overline{KM}/T$.
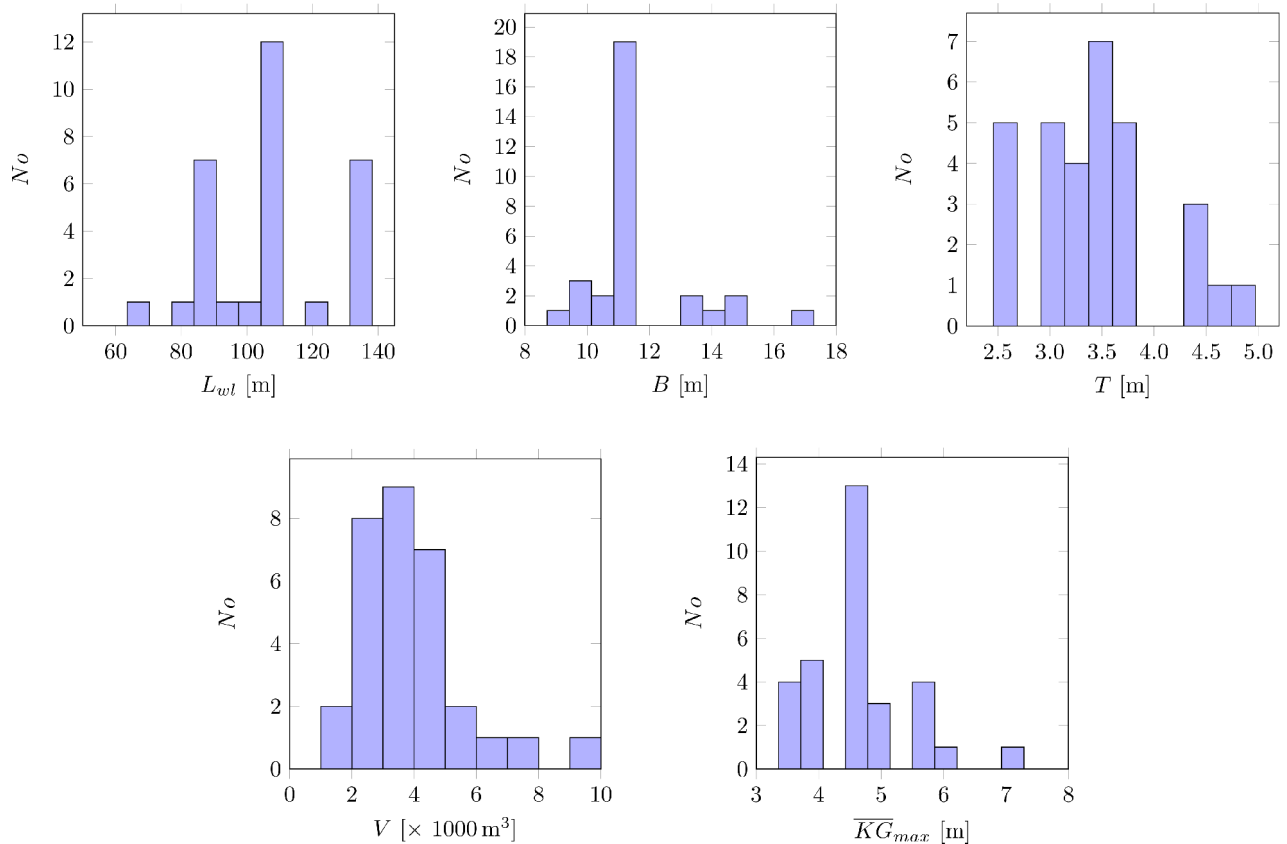
Figure A.1: Database overview. Distribution of main particulars at maximum draught.
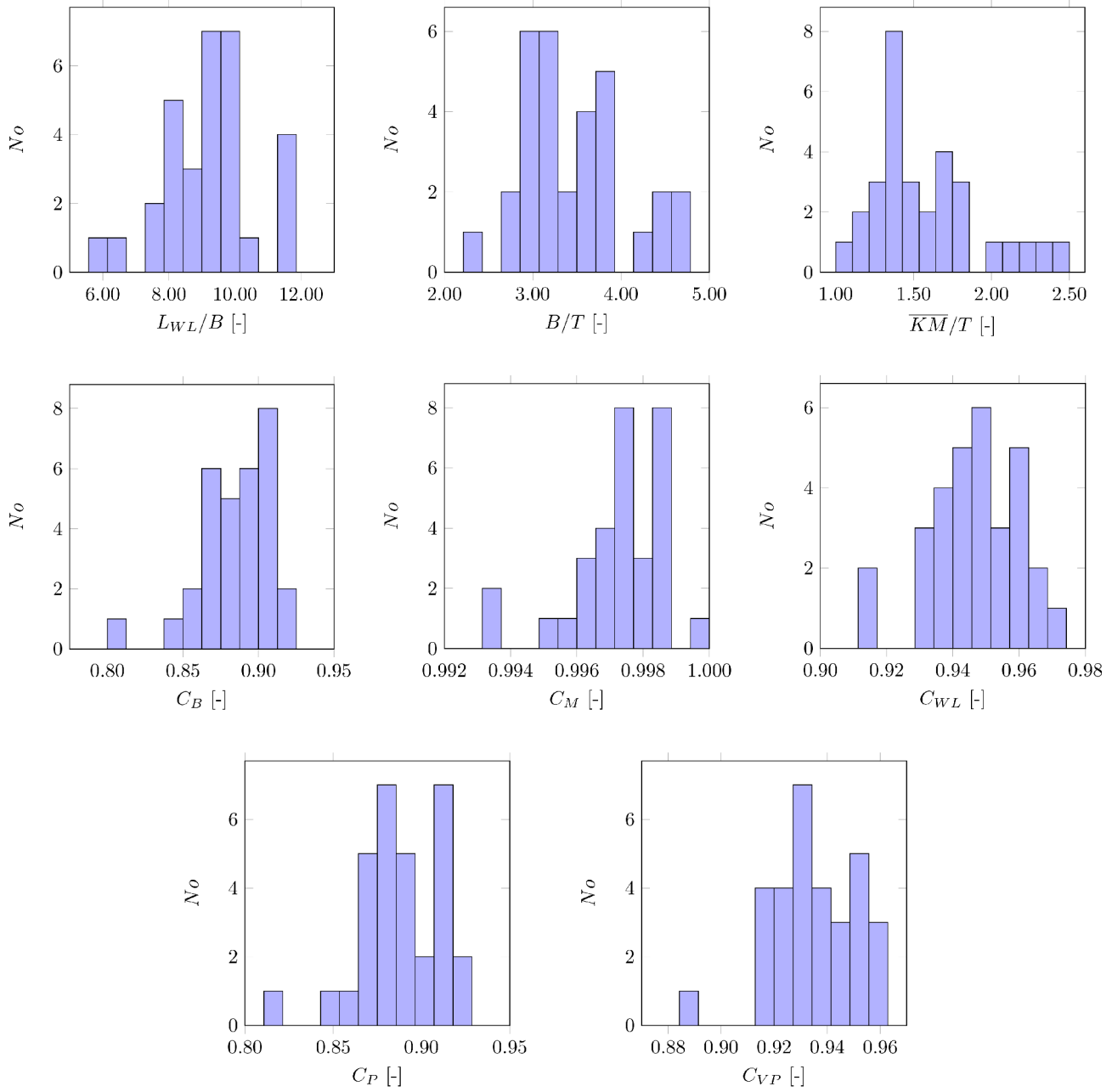
Figure A.2: Database overview. Distribution of main dimensionless coefficients at maximum draught.

Appendix B

Details of vessels in the calculation database - reduced 3DOF method

Figure B.1 reports the distribution of ratios between minimum and maximum draughts used in the analysis (T_{min}/T_{max}), and between the corresponding hull volumes (V_{min}/V_{max}).

Figure B.2 shows the distributions of some dimensionless ratios relevant to the metacentric height and to the vertical position of centre of gravity, at the maximum draught: $\overline{GM}_{min}/B$, $\overline{GM}_{max}/B$, and $\overline{KG}_{max}/T$.
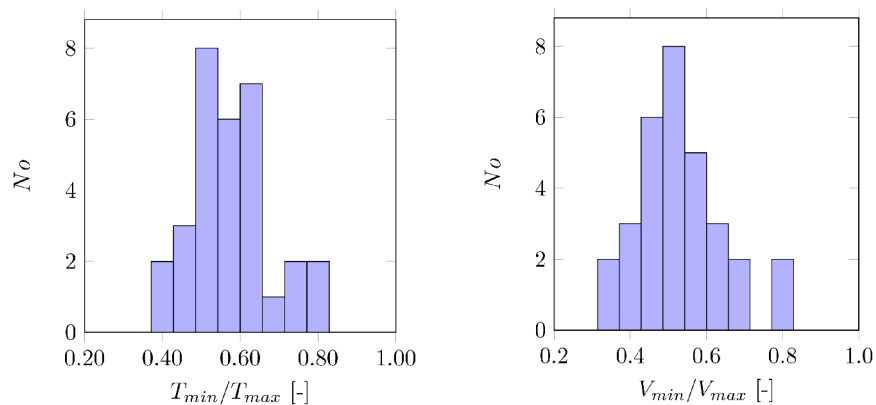
Figure B.1: Database overview. Distribution of ratios between minimum and maximum draughts and between corresponding volumes.
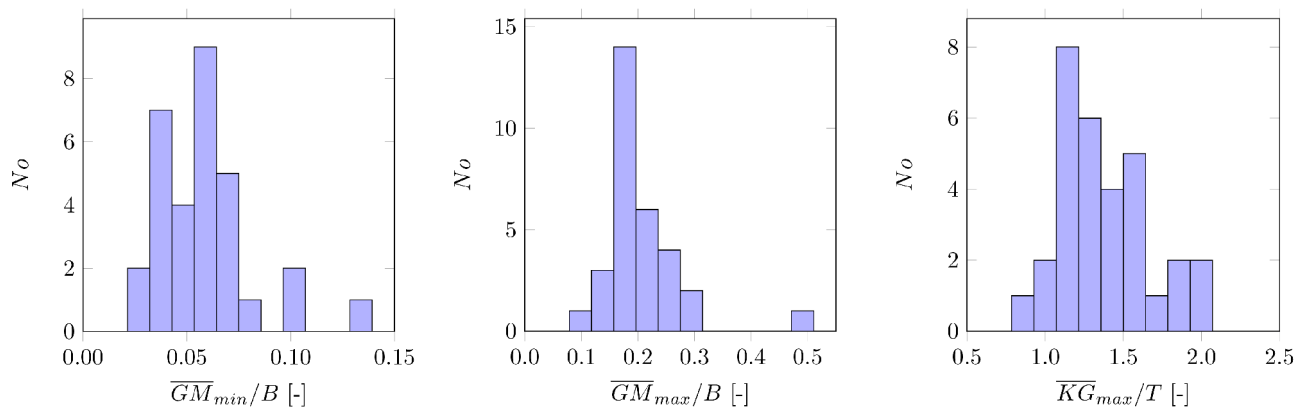
Figure B.2: Database overview. Distribution of dimensionless ratios relevant to metacentric height and vertical position of centre of gravity at maximum draught.

Appendix C
Simple regression models - Influenctial coefficient matrix table
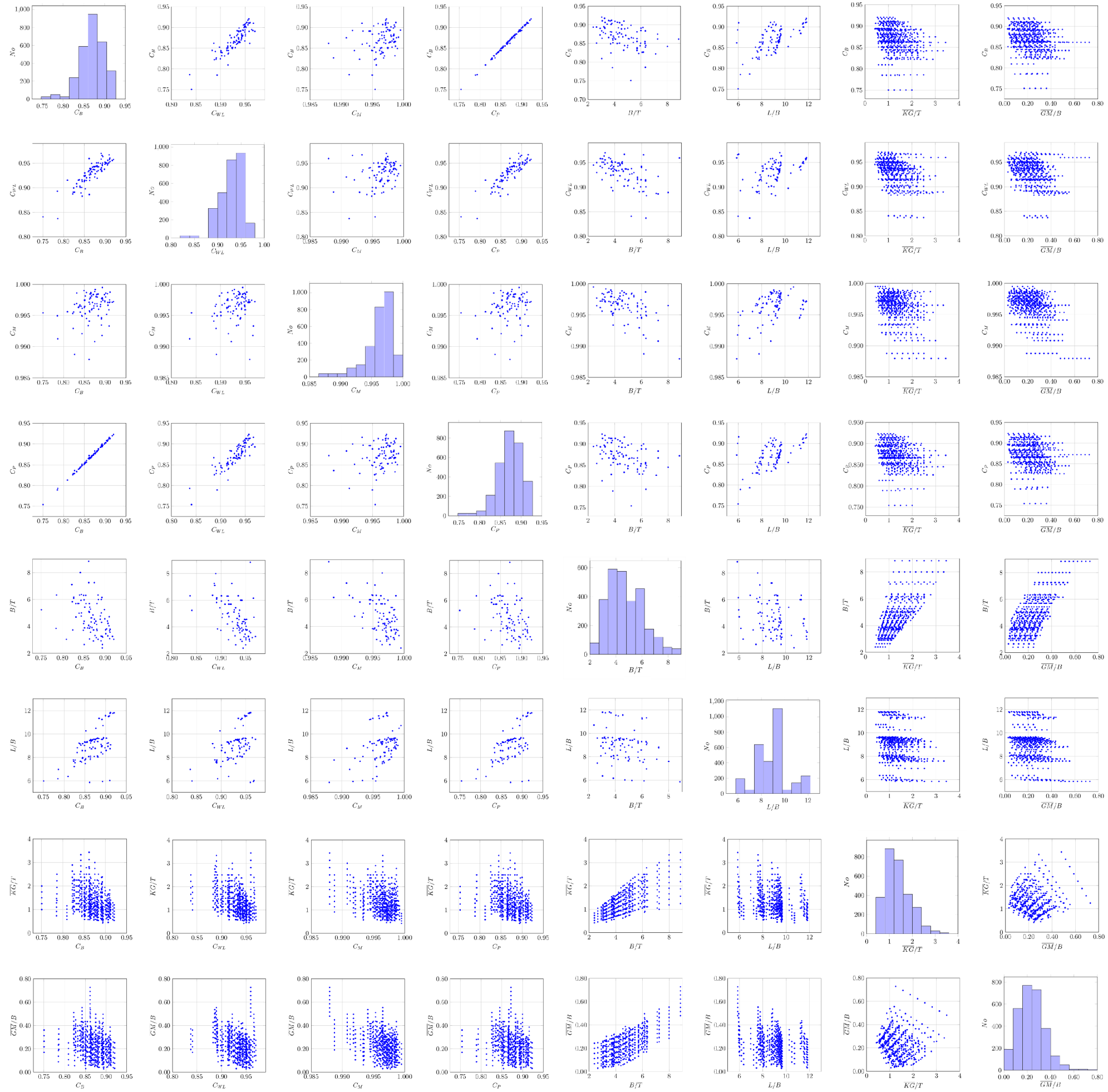
Appendix D

Simple regression models - validation set

This appendix provides comparisons between frequency dependent effective wave slope as determined from direct 3DOF calculations (see Section 7.2.1) and developed regression (see Section 9.4). Results are reported in Figures D.1 ÷ D.18.
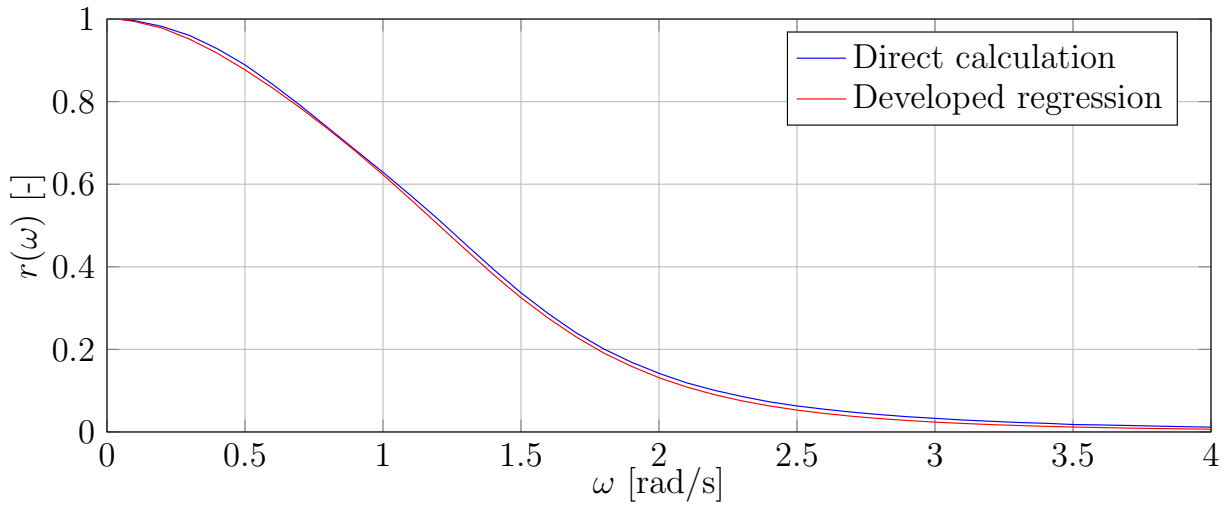
Figure D.1: Validation of $r(\omega)$, vessel V1, $T = 3.35\,\text{m}$, $k_{xx}/B = 0.35$, $\overline{GM} = 2.15\,\text{m}$.
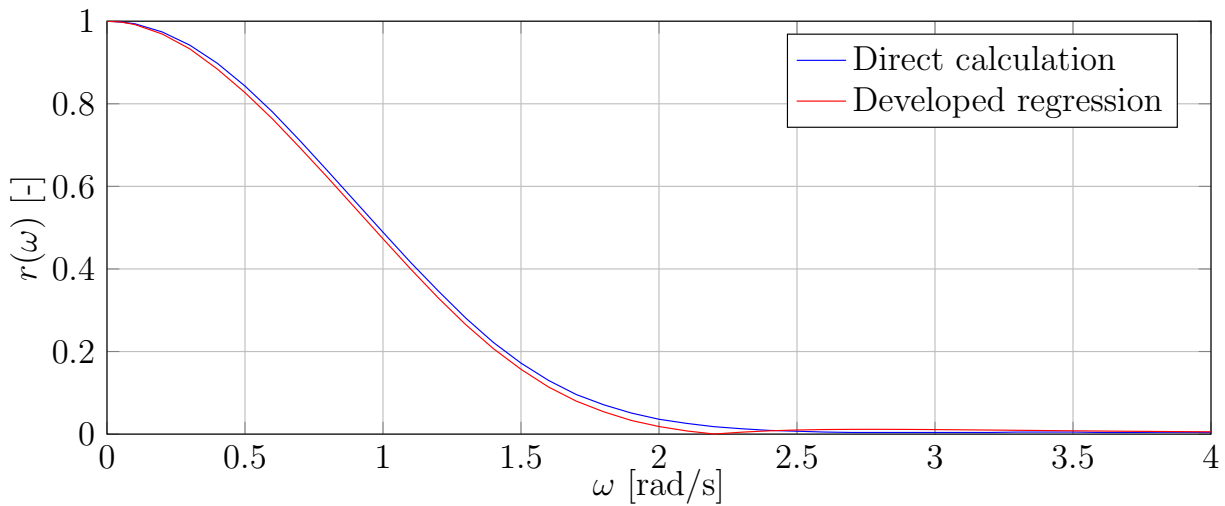

Figure D.2: Validation of $r(\omega)$, vessel V1, $T = 3.35\,\text{m}$, $k_{xx}/B = 0.35$, $\overline{GM} = 1.15\,\text{m}$.
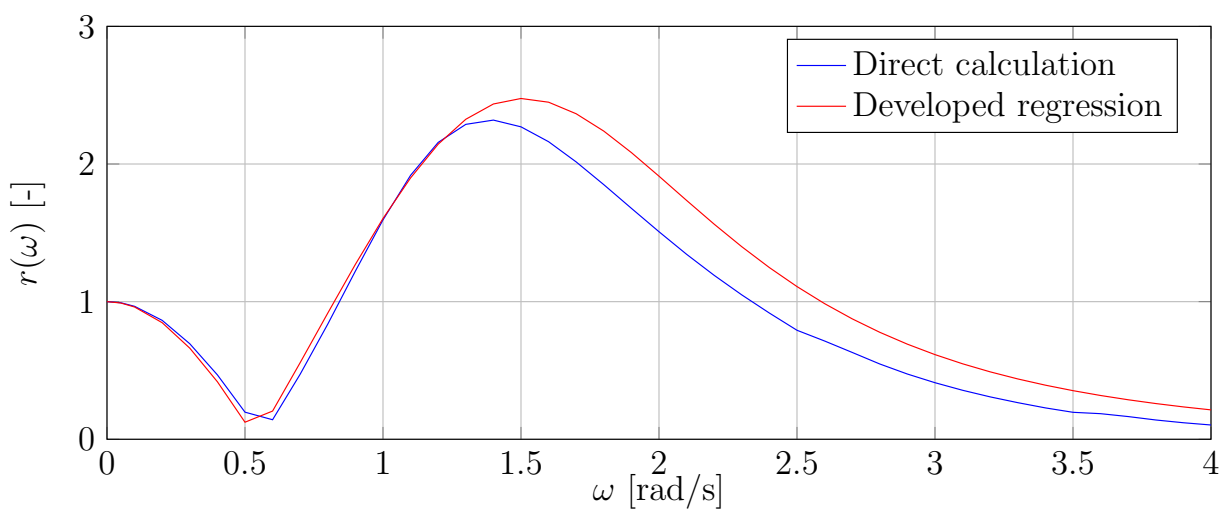

Figure D.3: Validation of $r(\omega)$, vessel V1, $T = 3.35\,\text{m}$, $k_{xx}/B = 0.35$, $\overline{GM} = 0.15\,\text{m}$.
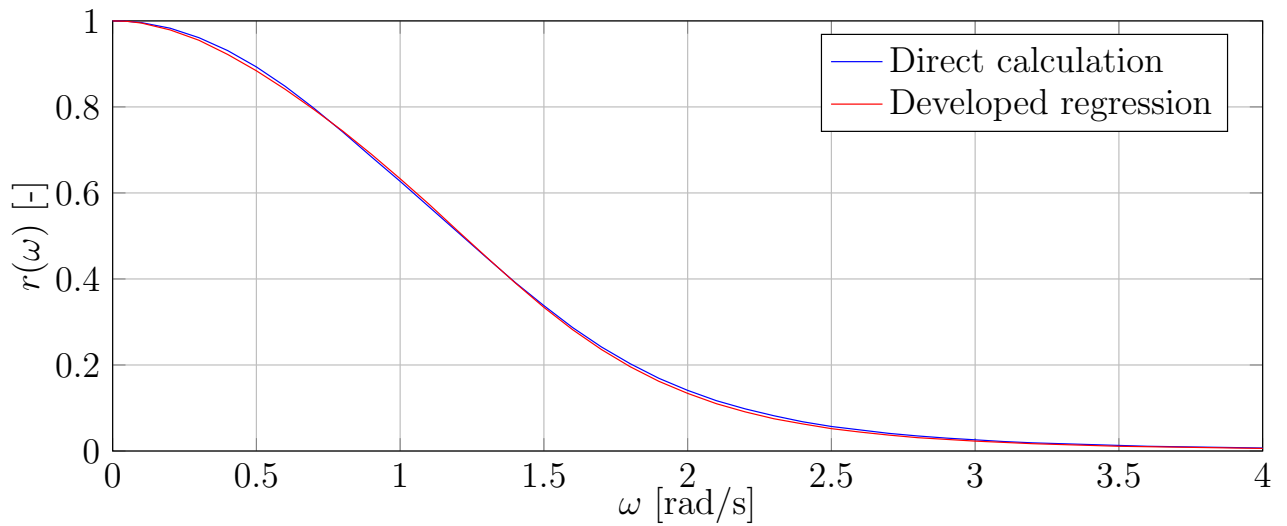
Figure D.4: Validation of $r(\omega)$, vessel V1, $T = 2.625\,\text{m}$, $k_{xx}/B = 0.30$, $\overline{GM} = 2.55\,\text{m}$.
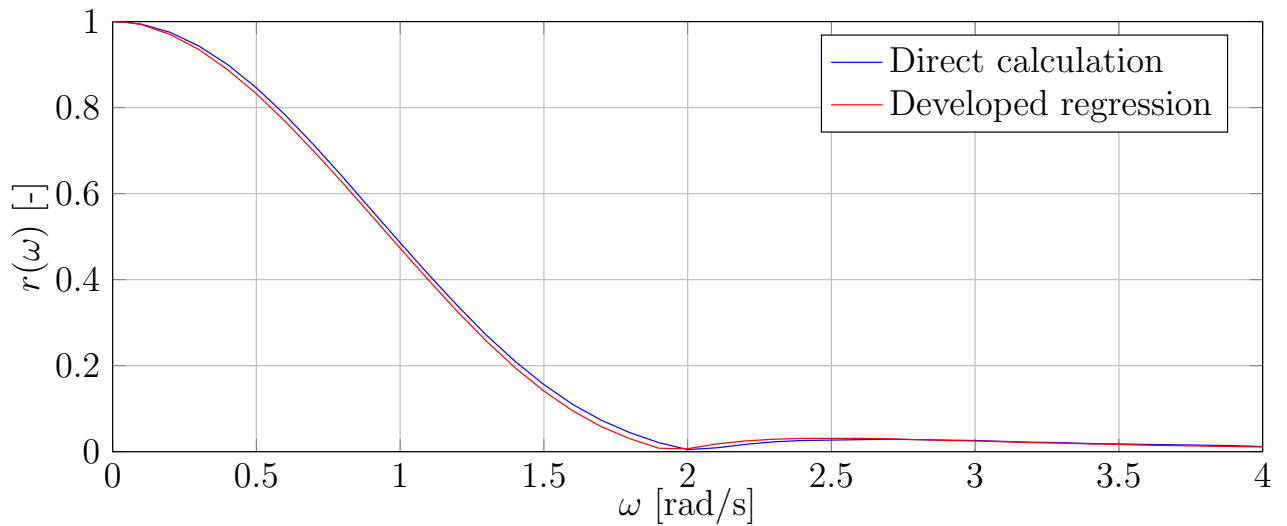
Figure D.5: Validation of $r(\omega)$, vessel V1, $T = 2.625\,\text{m}$, $k_{xx}/B = 0.30$, $\overline{GM} = 1.35\,\text{m}$.
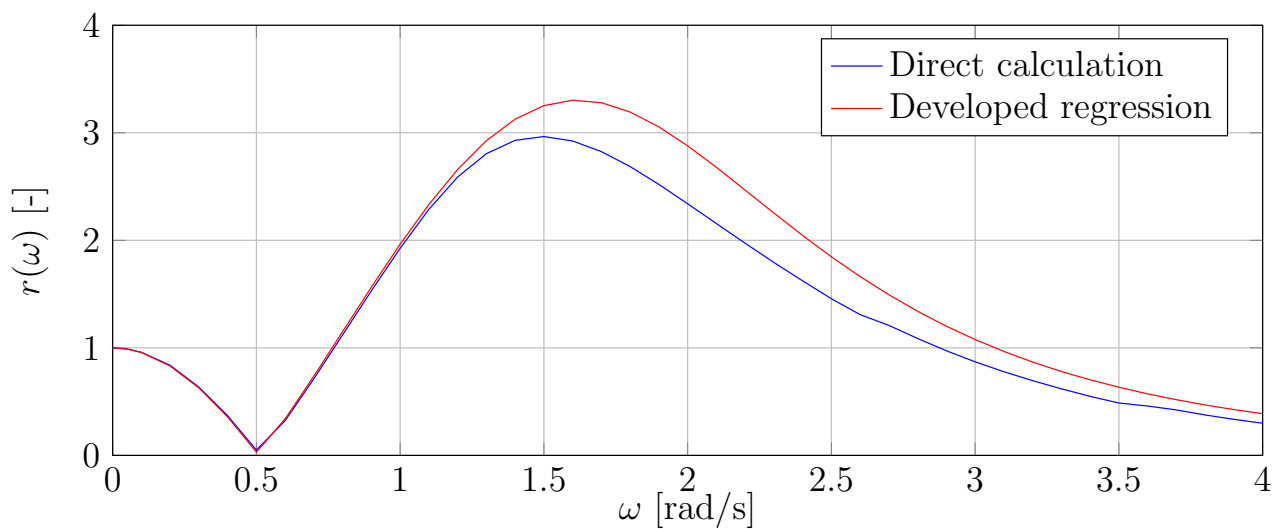
Figure D.6: Validation of $r(\omega)$, vessel V1, $T = 2.625\,\text{m}$, $k_{xx}/B = 0.30$, $\overline{GM} = 0.15\,\text{m}$.
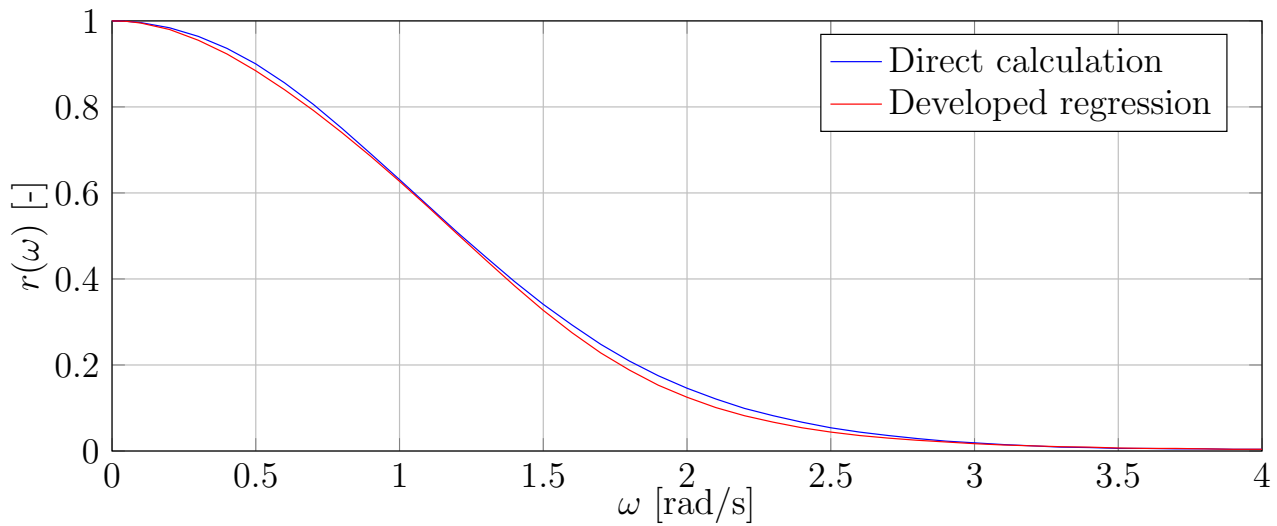
Figure D.7: Validation of $r(\omega)$, vessel V1, $T = 1.9\,\text{m}$, $k_{xx}/B = 0.40$, $\overline{GM} = 3.15\,\text{m}$.
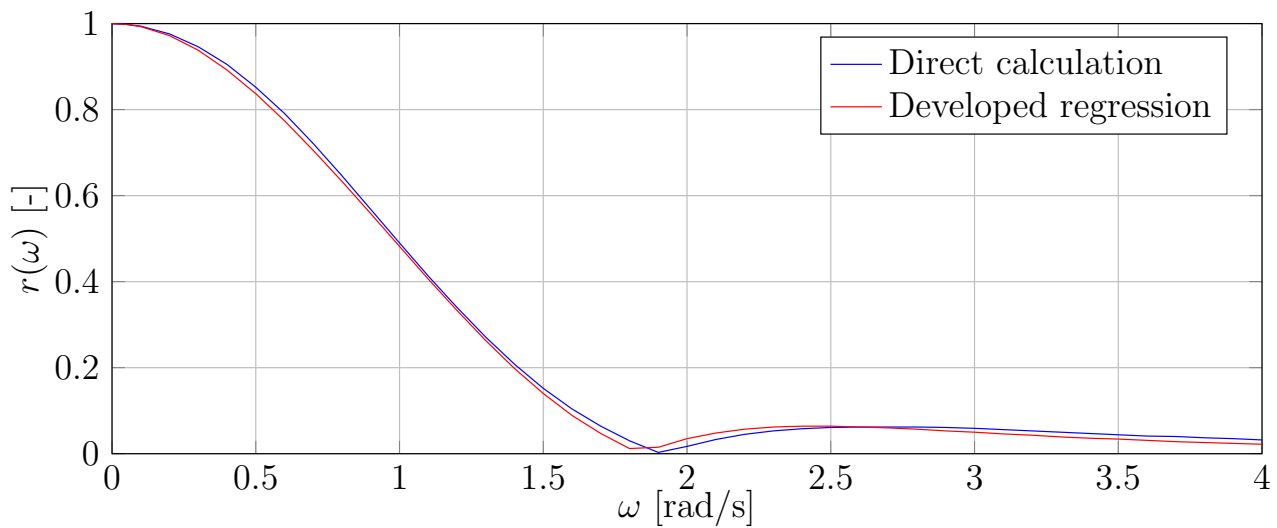

Figure D.8: Validation of $r(\omega)$, vessel V1, $T = 1.9\,\text{m}$, $k_{xx}/B = 0.40$, $\overline{GM} = 1.65\,\text{m}$.
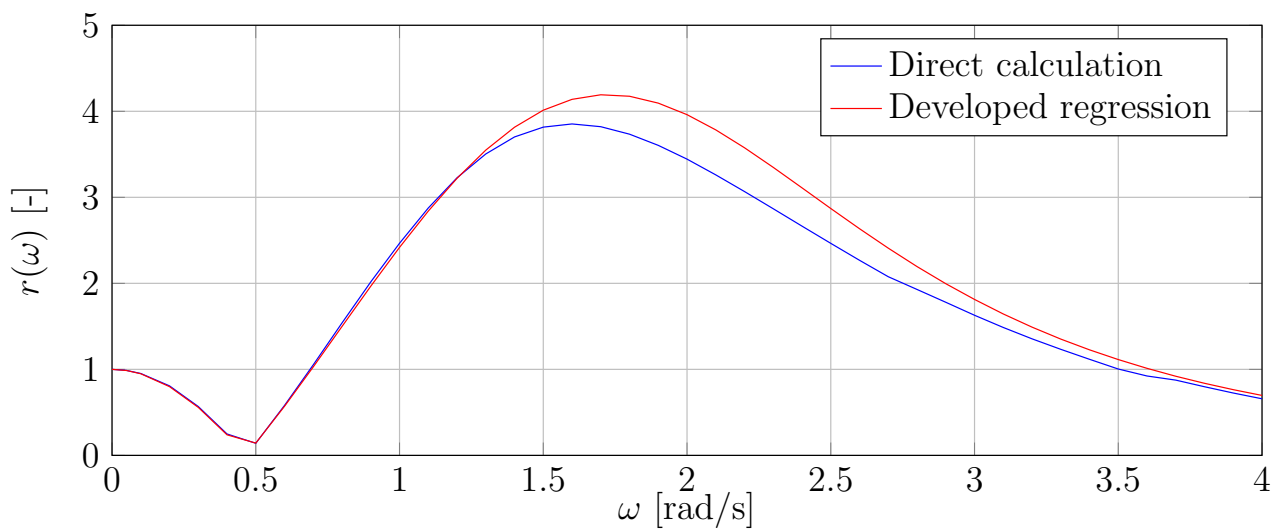
Figure D.9: Validation of $r(\omega)$, vessel V1, $T = 1.9\,\text{m}$, $k_{xx}/B = 0.40$, $\overline{GM} = 0.15\,\text{m}$.
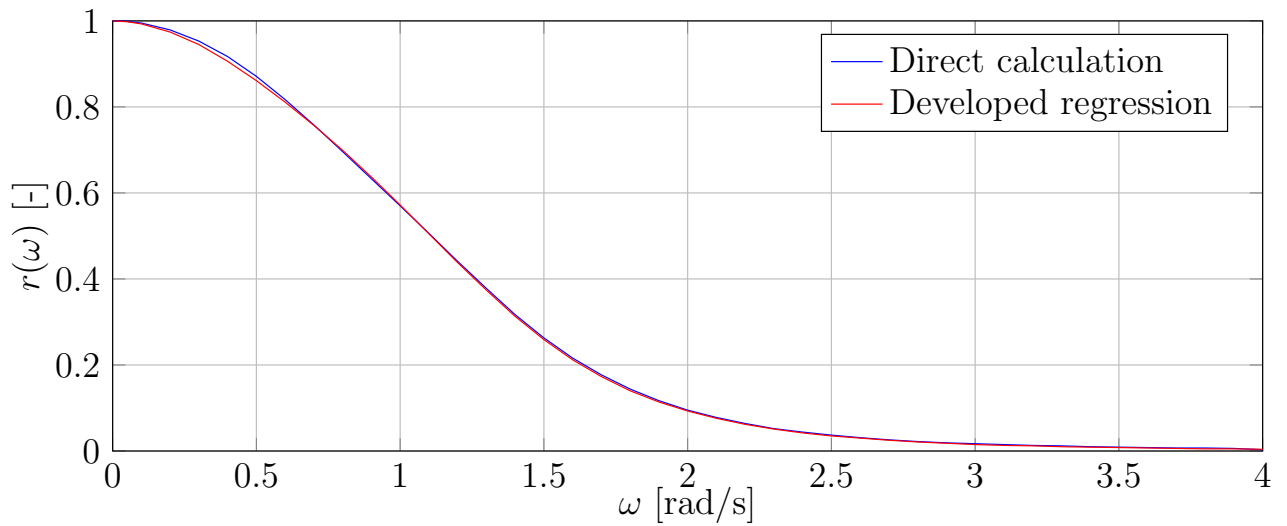
Figure D.10: Validation of $r(\omega)$, vessel V2, $T = 3.21\,\mathrm{m}$, $k_{xx}/B = 0.35$, $\overline{GM} = 3.15\,\mathrm{m}$.
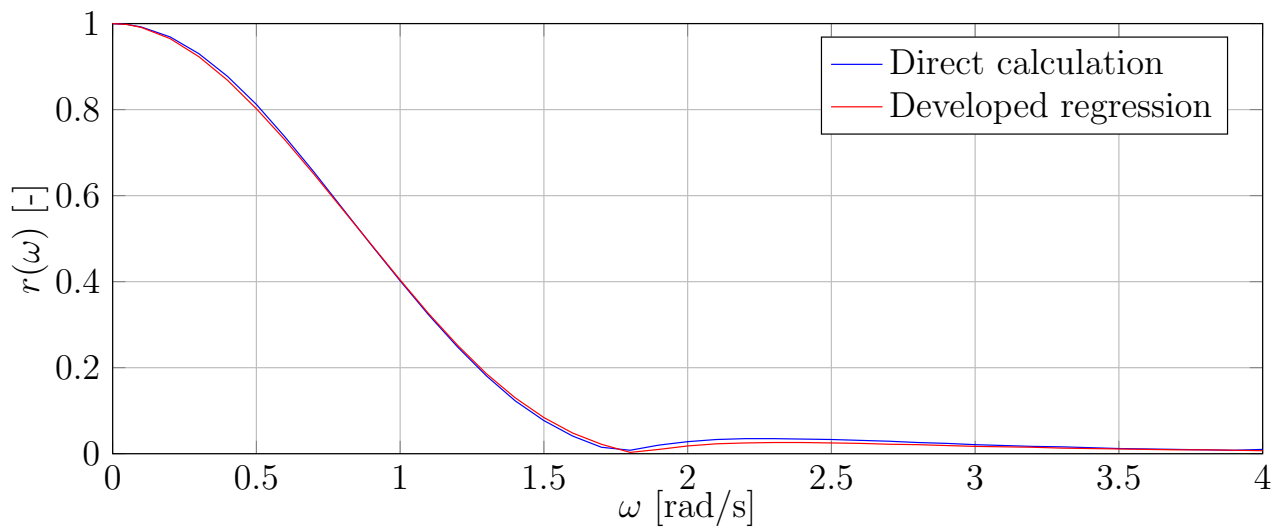
Figure D.11: Validation of $r(\omega)$, vessel V2, $T = 3.21\,\mathrm{m}$, $k_{xx}/B = 0.35$, $\overline{GM} = 1.65\,\mathrm{m}$.
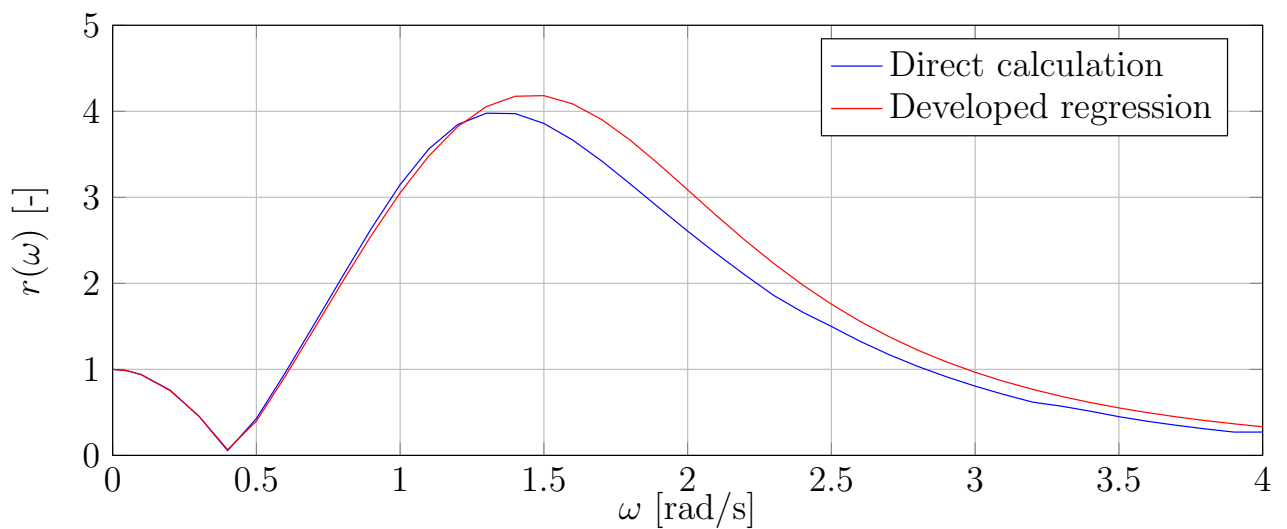
Figure D.12: Validation of $r(\omega)$, vessel V2, $T = 3.21\,\mathrm{m}$, $k_{xx}/B = 0.35$, $\overline{GM} = 0.15\,\mathrm{m}$.
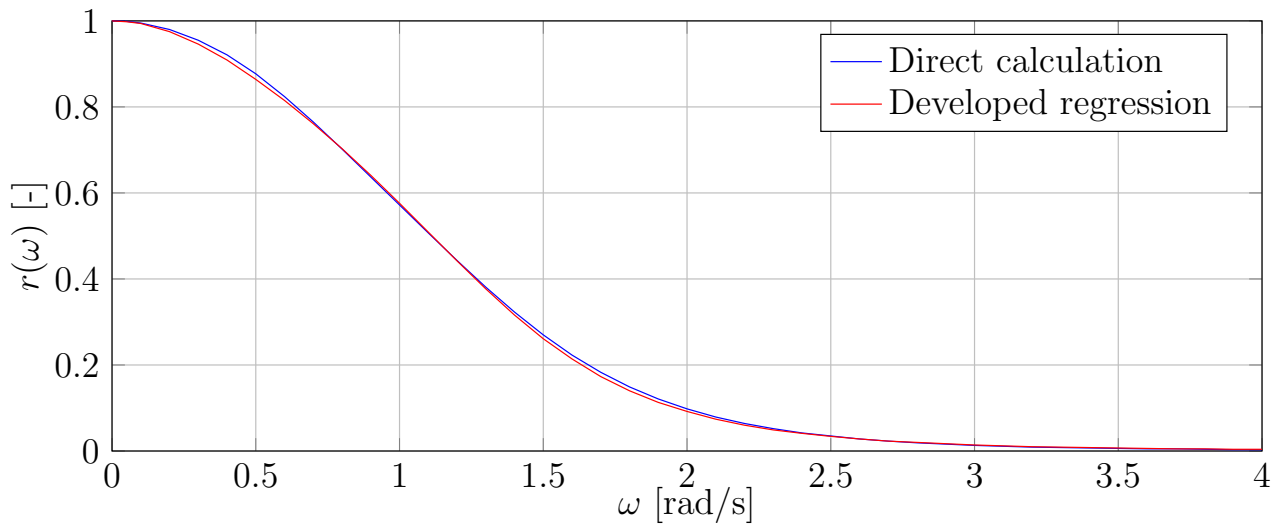
Figure D.13: Validation of $r(\omega)$, vessel V2, $T = 2.655\,\text{m}$, $k_{xx}/B = 0.40$, $\overline{GM} = 3.65\,\text{m}$.
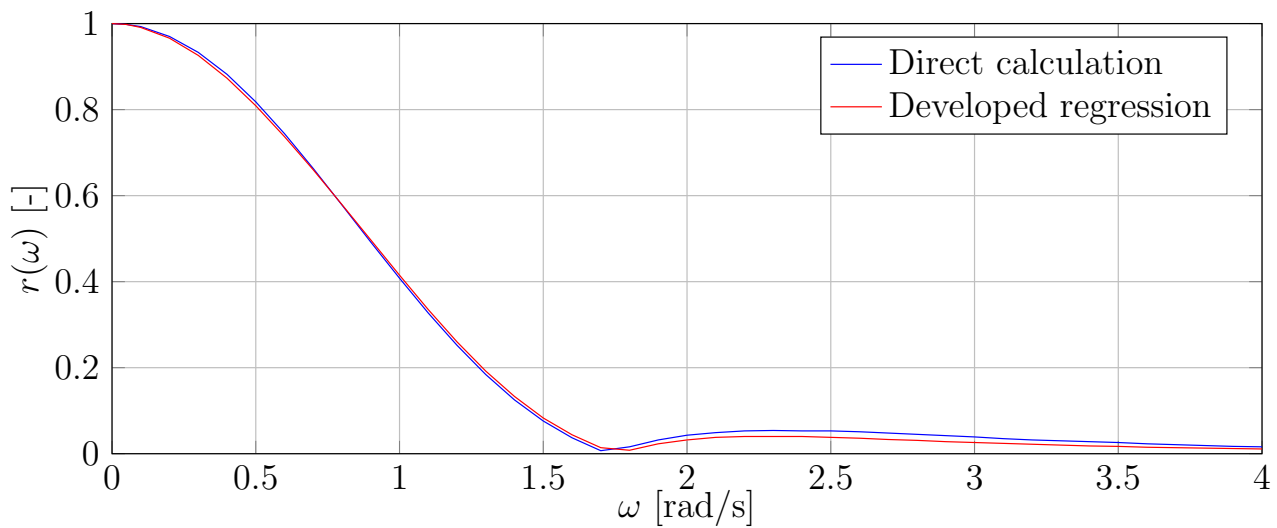

Figure D.14: Validation of $r(\omega)$, vessel V2, $T = 2.655\,\text{m}$, $k_{xx}/B = 0.40$, $\overline{GM} = 1.9\,\text{m}$.
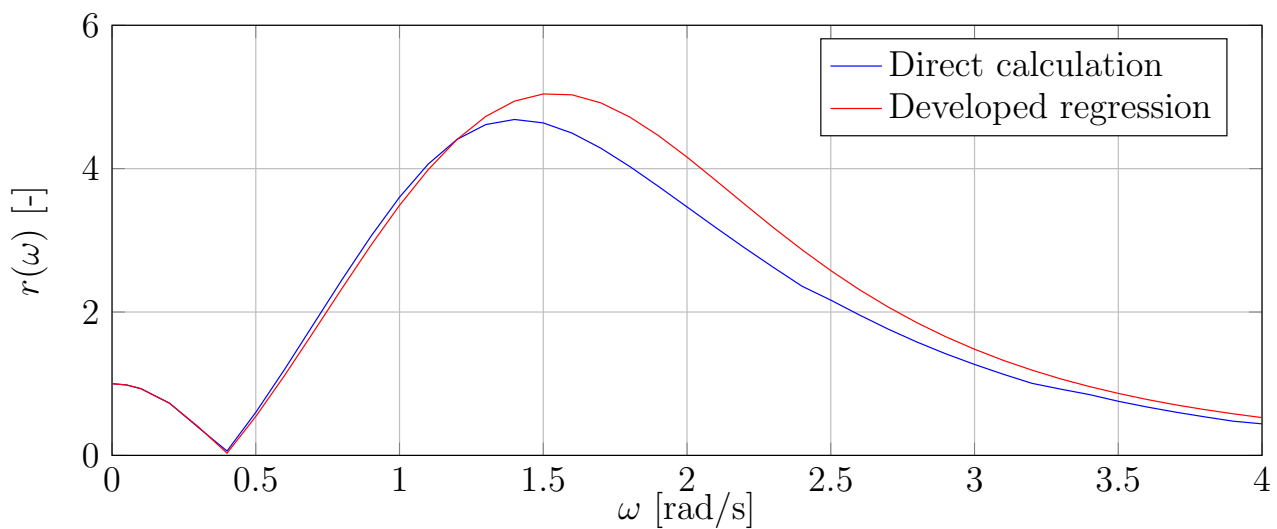

Figure D.15: Validation of $r(\omega)$, vessel V2, $T = 2.655\,\text{m}$, $k_{xx}/B = 0.40$, $\overline{GM} = 0.15\,\text{m}$.
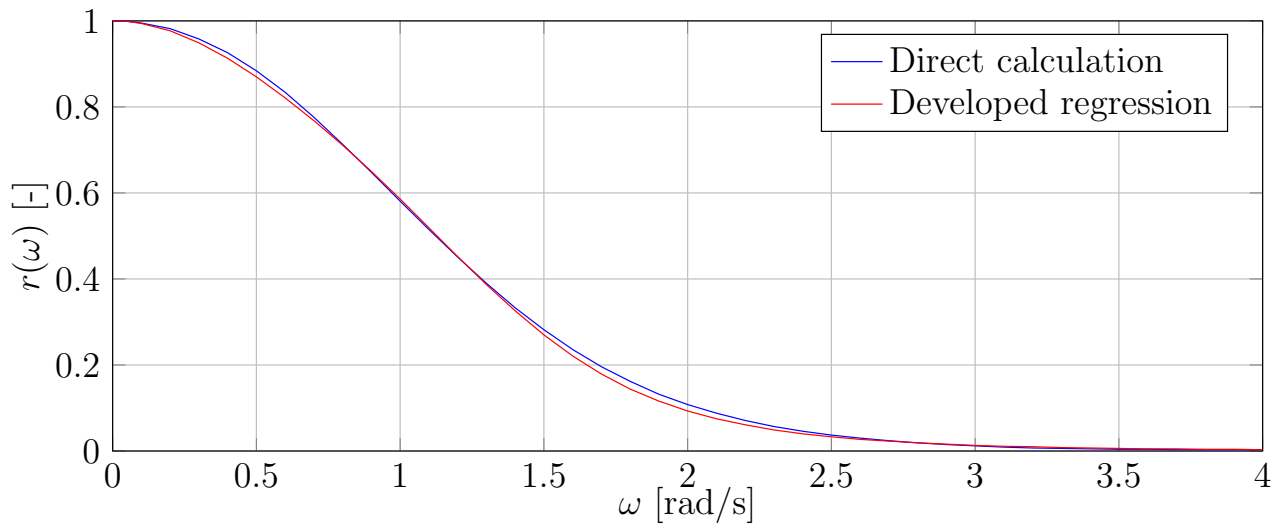
Figure D.16: Validation of $r(\omega)$, vessel V2, $T = 2.1\,\text{m}$, $k_{xx}/B = 0.30$, $\overline{GM} = 4.45\,\text{m}$.
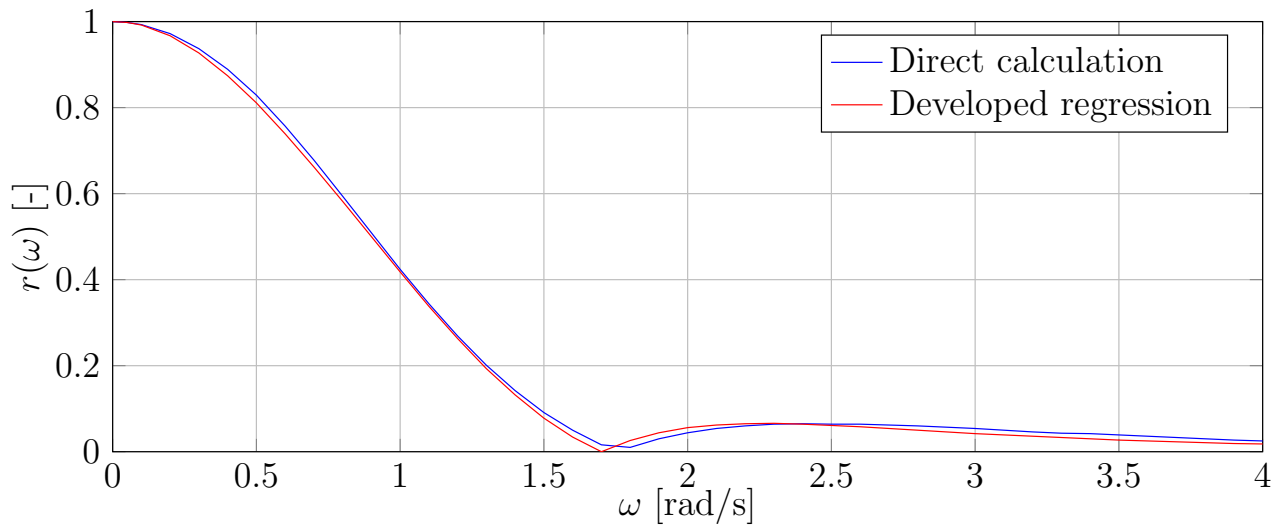

Figure D.17: Validation of $r(\omega)$, vessel V2, $T = 2.1\,\text{m}$, $k_{xx}/B = 0.30$, $\overline{GM} = 2.30\,\text{m}$.
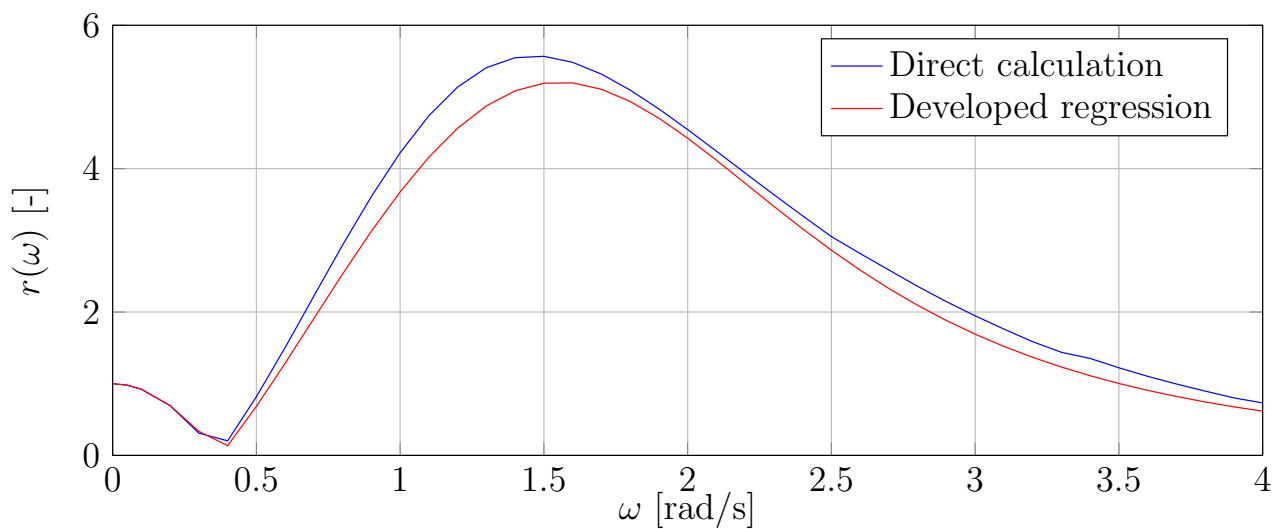
Figure D.18: Validation of $r(\omega)$, vessel V2, $T = 2.1\,\text{m}$, $k_{xx}/B = 0.30$, $\overline{GM} = 0.15\,\text{m}$.

Appendix E

Consolidated procedures for the novel approach to stability assessment of river-sea ships

E.1   Dead Ship Condition criterion for river-sea ships

The vulnerability to the Dead Ship Condition, according to the Vulnerability Level 2, is assessed by solving the one-degree-of-freedom differential equation of ship roll, where the excitations are beam irregular waves and gusting wind. The equation is to be solved in frequency domain in order to estimate the likelihood of stability failure (i.e. critical roll angles). The range of recommended frequency for the calculation is from $\omega_{min} = 0.000\,342\,\text{rad/s}$ up to $\omega_{max} = 3.42\,\text{rad/s}$ with the frequency step $\Delta\omega = 0.000\,342\,\text{rad/s}$. The integrations within the procedure are done by means of numerical integration using trapezoidal rule or any other method that provides sufficient accuracy, applying the proper combination of a numerical method and frequency step.

All equations in this section are already mentioned and discussed in the previous chapters, therefore, cross-referencing is provided for the additional explanation.

Environmental conditions

The sea elevation spectrum is to be calculated using the Mean JONSWAP wave spectrum. If short-term characterisation of environmental conditions, significant wave height H_S and in this case modal wave period T_m, are known the sea elevation spectrum can be obtained as (5.2):

$$S_{ZZ}(\omega) = A\gamma^B \cdot \frac{5}{16}\frac{H_S^2}{\omega_m}\left(\frac{\omega_m}{\omega}\right)^5 \cdot \exp\left[-\frac{5}{4}\left(\frac{\omega_m}{\omega}\right)^4\right]$$

where

$$A = 0.658$$

$$B = \exp\left[-\frac{1}{2\sigma^2}\left(\frac{\omega}{\omega_m}-1\right)\right]$$

$$\gamma = 3.3$$

$$\sigma = \begin{cases} 0.07, & \text{for } \omega < \omega_m \\ 0.09, & \text{for } \omega > \omega_m \end{cases}$$

$$\omega_m = \frac{2\pi}{T_m}$$

The wave slope spectrum is then calculated as (4.4):

$$S_{\alpha\alpha}(\omega) = \frac{\omega^2}{g^2} \cdot S_{ZZ}(\omega)$$

The natural roll frequency is to be calculated using the following equation (9.1):

$$\omega_\varphi = \sqrt{\frac{g\overline{GM}}{k_{xx}{}^2 + \delta k_{xx}{}^2}}$$

where the added roll radius of inertia δk_{xx} is to be calculated using the equation (9.4):

$$\delta k_{xx} = B \cdot (K_0 + K_1 + K_2 + K_3)$$
$$K_0 = 0.5909$$
$$K_1 = 0.05516\frac{B}{T} - 0.001876\left(\frac{B}{T}\right)^2 + 0.05674\frac{B}{T}C_{WL}$$
$$K_2 = 3.332C_B + 3.215C_B{}^2 - 0.07211C_B\frac{B}{T}$$
$$K_3 = -4.556C_{WL} + 6.8603C_{WL}{}^2 - 9.328C_{WL}C_B$$

The effective wave slope coefficient at natural roll frequency is to be calculates as (9.5):

$$r_\varphi = R_0 + R_1 + R_2 + R_3 + R_4$$
$$R_0 = -0.5969$$
$$R_1 = 3.416\frac{k_{xx}}{B} - 0.5722\left(\frac{k_{xx}}{B}\right)^2 - 2.814\left(\frac{k_{xx}}{B}\right)^3 + 7.543\left(\frac{k_{xx}}{B}\right)^2\frac{\overline{GM}}{B}$$
$$R_2 = -0.02502\frac{B}{T} + 0.002894\left(\frac{B}{T}\right)^2 + 0.04164\frac{B}{T}\frac{\overline{GM}}{B} - 0.06073\frac{B}{T}\frac{k_{xx}}{B}$$
$$R_3 = 1.198C_B - 0.8308C_B{}^2 - 0.1989C_B\frac{k_{xx}}{B} - 0.006306C_B\frac{B}{T}$$
$$R_4 = -0.2855\frac{\overline{GM}}{B} - 5.276\frac{\overline{GM}}{B}\frac{k_{xx}}{B} + 0.5694\frac{\overline{GM}}{B}C_B$$

while the effective wave slope as a function of frequency is calculated using the formula below (9.8):

$$r(\omega) = \left|\frac{1 + a\hat{k}}{1 + b\hat{k} + c\hat{k}^3}\right|$$

where

$$b = 0.5438 - 1.270\frac{\overline{OG}}{B} + 3.600\left(\frac{\overline{OG}}{B}\right)^2$$

$$c = 0.08857 - 0.4127\frac{\overline{OG}}{B} + 0.6709\left(\frac{\overline{OG}}{B}\right)^2$$

$$a = \frac{r_\varphi\left(1 + b\hat{k}_\varphi + c\hat{k}_\varphi{}^3\right) - 1}{\hat{k}_\varphi}$$

and where

$$\hat{k} = \omega^2 B/g$$

$$\hat{k}_\varphi = \omega_\varphi^2 B/g$$

The effective wave slope spectrum can be obtained using the wave slope spectrum and the effective wave slope (4.3):

$$S_{\alpha\alpha,c}(\omega) = r^2(\omega) \cdot S_{\alpha\alpha}(\omega)$$

It is considered that the mean wind speed can be determined from the significant wave height, as (5.1):

$$U_w = 11.75 \cdot H_S^{0.375}$$

and the spectrum of wind gust is to be calculated as (4.7):

$$S_v(\omega) = 4K \frac{U_w^2}{\omega} \cdot \frac{X_D^2}{(1 + X_D^2)^{\frac{4}{3}}}$$

with

$$K = 0.003$$

$$X_D = 600 \frac{\omega}{\pi U_w}$$

Then, the moment spectrum due to gusting wind can be obtained (4.6):

$$S_{\delta M_{wind,tot}}(\omega) = (\rho_{air} U_w C_{whm} A_L Z)^2 \cdot \chi^2(\omega) \cdot S_v(\omega)$$

Short-term roll motion statistics

The roll damping should be estimated by means of the Simplified Ikeda's method. The method is given in Kawahara et al. (2009), while the procedure for the equivalent linear roll damping coefficient μ_e is explained in Section 4.4.1. However, based on the work and conclusions presented in Chapter 6, the parameter A_E used for eddy damping estimation is to be substituted with the parameter A_{E-new}, calculated as (6.15):

$$A_{E-new} = A_{E1} + A_{E2-new} = \underbrace{(-0.0182x_2 + 0.0155)(x_1 - 1.8)}_{A_{E1}} -$$

$$\underbrace{+151.48x_2^5 - 567.603x_2^4 + 840.297x_2^3 - 612.498x_2^2 + 218.904x_2 - 30.497}_{A_{E2-new}}$$

The modified natural roll frequency should be corrected, using the residual metacentric height, obtained at the static heel angle due to the effect of constant wind speed U_w (4.11):

$$\omega_{\varphi,e} = \omega_\varphi \sqrt{\frac{\overline{GM}_{res}(\varphi_s)}{\overline{GM}}}$$

Then, the squares of relative and absolute roll transfer functions can be estimated, as (4.10):

$$H^2_{rel}(\omega) = \frac{\omega^4 + (2\mu_e\omega)^2}{(\omega^2_{\varphi,e}(\varphi_s) - \omega^2)^2 + (2\mu_e\omega)^2}$$

$$H^2(\omega) = \frac{\omega^4}{(\omega^2_{\varphi,e}(\varphi_s) - \omega^2)^2 + (2\mu_e\omega)^2}$$

and the spectrum of relative roll motion $S(\omega)$ can be obtained (4.2):

$$S(\omega) = H^2_{rel}(\omega) \cdot S_{\alpha\alpha,c}(\omega) + H^2(\omega) \cdot \frac{S_{\delta M_{wind,tot}}(\omega)}{(\Delta\overline{GM})^2}$$

Further step is to calculate the virtual capsize angles to leeward $\varphi_{cap,EA+}$ and windward $\varphi_{cap,EA-}$ side, taking into account the actual shape of the $\overline{GZ}$ curve (4.20):

$$\varphi_{cap,EA+} = \varphi_s + \sqrt{\frac{2}{\overline{GM}_{res}(\varphi_s)} \cdot \int_{\varphi_{crit,+}}^{\varphi_s} \overline{GZ}_{res}(\xi)\,\mathrm{d}\xi}$$

$$\varphi_{cap,EA-} = \varphi_s - \sqrt{\frac{-2}{\overline{GM}_{res}(\varphi_s)} \cdot \int_{\varphi_s}^{\varphi_{crit,-}} \overline{GZ}_{res}(\xi)\,\mathrm{d}\xi}$$

where

$$\overline{GZ}_{res}(\xi) = \overline{GZ}(\varphi) - l_{wind,tot}$$

Using known roll angle spectrum, the zeroth and second spectral moment can be obtained as (4.17):

$$m_0 = \int_0^\infty S(\omega)\,\mathrm{d}\omega$$

$$m_2 = \int_0^\infty \omega^2 S(\omega)\,\mathrm{d}\omega$$

Then, the standard deviation of roll is (4.19):

$$\sigma_\varphi = \sqrt{m_0}$$

Short-term stability failure indices

With the statistical parameters obtained, the risk indices to positive (leeward) RI_{EA+} and negative (windward) RI_{EA-} side should be calculated (4.18):

$$RI_{EA+} = \frac{\sigma_\varphi}{\Delta\varphi_{res,EA+}}; \qquad \Delta\varphi_{res,EA+} = \varphi_{cap,EA+} - \varphi_s$$

$$RI_{EA-} = \frac{\sigma_\varphi}{\Delta\varphi_{res,EA-}}; \qquad \Delta\varphi_{res,EA-} = \varphi_{cap,EA-} - \varphi_s$$

The short-term failure index is then to be calculated as (4.14):

$$C_{DSC,s} = 1 - \exp\left(-\lambda_{EA} \cdot T_{exp}\right)$$

where

$$\lambda_{EA} = \frac{1}{T_{Z,\varphi}} \cdot \left[\exp\left(-\frac{1}{2 \cdot RI_{EA+}^2}\right) + \exp\left(-\frac{1}{2 \cdot RI_{EA-}^2}\right)\right]$$

$$T_{Z,\varphi} = \frac{2\pi}{\omega_{Z,\varphi}}$$

$$\omega_{Z,\varphi} = \sqrt{\frac{m_2}{m_0}}$$

$$T_{exp} = 3600\,\text{s}$$

Long-term stability failure index

An appropriate short-term and long-term characterisation of environmental conditions that properly describe environment in which the ship is sailing have to be chosen. The short-term stability failure indices $C_{DSC,s}$ should be obtained for each combination of the significant wave height H_S and the modal wave period T_m, after which the long-term stability failure index C_{DSC} can be obtained as (4.21):

$$C_{DSC} = \sum_{i=1}^{n} C_{DSC,s,i} \cdot W_i$$

The ship is then considered not to be vulnerable to the Dead Ship Condition failure mode if the long-term stability failure index is not greater than the standard (4.22):

$$C_{DSC} \leq R_{DS0}$$

E.2 Excessive Acceleration criterion for river-sea ships

The vulnerability to the Excessive Acceleration, according to the Vulnerability Level 2, is assessed by solving the one-degree-of-freedom differential equation of ship roll, where excitation comes from beam irregular waves. The equation is to be solved in frequency domain in order to estimate the likelihood of stability failure (i.e. lateral acceleration for each location along the length of the ship where passengers or crew may be present). The recommended frequency range for the calculation is from $\omega_{min} = \max\{0.5/T_\varphi; 0.2\}$ up to $\omega_{max} = \min\{25/T_\varphi; 2.0\}$, while the frequency step is $(\omega_{max} - \omega_{min})/10000$. The integrations within the procedure are done by means of numerical integration using trapezoidal rule or any other method that provides sufficient accuracy, applying the proper combination of a numerical method and frequency step.

All equations in this section are already mentioned and discussed in the previous chapters, therefore, cross-referencing is provided for the additional explanation.

Environmental conditions

The sea elevation spectrum is to be calculated using the Mean JONSWAP wave spectrum. If the short-term characterisation of environmental conditions, the significant wave height H_S and in this case the modal wave period T_m, are known the sea elevation spectrum can be obtained as (5.2):

$$S_{ZZ}(\omega) = A\gamma^B \cdot \frac{5}{16}\frac{H_S^2}{\omega_m}\left(\frac{\omega_m}{\omega}\right)^5 \cdot \exp\left[-\frac{5}{4}\left(\frac{\omega_m}{\omega}\right)^4\right]$$

where

$$A = 0.658$$

$$B = \exp\left[-\frac{1}{2\sigma^2}\left(\frac{\omega}{\omega_m} - 1\right)\right]$$

$$\gamma = 3.3$$

$$\sigma = \begin{cases} 0.07, & \text{for } \omega < \omega_m \\ 0.09, & \text{for } \omega > \omega_m \end{cases}$$

$$\omega_m = \frac{2\pi}{T_m}$$

The wave slope spectrum is then calculated as (4.4):

$$S_{\alpha\alpha}(\omega) = \frac{\omega^2}{g^2} \cdot S_{ZZ}(\omega)$$

The natural roll frequency is to be calculated using the following equation (9.1):

$$\omega_\varphi = \sqrt{\frac{g\overline{GM}}{k_{xx}^2 + \delta k_{xx}^2}}$$

where the added roll radius of inertia δk_{xx} is to be calculated using the equation (9.4):

$$\delta k_{xx} = B \cdot (K_0 + K_1 + K_2 + K_3)$$
$$K_0 = 0.5909$$
$$K_1 = 0.05516\frac{B}{T} - 0.001876\left(\frac{B}{T}\right)^2 + 0.05674\frac{B}{T}C_{WL}$$
$$K_2 = 3.332C_B + 3.215C_B{}^2 - 0.07211C_B\frac{B}{T}$$
$$K_3 = -4.556C_{WL} + 6.8603C_{WL}{}^2 - 9.328C_{WL}C_B$$

The effective wave slope coefficient at natural roll frequency is to be calculates as (9.5):

$$r_\varphi = R_0 + R_1 + R_2 + R_3 + R_4$$
$$R_0 = -0.5969$$
$$R_1 = 3.416\frac{k_{xx}}{B} - 0.5722\left(\frac{k_{xx}}{B}\right)^2 - 2.814\left(\frac{k_{xx}}{B}\right)^3 + 7.543\left(\frac{k_{xx}}{B}\right)^2\frac{\overline{GM}}{B}$$
$$R_2 = -0.02502\frac{B}{T} + 0.002894\left(\frac{B}{T}\right)^2 + 0.04164\frac{B}{T}\frac{\overline{GM}}{B} - 0.06073\frac{B}{T}\frac{k_{xx}}{B}$$
$$R_3 = 1.198C_B - 0.8308C_B{}^2 - 0.1989C_B\frac{k_{xx}}{B} - 0.006306C_B\frac{B}{T}$$
$$R_4 = -0.2855\frac{\overline{GM}}{B} - 5.276\frac{\overline{GM}}{B}\frac{k_{xx}}{B} + 0.5694\frac{\overline{GM}}{B}C_B$$

while the effective wave slope as a function of frequency is calculated using the formula below (9.8):

$$r(\omega) = \left|\frac{1 + a\hat{k}}{1 + b\hat{k} + c\hat{k}^3}\right|$$

where

$$b = 0.5438 - 1.270\frac{\overline{OG}}{B} + 3.600\left(\frac{\overline{OG}}{B}\right)^2$$
$$c = 0.08857 - 0.4127\frac{\overline{OG}}{B} + 0.6709\left(\frac{\overline{OG}}{B}\right)^2$$
$$a = \frac{r_\varphi\left(1 + b\hat{k}_\varphi + c\hat{k}_\varphi{}^3\right) - 1}{\hat{k}_\varphi}$$

and where

$$\hat{k} = \omega^2 B/g$$
$$\hat{k}_\varphi = \omega_\varphi{}^2 B/g$$

The effective wave slope spectrum can be obtained using the wave slope spectrum and the effective wave slope (4.3):

$$S_{\alpha\alpha,c}(\omega) = r^2(\omega) \cdot S_{\alpha\alpha}(\omega)$$

Short-term roll motion statistics

The roll damping should be estimated by means of the Simplified Ikeda's method. The method is given in Kawahara et al. (2009), while the procedure for the equivalent linear roll damping coefficient μ_e is explained in Section 4.4.1. However, based on the work and conclusions presented in Chapter 6, the parameter A_E used for eddy damping estimation is to be substituted with the parameter A_{E-new}, calculated as (6.15):

$$A_{E-new} = A_{E1} + A_{E2-new} = \underbrace{(-0.0182x_2 + 0.0155)(x_1 - 1.8)}_{A_{E1}} -$$
$$\underbrace{+151.48x_2^5 - 567.603x_2^4 + 840.297x_2^3 - 612.498x_2^2 + 218.904x_2 - 30.497}_{A_{E2-new}}$$

From there, the linear damping coefficient B_{44} can be obtained (4.26):

$$B_{44} = 2 \cdot \mu_e(\sigma_{\dot{x}}) \cdot Q_{44}$$

and Q_{44} is the sum of the roll mass moment of inertia M_{44} and added roll mass moment of inertia A_{44}, obtained as:

$$Q_{44} = \frac{\Delta \cdot \overline{GM} \cdot T_\varphi^2}{4\pi^2}$$

where

$$T_\varphi = \frac{2\pi}{\omega_\varphi}$$

Therefore, the roll amplitude φ_a can be calculated using the following formula (4.25):

$$\varphi_a(\omega) = \sqrt{\varphi_r^2 + \varphi_i^2}$$

where

$$\varphi_r = \frac{a\left(C_{44} - Q_{44}\omega_e^2\right) + bB_{44}\omega_e}{\left(C_{44} - Q_{44}\omega_e^2\right)^2 + (B_{44}\omega_e)}$$

$$\varphi_i = \frac{b\left(C_{44} - Q_{44}\omega_e^2\right) - aB_{44}\omega_e}{\left(C_{44} - Q_{44}\omega_e^2\right)^2 + (B_{44}\omega_e)}$$

and where

$$a = 0$$
$$b = r(\omega)\Delta\overline{GM}k_w$$

From there, the transfer function of lateral acceleration can be found (4.28):

$$a_y^*(\omega) = K_L\left(g\sin\varphi_a + h\omega^2\varphi_a\right)$$

with

$$K_L = \begin{cases} 1.125 - 0.625x/L, & \text{if } x < 0.2L \\ 1.0, & \text{if } 0.2L \le x \le 0.65L \\ 0.527 + 0.727x/L, & \text{if } x > 0.65L \end{cases}$$

The first moment of lateral acceleration spectrum m_0 is to be calculated as (4.30):

$$m_0 = 0.75 \int_{\omega_{min}}^{\omega_{max}} \left| a_y^*(\omega) \right|^2 \cdot S_{ZZ}(\omega) \, \mathrm{d}\omega$$

Short-term stability failure indices

The short-term stability failure index $C_{EA,s}$ is calculated as (4.31):

$$C_{EA,s} = \exp\left(-\frac{R_2^2}{2\sigma_{ay}^2} \right)$$

where

$$\sigma_{ay} = \sqrt{m_0}$$
$$R_2 = 9.81 \, \mathrm{m/s^2}$$

Long-term stability failure index

An appropriate short-term and long-term characterisation of environmental conditions that properly describe environment in which the ship is sailing have to be chosen. The short-term stability failure indices $C_{EA,s}$ should be obtained for each combination of the significant wave height H_S and the modal wave period T_m, after which the long-term stability failure index C_{EA} can be obtained as (4.33):

$$C_{EA} = \sum_{i=1}^{n} C_{EA,s,i} \cdot W_i$$

The ship is then considered not to be vulnerable to the Excessive Acceleration failure mode if the long-term stability failure index is not greater than the standard (4.34):

$$C_{EA} \leq R_{EA2}$$

Biography

Stefan Rudaković (1989, Belgrade) received his B.Sc. from University of Belgrade, Faculty of Mechanical Engineering (2011) and M.Sc. from the same institution, from the Department of Naval Architecture (2014), graduating with the thesis "A probabilistic analysis of the influence of the freeboard on the stability of a small multipurpose cargo ship". Since 2014 he has been enrolled in Ph.D. studies at the same department.

During M.Sc. studies, Stefan carried out two internships: at "Vahali" shipyard in Belgrade and at "viadonau" in Vienna, Austria, both in 2012. He was awarded for excellent grades in 2012/13 school year, on the occasion of the Faculty Day. During Ph.D. studies, he carried out an internship at the classification society "Bureau Veritas" in Antwerp, Belgium (2015). Furthermore, he participated in Erasmus+ student exchange program during which he carried out a research for his Ph.D. thesis at the University of Trieste, Italy (2018).

Stefan has been employed at the Faculty of Mechanical Engineering since 2014. In 2014/2015, he was working as a junior researcher on a Technology Development Program of Serbian Ministry of Education and Science. From 2015 to 2019, he was working as a teaching assistant on several courses. Since 2019, he has been working as a laboratory associate.

From 2017, he has been engaged in Horizon2020 research project – NOVIMAR. In 2017 he organised a project "Confluence Belgrade", and led a team of students to the "Hydrocontest 2017" competition in Saint-Tropez, France.

Stefan was a member of a local organising committee of "16th International Ship Stability Workshop ISSW2017". He is a member of professional maritime organisations Royal Institution of Naval Architects (AMRINA) and Society of Naval Architects of Serbia (SNAS).

Изјава о ауторству

Име и презиме аутора: Стефан Рудаковић
Број индекса: Д8/14

Изјављујем

да је докторска дисертација под насловом

A NOVEL APPROACH TO STABILITY ASSESSMENT OF RIVER-SEA SHIPS

- резултат сопственог истраживачког рада;
- да дисертација у целини ни у деловима није била предложена за стицање друге дипломе према студијским програмима других високошколских установа;
- да су резултати коректно наведени и
- да нисам кршио ауторска права и користио интелектуалну својину других лица.

У Београду, 20.10.2020.   Потпис аутора

_____

Изјава о истоветности штампане и електронске верзије докторског рада

Име и презиме аутора: Стефан Рудаковић
Број индекса: Д8/14
Студијски програм: докторске академске студије
Наслов рада: **A novel approach to stability assessment of river-sea ships**
Ментор: проф. др Игор Бачкалов

Изјављујем да је штампана верзија мог докторског рада истоветна електронској верзији коју сам предао ради похрањивања у Дигиталном репозиторијуму Универзитета у Београду.

Дозвољавам да се објаве моји лични подаци везани за добијање академског назива доктора наука, као што су име и презиме, година и место рођења и датум одбране рада.

Ови лични подаци могу се објавити на мрежним станицама дигиталне библиотеке у електронском каталогу и у публикацијама Универзитета у Београду.

У Београду, 20.10.2020.   Потпис аутора

_____

Изјава о коришћењу

Овлашћујем Универзитецку библиотеку „Светозар Марковић" да у Дигитални репозиторијум Универзитета у Београду унесе моју докторску дисертацију под насловом:

A NOVEL APPROACH TO STABILITY ASSESSMENT OF RIVER-SEA SHIPS

која је моје ауторско дело.

Дисертацију са свим прилозима предао сам у електронском формату погодном за трајно архивирање.

Моју докторску дисертацију похрањену у Дигиталном репозиторијуму Универзитета у Београду и доступну у отвореном приступу могу да користе сви који поштују одредбе садржане у одабраном типу лиценце Креативне заједнице (Creative Commons) за коју сам се одлучио.

1. Ауторство (CC BY)
2. Ауторство - некомерцијално (CC BY-NC)
3. Ауторство - некомерцијално - без прераде (CC BY-NC-ND)
4. Ауторство - некомерцијално - делити под истим условима (CC BY-NC-SA)
5. Ауторство - без прераде (CC BY-ND)
6. Ауторство - делити под истим условима (CC BY-SA)

У Београду, 20.10.2020.   Потпис аутора

_____

1. **Ауторство**. Дозвољено умножавање, дистрибуција и јавно саопштавање дела, и прераде, ако се наведе име аутора на начин одређен од стране аутора или даваоца лиценце, чак и у комерцијалне сврхе. Ово је најслободнија од свих лиценци.

2. **Ауторство - некомерцијално**. Дозвољава умножавање, дистрибуцију и јавно саопштавање дела, и прераде, ако се наведе име аутора на начин одређен од стране аутора или даваоца лиценце. Ова лиценца не дозвољава комерцијалну употребу.

3. **Ауторство - некомерцијално - без прераде**. Дозвољава умножавање, дистрибуцију и јавно цаопштавање дела, без промене, преобликовања или употребе дела у свом делу, ако се наведе име аутора на начин одређен од стране аутора или даваоца лиценце. Ова лиценца не дозвољава комерцијалну употребу дела. У односу на све остале лиценце, овом лиценцом се ограничава највећи обим права употребе дела.

4. **Ауторство - некомерцијално - делити под истим условима**. Дозвољава умножавање, дистрибуцију и јавно саопштавање дела, и прераде, ако се наведе име аутора на начин одређен од стране аутора или даваоца лиценце и ако се прерада дистрибуира под истом или сличном лиценцом. Ова лиценца не дозвољава комерцијалну употребу дела и прерада

5. **Ауторство - без прераде**. Дозвољава умножавање, дистрибуцију и јавно саопштавање дела, без промена, преобликовања или употребе дела у свом делу, ако се наведе име аутора одређен од стране аутора или даваоца лиценце. Ова лиценца дозвољава комерцијалну употребу дела.

6. **Ауторство - делити под истим условима**. Дозвољава умножавање, дистрибуцију и јавно саопштавање дела, и прераде, ако се наведе име аутора на начин одређен од стране аутора или даваоца лиценце и ако се прерада дистрибуира под истом или сличном лиценцом. Ова лиценца дозвољава комерцијалну употребу дела и прерада. Слична је софтверским лиценцама, односно лиценцама отвореног кода.